Etude géochronologique, aspects géomorphologiques et géochimiques du volcanisme de l'île de Basse Terre (Guadeloupe), et datation des structures d'effondrement de flanc majeures de l'Arc des Petites Antilles

Agnes Samper

ÉCOLE DOCTORALE 143
Dynamique et physico-chimie
de la Terre et des planètes

UNIVERSITE PARIS XI
UFR SCIENTIFIQUE D'ORSAY

Thèse présentée
en vue de l'obtention du grade de Docteur ès Sciences de l'Université Paris XI Orsay
Spécialité Sciences de la Terre
par

Agnès SAMPER

Etude géochronologique, aspects géomorphologiques et géochimiques du volcanisme de l'île de Basse Terre (Guadeloupe), et datation des structures d'effondrement de flanc majeures de l'Arc des Petites Antilles

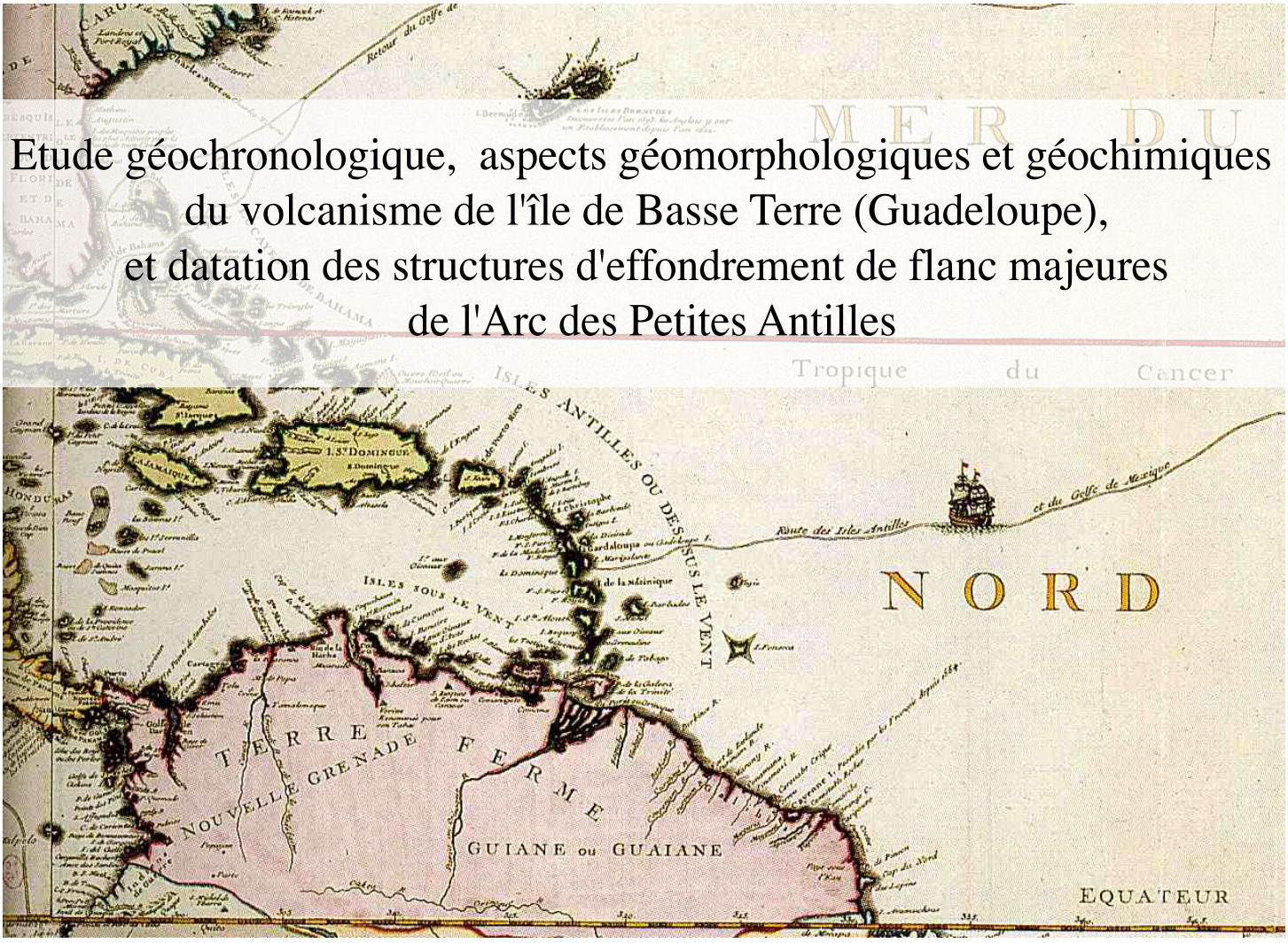

Thèse soutenue le 28 Septembre 2007 devant la Commission d'examen :

M Edouard KAMINSKI.....Rapporteur
M Benjamin van WYK de VRIES.....Rapporteur
M Vincent COURTILLOT.....Président du Jury
Mme Nicole METRICH.....Examinateur
M Pierre-Yves GILLOT.....Examinateur
M Xavier QUIDELLEUR.....Directeur de thèse

ÉCOLE DOCTORALE 143
Dynamique et physico-chimie
de la Terre et des planètes

UNIVERSITE PARIS XI
UFR SCIENTIFIQUE D'ORSAY

Thèse présentée
en vue de l'obtention du grade de Docteur ès Sciences de l'Université Paris XI Orsay
Spécialité Sciences de la Terre
par

Agnès SAMPER

Etude géochronologique, aspects géomorphologiques et géochimiques du volcanisme de l'île de Basse Terre (Guadeloupe), et datation des structures d'effondrement de flanc majeures de l'Arc des Petites Antilles

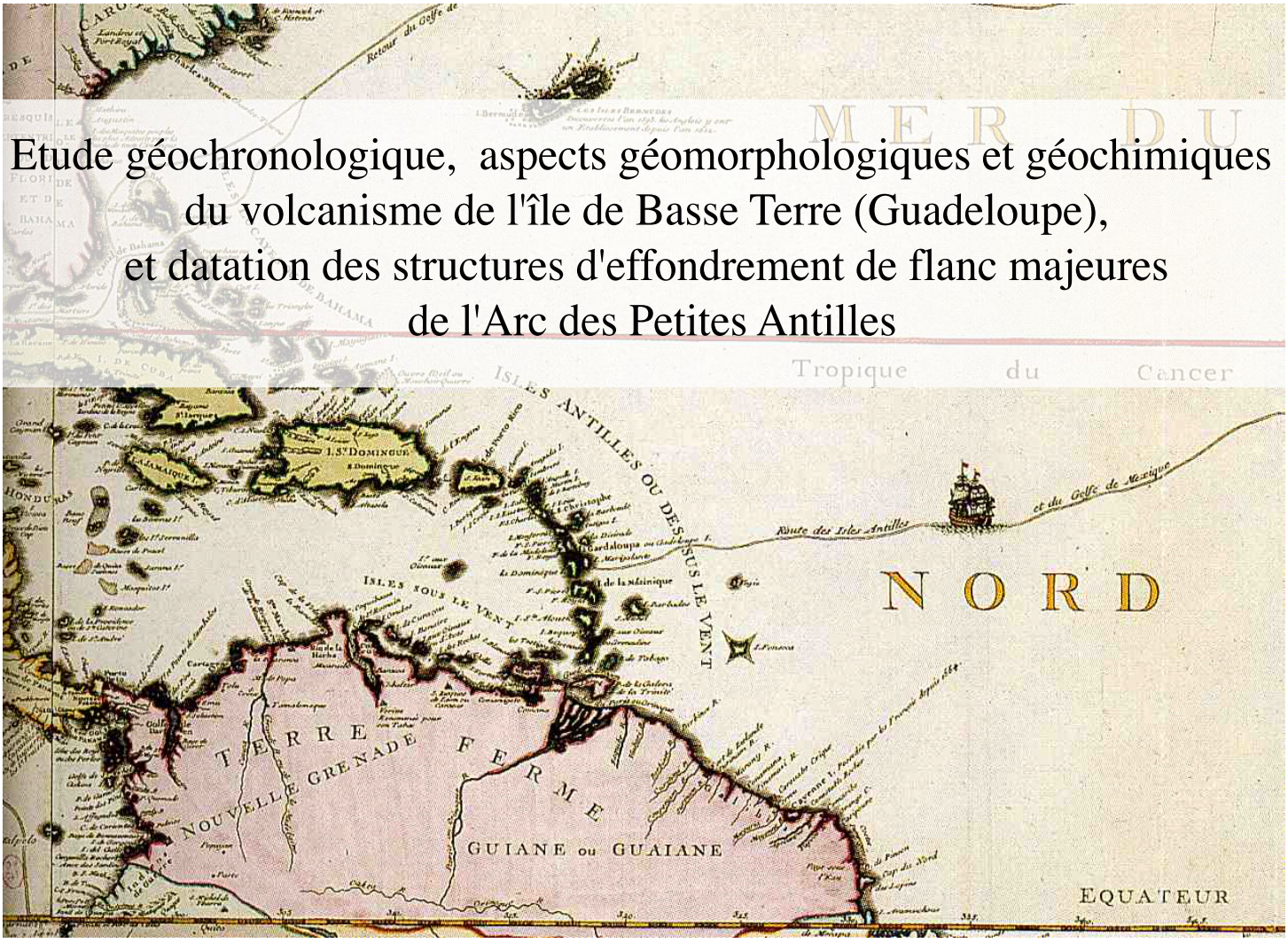

Thèse soutenue le 28 Septembre 2007 devant la Commission d'examen :

M Edouard KAMINSKI.....Rapporteur
M Benjamin van WYK de VRIES.....Rapporteur
M Vincent COURTILLOT.....Président du Jury
Mme Nicole METRICH.....Examinateur
M Pierre-Yves GILLOT.....Examinateur
M Xavier QUIDELLEUR.....Directeur de thèse

Remerciements

Ce travail de thèse n'aurait pu être réalisé sans la présence et le concours de nombreuses personnes au quotidien, collègues et amis.

Notamment toute l'équipe de géochronologie du laboratoire IDES qui m'a accueillie pendant ces cinq dernières années :
je tiens tout d'abord à remercier Xavier Quidelleur de m'avoir confié ce sujet, de m'avoir formée à cette efficace et redoutable technique de datation qu'est la méthode K-Ar Cassignol-Gillot, et de m'avoir fait confiance en me laissant champ libre pour essayer de faire le tour du sujet…de l'île de Basse-Terre.
Je tiens également à remercier Pierre Lahitte avec qui le dialogue scientifique s'est concrétisé cette dernière année par une collaboration prolifique sur les thématiques de volumes et de reconstruction des massifs de Basse-Terre, sa disponibilité et son écoute m'ont été précieuses.
Je remercie Pierre-Yves Gillot, Jean-Claude Lefèvre, Gilles Guérin, Raphaël Visocekas pour leur disponibilité et les discussions scientifiques, amicales et passionnées de tous les jours, ainsi qu'Anthony Hildenbrand et Guillaume Delpech ; Damien Mollex pour son aide précieuse sur le terrain et en laboratoire ; Gilles Guérin pour les discussions et le projet de travail commun de Thermoluminescence sur les quartz des Petites Antilles ; Jean-Pierre Villotte et François Elie ;

Je remercie Georges Boudon et toute l'équipe du Laboratoire de Géologie des Systèmes Volcaniques de l'Institut de Physique de Globe de Paris de m'avoir accueillie cette année ;
Georges Boudon, Jean-Christophe Komorowski, Anne Le Friant et Benoît Villemant pour les riches discussions concernant les Petites Antilles, discussions passées et encore à venir ; ainsi qu'Agnès Michel ; Pascale Besson, et bien entendu Michel, Omar et Fred et leur bonne humeur ;

Les équipes des observatoires volcanologiques et sismologiques des Petites Antilles pour leur accueil, aide et discussions.

Catherine Chauvel du Laboratoire de Géodynamique des Chaînes Alpines, Grenoble, pour m'avoir accueillie chaleureusement au sein de son laboratoire de géochimie isotopique au cours de trois séjours de trois semaines ;

Les membres du laboratoire IDES de l'Université Paris-Sud, Orsay ;
Mes collègues enseignants et la génération d'étudiants qui m'a permis de me forger une expérience d'enseignement au cours de ces dernières 5 années ;

Une forte pensée pour Henriette Lapierre qui nous a quittés l'an dernier, qui m'avait formée et fait confiance dès mon année de Maîtrise ;

Les compagnons de longue route du bâtiment 504 du bureau n°117 au canapé bleu, Virgile puis Tiffanie, puis du bureau n°119 au canapé cuir noir, Virgile et Erell, sans oublier Aurélie, Julie, Maud, sans qui l'ambiance de travail n'aurait pu être aussi joyeuse ainsi que Karmah, Olivier, Vincent, Alban, Thierry, Christelle, les Sebs ;
Marion et Shasa lors de mes escapades à Grenoble;

Les compagnons de route de cette dernière année : Anne, Hélène, Laurent, Patrick, Véronique, Yoann ainsi qu'Aurélie, Marie, et Thomas pour les pauses-café tardives de leur fin de rédaction.

Les trois restaurants libanais des alentours de Jussieu qui m'ont apporté un soutien certain cette année ;

Enfin, mes collègues et amis géologues de toujours Audrey, Cesar, Isa et Gwen, Chuy y Carmen ; toute la bande issue de Grenoble Stéphane et Aurèl, le Jé, Alex, Olivier, Chechen, Dennis ; la Venezuelan Connection de Chambéry et Paris : Crelia, el Aureliano, el Eduardo y el Raymi ; la Cameroon Connection : Dieudonné, David et Ferdinand ; et bien sûr encore eux Erell, Julie, Virgile, Anne et Yoann ;
Sans oublier Marianne, Robert, Nadège, Julien, La Division, Cocolai, y Noe mi prima preferida.
Je ne peux évidemment pas oublier de remercier les adventurous, apasionados, mystiques et toujours bavards Adam, Eduardo et Evan pour leur présence, soutien, et surtout leur précieuse amitié.
Enfin je n'oublierai pas ceux qui heureusement sont toujours là, mes parents, my sister, ma tasse de thé, mon vélo et la Lune.

Table des matières

Introduction Générale

Ce travail de thèse présente une étude des aspects temporels de la construction et destruction d'édifices volcaniques, dans le cadre de l'arc volcanique des Petites Antilles.

Nous nous sommes plus particulièrement intéressés aux épisodes de construction de l'île volcanique de Basse-Terre (Guadeloupe). Ce travail poursuit l'étude de la chronologie du volcanisme du Sud de Basse-Terre initiée par (Blanc, 1983) et poursuivie par (Carlut et al., 2000). Ces deux précédentes études ont fourni un total de 18 âges obtenus par la technique de datation K-Ar Cassignol-Gillot, qui ont ainsi permis de contraindre l'âge de la partie Sud de l'île entre 1 Ma et l'actuel.

Le but de notre étude fut d'étendre à l'ensemble de la Basse-Terre la caractérisation temporelle du volcanisme. Pour ce faire, l'échantillonnage exhaustif et la datation de cinquante-deux coulées de lave et édifices de l'île furent réalisés. Nous disposons donc actuellement d'une base de données temporelles de soixante-dix datations au total. Couplée à une analyse géomorphologique et géochimique, cette approche temporelle nous permet de proposer une histoire cohérente de la construction de l'île de Basse-Terre. Nous apportons en particulier de nouvelles contraintes temporelles quant aux épisodes d'effondrement de flanc qui ont affecté le Sud de la Chaîne Axiale, ainsi qu'une compréhension affinée des dernières phases d'activité du massif le plus récent de l'île, le complexe volcanique de Grande-Découverte.

Nous nous sommes également intéressés à la datation des phénomènes catastrophiques de déstabilisation de flancs aux Petites Antilles affectant les îles volcaniques de la Dominique, Martinique, et Sainte-Lucie.

Ce manuscrit est organisé en deux parties principales. La première concerne la construction de l'île volcanique de Basse-Terre, suivant des aspects géochronologiques, géomorphologiques et géochimiques. Sont présentées les histoires temporelles des massifs anciens du Nord de l'île, puis du plus récent situé au Sud de l'île, le complexe volcanique de Grande-Découverte. Dans une seconde partie, nous apportons des contraintes temporelles aux événements majeurs d'effondrement de flanc ayant affecté diverses îles de l'arc antillais, puis une proposition de corrélation causale entre ces phénomènes catastrophiques et les changements climatiques globaux est proposée. Enfin dans un dernier chapitre, nous présentons une synthèse générale de ce travail.

Introduction

Préambule

Dans ce premier chapitre, nous commencerons par une présentation du contexte géodynamique régional de l'arc des Petites Antilles en essayant de souligner succinctement ses particularités, puis nous présenterons le contexte structural, géologique et géochronologique de l'île de Basse-Terre, sujet principal de ce travail de thèse. Enfin, une synthèse des questions auxquelles tente de répondre cette étude, et un résumé de chaque article constituant chacun un chapitre de la thèse, cloront cette première partie.

I. Contexte Géodynamique de l'Arc des Petites Antilles

L'arc volcanique des Petites Antilles est le témoin de la subduction des plaques Amérique du Nord (NAM) et Amérique du Sud (SAM) sous la bordure Est de la plaque Caraïbes (CAR) (DeMets et al., 2000; Hawkesworth and Powell, 1980), suivant une direction de convergence SW et une vitesse de 2 cm/an (DeMets et al., 2000; Deng and R., 1995; Jordan, 1975; Minster and H., 1978; Tovish and Schubert, 1978). La plaque Caraïbes est délimitée en ses bords nord et sud par deux systèmes décrochant majeurs, de mouvement respectivement senestre au niveau des Grandes Antilles et dextre dans le nord Vénézuéla, qui marquent la transition avec les plaques NAM et SAM (Figure 1). Entre ces deux limites, la zone de subduction est fortement incurvée et l'arc des Petites Antilles, long de près de 850 km, présente un angle de courbure de l'ordre de 450 km. L'arc volcanique, constitué d'une douzaine d'îles, s'est vraisemblablement initié au Paléocène (Andreieff et al., 1981; Andreieff et al., 1984; Maury et al., 1990). Depuis, son évolution a été marquée par deux principales périodes qui contraignent sa morphologie actuelle en double-arc observable au nord de la Martinique (Fink, 1972; Martin-Kaye, 1969). Les îles d'Anguilla, St Martin, St Bartélémy, Barbuda, Antigua, Grande-Terre et Marie-Galante au Nord, puis au Sud la Martinique, Sainte-Lucie, Saint Vincent, l'archipel des Grenadines et Grenade ont dans un premier temps

constitué un arc unique, actif jusqu'au Miocène Inférieur à Moyen (Bouysse, 1979 ; Bouysse and Guennoc, 1983; Fink, 1972 ; Martin-Kaye, 1969 ; Maury et al., 1990; McCann and Sykes, 1984). Une absence de dépôts volcaniques postérieurs au Miocène Moyen dans les îles situées au Nord de la Martinique (Bouysse, 1979 ; Bouysse and Guennoc, 1983 ; Mascle and Westercamp, 1983) indique l'arrêt de l'activité volcanique de ces îles, vraisemblablement au Miocène Inférieur à Moyen (Bouysse, 1979 ; Bouysse and Guennoc, 1983; Martin-Kaye, 1969). Le hiatus magmatique qui s'en suivit jusqu'au Miocène Supérieur à Pliocène (Bouysse, 1979 ; Bouysse and Garrabe, 1984 ; Martin-Kaye, 1969 ; McCann and Sykes, 1984) serait dû à un probable changement de l'orientation de la lithosphère subductante (NAM) (Bouysse, 1979; Bouysse and Westercamp, 1990) ou à un aplanissement de son angle de subduction. Ces modifications du régime de convergence, initiées à la suite d'un changement géodynamique, ou de la subduction de reliefs sous-marins tels que les rides asismiques de Tiburon et Barracuda (Bouysse and Westercamp, 1990) ont causé le saut du front de subduction vers l'Ouest. Ainsi, tandis que le dépôt de calcaires de plate-forme se développait sur la plupart des îles de la branche de l'arc avorté, l'activité volcanique s'initiait dès le Miocène-Pliocène au sein d'un second arc localisé plus à l'Ouest (Maury et al., 1990; Wadge, 1986),. L'arc interne récent est composé du Nord au Sud des îles de Saba, Saint Eustache, Saint Kitts, Nevis, Redonda, Montserrat, Basse-Terre, Les Saintes, et la Dominique. Le front volcanique Plio-Pléistocène est actuellement localisé sur les deux branches Nord et Sud, qui forment un seul et même arc volcanique actif. Sur chacune des îles, l'extension du volcanisme Pléistocène serait limitée à l'intérieur d'une zone large de 10 km (Wadge and Shepherd, 1984).

De récentes études concernant le régime des failles actives de l'arc des Petites Antilles mettent en évidence une partition du régime tectonique de l'arc (Feuillet et al., 2002). La partie Nord de l'arc comprise entre les îles de la Dominique et d'Antigua, est le site d'une

extension parallèle à la zone de subduction qui se traduit par une famille de failles normales décrochantes sénestres, parallèles à la zone de l'arc, et situées en arrière de celui-ci (Feuillet, 2000; Feuillet et al., 2002). Une deuxième famille de failles normales perpendiculaires à la zone de subduction coupe l'avant-arc. Une absence d'extension parallèle à l'arc est observable dans la partie Sud de l'arc. La composante de mouvement sénestre qui disparaît au Sud de la Guadeloupe, puis devient dextre, caractérise le changement de régime tectonique (Feuillet, 2000). Une déformation superficielle à dominante compressive se concentre alors en avant des îles de la Martinique à Grenade, au niveau du prisme d'accrétion de la Barbade, large d'environ 400 km. La différence des régimes tectoniques des parties Nord et Sud de l'arc s'expliquerait par le fait que la plaque Caraïbes (CAR) soit prise en étau au sein du mouvement convergent des plaques Nord-Américaine (NAM) et Sud-Américaine (SAM) (Feuillet, 2000). La déformation dans la partie Nord de l'arc serait alors principalement dominée par l'interaction entre les plaques NAM et CAR. La composante de mouvement sénestre induite, parallèle à la fosse, est accommodée en arrière de l'arc par du partitionnement (DeMets et al., 2000; Feuillet, 2000; Feuillet et al., 2002). Les systèmes de rift de direction E-W, situés en position avant-arc et perpendiculaires au mouvement de subduction ont été décrits dans toute la partie Nord de l'arc (Feuillet, 2000; Feuillet et al., 2002) et ce, dès le passage d'Anegada qui marque la distinction morphologique entre l'arc des Petites Antilles, et les Iles Vierges et Porto-Rico (Grandes Antilles). L'ouverture du rift NE-SE d'Anegada, suivant une direction NW-SE localement perpendiculaire à la zone de convergence, se serait initiée dès le Pliocène (Mann et al., 2005).

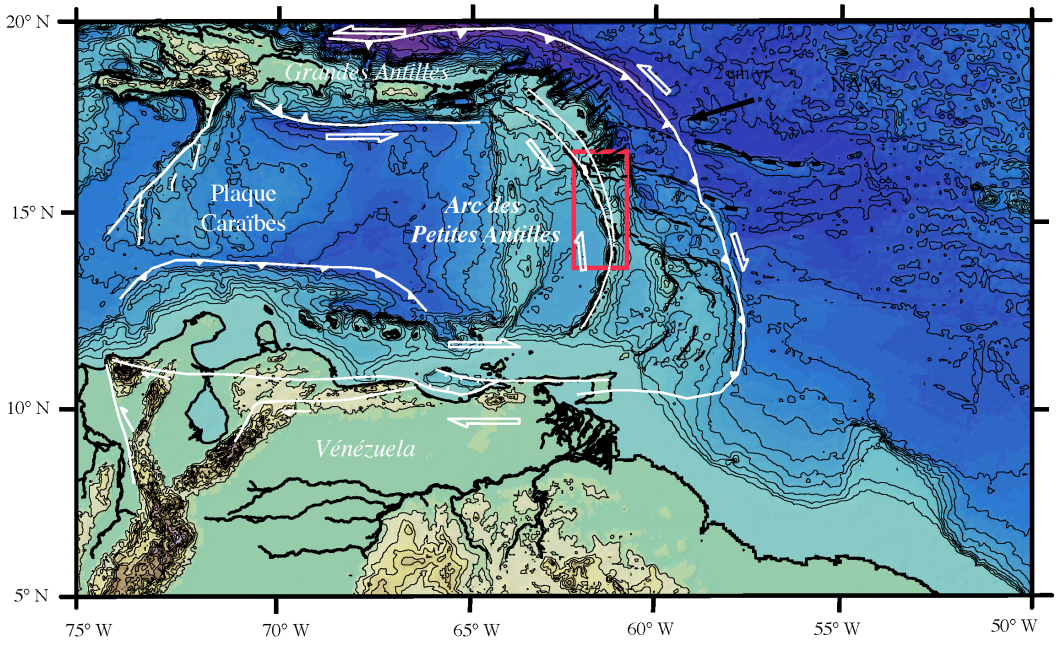

.

Figure 1. Contexte géodynamique et tectonique de l'arc des Petites Antilles, d'après Feuillet et al. (2002). Bathymétrie d'après Smith and Sandwell (1997). Le double-arc des Petites Antilles est souligné en blanc. Le cadre rouge délimite les îles de l'arc des Petites Antilles dont il est question dans cette étude (du nord au sud : Basse-Terre, Dominique, Martinique et Sainte-Lucie). L'île de Basse-Terre est colorée en blanc.

II. Le volcanisme de l'Archipel de Guadeloupe : état des connaissances

II.1 Contexte Tectonique de l'Archipel de Guadeloupe

L'archipel de Guadeloupe est situé dans la partie Nord de l'arc des Petites Antilles (Figure 1). Appartenant à la fois à l'arc ancien avorté et à l'arc actif, il est constitué de cinq principales îles. Situées à l'Est, La Désirade, Grande-Terre et Marie-Galante sont des îles des Antilles Calcaires. Elles sont recouvertes d'épaisses séquences de plate-forme carbonatée récifale d'âge Plio-Quaternaire, déposées de façon relativement continue jusqu'à leur émersion au Pléistocène (Bouysse and Garrabe, 1984 ; Garrabé, 1983; Léticée et al., 2005). A l'Ouest, l'île de Basse-Terre et en son Sud l'archipel des Saintes sont les témoins de l'activité de l'arc récent.

La figure 2, d'après (Feuillet, 2000; Feuillet et al., 2002), illustre la particularité du régime tectonique affectant les îles du Nord de l'arc actif, exposée précédemment dans ce chapitre. L'archipel de Guadeloupe est découpé par trois systèmes principaux de failles normales. Le système de Basse-Terre – Montserrat, parallèle à l'arc, composé de failles normales en échelon à composante sénestre relie l'île de Montserrat à celle de Basse-Terre. Affectant l'île de Grande-Terre, il se connecte au système de graben E-W de La Désirade (Système de l'Eperon Bertrand-Falmouth), au niveau du massif volcanique de Soufriere Hills de Montserrat. Identifié à terre au niveau de Bouillante dans la région Sud-Ouest de Basse-Terre, il se connecte à celui de Marie-Galante au niveau du complexe récent actif de la Grande-Découverte, suggérant un couplage entre la tectonique extensive et l'emplacement des structures volcaniques (Feuillet, 2000; Feuillet et al., 2001; Feuillet et al., 2002).

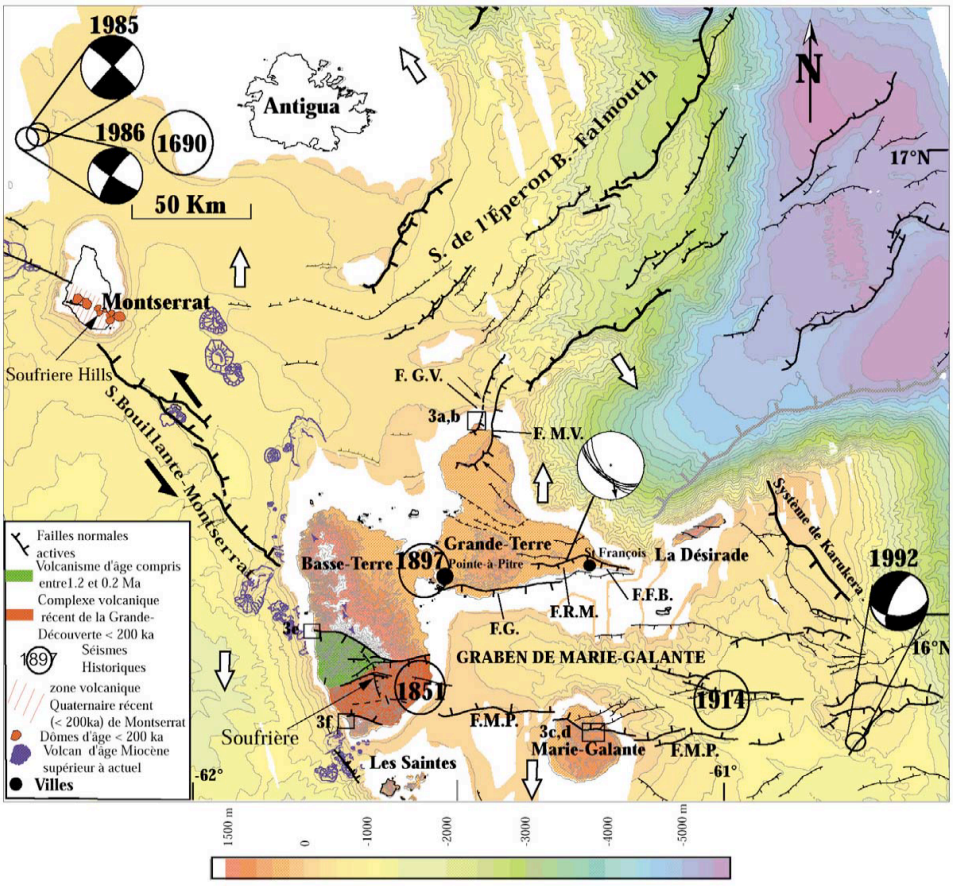

Figure 2. Contexte tectonique régional de l'archipel de Guadeloupe (Feuillet et al., 2002).

II.2 Géologie de l'île de Basse-Terre

Les divers ensembles volcaniques

Toutes les études réalisées sur l'île de Basse-Terre se sont accordées sur la reconnaissance et la désignation des principaux ensembles volcaniques composant l'île, ainsi que sur les directions structurales majeures (Figure 3) (Blanc, 1983; Bouysse, 1985; De Reynal de St Michel, 1966; Gstalter, 1986; Westercamp and Tazieff, 1980).

L'île de Basse-Terre est communément divisée en six massifs volcaniques se disposant entre ses extrémités Nord et Sud. Le Complexe Basal et la Chaîne Septentrionale suivent une direction N-S tandis que la Chaîne Axiale et en son Sud le massif de la Grande Découverte sont construits suivant une direction NW-SE. Le Complexe Basal comprend des coulées massives et quelques dômes isolés ; la Chaîne Septentrionale, érodée, est constituée d'un alignement d'édifices et coulées. La Chaîne Axiale est construite par l'alignement d'édifices composites imbriqués. Le massif de la Grande-Découverte comporte deux complexes volcaniques distincts : le volcan composite de Grande-Découverte et le système de Trois-Rivières-Madeleine qui comprend d'épaisses coulées, divers dômes et édifices isolés dont le dôme andésitique de la Madeleine. La Chaîne de Bouillante, constituée de petits centres éruptifs distincts, longe la Chaîne Axiale sur son bord Ouest. Le volcanisme essentiellement sous-marin, maintenant émergé des Monts Caraïbes, est localisé hors des axes majeurs N-S et NW-SE (Figure 3). L'activité volcanique est actuellement concentrée au sud de l'île au sein du massif de la Grande-Découverte. Le dôme de la Soufrière, qui a subi plusieurs éruptions phréatiques depuis sa mise en place en 1440 AD, en est le témoin le plus récent. La partie Nord-Est de l'île, nommée Plaine Nord-Orientale, est constituée de matériaux latéritiques (Bouysse, 1985; De Reynal de St Michel, 1966; Westercamp and

Tazieff, 1980). Vraisemblablement d'âge plus ancien que l'ensemble des massifs volcaniques, elle est ainsi assimilée au substratum de l'île (Figure 3).

Les Cartes géologiques disponibles

Il existe deux cartes géologiques de l''île de Basse-Terre. La plus ancienne, réalisée par (De Reynal de St Michel, 1966) concerne l'ensemble de l'île. La reconnaissance des diverses unités se base principalement sur des caractérisations et corrélations pétrologiques. Cependant en raison de la relative monotonie pétrographique des laves, cette étude s'avère insuffisante à la compréhension de l'ensemble du volcanisme de l'île et à l'établissement d'une histoire cohérente.

La seconde carte géologique disponible est centrée sur le sud Basse-Terre et en particulier sur le massif de la Grande Découverte (Boudon et al., 1988). Elle présente une étude et un lever des structures et dépôts volcaniques, et incorpore les datations K-Ar (Blanc, 1983; Carlut et al., 2000), ^{14}C ou de thermoluminescence alors disponibles. Elle propose une histoire cohérente de l'activité volcanique du Sud Basse-Terre et de la mise en place des diverses morphologies, notamment de la construction du cône de Grande-Découverte et des différents épisodes explosifs et d'effondrement qui l'ont rythmée.

Des études fines et exhaustives des dépôts pyroclastiques à terre et en mer en cours ont conduit jusqu'à présent à l'identification de onze épisodes d'effondrement de flanc supplémentaires pour la période de 45000 ans à l'actuel (Komorowski et al., 2005). Cette cartographie fine de l'extension des dépôts a pour but de mieux contraindre l'aléa volcanique, en particulier celui associé à un possible effondrement du dôme de la Soufrière ou éruption sub-plinienne de celui-ci (Komorowski et al., 2005).

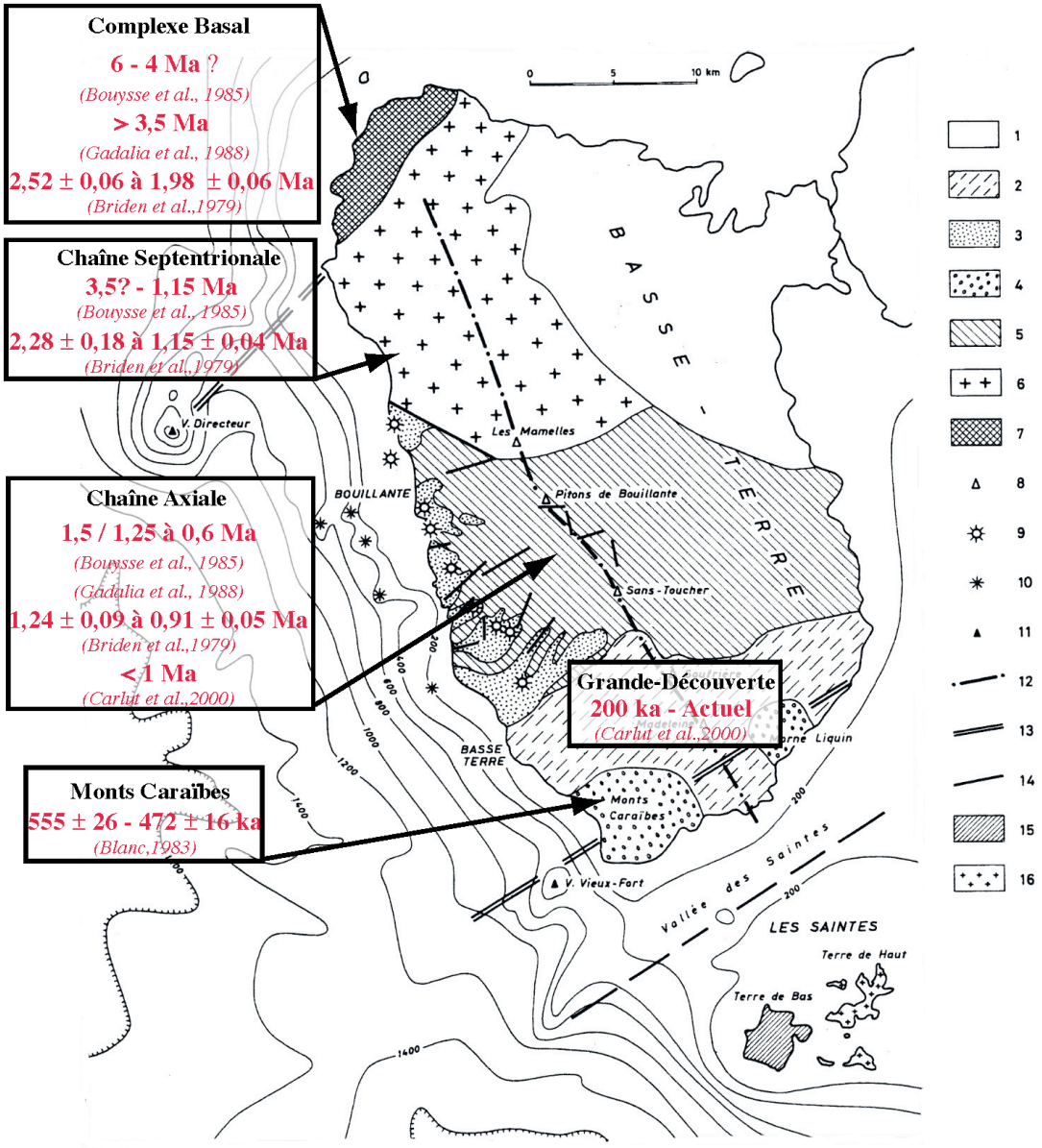

Figure 3. Carte géologique et structurale simplifiée de l'île de Basse-Terre, d'après (Bouysse, 1985c) 1. plaine alluviale du NE; 2. volcanisme Madeleine-Soufrière; 3. volcanisme Chaîne de Bouillante; 4. volcanisme Monts Caraïbes-Morne Liquin; 5. volcanisme Pitons de Bouillante-Sans Toucher; 6. volcanisme Chaîne Septentrionale; 7. Complexe volcanique de base; 8. principales élévations à terre; 9. appareil volcanique émergé de la Chaîne de Bouillante; 10. appareil volcanique submergé de la Chaîne de Bouiillante; 11. volcans sous-marins de Vieux-Fort et du Directeur; 12. axe médian volcanique; 13. grand accident transverse hypothétique; 14. accident; 15. volcanisme de Terre de Bas; 16. volcanisme de Terre de Haut. En rouge: données chronologiques disponibles dans la littérature.

II.3 Les données chronologiques disponibles

Les ensembles volcaniques de l'île de Basse-Terre

La forte pluviométrie du climat tropical guadeloupéen et le développement important de sols épais rendent difficile le travail de lever géologique et de leur interprétation. En outre, l'érosion différentielle d'édifices volcaniques de morphologie et/ou de pétrographie variée a parfois pu conduire à des erreurs d'interprétation chronologique. Ce fut le cas par exemple du Piton de Sainte-Rose, appartenant au Complexe Basal, mais auquel fut attribuée une origine beaucoup plus récente en raison de sa morphologie préservée (De Reynal de St Michel, 1966).

Diverses datations absolues K-Ar ont été réalisées par le passé. Une synthèse des données géochronologiques publiées est présentée en Figure 3. La disparité temporelle qui en ressort souligne la diversité des méthodologies suivies autant en ce qui concerne la qualité de l'échantillonnage, la préparation des échantillons et la technique de datation K-Ar utilisée.
Plus récemment, les travaux de (Blanc, 1983) et (Carlut et al., 2000), réalisés sur le Sud de Basse-Terre ont en effet montré l'inadéquation des âges précédemment publiés. Notamment par la réalisation d'une étude systématique de mesures paléomagnétiques couplée à des datations K-Ar, (Carlut et al., 2000) a démontré l'inexactitude des valeurs paléomagnétiques réalisées et publiées jusque là (Briden et al., 1979).

L'archipel des Saintes

L'étude exhaustive de l'archipel par (Jacques, 1988) conduisit à l'établissement de la carte géologique des Saintes. Les datations K-Ar réalisées sur diverses formations de Terre de Haut et de Terre de Bas contraignent l'initiation de l'émersion de ces îles au Pliocène. Cinq phases d'activité furent définies à partir d'un ensemble de douze âges K-Ar se distribuant entre 4.7 et 0.6 Ma. Les phases I à III [4.7 - 2.4 Ma] concernent uniquement l'édification de Terre de

Haut. Aux environs de 2 Ma, la phase IV constitue la phase majeure d'édification de Terre-de-Bas, tandis que Terre-de-Haut enregistre ses phases d'activité les plus récentes. Ainsi la phase V [1,3 – 0,6 Ma] est limitée à l'activité terminale de Terre-de-Bas.

Le volcanisme sous-marin de l'archipel de Guadeloupe

Des campagnes bathymétriques menées dans les années soixante (Fink, 1972) puis quatre-vingt (ARCANTE 2-THERMOSITE 1980, SEACARIB 1 1985, (Bouysse, 1988; Bouysse, 1985)) au large des côtes de diverses îles des Petites Antilles, ont permis la reconnaissance de morphologies caractéristiques d'édifices volcaniques sous-marins. Trois zones principales ont, en particulier, été identifiées aux abords de la côte ouest de la Basse-Terre (Figure 3). A une distance de 3 km au sud-est des Monts Caraïbes, le volcan du Vieux-Fort se situe à une profondeur de 400 m. Deux datations sur roche totale de blocs andésitiques dragués donnent deux âges semblables de 2,09 ± 0,32 Ma et 3,05 ± 1,00 Ma (Bouysse, 1985). Entre 4,5 à 6,5 km au large de la Chaîne de Bouillante, cinq monts sous-marins ont été identifiés à des profondeurs moyennes de 800 à 200 m ; l'îlet à Pigeons étant considéré comme un petit centre éruptif émergeant à 4 km au NNE de Bouillante. Une troisième zone de volcanisme sous-marin est située à près de 13,5 km des côtes : entre les profondeurs de 1000 à 200 m (Bouysse, 1988) un relief long d'une dizaine de kilomètres représente l'éperon du Volcan du Directeur. (Gadalia et al., 1988) et (Bouysse, 1988) proposent que cet édifice soit localisé sur le prolongement en mer de la faille NO-SE identifiée à terre à l'Anse à Zombi, faille raccordée à l'accident tectonique majeur de Bouillante-Montserrat (Feuillet, 2000). Sur la base de roches volcano-sédimentaires draguées, (Bouysse, 1985) proposent la mise en place de cet édifice entre 3,7 et 3,4 Ma et une datation K-Ar réalisée sur les plagioclases d'une cendre volcanique donne un âge de 2,82 ± 0,90 Ma.

Les échantillons dragués présentant des risques manifestes et élevés d'altération hydrothermale, et ces âges K-Ar ayant été réalisés sur roches totales ou sur phénocristaux, ces âges sont peu fiables, et nous ne les considèreront plus pour la suite de cette étude.

II.4 Essais de corrélations spatio-temporelles

Les diverses études précédant les travaux de (Feuillet, 2000; Feuillet et al., 2001; Feuillet et al., 2002) ont tenté d'établir des corrélations volcano-structurales à terre, et en mer. Les axes principaux N-S du Nord Basse-Terre, et NW-SE du Sud Basse-Terre ont été reconnus très tôt (Bouysse, 1985; Gadalia et al., 1988; Westercamp and Tazieff, 1980). Des axes NE-SW parallèles à celui de la Vallée des Saintes séparant le Sud Basse-Terre de l'archipel des Saintes ont été proposés pour relier le volcanisme des Monts Caraïbes à celui du Morne Liquin, de même pour le volcan sous-marin du Directeur et du Complexe Basal. Si les principales directions ont bien été établies, les essais de corrélations spatio-temporelles tectono-volcaniques basées sur la reconnaissance des structures et les âges disponibles ont conduit souvent à des interprétations incertaines et à certaines confusions. L'une d'elles est notamment la confusion de la notion de front volcanique et de failles d'extrusion du volcanisme qui a pu conduire à interpréter le front volcanique comme animé d'un « comportement » spatial variable au cours du temps (Gadalia et al., 1988). Cet exemple illustre que les divers objets géologiques et leurs échelles spatio-temporelles ont souvent été mal identifiés et distingués, aboutissant à une confusion du rôle joué par chacun dans les processus du magmatisme en profondeur, et du volcanisme en surface. La délimitation spatiale en surface du front de subduction est de l'ordre de la dizaine de kilomètres, de permanence de plusieurs millions d'années, en l'occurrence depuis le Pliocène dans l'arc des Petites Antilles (Wadge and Shepherd, 1984). Si le front volcanique est l'expression en surface d'une genèse de magma en profondeur contrainte par les conditions de la subduction

(angle et vitesse de plongée de la plaque subductante, profondeur de genèse du magma), il a été proposé plus récemment que le réseau de failles découpant la plaque sus-jacente puisse jouer un rôle majeur dans le contrôle de l'extraction des magmas au cours du temps (Feuillet, 2000; Feuillet et al., 2001; Feuillet et al., 2002; Wadge, 1986).

III Problématique

Partie I : Etude de l'île de Basse-Terre

Une simple observation morphologique renseigne sur la chronologie relative des quatre principaux massifs (Figure 4). C'est en effet dans la partie Sud de l'île que se situent les altitudes les plus importantes et les morphologies les mieux préservées, manifestement moins affectées par l'érosion et donc d'âge plus jeune. Cette approche morphologique est bien entendue insuffisante à une reconstruction temporelle cohérente de l'île de Basse-Terre. De même, l'analyse pétrographique et géochimique a échoué dans la compréhension globale du volcanisme de l'île (Gadalia et al., 1988; Gunn et al., 1980).

Au vu du peu de données géochronologiques existantes, la couverture temporelle de l'île est manifestement trop réduite. La plupart des sites datés sont localisés en bord de côte ou en bord de route, donc en bordure des massifs volcaniques et non en leur centre. En ce qui concerne le Nord Basse-Terre, une incohérence générale se dégage des âges disponibles. De plus, nombre de ces datations ont été réalisées sur roches totales ou sur roches altérées, ce qui rend incertaine la fiabilité de ces âges. Ainsi que cela sera évoqué dans les différents articles de cette thèse, la réalisation de datations ^{40}K-^{40}Ar sur roche totale est propice à des erreurs importantes sur les âges obtenus en raison de possibles excès d'argon dans les phénocristaux, et de pertes de potassium occasionnées par le lessivage de la roche au cours du temps.

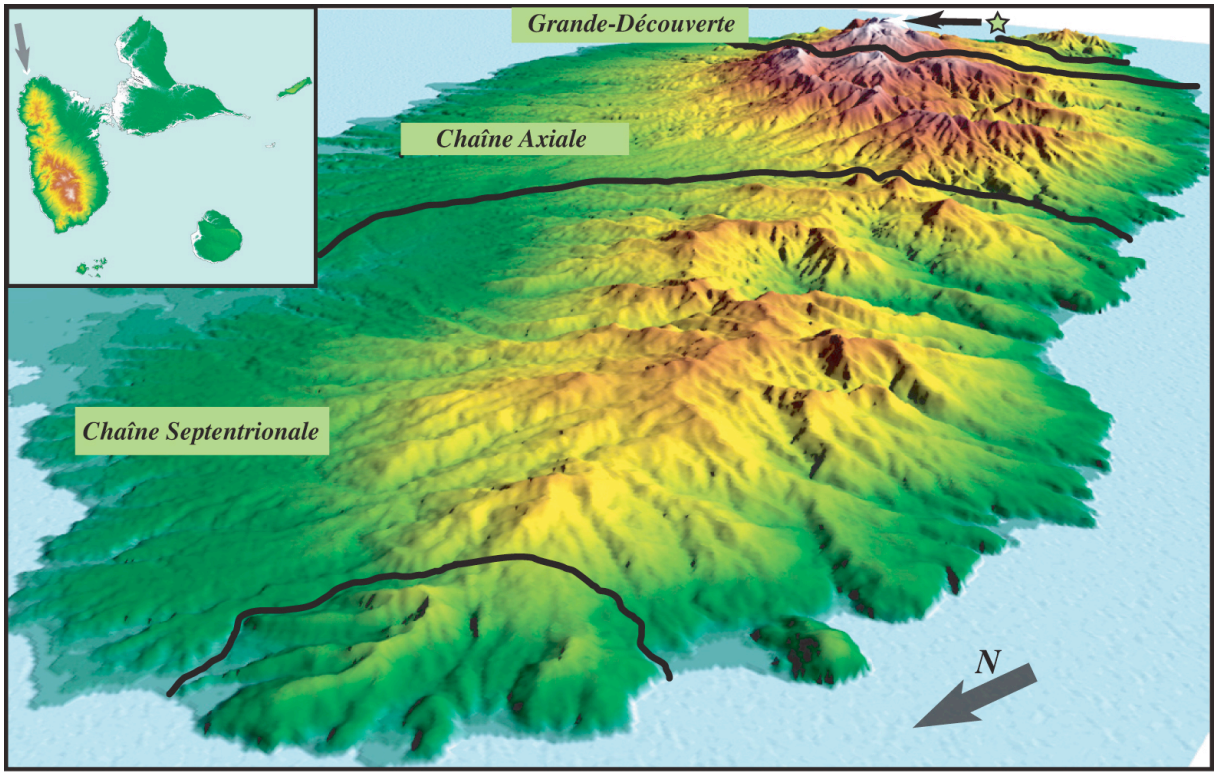

Figure 4: l'île de Basse-Terre vue du Nord illustrant la décroissance de l'effet de l'érosion du Nord au Sud de l'île

L'histoire volcanique générale de l'île est ainsi peu contrainte. Un des premiers objectifs de ce travail de thèse fut d'obtenir des données temporelles fiables et abondantes. Nous avons donc entrepris d'échantillonner l'ensemble des massifs volcaniques de l'île. En raison du climat tropical, le développement de sols épais rend la préservation des produits volcaniques difficile et leur affleurement restreint. Nous nous sommes donc intéressés au volcanisme effusif sub-aérien, l'échantillonnage étant cependant fonction de la possibilité de pénétration dans la forêt tropicale et les reliefs. Les coulées de laves accessibles en bord de routes, falaises, et carrières ont été prélevées, mais c'est l'exploration systématique des chemins existants et principalement des rivières qui a permis l'obtention d'un échantillonnage à l'intérieur des massifs et donc de ce fait beaucoup plus abondant que par le passé.

La technique de datation K-Ar Cassignol-Gillot a été systématiquement appliquée à la mésostase de chaque échantillon, cette phase étant la dernière à avoir cristallisé lors de la mise en place de la coulée et de son refroidissement à l'air libre. Il est également nécessaire de signaler qu'une sélection drastique des échantillons a été réalisée (cf Partie I). Ainsi tous les échantillons prélevés n'ont pu être datés car ne correspondant pas à nos critères de sélection.

Cinquante-deux âges nouveaux obtenus au cours de cette étude viennent compléter les dix-huit préexistants obtenus sur les massifs du Sud de l'île, la Chaîne Axiale et le Massif de Grande-Découverte (Blanc, 1983 ; Carlut et al., 2000).

L'utilisation de cette nouvelle base de donnée temporelle riche de soixante-dix datations a ainsi pour objectifs de :

* Préciser l'âge d'initiation du volcanisme effusif sub-aérien à Basse-Terre
* Définir les limites temporelles de chacun des massifs volcaniques constituant l'île
* Proposer un scénario cohérent de la construction de la partie sub-aérienne de l'île

* Préciser l'évolution temporelle du volcanisme au sein de chaque massif, en étudiant la morphologie des structures

* Réaliser lorsque cela semble cohérent, des corrélations volcano-tectoniques à l'échelle de chaque massif, de l'île, et de l'archipel

* Proposer une réflexion globale sur le volcanisme de l'archipel guadeloupéen

Partie II : Datation des structures d'effondrement de flanc dans l'arc antillais

Nous nous sommes également intéressés au cours de ce travail à la datation à terre des phénomènes d'effondrement de flanc majeurs qui ont affecté, et parfois à répétition, les îles de l'arc antillais. Les structures de Plat-Pays en Dominique, Des Carbets en Martinique et de Qualibou à Sainte-Lucie, bien reconnaissables par leur morphologie caractéristique en fer à cheval ouvertes sur l'Ouest, ont été échantillonnées dans le but de contraindre l'âge de ces effondrements dont pour la plupart, des dépôts volumineux ont été identifiés en mer au cours de précédentes études (Deplus et al., 2001; Le Friant, 2001; Le Friant, 2002).

La méthodologie adoptée fut ainsi d'échantillonner autant que possible chaque édifice antérieur et postérieur à l'épisode de déstabilisation, afin de contraindre un intervalle de temps le plus restreint possible pour chacun de ces épisodes.

Enfin, une comparaison des âges estimés pour chacun de ces épisodes catastrophiques avec l'échelle des temps des périodes de glaciation et déglaciation nous permet de proposer une corrélation entre l'occurrence de ces événements et les changements climatiques affectant l'ensemble du globe.

Ce manuscrit est ainsi organisé en deux parties autour de ces deux problématiques principales qui sont l'étude du volcanisme effusif de l'île de Basse-Terre, et la caractérisation temporelle des phénomènes d'effondrement majeurs de l'arc antillais. Chacune de ces parties comporte deux articles rédigés en anglais dont nous présentons ci-après les résumés traduits en français.

Partie I : Etude géochronologique, aspects géomorphologiques et géochimiques d'une île volcanique : l'île de Basse-Terre, Archipel de la Guadeloupe

Article 1

Timing of effusive volcanism and collapse events within an oceanic arc island : Basse-Terre, Guadeloupe archipelago.

A. Samper, X. Quidelleur, P. Lahitte, D. Mollex.

Une étude de l'évolution temporelle du volcanisme effusif a été réalisée à l'échelle d'une île volcanique active, au sein de l'Arc des Petites Antilles. Trente-deux âges K-Ar ont été obtenus sur une sélection d'échantillons prélevés sur l'ensemble de l'île de Basse-Terre, Guadeloupe, grâce à l'utilisation de la technique K-Ar Cassignol-Gillot. Cette étude, couplée à des données géomorphologiques et géochimiques, conduit à un modèle d'évolution générale de l'île de Basse-Terre. Les données de paléomagnétisme disponibles pour certains sites sont en accord avec l'échelle des inversions paléogéomagnétiques. La durée des processus volcaniques est contrainte pour les trois massifs les plus septentrionaux entre 2.79 ± 0.04 et 0.435 ± 0.008 Ma. Tandis que la période d'activité du Complexe Basal n'excède pas 110 ka (2.79 ± 0.04 – 2.68 ± 0.04 Ma), celle des Chaînes Septentrionales et Axiales s'étend sur à peu près 600 ka, respectivement de 1.81 ± 0.03 à 1.15 ± 0.02 Ma, et de 1.02 ± 0.03 à 0.435 ±

0.008 Ma. Cette étude géochronologique démontre la migration temporelle nord-Sud du volcanisme à travers l'ensemble de l'île, suivant une vitesse de 18 km/Ma sur les 2.8 Ma, et 25 km/Ma pour les derniers 1.8 Ma. Le Complexe Basal et la Chaîne Septentrionale illustrent l'occurrence de volcanisme fissural sur un tiers de l'île, suivant un axe NNW-SSE, tandis que la Chaîne Axiale se compose de volcans composites imbriqués et alignés suivant une direction NO-SE. La partie sud de la Chaîne Axiale a été affectée par deux effondrements de flancs de très grande ampleur orientés en direction du SO pour le premier (640 ka ; 5 à 10 km^3), et en direction du SE pour le second (550 ka ; 20 à 25 km^3). Le taux d'érosion des surfaces d'effondrement atteint 84 km^3/Ma (1250 t/km^2/an) au cours des derniers 650 ka, et 30 km^3/Ma (5250 t/km^2/an) au cours des derniers 200 ka, avant que le volcan du Sans Toucher ne se construise dans les structures d'effondrement. Les roches volcaniques du nord Basse-Terre sont principalement des andésites basaltiques et des andésites, dont les signatures géochimiques, typiques de magmas non primitifs, sont propres aux îles du centre de l'arc des Petites Antilles. Finalement, la mise en place des massifs volcaniques de Basse-Terre peut être reliée séquentiellement à la fois au système régional de failles actives de direction principale NW-SE autour de l'archipel de la Guadeloupe, et à la propagation vers l'est des systèmes de rift de la Désirade, puis de Marie-Galante.

Article 2

Effusive history of southern Basse-Terre (Guadeloupe, French West Indies) during the last 400 kyr, from new K-Ar Cassignol-Gillot ages

Samper A., Quidelleur X., Lahitte P., Komorowski J.C., Boudon G.

Le complexe volcanique de la Grande Découverte, actif depuis au moins 0,2 Ma, est le complexe volcanique le plus récent de l'île de Basse-Terre (Guadeloupe, Arc des Petites

Antilles). Une étude géochronologique détaillée utilisant la technique K-Ar Cassignol-Gillot a été entreprise dans le but d'étudier le rythme de l'activité effusive de ce système volcanique de longue durée. Vingt âges nouveaux permettent de définir que le GDVC a expérimenté pour le moins six grands épisodes effusifs, entre 200 ka et l'actuel. Au Nord, le GDV (Volcan de Grande-Découverte) est actif depuis au moins 200 ka, et au sud, la mise en place du TRMC (Complexe de Trois-Rivières-Madeleine) a débuté il y a 100 ka. Les volumes des GDV et TRMC atteignent respectivement 16,1 km^3 et 2,4 km^3. Ceux-ci, extrudés à des taux de 6,4 10^{-5} km^3/yr et 2,4 10^{-5} km^3/yr, correspondent à 87% et 13% du volume total du GDVC. Les signatures des éléments majeurs et traces sont très proches pour les deux systèmes, suggérant sous l'ensemble du GDVC un système d'alimentation commun, et complexe. Cependant, des observations morphologiques suggèrent que le volcanisme du TRMC fut émis par des évents distincts de celui du GDV, en l'occurrence probablement un réseau de fissures de direction principale E-W lié au rift de Marie-Galante. L'âge moyen de 62 ± 5 ka, obtenu pour l'Alignement E-W La Madeleine-Le Palmiste (MPA, 1,7 km^3), suggère qu'une phase importante de propagation à terre du rift de Marie-Galante s'est produite à cette période. Une phase d'activité récente effusive, de moins de 10 ka, est maintenant décrite pour chacun des massifs. Bien que le risque associé au volcanisme effusif soit bien moins important que celui représenté par l'effondrement potentiel du dôme de la Soufrière, l'extrusion de volumes relativement élevés (jusqu'à près de 0,25 km^3, Coulée de La Coulisse) suggère que l'évaluation du risque volcanique basée principalement sur l'enregistrement géologique de l'activité du dôme de la Soufrière, devrait à présent tenir compte de cette zone active nouvellement identifiée.

Partie II : Apports géochronologiques à la caractérisation des phénomènes d'effondrement de flanc majeurs de l'Arc des Petites Antilles. Applications aux îles de La Dominique, Martinique, Sainte-Lucie et Basse-Terre.

Article 3

Radiometric Dating of Three Large Volume Flank-collapses in The Lesser Antilles Arc

A. Samper, X. Quidelleur, G. Boudon, A. Le Friant, J.C. Komorowski

Il est à présent admis que les effondrements de flancs sont un processus récurrent de l'évolution des volcans des Petites Antilles. Des dépôts d'avalanche de débris de grande extension comportant des volumes associés pouvant atteindre jusqu'à 20 km^3 ont été identifiés au large des côtes des îles de la Dominique, Martinique et Sainte-Lucie. Nous présentons ici de nouvelles datations radiométriques de trois événements majeurs anciens, obtenues par la technique K-Ar Cassignol-Gillot. Au niveau de la dépression de Qualibou de l'île de Sainte-Lucie, l'effondrement s'est produit antérieurement à la mise en place d'un dôme daté à 95 ± 2 ka Par. Sur l'île de la Dominique, où des effondrements à répétition ont été reconnus, l'événement de Plat-Pays s'est probablement produit après 96 ± 2 ka. A l'intérieur de la dépression formée par l'effondrement, Scotts Head, qui est interprété comme un megabloc proximal de taille pluri-kilométrique issu de l'avalanche de la Soufrière, a été daté à 14 ± 1 ka, ce qui fournit une limite inférieure plus récente pour cet événement. Sur l'île de la Martinique, trois différents dômes, présents au sein de la structure des Carbets, et datés à 337 ± 5 ka, permettent de contraindre l'âge de cet événement de grande amplitude. Finalement, ces résultats, obtenus à partir de trois des effondrements de flanc les plus volumineux de l'arc des Petites Antilles, fournissent des contraintes utiles à l'estimation de la récurrence de ces

événements, qui représentent un des risques majeurs liés à la présence des volcans dans l'arc des Petites Antilles.

Article 4

Causal link between Quaternary paleoclimatic changes and volcanic islands evolution

Quidelleur, X., Hildenbrand, A. and Samper, A.

Des glissements gigantesques et les tsunamis qui en résultent représentent le risque géologique principal lié à l'évolution d'une île volcanique [*McMurtry et al.*, 2004; *Moore et al.*, 1994; *Ward and Day*, 2001]. Grâce à des données bathymétriques et des études géologiques menées à terre, des ruptures de flancs ont été identifiées autour de nombreuses îles volcaniques, et ce dans la plupart des contextes géodynamiques. Cependant, les conditions rendant possibles ces phénomènes et les déclenchant sont encore peu comprises, diverses causes internes et externes pouvant agir simultanément jusqu'à atteindre le seuil critique [*McGuire*, 1996]. Nous montrons dans cette étude que la plupart des glissements qui impliquent d'importants volumes (>10 km^3) se produisent à la fin des périodes glaciaires et nous proposons qu'une relation causale entre des effondrements de flanc affectant des îles volcaniques et des changements climatiques globaux a existé durant au moins les derniers 900 ka. De plus, les âges de grande précision présentés ici favorisent l'hypothèse suivant laquelle des événements d'effondrement de flanc majeurs se sont produits pendant le début des transitions glaciaires à interglaciaire, lorsqu'une montée rapide du niveau de la mer est entraînée par l'apport soudain d'eau de fonte des calottes polaires. Nous proposons qu'à la suite de phases d'érosion sub-aérienne contemporaines des périodes de bas niveau marin, une montée rapide du niveau de la mer induise une érosion côtière et des variations soudaines des conditions de pression de pores au niveau des couches basales, ce qui favoriserait la rupture de l'édifice. Enfin, l'effet du réchauffement climatique mis en évidence ici au travers des

variations du niveau marin aidera à mieux apprécier le risque géologique lié aux effondrements des îles océaniques.

Partie I

Etude géochronologique, aspects géomorphologiques et géochimiques d'une île volcanique: l'île de Basse-Terre, Archipel de la Guadeloupe

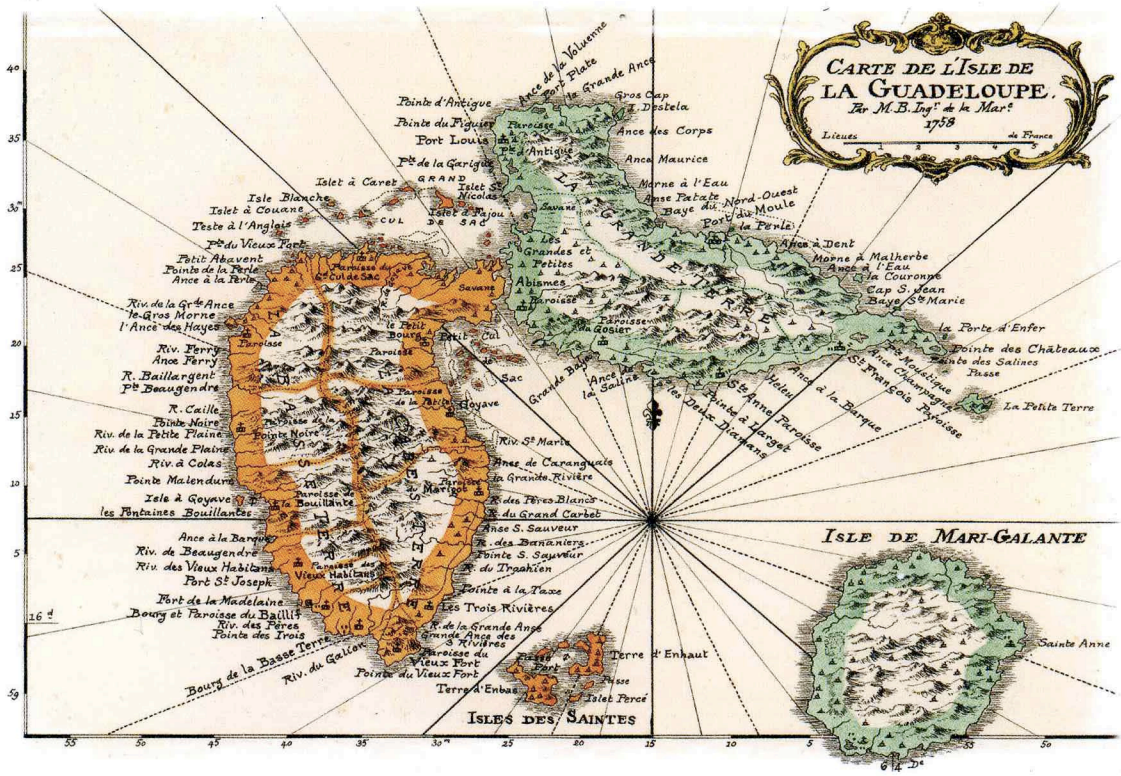

Available online at www.sciencedirect.com
ScienceDirect
Earth and Planetary Science Letters 258 (2007) 175–191
EPSL
www.elsevier.com/locate/epsl

Timing of effusive volcanism and collapse events within an oceanic arc island: Basse-Terre, Guadeloupe archipelago (Lesser Antilles Arc)

A. Samper, X. Quidelleur *, P. Lahitte, D. Mollex

Equipe de Géochronologie UPS-IPGP, Laboratoire IDES, UMR 8184 CNRS-UPS, Dpt. Sciences de la Terre Bâtiment 504, Université Paris-Sud, 91405 Orsay, France

Received 30 August 2006; received in revised form 16 March 2007; accepted 19 March 2007
Available online 24 March 2007
Editor: C.P. Jaupart

Abstract

Timing of effusive volcanism has been investigated at the scale of an active volcanic island within the Lesser Antilles outer arc. Thirty-two new accurate K–Ar ages were obtained throughout the island of Basse-Terre, Guadeloupe, by the use of the K–Ar Cassignol–Gillot technique. Coupled with geomorphological and geochemical data, this study provides a general evolution model for Basse–Terre. Where available, paleomagnetic data are in agreement with the geomagnetic polarity time scale. Time scales of volcanic processes for the three northernmost massifs of the island have been constrained between 2.79±0.04 and 0.435±0.008 Ma. Whereas the Basal Complex lasted only 110 kyr (2.79±0.04 – 2.68±0.04 Ma), the Septentrional and the Axial Chains spread each over about 600 kyr, from 1.81±0.03 to 1.15±0.02 Ma, and from 1.02±0.03 to 0.435±0.008 Ma respectively. This geochronological study demonstrates the temporal North to South migration of volcanism throughout the whole island, at a rate of 18 km/Myr over the last 2.8 Myr, and 25 km/Myr for the last 1.8 Myr. The Basal Complex and Septentrional Chain illustrate the occurrence of fissural volcanism over one third of the island along a NNW–SSE striking axis, whereas the Axial Chain is composed of imbricate composite volcanoes aligned along a NW–SE direction. The southern part of the Axial Chain has been affected by two huge flank-collapses, the first event (640 ka; 5 to 10 km^3) was SW oriented while the second (550 ka; 20 to 25 km^3) was SE oriented. Erosion of the collapse areas reaches 84 km^3/Myr (1250 t/km^2/yr) within the last 650 kyr, and 30 km^3/Myr (5250 t/km^2/yr) during about 200 kyr, before the Sans Toucher volcano grew within the collapse structures. Northern Basse-Terre volcanics are mostly basaltic andesites and andesites, and geochemical characteristics belong to a typical Lesser Antilles Central Islands range, representative of non-primitive magmas. Finally, Basse-Terre volcanic massifs emplacement is sequentially related to both regional active faulting around Guadeloupe archipelago along a main NW-SE striking direction, and the westwards propagation of the Désirade, and then Marie-Galante rift systems.

Keywords: geochronology; geochemistry; K–Ar dating; oceanic islands arc; Lesser Antilles; Guadeloupe

1. Introduction

Only a few studies focusing on timing of volcanic processes are presently available for subduction-arc settings. In particular, when applied to specific volcanic

* Corresponding author.
E-mail address: xavier.quidelleur@u-psud.fr (X. Quidelleur).

0012-821X/$ - see front matter © 2007 Elsevier B.V. All rights reserved.
doi:10.1016/j.epsl.2007.03.030

arcs, the acquisition of a detailed and complete chronological framework at the scale of a whole volcanic island proves to be of great interest in order to characterize the evolution of arc volcano systems through time and their processes. At the scale of the arc, constraints about the location of active loci through time within each island provide valuable information about magma extraction and spatial migration rates relative to the volcanic front. In the Lesser Antilles Arc the amount of accurate time constraints available is still insufficient and is really needed for a better understanding of the volcanism of this arc-system. Moreover, accurate dating of successive volcanic units can help constrain volcanic hazards through time such as flank-collapse events, which have been recognized as a recurrent characteristic of the Lesser Antilles Arc evolution [1,2].

Previous studies focused on Basse-Terre (Guadeloupe archipelago, French West Indies) [3–7], described the main volcano-structural units of the island, as well as an overall NNW–SSE trend of volcanism migration throughout the island [3–7]. However no detailed timing of the different volcanic stages was available. In this study, we present the evolution through time of effusive volcanism within the whole volcanic island of Basse-Terre, by the use of accurate K/Ar geochronology, combined with geochemistry and geomorphology. Previous K/Ar ages from Basse-Terre Island [8] were shown to be inaccurate, probably because of the use of slightly weathered whole-rock material [5,9]. We have applied here the K/Ar Cassignol–Gillot technique [10,11] to selected groundmass from fresh effusive rocks sampled in thirty-two sites located from the northern end of the island to the north of the Composite Volcano of La Grande Decouverte (CVGD), occupying the southern part of the island. This work completes previous K/Ar geochronological investigations limited to the south of the island, where volcanism has been constrained with the same technique to less than 1 Ma [5,9].

2. Geodynamic setting

The Lesser Antilles arc volcanism is generated by the subduction of the Atlantic seafloor beneath the Caribbean plate [12,13] with a relatively low rate of about 2 cm/yr [13–15]. The arc spreads over 850 km long between eastern Venezuela and the Anegada Passage to the north, and displays a strong radius of curvature of about 450 km (Fig. 1). North of the Martinique Island, the Lesser Antilles diverge into two distinct arcs.

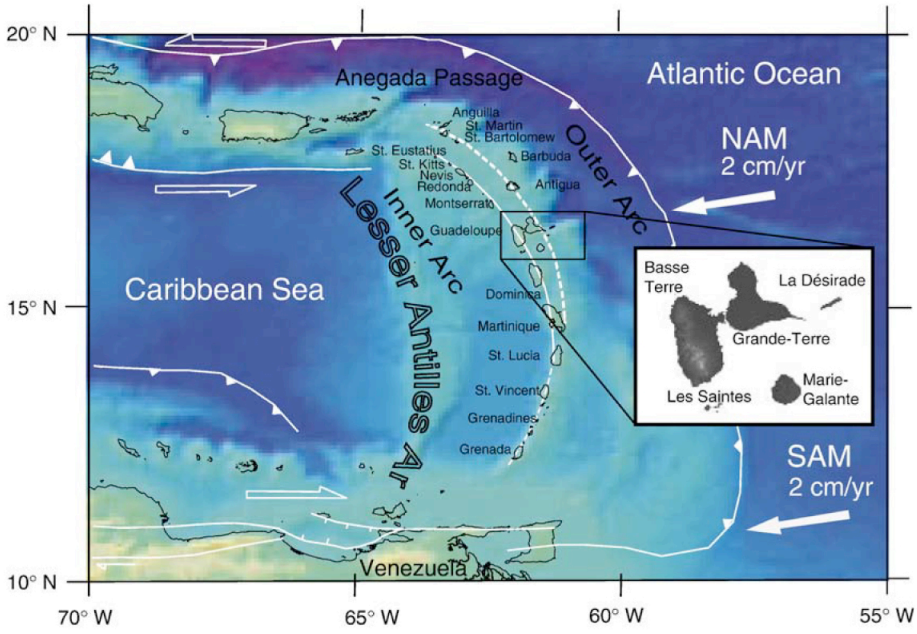

Fig. 1. Geodynamic setting of the Lesser Antilles Arc. Bathymetry from [59] and localization of main faults from [56]. Insert shows the location of the Guadeloupe Archipelago within the Lesser Antilles Arc.

Tectonic adjustments during the mid-Miocene probably modified the orientation of the northern subducting slab, enhancing migration of the volcanic front to the west and the initiation of a new active arc [16,17]. A dozen of volcanoes considered as active are located in the presently western younger arc, where volcanic activity has been observed since Pliocene [7,18]. The northern eastern arc (so-called the Limestone Caribbees) stretches from Anguilla Island to the eastern Martinique. No volcanic activity younger than mid-Miocene [16,19–22] has been reported for these islands, which are mainly covered by Miocene to Pleistocene–Quaternary limestones [21,23]. Older sediments of Paleocene to Eocene age have been found on some islands from the northern arc such as Anguilla, St. Martin, St. Bartholomew [7,24,25]. The southern volcanic Caribbees extend from Martinique to Grenada Islands and commonly display Pliocene and Quaternary volcanic units superimposed over pre-Miocene volcanics and sedimentary units [7].

La Guadeloupe archipelago is part of both the outer and the inner northern arcs (Fig. 1). To the East, the islands of Grande-Terre, La Désirade, Petite-Terre and Marie-Galante belong to the Limestone Caribbees, while, to the West, Basse-Terre and Les Saintes Islands belong to the recent volcanic western arc. Unlike most of the Limestone Caribbees of the outer arc, no volcanic basement can be found on Grande-Terre and Marie-Galante. These islands display the thickest (120 m) and more complete platform reef sequence of Plio–Quaternary age found in the Lesser Antilles Arc [23,26].

3. The geology of Basse-Terre

Together with Dominica and Martinique, the island of Basse-Terre belongs to the central segment of the active volcanic arc (Fig. 1). Based on morphological evidences, four main massifs associated with successive volcanic stages have been identified. To the North, the Basal Complex and the Septentrional Chain have been identified as the remnants of the oldest volcanic massifs of the island [4,27]. Southern Basse-Terre is composed of the Axial Chain and the Grande Découverte massif. The Soufrière volcano is the presently active stage of the younger than 0.2 Ma CVGD [5,9]. We present below a brief description of the successive volcanic stages and the age constraints previously available for each of the four main massifs of Basse-Terre.

3.1. Northern Basse-Terre

The Basal Complex is only found to the North, between Pointe Allègre and the town of Deshaies (Fig. 2). It is made of sub-aerial massive lava flows marking the coastline. Inland, these lava flows extend as high as 100 m above sea level (asl), and eroded volcanic edifices of 200 to 300 m high are observed. The Basal Complex was first interpreted as being pre-Miocene [3], but later studies suggested younger ages ranging from Mio-Pliocene: 6–4 Ma [7,28] to Mid-Pliocene: 4–2 Ma [4].

South of the Basal Complex, the Septentrional Chain which extends over one third of the island, draws a NNW–SSE line [4] of more than twenty 600 to 700 m asl eroded edifices that display thick E–W directed lava flows (Fig. 2). Earlier Late Miocene ages [3] were later revised to Pliocene (3.5–1.2 Ma) [7] or Late Pliocene–Pleistocene ages (2.28–1.15 Ma) [8]. The two dacitic domes of Les Mamelles, located at the southern end of the chain, have been described as the last volcanic episode of this chain (Fig. 2) [4].

3.2. Southern Basse-Terre

Two main massifs have been identified in southern Basse-Terre (Fig. 2). The Axial Chain, which is about 400 to 1000 m asl, is structured by imbricate or compound, sometimes truncated, edifices aligned in a NW–SE direction (Pitons de Bouillante, Sans Toucher, Icaques, and Capesterre volcanoes), associated to numerous lava flows. The onset of the Pitons de Bouillante and Sans Toucher edifices has been related to fissural volcanism, which started with extensive submarine volcanism erupting hyaloclastites, followed by andesitic subaerial effusive phases [7]. Previous unreliable whole-rock K/Ar ages suggested that the Axial Chain volcanic activity spanned through Pleistocene [4,8], while K/Ar Cassignol–Gillot data constrained its activity between 1.023 ± 25 and 0.445 ± 0.006 Ma [5,9]. The E–W striking Vieux-Habitants–Matéliane escarpment cuts the Axial Chain from its eastern to western extremities. It is a large horse-shoe-shaped structure (Fig. 2) interpreted as the remnant rim of a large volcano affected by flank-collapse events [29]. Its eastern part has been associated with the onland termination of the Marie–Galante rift system [30]. The Bouillante chain, located west of the Axial Chain along the Caribbean coast, is made of a succession of small eruptive centers of hydromagmatic dynamism [6,19]. It was thought to have been active between 1.2 and 0.9 Ma [8], later revised between 0.8 and 0.2 Ma [5,9]. The Monts Caraïbes massif lies to the southern end of the island of Basse-Terre (Fig. 2). Its construction was initiated by intensive submarine activity of surtseyan type [4]. It carried on with explosive hydromagmatic activity, followed by emplacement of sub-aerial effusive lava flows intercalated with phreatomagmatic products, and

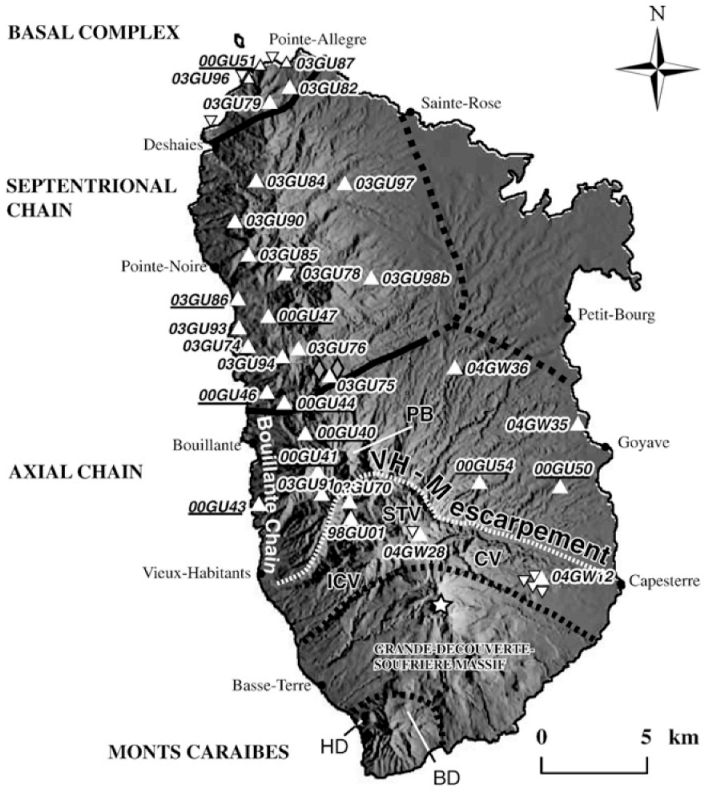

Fig. 2. Basse-Terre Island shaded digital elevation model (light from NE; data IGN). Localization of the 41 sampling sites within the three northern massifs studied here: Basal Complex, Septentrional Chain and Axial Chain–Mont Caraïbes. White triangles for K–Ar dated samples from this study; white inverted triangles for non-dated samples. All samples have been analyzed for major and trace-elements. Lava flows sampled for paleomagnetic measurements are underlined. Grey diamonds show the localization of the dacitic domes of Les Mamelles, and the white star the active volcano of La Soufriere within the Grande-Découverte-Soufrière Massif. PB for Pitons de Bouillante, IcV for Icaques Volcano, STV for Sans-Toucher Volcano, CV for Capesterre Volcano, HD for Houëlmont Dome, BD for Boucanier Dome. White dotted line for the Vieux Habitants–Matéliane (VH–M) escarpment.

ended with the extrusion of the domes of Houëlmont and Boucanier [4,31]. On the Caribbean side, normal faulting oriented along an E–W direction, with mostly northward dip, suggests uplifting of the massif relative to the northern recent volcanic complex of La Grande–Découverte [32]. Earlier K–Ar ages between 1.8 and 1.4 Ma [8] were shown to be inaccurate and revised to much younger values of 555±26 and 472±16 ka for two lava flows [5], in agreement with their normal magnetic polarity [9]. This constrained the activity of the Monts Caraïbes between about 0.6 and 0.4 Ma. Based on these age data, the Bouillante Chain and the Monts Caraïbes are here associated with the Axial Chain Massif.

Located south of the Axial Chain, the CVGD is the most recent volcanic complex of Basse-Terre. Initiated at 205±28 ka [9], its construction has been divided into three main stages: Grande–Découverte (200 to 42 ka), Carmichaël (42 to 11.5 ka) and La Soufrière (8.5 ka to present) [5,31]. Volcanic activity in the past few hundred years has occurred at the la Soufrière dome that was emplaced in 1440 A.D. [33]. Reaching 1467 m asl, it is the highest volcano of the Lesser Antilles Arc.

4. Analyses

4.1. Sampling

During winter 2000 and June 2003, forty-one lava flows were sampled in Central and Northern Basse-Terre, within the Basal Complex, the Septentrional and

Axial Chains. From each lava flow, hand-sized blocks were taken for geochronological and geochemical investigations, and at some sites drill-cores were sampled for paleomagnetic measurements. Due to the easterly winds, heavy rainfalls favor erosion on the eastern side of the island, where lateritic soils are well developed, while cliffs and higher slopes are found to the west. Since all massifs are densely vegetated and soils are largely developed under this tropical climate, exposures are thus rather scarce and limited to rivers, road cuts and quarries, coastal and interior cliffs.

4.2. Geochemical data

Whole-rock major and trace element analyses were performed at the SARM-CRPG (CNRS, Nancy, France). Samples were fused with $LiBO_2$ then dissolved with HNO_3. Major element contents were determined by ICP-AES (Jobin-Yvon JY 70) and trace element concentrations by ICP-MS (Perkin Elmer 5000). Uncertainties for each element can be found at: http://www.crpg.cnrs-nancy.fr/SARM/index.html.

4.3. K/Ar procedure

Thirty-two lava flows (Fig. 2) have been dated in the UPS-IPGP geochronology laboratory at Orsay (France), using the K/Ar Cassignol–Gillot technique [10,11]. After selection of the samples by examination of petrographic thin sections, samples were crushed to a 125–250 μm size fraction and ultrasonically cleaned 15 min in a 10% nitric acid solution. In order to avoid K loss due to weathering, as well as excess argon carried by mafic minerals and low K content plagioclases [34,35], analyses were performed on the carefully separated groundmass phase obtained in a narrow density range, by the use of heavy liquids. A magnetic separator was then used to remove remaining microlithic plagioclases. K was measured by flame emission spectrometry and compared with reference values of MDO–G and ISH–G standards [36]. Ar was measured with a mass spectrometer identical to the one described by [11]. The inter-laboratory standard GL–O, with the recommended value of 6.679×10^{14} atom/g of $^{40}Ar^*$ [37], was used for ^{40}Ar signal calibration. Typical uncertainties of 1% are achieved for the ^{40}Ar signal calibration and for the K determination. The uncertainty on the $^{40}Ar^*$ determination is a function of the radiogenic content of the sample. The detection limit of the system is presently of 0.1% of $^{40}Ar^*$ [38], which makes the Cassignol–Gillot technique especially suitable for these samples. In order to avoid isotopic fractionation, no pre-degassing of the sample was performed [11]. Decay constants and isotopic ratios of Steiger and Jager [39] were used. K contents and Ar measurements were duplicated for each sample. Uncertainties herein are given at the 1σ level.

4.4. Paleomagnetic procedure

Paleomagnetic cores from 10 flows were drilled with a portable gasoline-powered drill and were oriented with a magnetic compass. In order to account for the IGRF declination, following previous determination [9] a mean correction of 14° was applied for each site. Since only the polarity of the flows was investigated here, only four cores per flows were treated with stepwise procedures with about 10 steps. Two specimens experienced alternating field demagnetization, and two others thermal treatment. Measurements were performed using a JR5 (Brno) spinner magnetometer. Measurements and demagnetization were performed in the shielded room of the Institut de Physique du Globe de Paris (IPGP) paleomagnetic laboratory. Evolution of the magnetization vector was scrutinized using Zijderveld [40] diagrams and primary NRM directions were determined using least squares principal component analysis [41].

5. Results

5.1. Geochemistry and petrology

Forty-eight lava flows (Fig. 2) including thirty-two new dated lavas, nine undated samples and seven previously dated lavas [5,9] have been analyzed for major and trace elements, in addition with major elements data previously available for four samples [5]. Although SiO_2 content ranges from 47 to 64 wt.% (Fig. 3a, b), most samples are andesites with only a few basalts and basaltic andesites, and only one dacite from the Axial Chain (ACbC, Fig. 3a). All textures are porphyric. Phenocrysts, being mainly plagioclase ± clinopyroxene, ± orthopyroxene, ± oxides, vary from 25 to 65% content, depending on the massifs. Groundmass is typically microlite and oxide-rich. Basse-Terre lavas belong to the Medium K and Low K types (K_2O: 0.4–1.4 wt.%; Fig. 3a) and display calc–alkaline to tholeitic REE chondrite-normalized patterns with 20 to 50 times the chondrites, and chondrite-normalized La/Sm ratios ranging from 1 to 2.5 (Fig. 3d, [42]). Fig. 3c shows that MgO values are lower than 6 wt.% (from 0.85 to 5.9%), which is comparable to the northern and central arc volcanic islands [43].

Three out of the four basaltic lava flows sampled (Fig. 3a) belong to the Septentrional Chain. When compared to the other rocks of the Septentrional Chain,

these rocks display lower La/Sm ratios between 1.3 and 1.4 (00GU44, 00GU46, 03GU75, Fig. 3d). The fourth basalt identified, from the Monts Caraïbes, belongs to a group made by both the Basal Complex and the Axial Chain, displaying La/Sm ratios between 1 and 1.3. Note that olivine have been observed in only one basalt (03GU75).

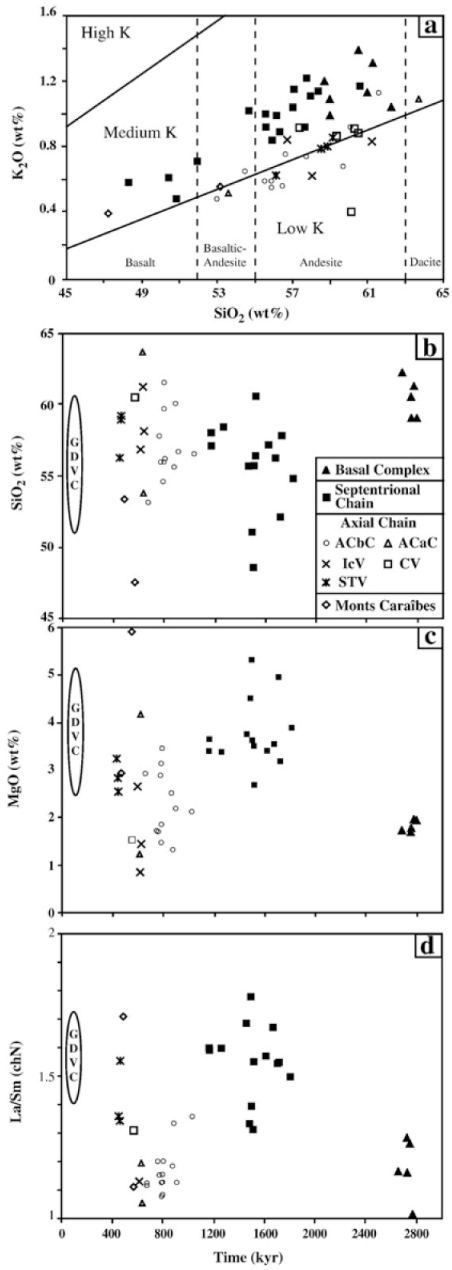

Fig. 3. (a) K_2O versus SiO_2 diagram for Basse-Terre lavas. Fields are from [60] and analyses from this study and [5]. Note that Basal Complex and Septentrional Chain samples (closed symbols) are within the Medium K field, whereas Axial Chain samples are on the Medium K-Low K boundary. Subdivision within the Axial Chain as in Fig. 2, with AcBC and AcAC, for Axial Chain before and after collapse, respectively. (b), (c) and (d): SiO_2, MgO and La/Sm versus time (in ka) for Basse-Terre lavas. The range observed for Grande Découverte Volcanic Complex (GDVC) lavas is also indicated [42].

5.2. K/Ar dating

Thirty-two new K–Ar ages (Tables 1a and 1b) were obtained from the Basal Complex, the Septentrional Chain and the Axial Chain. Ages range from 2.79±0.04 Ma in the north of the Basal Complex to 435±8 ka in the Axial Chain (Fig. 4 and Tables 1a and 1b). Radiogenic ^{40}Ar concentrations are between 3.5 and 61.0%. Almost all duplicates are compatible at the 1σ level, except 03GU78 and 04GW12, which have been duplicated at the 2σ level only. Although, this dataset is limited to outcropping subaerial lava flows, which could be sampled, it allows us to constrain through time the volcanic activity within Basse-Terre.

The Basal Complex (Fig. 4) is mainly composed of effusive lava flows and coastal domes, built over a short time period within the Pliocene between 2.79±0.04 and 2.68±0.04 Ma (Table 1a). Two lava flows from the coves of Clugny and Tillet (03GU87 and 00GU51; Fig. 2) yield ages of 2.77±0.04 and 2.75±0.04 Ma), respectively. On the Caribbean coast, the upper lava flow of the coastal edifice of Morne Petit Bas Vent (03GU96) is dated at 2.77±0.04 Ma as well. The lava flow of Le Piton (03GU82), sampled in the Rivière du Vieux Fort, is the oldest volcanic formation identified in Basse-Terre (2.79±0.04 Ma), and is overlaid by the dome of Piton de Sainte-Rose (2.68±0.04 Ma; 03GU79). The ages obtained over the whole massif suggest that the Basal Complex building stage lasted about 110 kyr.

Fifteen ages, ranging from 1.81±0.03 to 1.15±0.02 Ma have been obtained within the Septentrional Chain (Table 1a). They are distributed along the chain (Fig. 4), and do not show any preferential direction of migration. The spatial distribution of lava flows and domes dated around 1.65 Ma suggests that activity likely occurred contemporaneously in different loci along the Chain (Fig. 4). Moreover, indistinguishable ages for neighbor flows and edifices help to identify

Table 1a
New K–Ar ages from the Basal Complex and the Septentrional Chain

Sample	Longitude	Latitude	K (%)	$^{40}Ar^* \times 10^{12}$ (atom/g)	$^{40}Ar^*$ (%)	Age±1σ (Ma)	Mean age±1σ (Ma)
03GU82	61°45.11′	16°20.33′	1.144	3.316	28.8	2.77±0.04	2.79±0.04
				3.369	26.6	2.82±0.04	
03GU87	61°45.22′	16°21.20′	1.126	3.256	30.3	2.77±0.04	2.77±0.04
				3.272	22.8	2.78±0.04	
03GU96	61°46.61′	16°20.66′	1.325	3.806	39.0	2.75±0.04	2.77±0.04
				3.875	30.6	2.80±0.04	
00GU51	61°46.15′	16°20.10′	1.035	2.998	31.9	2.77±0.04	2.75±0.04
				2.951	26.7	2.73±0.04	
03GU79	61°45.82′	16°19.82′	0.975	2.741	56.0	2.69±0.04	2.68±0.04
				2.718	61.0	2.67±0.04	
00GU47	61°45.92′	16°12.48′	1.218	2.290	17.8	1.80±0.03	1.81±0.03
				2.316	18.5	1.82±0.03	
03GU84	61°46.32′	16°17.13′	1.615	2.884	39.5	1.71±0.02	1.72±0.03
				2.917	47.8	1.73±0.02	
03GU78	61°45.34′	16°13.93′	0.725	1.236	3.5	1.68±0.05	1.71±0.03
				1.337	4.7	1.72±0.05	
03GU86	61°46.99′	16°13.10′	1.227	2.139	47.7	1.67±0.02	1.67±0.02
				2.148	42.4	1.68±0.02	
03GU85	61°46.60′	16°14.59′	1.315	2.224	43.1	1.62±0.02	1.64±0.02
				2.279	55.3	1.66±0.02	
03GU93	61°46.96′	16°12.09′	1.575	2.623	7.4	1.59±0.03	1.61±0.03
				2.671	6.2	1.62±0.03	
03GU90	61°47.08′	16°15.74′	1.129	1.886	25.4	1.60±0.02	1.61±0.02
				1.914	33.9	1.62±0.02	
03GU97	61°43.18′	16°17.01′	0.865	1.360	43.0	1.51±0.02	1.51±0.02
				1.372	52.6	1.52±0.02	
00GU46	61°45.98′	16° 9.88′	0.755	1.179	24.3	1.49±0.02	1.49±0.02
				1.168	20.2	1.48±0.02	
03GU75	61°43.90′	16°10.43′	0.400	0.606	7.9	1.45±0.03	1.46±0.02
				0.610	7.5	1.46±0.03	
00GU44	61°45.37′	16° 9.88′	0.739	1.136	24.3	1.47±0.03	1.46±0.02
				1.116	28.0	1.44±0.03	
03GU98	61°42.26′	16°13.77′	1.075	1.412	48.3	1.26±0.02	1.26±0.02
				1.413	54.2	1.26±0.02	
03GU74	61°45.43′	16°11.09′	1.314	1.579	33.8	1.15±0.02	1.16±0.02
				1.611	48.5	1.17±0.02	
03GU94	61°46.64′	16°11.45′	1.234	1.489	41.1	1.16±0.02	1.16±0.02
				1.503	42.4	1.17±0.02	
03GU76	61°44.86′	16°11.37′	1.361	1.611	44.8	1.13±0.02	1.15±0.02
				1.651	56.0	1.16±0.02	

$^{40}Ar^*$: radiogenic argon.

volcanic complexes within the Chain. For example, the dome of Morne à Louis (743 m, 03GU76, 1.15± 0.02 Ma) and the neighbor flows both dated at 1.16± 0.02 Ma (03GU74 and 03GU94) can be related to the same volcanic episode (Fig. 4). The existence of preferential eruptive loci and their reactivation through time is suggested by the overlapping of 00GU47 flow (1.81± 0.03 Ma) by both 03GU93 (1.61±0.03 Ma) and 03GU86 (1.67±0.02 Ma) lava flows. At the southern end, the dacitic domes of Les Mamelles, which could not be dated because of hydrothermal weathering, cover a group of three thick basaltic lava flows (03GU75, 00GU44, 00GU46; Figs. 2 and 4) yielding indistinguishable ages around 1.48±0.02 Ma (Table 1a).

Axial Chain volcanic morphologies, which are more preserved than in northern Basse-Terre, show that voluminous effusive volcanism has been dominating throughout the lifetime of the chain. The border with the Septentrional Chain is well marked by north-facing lava flows which delimit the northern extension of the Axial Chain and attest for no overlapping between the two massifs. Numerous lava flows extending from eroded edifices in an eastward to northwestward radial pattern reach the eastern and western coasts of the island (Fig. 4).

Table 1b
New K–Ar ages from the Axial Chain

Sample	Longitude	Latitude	K (%)	$^{40}Ar^* \times 10^{12}$ (atom/g)	$^{40}Ar^*$ (%)	Age±1σ (ka)	Mean age±1σ (ka)
04GW36	61°39.33′	16°10.69′	0.729	0.690	22.6	907±13	898±13
				0.679	33.4	892±13	
00GU41	61°44.19′	16°7.18′	1.154	1.067	6.8	885±18	875±21
				1.039	4.9	862±21	
03GU91	61°44.04′	16°06.55′	0.752	0.670	6.1	852±18	864±19
				0.687	6.1	875±19	
00GU40	61°44.63′	16°08.47′	0.675	0.561	15.1	795±12	791±12
				0.555	17.3	786±12	
03GU70	61°43.08′	16°06.13′	0.539	0.446	5.8	793±18	784±19
				0.435	4.8	773±20	
00GU43	61°46.29′	16°06.06′	0.559	0.442	11.1	757±13	759±14
				0.445	7.1	763±15	
00GU54	61°38.48′	16°06.77′	0.497	0.344	12.3	663±11	659±11
				0.339	8.2	652±12	
04GW35	61°34.99′	16°08.74′	0.597	0.377	12.2	604±10	611±10
				0.385	14.8	618±10	
00GU50	61°35.63′	16°06.60′	0.945	0.609	15.4	617±10	616±10
				0.607	11.4	615±10	
04GW12	61°36.54′	16°03.48′	0.823	0.482	32.7	568±8	554±8
				0.469	26.0	546±8	
04GW28	61°40.68′	16°04.93′	1.046	0.483	28.5	442±6	447±6
				0.493	36.8	452±7	
98GU01	61°43.04′	16°05.55′	0.651	0.297	8.2	437±8	435±8
				0.295	10.8	434±7	

$^{40}Ar^*$: radiogenic argon.

We obtained twelve new ages between 898±13 ka and 435±8 ka (Table 1b), which double the data set previously available for the Axial Chain and the Monts Caraïbes [5,9]. Note that paleomagnetic site 98GU01 [9] was mistaken with site H1702 (Morne Soldat) of [5]. The two sites are actually distinct, having been sampled on both sides of the river Grande Rivière des Vieux Habitants (Fig. 4). For the present study 98GU01 [9] was dated and its age of 435±8 ka (Table 1b) clearly associates it with the Sans Toucher Volcano phase.

5.3. Paleomagnetic directions

Eight flows yielded well-defined mean directions with alpha 95 confidence cones lower than 8°. Two flows (00GU40 and 00GU51) showed poorly defined mean directions with alpha 95 of 12 and 23°, respectively, but the magnetic polarity is unambiguously determined. Mean directions for flows with well-defined polarity are shown in Fig. 5a. Five flows recorded normal polarity, while five are reverse. Note that the mean direction (Dec.: −7° and Inc.: 34°), although based from only 10 data, is undistinguishable from the expected value (Dec.: 0° and Inc.: 30°) at this site in the geocentric axial dipole hypothesis.

6. Discussion

6.1. Age reliability

Compared to the few previous geochronological studies, our ages are younger and show a very good coherency within each massif, and at the scale of the whole island. For instance, the small range, from 2.79±0.04 to 2.75±0.04 Ma, obtained for 4 independent K–Ar determinations of lava flows from the Basal Complex (Table 1a) highlights the geological meaning of our results. Similarly, all three ages obtained within the Morne à Louis area for the terminal phase of the Septentrional Chain cluster around 1.16±0.02 Ma (Table 1a).

Additional support is provided by the perfect agreement between the available paleomagnetic polarity (Fig. 5a) and K–Ar ages compared with the geomagnetic polarity time scale (GPTS) (Fig. 5b). All normal and reverse flows agree with the GPTS [44], even for those emplaced shortly before and after the Matuyama–Brunhes transition (MBT), which is dated by the same technique at 786±8 ka [45]. Note that this was already the case for transitional flows from Basse-Terre sampled within the MBT [9].

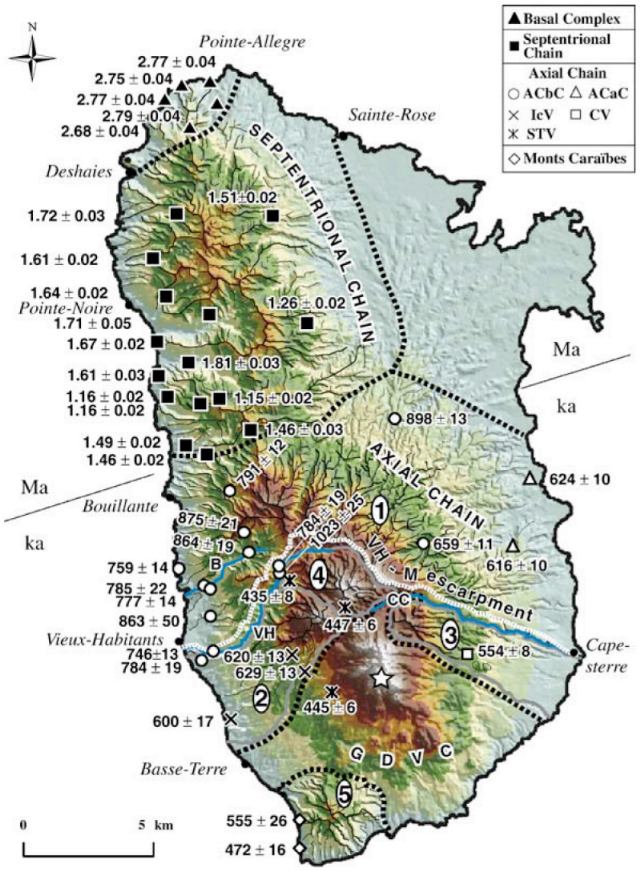

Fig. 4. Basse-Terre Island shaded digital elevation model (light from NE; data IGN) with inferred limits of Basal Complex, Septentrional Chain and Axial Chain massifs (dotted lines). Cassignol-Gillot K-Ar ages available within each massif (Tables 1a and 1b, and [5,9]). Same symbols as in Fig. 3. The Monts Caraïbes (5), Beaugendre (B), Vieux-Habitants (VH) and Class and Capesterre (CC) rivers are indicated. White dotted line for the Vieux-Habitants–Matéliane (VH–M) escarpment. The White star shows the location of La Soufrière.

6.2. Evolution of geochemistry through time

Basse-Terre geochemical characteristics, typical of evolved magmas, are relatively homogeneous and fall in the range observed for the Lesser Antilles Central Islands [43]. However at the scale of the whole island, small heterogeneities between each volcanic chain can be identified through time, from major and trace elements (Fig. 3b, c, d). Septentrional Chain lavas show values close to that of the GDVC, whereas Axial Chain lavas depict characteristics spreading from the ones of the Basal Complex to those of the Septentrional Chain and GDVC. Indeed, rocks younger than 500 ka show La/Sm ratios close to that of the Septentrional Chain and GDVC rocks (Fig. 3d). Thus, within the Axial Chain, the whole island lava range is covered in 600 kyr, which suggests for this massif a quicker evolution of magma range. However, within each massif, no more specific correlation could be found with time and space, suggesting that volcanic edifices and complexes display isolated geochemical evolution.

6.3. Volcanism migration

Morphologies within Basse-Terre show a southward decrease in erosion maturity, which led to the early suggestion that southern volcanic massifs were somehow younger [7]. With the complete reliable data set

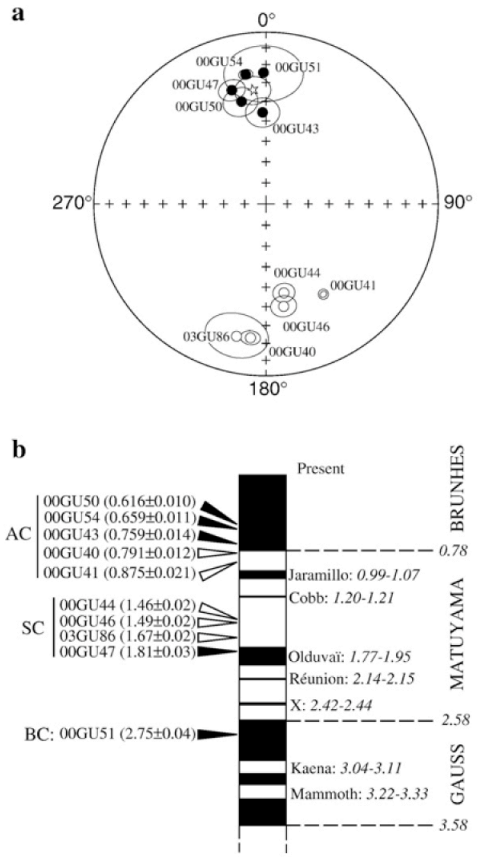

Fig. 5. Paleomagnetic results for lava flows from BC ($n=1$), SC ($n=4$) and AC ($n=5$). (a) Stereographic projection of the mean paleomagnetic direction obtained for each flow and the associated α_{95} confidence cone (black and white symbols: positive and negative inclinations, respectively). The direction of the present-day magnetic field at La Guadeloupe is shown by the open star. (b) Comparison between the magnetic polarity of dated flows from this study with the geomagnetic polarity time scale [44]. Closed and open arrows are for flows with normal and reverse polarity, respectively. All ages are in Ma.

now available (Tables 1a and 1b), we demonstrate that a north to south migration of volcanism has occurred since 2.8 Ma within the whole island of Basse-Terre. These results favor a complete reinterpretation of the age of initiation of subaerial effusive volcanism, as well as the timing of the overall effusive volcanic stages and their spatial distribution within Basse-Terre Island. In order to highlight the ages of the successive effusive events, we have used the age-probability spectra [46]. As each age has been obtained on distinct lava flows and lava domes well distributed geographically, the Fig. 6 represents the duration of the different stages and periods of dormancy that can be inferred from out data set for the Basal Complex, the Septentrional and Axial Chains. The value of the relative probability (*Y* axis) is influenced by the number of samples with close ages (*X* axis).

Subaerial effusive volcanism within Basse-Terre initiated at 2.79±0.04 Ma in the Basal Complex and lasted only about 110 kyr. Following an inferred maximum dormancy period of 900 kyr (Fig. 6), volcanic activity distributed along the NNW–SSE trending axis of the Septentrional Chain, between 1.81±0.03 and 1.15±0.02 Ma. No clear trend of migration of volcanic activity is observed during this 0.7 Myr interval (Fig. 4), but it seems that activity dominated in the North during the earliest half of this time interval, whereas it is more concentrated to the South during the latest. However, effusive activity has been probably contemporaneous in different loci along the axis, with peaks around 1.7, 1.5 and 1.15 Ma (Fig. 6). Nevertheless, we suggest that between 1.81 and 1.15 Ma, a continuous distributed effusive activity characteristic of volcanic complexes built by fissural volcanism, controlled the Septentrional Chain construction along a NNW–SSE axis, with a recurrence time of about 100–150 kyr (Fig. 6).

The Axial Chain has been active between 1023±25 and 435±8 ka (Fig. 4) over a time interval of 600 kyr similar to that of the Septentrional Chain. Only a short gap of activity of 100 kyr (Fig. 6) is observed between the Axial and the Septentrional Chains. Fig. 6a highlights the occurrence of three main volcanic phases around 780, 620 and 430 ka within the Axial Chain. Spatial distribution of ages and morphologies allows us to distinguish five main zones (Fig. 4). The first one is located north of the Vieux-Habitants–Matéliane (VH–M) scarp. To the west, twelve ages are spatially distributed between 1023±25 and 746±13 ka with a pronounced cluster around 780 ka. To the east, four ages are available from 898±13 to 616±10 ka. A volcanic activity recurrence time of about 100–120 kyr can be estimated within this first zone (Fig. 6). Note that such value is similar to the one observed for the Septentrional Chain. South of the VH–M escarpment, the second zone consists of the Icaques Volcano emplaced between 629±13 and 600±17 ka [5], contemporaneously with the terminal phase of the eastern part of the first zone. In the third zone (Fig. 4), located southeast of the VH–M scarp, a lone age of 554±8 ka has been obtained close to the Capesterre Volcano. The fourth zone is the Sans Toucher Volcano (447±6 and 435±8 ka) located within the VH–M horse-shoe-shaped depression (Fig. 4). An

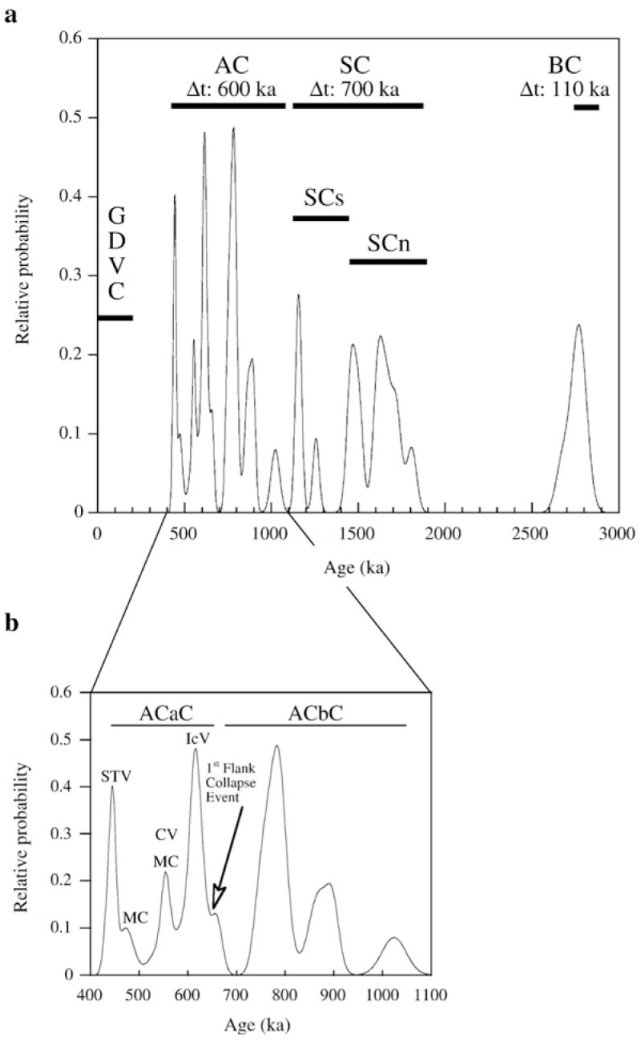

Fig. 6. (a) Age probability density [46] outlining effusive phases maxima and massif maximum duration length for BC (5 ages), SC (15 ages) and AC (23 ages from this study, [5,9]. (b) Close up of the 1100–400 ka interval during the AC activity (12 ages from this study, 4 ages [9] and 7 from [5]). See Fig. 3 caption for stages name.

age of 445±6 ka (98GU14, [9]) was obtained southeast of the Icaques Volcano and can therefore be related to the Sans Toucher Volcano. The contemporaneous Monts Caraïbes massif can be considered as the fifth zone of the Axial Chain. If ages within the first zone appear to follow an overall southwards migration along a NW–SE axis, this is not observed south of the VH–M escarpment. However, the three edifices of Icaques, Capesterre and Sans Toucher volcanoes emplaced there along the same NW–SE trending lineament. Recurrence time decreased to only 40 kyr (Fig. 6), which suggests that a change in the eruptive processes occurred at about 650 ka. This can be related with the occurrence of flank-collapse events as discussed below.

Overall, a N–S magmatic migration rate of 18 km/Myr has been obtained here for the whole Basse-Terre

Island. It increases up to 25 km/Myr, when only post Basal Complex volcanism, which represents 98% of subaerial volcanism, is considered. This is twice to four times higher than values previously calculated from poor reliability ages for trench parallel magmatic migration rates within the Lesser Antilles Arc [18].

We have calculated a subaerial extrusive volume of 180 km^3 for the Axial Chain for the 1.02–0.64 Ma interval, before collapses occurred, with an extrusion rate of 4.5×10^{-4} km^3/yr. It is on the same order than some volcanic complexes from other subduction zones, where magmatic production rates are available over a comparable time length. At Hakone Volcano (Japan), 150 km^3 were extruded over 400 kyr, which yields a rate of 3.7×10^{-4} km^3/yr [47,48], and at Mt Adams (Cascades, USA), a rate of 5.8×10^{-4} km^3/y, was calculated from a volume of 303 km^3 emitted over 520 kyr [48,49]. Note that the convergence rate for these contexts is comparable with the Lesser Antilles Arc, between 2 and 3 cm/yr [50].

6.4. Flank-collapse structures

Besides its morphology (Fig. 4), available K–Ar ages (Table 1b) strongly suggest that the Beaugendre depression cannot be related to any flank-collapse event. Effectively the oldest age of the Axial Chain (1.023 Ma, [5]) is obtained on the Morne Soldat edifice, located within the depression. Moreover, paleomagnetic directions obtained from lava flows in the area (Fig. 5 and [9]) demonstrated that those did not experience any displacement since their emplacement.

On the other hand, our K–Ar ages and the morphology of the VH–M scarp can only be interpreted as the result of a multiple stages collapse sequence (Figs. 4 and 7). The first flank-collapse of the southern Axial Chain (Fig. 7-1) occurred along an E–W line, which present day remnant scar extends from Matéliane Volcano to Morne Soldat Volcano (Fig. 7-2). Then, the Icaques Volcano emplaced in the post-collapse depressions between 629±13 and 600±17 ka [5] (Fig. 7-3). We suggest that the present day morphology of the VH–M arcuate structure is the result of northwards regressive erosion subsequent to post-collapse volcanic emplacement. Effectively, in order to develop its morphology and size, the Beaugendre river needs to be fed by a larger drainage area than its present-day basin (Fig. 4). The thin present-day morphology of its southern rim, shared with the VH–M escarpment, is not compatible with the Beaugendre depression size, which we interpret as due to a larger drainage area. It most probably included a significant relief south of the present-day VH–M escarpment, which has since been removed through northwards regressive erosion of the VH–M escarpment. This leads us to suggest that the VH–M escarpment used to be located southwards when it formed after the flank-collapse event. Thus, we consider that the initial horseshoe-shaped structures do not lie along the present day VH–M escarpment but further south (Fig. 7). Such regressive erosion has also been observed at La Palma (Canary Islands), where following the Cumbre Nueva collapse [51,52], fast erosion was enhanced by the small space left for evacuating streams in the area between collapse walls and post-collapse volcanoes. Watersheds preferentially develop at these limits, leading to the formation of big scale erosion calderas. Then, a second collapse SE directed occurred (Fig. 7-4), and was rapidly followed by the emplacement of the Capesterre Volcano around 550 ka (Fig. 7-5). The northward regressive erosion resumed, and the area created was filled with products from the Sans Toucher Volcano, between 447±6 and 435±8 ka (Fig. 7-7). Following a time interval where erosion pursued and volcanic activity was limited to the south (Fig. 7-8), the emplacement of the GDVC since 200 ka yielded the present day Basse-Terre morphology (Fig. 7-9 and b). Note that although large-scale debris avalanches deposits associated with collapses have been identified in the Grenada Basin offshore along the Lesser Antilles arc [1], no debris-avalanche deposits were found off Basse-Terre. Most probably, flank-collapse products were drained eastwards by a channels swarm directly towards the Grenada Basin [1,2], or were latter covered by thick sedimentary deposits [2].

6.5. Timing of collapse, filling and erosion rates

We constrain the first flank-collapse event between 659±11 (00GU54, Matéliane Volcano) and 629±13 ka ([5], Icaques Volcano) (Fig. 4). As previously observed at Oahu [53], Tahiti [54], and in the Canary Islands [52], subsequently post-collapse volcanic emplacement happened very quickly. Our data show that it started to the west with the Icaques Volcano, which is characterized by fast growing rate during about 30 kyr, from 629±13 to 600±17 ka. The age of 554±8 ka for a basal lava flow suggests that the Capesterre Volcano emplaced to the east, about 50 kyr later than the Icaques Volcano. In the hypothesis of a two stages collapse scenario, this age can be considered as a good estimate for the second collapse timing. We have estimated the total volume lost by collapse of the Matéliane Volcano to about 30 km^3, between 5 and 10 km^3 for the first event and about 20 to 25 km^3 for the second. A maximum time of 200 kyr is assessed for eroding the Matéliane edifice northwards and to free enough space (6 km^3) for the emplacement of

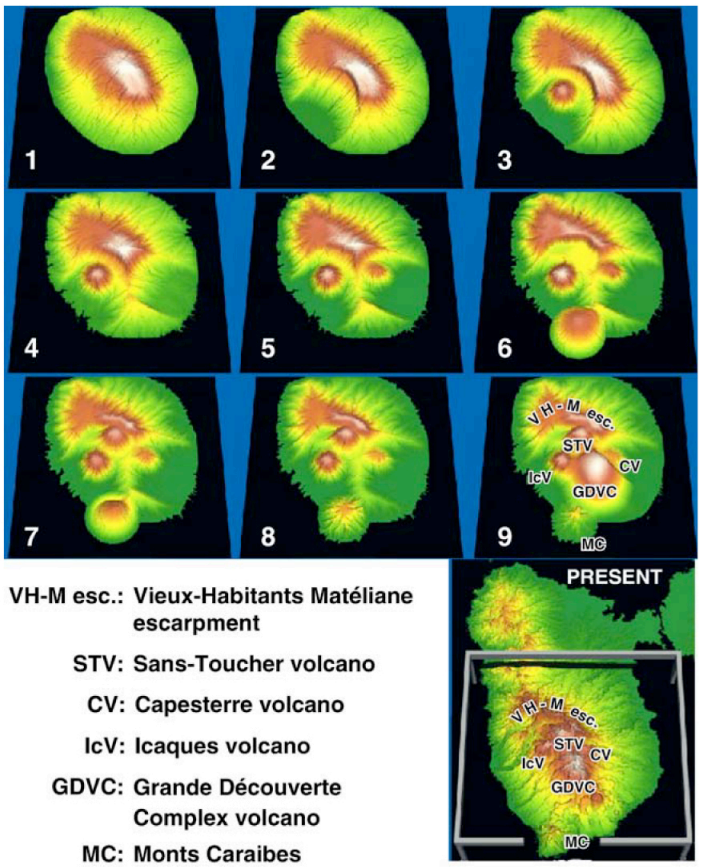

Fig. 7. Evolution of AC through time.1, 1050–0.650 Ma: AC building stage. 2, 0.650–0.630 Ma: first SW oriented flank-collapse. 3, 0.630–0.600 Ma: Icaques Volcano building stage within the collapse scar and initiation of NE regressive erosion. 4, before 0.550 Ma: second SE oriented flank-collapse. 5, around 0.550 Ma: Capesterre Volcano building stage within the latter collapse scar. 6, up to 0.450 Ma: regressive erosion of both SW and SE collapse scars enhanced by the presence of both Icaques and Capesterre Volcanoes: northwards regressive erosion increases, as southwards stream circulation is blocked. Monts Caraïbes building stage. 7, around 0.450 Ma: Sans Toucher Volcano building stage. 8, between 0.450 and 0.200 Ma: global erosion. 9, Since 0.200 Ma: Grande–Découverte Composite Volcano construction [5,9,61]. Also shown is the present time Basse-Terre DEM to be compared to the above stage 9.

the Sans Toucher volcano, between 630 ka (Icaques Volcano) and 445 ka (Sans Toucher Volcano) (Figs. 4 and 8). The total volume lost south of the flank-collapse scars reaches 84 km^3. Thirty cubic kilometers were lost by two flank-collapse episodes, whereas 54 km^3 were lost over 650 kyr by regressive erosion of the southern Axial Chain (Sans Toucher area and in between Icaques and Capesterre Volcano). This yields an erosional rate by regressive erosion estimated at about 84 km^3/Ma (8.4×10^{-5} km^3/yr or 1250 t/km^2/yr, considering a mean density of 2.7) for the last 650 kyr, and up to 5250 t/km^2/yr for the 6 km^3 erosion of the area where the Sans Toucher volcano later emplaced, during the 200 kyr interval following the Icaque collapse. Note that these estimates are comparable with the erosion rate of 2000 to 4500 t/km^2/yr, recently estimated for the last 200 kyr at the CVGD from U series isotopic data [55].

6.6. Structural control

Fissural volcanism along a NNW–SSE axis seems to have controlled the Basal Complex and the Septentrional Chain constructions. This direction is normal to the Désirade graben, which has a termination located to the

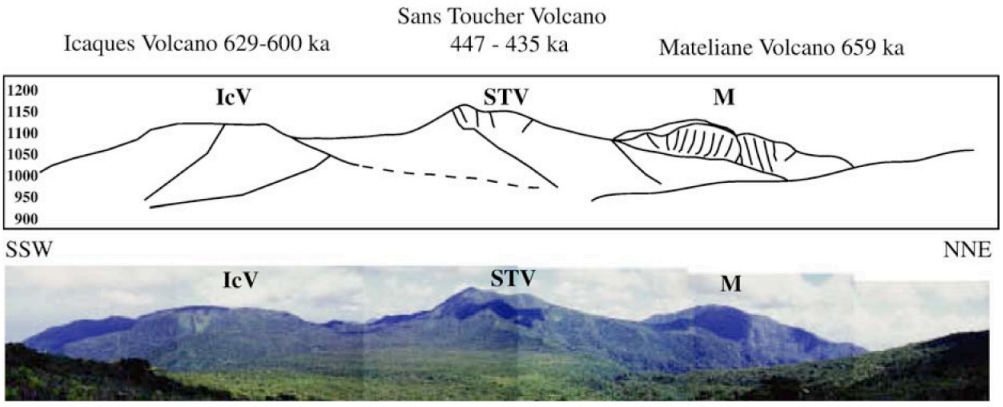

Fig. 8. SSW–NNE profile and photo through the Axial Chain showing the location of the Sans Toucher Volcano (STV) in between Icaques Volcano (IcV) and the Vieux-Habitants–Matéliane (VH–M) escarpment.

East of Grande Terre. Following earlier suggestion [32], we can thus interpret the ages obtained for the Basal Complex as coeval with the initial stage of propagation of the Désirade graben towards Basse-Terre at about 3 Ma, and the timing of the Basal Complex and Septentrional Chain activity as an active period of this graben, the activity of which decreased around 1 Ma. Relatively to northern Basse-Terre, the Axial Chain migration axis is oriented slightly westwards towards a NW–SE direction (Fig. 4). The latter direction is similar and in continuity with the 150° N striking Basse-Terre–Montserrat normal fault system [56] to the North, and the Ty fault [32] to the south within the CVGD massif. We thus propose that during the Axial Chain main volcanic activity, between 1.0 and 0.6 Ma, effusive volcanism was controlled by the en-échelon Dominica–Basse-Terre–Montserrat normal faults system which accommodates a left-lateral component of slip along the arc [56]. At the end of the Axial Chain construction, the well constrained age of the Icaques collapse, between 659±11 and 629±13 ka (Fig. 7a), or the age of the supposed Capesterre collapse around 554±8 ka (Fig. 7a) can be interpreted as the onset of the onland propagation of the Marie–Galante graben, in which all the recent activity of the CVGD is located [30,32]. The Icaques collapse, which occurred around a large scale $\delta^{18}O$ shift, from isotopic stages 16 to 15 [57], was then probably triggered by the combination of active tectonic propagation of the Marie–Galante rift system and the rapid climatic change, between glacial to interglacial conditions, and the associated sea-level variations [58].

6.7. Comparison with the island of Montserrat

The islands of Basse-Terre and Montserrat have been constructed over the same time period, from about 2.8 Ma (Fig. 6) and 2.6 Ma [34], respectively, to present. Both followed a North to South emplacement scheme. Montserrat comprises three major massifs (Silver Hills, Centre Hills and South Soufrière Hills–Soufrière Hills), whereas four have been described on Basse-Terre (Basal Complex, Septentrional Chain, Axial Chain and CVGD). The northernmost small massif of Silver Hills (2.6±0.06 and 1.16±0.05 Ma, [34]) seems to cover the same time-period than both the Basal Complex and the Septentrional Chain in Basse-Terre. Centre Hills (From 954±12 to 550±23 ka; [34]) on Montserrat and the Axial Chain (this study) roughly cover the same time-period. The southern Soufrière Hills–South Soufrière Hills Massif is limited to the last 170 kyr [34]. The total area of Montserrat (85 km^2), built over the last 2.6 Myr, being far smaller than the one of Basse-Terre (950 km^2), suggests that magmatic eruptive rates have been much smaller on Montserrat. This is illustrated by the time-averaged volcanic migration rate of 6 km/Ma [34], which is three to four times less than in Basse-Terre. This can be interpreted as a dominant tectonic control of effusive activity by the Basse-Terre–Montserrat fault system. Note that no inland propagation of a major rift system, such as the Désirade Graben in Guadeloupe, where escarpments are about 4000 m high [19,56], is identified towards Montserrat. Hence, although the role of such major fault systems in magma extraction processes is not constrained and is still poorly understood,

their influence should be considered for a better understanding of magma extraction in Basse Terre and in the Lesser Antilles Arc.

7. Conclusions

A complete geochronological data set consisting of thirty-two new accurate K–Ar ages has been acquired on lavas sampled in Northern and Central Basse-Terre. Coupled with geomorphological and geochemical data, it allows us to propose a general evolution model for Basse-Terre.

1 Basse-Terre volcanism presents an overall geochemical homogeneity characteristic of the evolved magmas from the Central Islands of the Lesser Antilles Arc. Slight modification of geochemistry through time coincides with the emplacement of each new volcanic chain, which could be linked to regional tectonic control.
2 The volcanic evolution of Basse-Terre is characterized by an overall North to South trend of migration that occurred in four main stages throughout the four main massifs of the island. Effusive activity occurred from 2.79±0.04 to 0.435±0.08 Ma north of the massif of Grande Découverte–Soufrière (from 0.2 Ma to present). The Basal Complex, from 2.79±0.04 to 2.68±0.04 Ma, is the initial sub-aerial volcanism in Basse-Terre. The Septentrional Chain, from 1.81±0.03 to 1.15±0.02 Ma highlights the occurrence of fissural volcanism over one third of the island along a NNW–SSE striking axis. The Axial Chain, 1.023±0.025–0.435±0.08 Ma, composed of imbricate volcanoes aligned along a NW–SE direction, has been affected on its southern part by two flank-collapse events around 630 and 550 ka. The first inherited SW depression was in-filled rapidly by the Icaques Volcano in less than 30 kyr, and the second by the Capesterre volcano. Regressive erosion in the collapsed areas occurred at a rate of 8.4×10^{-5} km^3/yr. Within the following 200 kyr about 6 km^3 were eroded at a rate of 3.0×10^{-5} km^3/yr in between the collapse scar and the newly formed volcanoes, leaving enough space for the Sans Toucher volcano to emplace around 445 ka.
3 Our age data constrain the southward volcanic migration rate to 18 to 25 km/Myr, three to four times higher than at Montserrat [34], and twice to six times higher than earlier estimations obtained within the arc [18]. Volcanic eruption rate of the Axial Chain has been estimated at 4.5×10^{-4} km^3/yr between 1 and 0.6 Ma.
4 Finally, differences in the expression of volcanism observed between each massif can be linked to regional active tectonic setting. The two main directions of active faulting around Basse-Terre, NW–SE on its Caribbean side, NE–SW and E–W on its Atlantic side converge towards the island [32]. The Désirade graben propagated westwards synchronously with the 2.8 Ma initiation of volcanic activity of northern Basse-Terre. The NW–SE propagation of the en-échelon normal faults system of Basse-Terre–Montserrat can be linked to the main direction of construction of the Axial Chain, while the E–W on land propagation of the Marie–Galante rift could have partly triggered the flank-collapse event that affected the Axial Chain around 640 ka. Therefore, the Axial Chain volcanic history can be considered as resulting from the activity of two competitive active normal-fault systems.

Acknowledgements

Many thanks to the OVSG volcanic observatory staff at Houëlmont, and its successive directors J.C. Komorowski and F. Beauducel, for help and discussion. Modifications suggested by two anonymous referees significantly improved the first version of this manuscript. Comments and suggestions by P.Y. Gillot and A. Hildenbrand were also greatly appreciated. This study was funded by CNRS-INSU DyETI and EU EXPLORIS programs. This is LGMT contribution number 63.

References

[1] C. Deplus, A. Le Friant, G. Boudon, J.C. Komorowski, B. Villemant, C. Harford, J. Segoufin, J.L. Cheminée, Submarine evidence for large-scale debris avalanches in the Lesser Antilles Arc, Earth Planet. Sci. Lett. 192 (2) (2001) 145–157.
[2] A. Le Friant, Les déstabilisations de flanc des volcans actifs de l'arc des Petites Antilles: origines et conséquences, Thèse de Doctorat de l'Université Paris 7— Denis Diderot. UFR Sciences Physiques de la Terre, 2001.
[3] M. De Reynal de St Michel, Carte géologique détaillée de la France. Département de la Guadeloupe au 1/50000. Feuilles de Basse Terre et des Saintes, Imprimerie Nationale, Ministère de l'industrie Paris, 1966.
[4] D. Westercamp, H. Tazieff, Martinique, Guadeloupe, Saint-Martin, La Désirade, Paris, 1980, 136 pp.
[5] F. Blanc, Corrélations chronologiques et géochimiques des formations volcaniques du sud de la Basse-Terre de Guadeloupe (Petites Antilles). Début du cycle récent, 3e cycle Thesis, Univ. Sci. Medic. Grenoble, 1983.
[6] A. Gadalia, N. Gstalter, D. Westercamp, La chaîne volcanique de Bouillante, Basse-Terre de Guadeloupe, (Petites Antilles): Identité pétrographique, volcanologique et géodynamique, C. R. Acad. Sci. Paris, Earth and Planetary Sciences Géologie de la France, vol. 2–3, 1988, pp. 101–130.

[7] R.C. Maury, G.K. Westbrook, P.E. Baker, P. Bouysse, D. Westercamp, Geology of the Lesser Antilles, The Geology of North America vol. H, The Caribbean Region, 1990, pp. 141–166.
[8] J.C. Briden, D.C. Rex, A.M. Fallar, J.F. Tomblin, K–Ar geochronology and palaeomagnetism of volcanic rocks from the Lesser Antilles Island Arc, Philos. Trans. R. Soc. Lond. Ser. A: Math. Phys. Sci. 291 (1979) 485–528.
[9] J. Carlut, X. Quidelleur, V. Courtillot, G. Boudon, Paleomagnetic directions and K/Ar dating of 0–1 Ma lava flows from La Guadeloupe Island (French West Indies): Implications for time averaged field models, J. Geophys. Res. 105 (2000) 835–849.
[10] C. Cassignol, P.-Y. Gillot, Range and Effectiveness of Unspiked Potassium–Argon Dating: Experimental Groundwork and Applications, John Wiley, New York, 1982, 159–179 pp.
[11] P.Y. Gillot, Y. Cornette, The Cassignol technique for potassium–argon dating, precision and accuracy: examples from late Pleistocene to recent volcanics from southern Italy, Chem. Geol. 59 (1986) 205–222.
[12] C.J. Hawkesworth, M. Powell, Magma genesis in the Lesser Antilles island arc, Earth Planet. Sci. Lett. 51 (1980) 297–308.
[13] C. DeMets, P.E. Jansma, G.S. Mattioli, T.H. Dixon, F. Farina, R. Bilham, E. Calais, P. Mann, GPS geodetic constraints on Caribbean–North America plate motion, Geophys. Res. Lett. 27 (2000) 437–440.
[14] T.H. Jordan, The present-day motion of the Caribbean plate, J. Geophys. Res. 80 (1975) 4433–4439.
[15] G. Wadge, Comparison of volcanic production rates and subduction rates in the Lesser Antilles and Central America, Geology 12 (1984) 555–558.
[16] P. Bouysse, Caractères morphostructuraux et évolution géodynamique de l'arc insulaire des Petites Antilles (Campagne Arcante 1), Bull. Bur. Rech. Geol. Min. Fr. 2 (1979) 185–210.
[17] P. Bouysse, D. Westercamp, Subduction of Atlantic aseismic ridges and late Cenozoic evolution of the Lesser Antilles Island Arc, Tectonophysics 175 (1990) 349–380.
[18] G. Wadge, The dykes and structural setting of the volcanic front in the Lesser Antilles Island arc, Bull. Volcanol. 48 (1986) 349–372.
[19] P. Bouysse, P. Guennoc, Data on the structure of the insular arc in the Lesser-Antilles, between St-Lucia and Anguilla, Mar. Geol. 53 (1–2) (1983) 131–166.
[20] W.R. McCann, L.R. Sykes, Subduction of aseismic ridges beneath the Caribbean plate; implications for the tectonics and seismic potential of the northeastern Caribbean, J. Geophys. Res. 89 (1984) 4493–4519.
[21] P. Bouysse, F. Garrabe, Neogene tectonic evolution of the limestone Caribbees in the Guadeloupe archipelago, C. R. Acad. Sci. II 298 (17) (1984) 763–766.
[22] A. Mascle, D. Westercamp, Géologie d'Antigua, Petites Antilles, Bull. Soc. Geol. Fr. Sér. 7, t. 15, no. 6 (1983) 855–866.
[23] F. Garrabé, Evolution sédimentaire et structurale de la Grande-Terre de Guadeloupe, Thèse de Doctorat de l'Université Paris-Sud, 1983.
[24] P. Andreieff, G. Bizon, P. Bouysse, Révision de l'âge des formations sédimentaires de l'île de Saint-Martin; implications sur la chronologie du volcanisme de l'arc insulaire des Petites Antilles, C. R. Acad. Sci. II 292 (1981) 79–82.
[25] P. Andreieff, J.R. Bonneton, J.M. Vila, D. Westercamp, Découverte du Paléocène supérieur à Anguilla, à l'extrémité nord de l'arc des Petites Antilles, 10è Réunion Annuelle Sciences de la Terre, Bordeaux, France, 1984, p. 15.
[26] J.L. Léticée, A. Randrianosolo, J.J. Cornée, P. Münch, J.F. Lebrun, J.P. Saint-Martin, M. Villeneuve, Mise en évidence d'une discontinuité émersive majeure au sein de la plate-forme récifale plio-pléistocène de l'avant-arc des Petites Antilles, C.R. Geosci. 337 (2005) 617–624.
[27] P. Bouysse, P. Andreieff, M. Richard, J.C. Baubron, A. Mascle, R.C. Maury, D. Westercamp, Aves Swel and Northern Lesser Antilles ridge: rock-dredging results from Arcante 3 Cruise, Géodynamique des Caraïbes, Editions Technip, 1985, pp. 65–76.
[28] P. Bouysse, D. Westercamp, P. Andreieff, J.C. Baubron, G. Scolari, Le volcanisme sous-marin néogène récent au large des côtes Caraïbes des Antilles françaises. Relations avec le volcanisme à terre et évolution du front volcanique, Géol. Fr. 1 (1985) 101–114.
[29] J.C. Komorowski, G. Boudon, M. Semet, F. Beauducel, C. Anténor-Balzac, S. Bazin, G. Hammouya, Guadeloupe, in: S.R. Unit (Ed.), Volcanic hazard atlas of the Lessser Antilles, University of the West Indies, St Augustine, Trinidad, W.I., 2005, pp. 67–104.
[30] N. Feuillet, I. Manighetti, P. Tapponier, Active arc-transverse normal faulting in Guadeloupe (French Lesser Antilles), Earth Planet. Sci. Lett. 333 (2001) 583–590.
[31] G. Boudon, M.P. Semet, P.M. Vincent, The Evolution of la Grande Découverte (la Soufrière) volcano, Guadeloupe (F.W.I.), in: J. Latter (Ed.), Volcanic Hazards: Assessment and Monitoring. IAVCEI Proceedings in Volcanology, Berlin, 1989, pp. 86–109.
[32] N. Feuillet, I. Manighetti, P. Tapponnier, Arc parallel extension and localization of volcanic complexes in Guadeloupe, Lesser Antilles, J. Geophys. Res. 107 (B12) (2002) 1–29.
[33] M. Semet, N. Vatin-Pérignon, P.-M. Vincent, J.-L. Joron, L'éruption volcanique du XVIème siècle de la Soufrière de Guadeloupe, mélanges de magmas et dynamisme éruptif, Bull. PIRPSEV, CNRS-INAG, Paris, France, vol. 60, 1981, pp. 1–63.
[34] C.L. Harford, M.S. Pringle, R.S.J. Sparks, S.R. Young, The volcanic evolution of Montserrat using $^{40}Ar/^{39}Ar$ geochronology, Memoirs, vol. 21, Geological Society, London, 2002, pp. 93–113, The Geological Society of London, 2002.
[35] X. Quidelleur, A. Samper, G. Boudon, A. Le Friant, J.C. Komorowski, 2004. Radiometric dating of large volume flank collapses in the Lesser Antilles arc. Eos Trans. AGU, 85 (47), San Fransisco, Fall Meet. Suppl., Abstract V41B-1397.
[36] P.Y. Gillot, Y. Cornette, N. Max, B. Floris, Two reference materials, trachytes MDO-G and ISH-G, for argon dating (K–Ar and 40Ar/39Ar) of Pleistocene and Holocene rocks, Geostand. Newsl. 16 (1) (1992) 55–60.
[37] G.S. Odin, et al., Interlaboratory standards for dating purposes, in: G.S. Odin (Ed.), Numerical Dating in Stratigraphy, vol. 1, John Wiley and Sons, Chichester, 1982, pp. 123–150.
[38] X. Quidelleur, P.Y. Gillot, V. Soler, J.C. Lefèvre, K/Ar dating extended into the last millennium: application to the youngest effusive episode of the Teide volcano (Spain), Geophys. Res. Lett. 28 (2001) 3067–3070.
[39] R.H. Steiger, E. Jäger, Subcommission on Geochronology: convention on the use of decay constants in Geo and Cosmochronology, Earth Planet. Sci. Lett. 36 (1977) 359–362.
[40] J.D.A. Zijderveld, A.C. demagnetization of rocks: analysis of results, in: D.W. Collinson, K.M. Creer, S.K. Runcorn (Eds.), Methods in Paleomagnetism, Elsevier, New York, 1967, pp. 254–286.
[41] J. Kirschvink, The least-squares line and plane and the analysis of paleomagnetic data: examples from Siberia and Morocco, Geophys. J. R. Astron. Soc. 62 (1980) 699–718.

[42] A. Samper, C. Chauvel and X. Quidelleur, Geochemical and isotopic study of K–Ar dated volcanics from Basse Terre, Guadeloupe, Lesser Antilles Arc, in: EGU 2005 Meeting, Geophys. Res. Abs., ed. 7, EGU05-A-09657, Vienna, 2005.
[43] R. Macdonald, C.J. Hawkesworth, E. Heath, The Lesser Antilles volcanic chain: a study in arc magmatism, Earth-Sci. Rev. 49 (2000) 1–76.
[44] S. Cande, D. Kent, Revised calibration of the geomagnetic polarity time scale, J. Geophys. Res. 100 (B4) (1995) 6093–6095.
[45] X. Quidelleur, J. Carlut, V. Soler, J.-P. Valet, P.-Y. Gillot, The age and duration of the Matuyama–Brunhes transition from new K–Ar data from La Palma (Canary Islands) and revisited $^{40}Ar/^{39}Ar$ ages, Earth Planet. Sci. Lett. 208 (2003) 149–163.
[46] A. Deino, R. Potts, Age-probability spectra for examination of single-crystal $^{40}Ar/^{39}Ar$ dating results: examples from Olorgesailie, Southern Kenya Rift, Quat. Int. 13/14 (1992) 47–53.
[47] J.A. Crisp, Rates of magma emplacement and volcanic output, J. Volcanol. Geotherm. Res. 20 (3–4) (1984) 177–211.
[48] S.M. White, J.A. Crisp, F.J. Spera, Long-term volumetric eruption rates and magma budgets, Geochem. Geophys. Geosyst. 7 (2006).
[49] W. Hildreth, M.A. Lanphere, Potassium-Argon Geochronology of a Basalt–Andesite–Dacite Arc System — the Mount Adams Volcanic Field, Cascade Range of Southern Washington, Geol. Soc. Am. Bull. 106 (11) (1994) 1413–1429.
[50] A. Heuret, S. Lallemand, Plate motions, slab dynamics and back-arc deformation, Phys. Earth Planet. Inter. 149 (1–2) (2005) 31–51.
[51] A. Hildenbrand, P.Y. Gillot, V. Soler, P. Lahitte, Evidence for a persistent uplifting of La Palma (Canary Islands), inferred from morphological and radiometric data, Earth Planet. Sci. Lett. 210 (2003) 277–289.
[52] J.C. Carracedo, S.J. Day, H. Guillou, F.J.P. Torrado, Giant Quaternary landslides in the evolution of La Palma and El Hierro, Canary Islands, J. Volcanol. Geotherm. Res. 94 (1–4) (1999) 169–190.
[53] T.K. Presley, J.M. Sinton, M. Pringle, Postshield volcanism and catastrophic mass wasting of the Waianae volcano, Oahu, Hawaii, Bull. Volcanol. 58 (1997) 597–616.
[54] A. Hildenbrand, P.-Y. Gillot, I. Le Roy, Volcano-tectonic and geochemical evolution of an oceanic intra-plate volcano: Tahiti-Nui (French Polynesia), Earth Planet. Sci. Lett. 217 (2004) 349–365.
[55] S. Rad, P. Louvat, C. Gorge, K. Gaillardet, C.J. Allegre, River dissolved and solid loads in the Lesser Antilles: new insight into basalt weathering processes, J. Geochem. Explor. 88 (1–3) (2006) 308–312.
[56] N. Feuillet, Sismotectonique des Petites Antilles. Liaison entre activité sismique et volcanique, Thèse de Doctorat de l'Université Paris 7 — Denis Diderot. UFR Sciences Physiques de la Terre, 2000.
[57] L.E. Lisiecki, M.E. Raymo, A Pliocene–Pleistocene stack of 57 globally distributed benthic $\delta^{18}O$ records, Paleoceanography 20 (2005).
[58] X. Quidelleur, A. Hildenbrand, A. Samper, 2006. Causal link between Quaternary paleoclimatic changes and volcanic islands evolution, Eos Trans. AGU, 87 (52), San Fransisco, Fall Meet. Suppl., Abstract OS43C-0657.
[59] W.H.F. Smith, D.T. Sandwell, Global sea floor topography from satellite altimetry and ship depth soundings, Science 277 (5334) (1997) 1956–1962.
[60] J.B. Gill, Orogenic Andesites and Plate Tectonics, Springer-Verlag, New York, 1981, 390 pp.
[61] A. Samper, X. Quidelleur, D. Mollex, J.C. Komorowski, G. Boudon, 2004. Time evolution of the Basse Terre island (Guadeloupe, French West Indies) effusive volcanism from new K-Ar Cassignol-Gillot ages. Eos Trans. AGU, 85 (47), San Fransisco, Fall Meet. Suppl., Abstract V53A-0601.

Effusive history of southern Basse-Terre (Guadeloupe, French West Indies) during the last 400 kyr from new K-Ar Cassignol-Gillot ages

Samper A. [1, 2, *], Quidelleur X. [1, *], Lahitte P. [1], Komorowski J.-C. [3,], Boudon G. [3,]

[1] Laboratoire IDES, UMR 8184 CNRS-UPS, Dept Sciences de la Terre bâtiment 504, Université Paris-Sud, 91405 Orsay, France.

[2] Institut de Physique du Globe de Paris (IPGP), et Université Paris-Diderot (UP7), CNRS, Laboratoire de Géologie des Systèmes Volcaniques, Tour 46, 2 place Jussieu, 75005 Paris, France.

[3] Institut de Physique du Globe de Paris (IPGP), CNRS, Laboratoire de Géologie des Systèmes Volcaniques, Tour 46, 2 place Jussieu, 75005 Paris, France.

*Corresponding authors: agnes.samper@u-psud.fr, xavier.quidelleur@u-psud.fr

to be submitted to JVGR

Word counts: 8688

Abstract

The Grande Découverte Volcanic Complex, active since at least 0.2 Ma, is the most recent volcanic complex of the Basse-Terre Island (Guadeloupe, Lesser Antilles Arc). A detailed geochronological study using the K-Ar Cassignol-Gillot technique has been undertaken in order to investigate the pace of effusive activity of this long-lived volcanic system. Twenty new ages permit to define that the GDVC experienced at least six main effusive stages, from 200 ka to present time. To the north the GDV (Grande Découverte Volcano) has been active since at least 200 ka, and to the south the TRMC (Trois Rivières-

Madeleine Complex), started to emplace 100 ka ago. GDV and TRMC volumes are respectively of 16.1 km^3 and 2.4 km^3. These, extruded at rates of 6.4 10^{-5} km^3/yr and 2.4 10^{-5} km^3/yr, correspond to 87% and 13% of the total volume of GDVC. Major and trace element signatures are very close for both systems, suggesting a common and complex magma plumbing system beneath the overall GDVC. However, morphological investigations suggest that the whole TRMC volcanism was emitted from vents distinct from the GDV, most probably a large E-W fissure network linked to the Marie Galante rift. The mean age of 62 ± 5 ka, obtained for the E-W Madeleine-Le Palmiste Alignment (MPA, 1.7 km^3) suggests that an important phase of the on-land propagation of the active rift of Marie-Galante occurred at that time. A less than 10 kyr volcanic activity is now described for both massifs. Although the risk associated with such effusive volcanism is far lower than the one represented by the potential collapse of the Soufrière dome, the emplacement of relatively large volumes (up to 0.25 km^3, La Coulisse lava flow) suggests that volcanic risk evaluation, which was mainly based on past geological records of La Soufrière dome activity, needs to be now revised to account for this active area.

Keywords: Geochronology, Lesser Antilles arc, Active Volcanic Complex, Grande-Découverte – Soufrière massif, extrusion rates

1. Introduction

The lifetime of an active composite volcano is punctuated by construction phases alternating with destructive episodes, both of which contributing to shape the edifice. If it is well assessed that composite volcanoes are built through pulses of activity (Davidson and De Silva, 2000), quantities of volumes erupted and time length of each effusive phase depend on the volcanic complex considered, as those parameters are linked to geological and geodynamic settings. Identifying most of the main eruptive stages that occurred through the lifetime of a composite volcano leads to a better understanding of its global past behavior. In particular, the use of an efficient geochronological tool for dating most of effusive phases can be extremely relevant in establishing an accurate and comprehensive chronology of the story of the volcano, as much as field conditions make an exhaustive sampling of the edifice possible. In particular, when linked to geomorphological studies and volume estimations, it makes possible the establishment of long-term extrusion rates, the use of which through comparison with analogs leads towards an extended and best characterization (White et al., 2006). Here we present the results of K-Ar dating of a volcanic complex of the Lesser Antilles Arc, the Grande Découverte Volcanic Complex (GDVC), located in the southern part of the island of Basse-Terre, Guadeloupe. This study, dedicated to an active volcanic complex aims at identifying the main successive effusive phases and at better constraining their chronology, and when possible their extrusion rates. We recently investigated the timing of the northern part of this volcanic island (Samper et al., 2007) and confirmed that since the last 2.8 Ma volcanism has been migrating southwards throughout the whole island until its present day location within the GDVC. Based on their different morphology and location, the GDVC can be divided into two distinct massifs, the Grande Découverte Volcano *s. s.* (GDV) and the Trois Rivières – Madeleine Complex (TRMC). Following the same approach as for northern

Basse-Terre (Samper et al., 2007), we have used here the K-Ar Cassignol-Gillot technique on effusive lava flows and lava domes, together with geochemical data and a geomorphological study of the massif, in order to reconstruct the multi-stage eruptive history of the GDVC in southern Basse-Terre.

2. Geological Setting

The volcanic island of Basse-Terre, part of the Guadeloupe archipelago, belongs to the central part of the Lesser Antilles Arc. It is located in the inner arc within the Plio-Pleistocene volcanic front (Fig. 1). From late Pliocene to late Pleistocene, competition between the NW-SE Basse-Terre-Montserrat en echelon normal fault system, and the La Désirade, then the Marie-Galante, E-W rift systems led to the presently volcanic morphology of Basse-Terre (Feuillet et al., 2002; Samper et al., 2007). Basse-Terre volcanic activity can be divided into two main long time episodes (Samper et al., 2007). From 2.8 to 1.15 Ma sub-aerial activity has been set in the northern half of the island along a N-S trending lineament (Fig. 1). The Basal Complex, constrained between 2.79 and 2.69 Ma, is the northernmost and smallest massif of the island. The NNW-SSE Septentrional Chain (SC), characterized by fissural volcanism, emplaced south of the Basal Complex (BC) between 1.8 and 1.15 Ma. The last 1 Ma activity southwards migration has been set along a NW-SE direction. The Axial Chain (AC), made of several composite volcanoes, extends over most of the half southern part of Basse-Terre and its activity spreads over about 0.6 Myr from 1 to 0.435 Ma. The GDVC occupies the extreme southern part of Basse-Terre Island. It is the most recent volcanic complex of the whole island and represents the last episode of the 2.8 Myr north-south volcanic migration throughout entire Basse-Terre (Samper et al., 2007). Two main volcanic

fields have been recognized there, the GDV and the TRMC (Komorowski et al., 2005). The GDV is built upon older lava flows sequences from the southern end of the Axial Chain (Boudon et al., 1988; Komorowski et al., 2005). Onset of the GDV was estimated at about 200 kyr by the use of stratigraphic and petrologic arguments (Boudon et al., 1989; Boudon et al., 1992) and has been supported by a K-Ar age of 205 ± 28 ka obtained on the uppermost lava flow section from the northern rim of the Grande Découverte caldera (Carlut et al., 2000).

Three main volcanic phases have been defined for the GDVC. The first stage, known as the Grande Découverte phase, is constrained between 205 ± 28 and about 42 ka, the latter being a ^{14}C age obtained for the Pintade explosive sequence (Komorowski et al., 2005). Three widespread pyroclastic pumice deposits that can be found in various places within the Grande Découverte massif have been dated within the 200 – 42 ka interval. The occurrence of the Anse des Pères (140 ± 14 ka) and Montval (108 ± 10 ka) (Blanc, 1983)) quartz dacitic pumices suggests that periodically, the dominant effusive activity has been interrupted by major eruptions forming explosive calderas, and by several flank-collapse episodes. However, recent work on thermoluminescence dating on quartz from St. Lucia dacites suggests that these ages should only be considered with caution (Guérin and Samper, 2007). The Pintade andesitic pumice deposit, 42,350 +1,975/-1,585 yr BP (Boudon et al., 1988) is thought to represent the deposits associated with the formation of the Grande Découverte caldera, which ended the Grande Découverte phase. The Carmichaël composite volcano emplacement took place within the Grande Découverte caldera. Its activity, which consisted of a succession of lava flows and lava domes associated with pyroclastic phases (Komorowski et al., 2005), spanned until 11.5 ka, when it was destructed by at least two edifice-collapse eruptions at about 13.5 and 11.5 ka, which led to the formation of the Carmichaël crater (Boudon et al., 1988; Boudon et al., 1987; Boudon et al., 1989).

Thus, the occurrence of significant pyroclastic deposits and relevant morphological structures led to define the activity of the GDV as consisting mainly of the alternation of construction and destruction phases, through the succession of several andesite dome eruptions associated to destruction pyroclastic phases (Komorowski et al., 2005). Indeed, eleven more collapse events considered as having produced over the last 45 kyr have been identified so far (Komorowski et al., 2005). On the basis of overlapping and intercalated pyroclastic flows identified within the Grande Découverte massif, three main phases have been recognized for the Carmichaël Volcano. The first, constrained between 42 and 35 kyr BP, is characterized by two major eruptions at 42 kyr BP (Pintade event) and 26 kyr BP (St Phy event), that cover southern Basse-Terre over 120 km^2 with thick pyroclastic sequences which individual volumes have been estimated between 0.5 and 3 km^3. The second phase is constrained between 29 and 21 kyr BP, and the third one, from 18 to 14 kyr BP. The Soufrière phase began within the Amic crater at about 8.5 kyr BP, formed by the collapse of a previous edifice. This phase is characterized by the alternation of lava dome eruptions and prolonged periods of phreatic explosive to non-explosive activity (Komorowski et al., 2005). The three last edifices to have emplaced on top of the Grande-Découverte Composite Volcano are the monogenetic edifices of L'Echelle, La Citerne and the dome of la Soufrière s.s. (1440 A.D.) (Boudon et al., 1988; Semet et al., 1981) which has undergone several phases of phreatic activity in the past few hundred years.

The TRMC, located south of the GDV (Fig. 1), includes on its northern border the E-W alignment of Le Palmiste lava flow, Gros Fougas and La Madeleine edifices, and is bordered to the southwest by the Monts Caraïbes (Fig. 1). It is made mainly of the viscous prominent lava dome of La Madeleine, dome related lava flows, thick lava flows and some monogenetic centers. In this area, on the opposite of the GDV, only minor pyroclastic deposits associated to lava domes are present (Komorowski et al., 2005). No

geochronological data were previously available to constrain the eruptive successions of this area.

3. Analyses

3.1. Sampling

Due to tropical climate, and because easterly winds are stopped on the topographic highs of the GDVC, strong erosion and the development of thick soils and dense vegetation is favored throughout the whole massif. Although exposures are rather scarce and limited to rivers, path and road cuts, and quarries, sampling has been done in some of the highest inner parts of the massif. Overall, during winter 2001 and March 2004, thirty-nine hand-sized lava blocks were taken on lava flows and domes for both geochronological and geochemical studies. The SAM58 sample comes from a borehole realized downwards the La Soufrière dome on the Savane à Mulet site, from a 58 meter underground level.

3.2. Geochemical data

Whole-rock major and trace element analyses were performed at the SARM-CRPG (CNRS, Nancy). Samples were fused with $LiBO_2$ then dissolved with HNO_3. Major element contents were determined by ICP-AES (Jobin-Yvon JY 70) and trace element concentrations by ICP-MS (Perkin Elmer 5000). Uncertainties for each element can be found at: http://www.crpg.cnrs-nancy.fr/SARM/index.html.

3.3. K-Ar procedure

After selection of the samples by examination of petrographic thin sections, the remaining twenty lava flows (Fig. 1) were dated in the UPS-IPGP geochronology laboratory at Orsay (France) using the K-Ar Cassignol-Gillot technique (Cassignol and Gillot, 1982; Gillot and Cornette, 1986). The same procedure as described in (Samper et al., 2007) has been followed. Samples were crushed to a 125-250 μm size fraction and ultrasonically cleaned 15 mn in a 10 % nitric acid solution. In order to avoid K loss due to weathering, as well as excess argon carried by mafic minerals and low K content plagioclases (Harford et al., 2002; Samper et al., 2007), analyses were performed on the narrow density range groundmass phase which was carefully separated by the use of heavy liquids. A magnetic separator was then used to remove remaining microlithic plagioclases. K was measured by flame emission spectrometry and compared with reference values of MDO-G and ISH-G standards (Gillot et al., 1992). Ar was measured with a mass spectrometer identical to the one described by Gillot (Gillot and Cornette, 1986). The interlaboratory standard GL-O, with the recommended value of 6.679 x 10^{14} atom/g of ^{40}Ar* (Odin and al., 1982), was used for ^{40}Ar signal calibration. Typical uncertainties of 1 % are achieved for the ^{40}Ar signal calibration and for the K determination. The uncertainty on the ^{40}Ar* determination is a function of the radiogenic content of the sample. The detection limit of the system is presently of 0.1 % of ^{40}Ar* (Quidelleur et al., 2001), which makes the Cassignol-Gillot technique especially suitable for samples from young volcanic complexes, as those investigated here. In order to avoid isotopic fractionation, no pre-degassing of the sample was performed (Gillot and Cornette, 1986). Decay constants and isotopic ratios of Steiger and Jager (Steiger and Jäger, 1977) were used. K contents and Ar measurements were duplicated for each sample. Uncertainties herein are given at the 1σ level.

3.4. Methodology for volumes and extrusion rates estimations

K-Ar geochronology is coupled with quantitative volume determinations in order to constrain volumes and magma extrusion rates over small increments of time, equivalent to the duration of effusive constructional phases (i.e., from tens to thousands of years).

In order to better assess the limits and volumes of volcanic features, we used a combination of DEM, orthophotos, and topographic maps in conjunction with fieldwork, with the aim of defining a systematical volume determination method. The DEM scale is of 1:50,000, and corresponds to a lateral resolution of 50 m and a vertical resolution of 2 m. The Universal Transverse Mercator (UTM) projection and the World Geodetic System 84 (WGS 84) model are both used, making possible to superimpose the DEM on aerial photos, which display a scale of 1:20,000 and a resolution of 1 m/pixel. All this makes easier the identification of the outlines of individual lavas flows, cones, and lava domes. In order to evaluate the volumes of such volcanic features, we created a three-dimensional surface of the geologic map by the use of the GIS software ArcGIS 9.1. Using GIS techniques, we also modeled topography and paleo-landscapes. Guided by field relationships and present-time topography we reconstructed several pre-eruptive topographies. Successive three-dimensional basal levels were created by interpolation of elevations from the volcanic unit outlines. Points used to create the base of each sloping surface are derived from a detailed analysis of the surrounding topography of the previous volcanic phases. The most challenging aspect of volume calculations lies in the determination beneath each volcanic phase of the slope of the basal surface, its elevation and topography. Errors are the smallest for units with well-exposed boundaries, including scoria cones, isolated domes and lava flows such as Le Palmiste lava flow or Morne Gros Fougas cone (Fig.1). Nevertheless large errors can occur where the

volumes to be determined are weighted by older units around, or when overlying flows hide the thickness of the units around. Estimations of volumes were managed using several successive paths, which are the following: estimation of the thickness of a weighted lava flow and where visible, calculation of the underlying slope. Then the extension of the area up to the contact and the estimation of the elevation at the base of the lava flow were realized. Finally, volumes (V) were calculated for each unit or phase from the following integration $V = \Sigma_{ij} \Delta x.\Delta y.\Delta Z_{ij}$ where $\Delta x = 50$ m is the linear dimension of the square DEM cell and ΔZ_{ij} is the height elevation variation between the modeled basal surfaces and the top topographic surfaces. Extrusion rates were then simply derived from the volumes calculated and the duration of activity inferred from the dating results.

4. Results

4.1. K-Ar results

We present in Table 1 twenty new K-Ar ages obtained on effusive phases from the GDVC. Our study provides seven new K-Ar ages on the GDV, which completes the data set of nine K-Ar ages previously available for the composite edifice. We also realized thirteen K-Ar ages within the TRMC where no data were previously available. Radiogenic ^{40}Ar concentrations range from 0.0 to 14.5 %, and all analyses have been duplicated at the 1σ level. Four recent (<10 ka) ages have been obtained within both volcanic complexes.

Previous K-Ar data from the GDVC constrained its effusive activity between 205 ± 28 and 47 ± 21 ka (Blanc, 1983; Carlut et al., 2000). Our new data set extends this record up to more recent periods (Table 1). We also constrain the activity of the TRMC between 89 ± 2 ka (00GU53) and present time (04GW05, 0 ± 20 ka).

The twenty-nine K-Ar ages now available (Table 1) have been used in age-probability spectra ((Deino and Potts, 1992); Fig. 2). We are well aware that such approach is biased by the distribution of sampling sites, but it allows us to identify the succession of the main active and repose periods of the whole massif. We show that six main effusive phases (Fig. 1 and 2) at 250 – 150, 150 -100, 100 – 70, 70 – 45, 45 – 15, and <15 ka have occurred. On the basis of two old ages (04GW04, 314 ± 12 ka and 04GW14, 261 ± 7 ka; Fig. 1) obtained within the TRMC area we propose to define the lower bound of the GDVC at 250 ka to distinguish the former and less constrained older activity.

On the basis of the twenty-nine K-Ar ages now available for effusive phases, together with previous geological constraints (Boudon et al., 1988), we present in Fig. 3 an interpretative simplified geochronological map of the whole GDVC.

4.2. Geochemistry results

The twenty-nine dated lavas have been plotted in K_2O vs SiO_2 diagrams (Gill, 1981) for each of the six eruptive phases identified (Fig. 4.). As already observed for the 2.8 – 0.435 Ma Northern Basse-Terre lavas (Samper et al., 2007), lavas younger than 0.25 Ma, investigated here, also belong to the Medium and Low K types (Fig. 4). Most samples are andesites and basaltic andesites, while the lava dome of Morne Liquin of the <15 ka phase (04GW05, Table 1 and Figure 1) is the only basalt. Fig. 5 shows the evolution of major elements as a function of time. An overall decrease of SiO_2 and K_2O can be observed through time, suggesting eruption of slightly more primitive magmas, while MgO, Fe_2O_3, Na_2O and Al_2O_3 do not display any clear trend.

Similarly to the Northern Basse-Terre massifs (Samper et al., 2007), GDVC lavas show systematic MgO concentrations lower than 6 wt % (from 1.91 to 5.88 %, Fig. 6a), which is a recurrent feature of the Central and Northern islands of the Lesser Antilles arc (Macdonald et al., 2000). MgO do not show any clear trend though time, although an overall increase can be inferred (Fig. 6a). GDVC lavas display narrow values for La/Yb chondrite-normalized ratios, which remain more or less constant through time (Fig. 6b). These values, between 1.96 and 2.5, indicate slight LREE enrichment typical of Medium K calc-alkaline rocks (Gill, 1981). Note that the two lava domes of the 450-250 ka TRMC area, Petite Montagne (04GW14) and Morne Laffite (04GW04), display respectively the lowest and uppermost values of the data set for both Mg# and La/Yb ratio (Fig. 6b and 6d). When compared with the Northern Basse-Terre massifs (Samper et al., 2007), Mg# values and La/Yb ratios for GDVC lavas are similar with the 1.8 – 1.15 Ma SC lavas. These values, which are much higher than for lavas from the 2.8 Ma BC and the 1 Ma – 0.435 ka AC (Fig. 6c and d), characterize more differentiated lavas, but do no show characteristic differentiation trends such as observed for BC and AC lavas (Fig. 6d). The higher values of the La/Yb ratio could be interpreted as a higher partial fusion of the source for both SC and GDVC lavas.

Rare Earth Elements (REE) and multi-elements patterns display similar calc-alkaline patterns for both GDV and TRMC areas (Fig. 7a to d). Slight enrichments in LREE (Fig. 7a and b) typical of Medium-K suites and other typical subduction-related features can be observed, such as LILE, U, Pb and Sr enrichments, Nb and Ta depletions (Fig. 7c and d). Numerous lavas show negative Ce anomalies, which have been described as the effects of post-magmatic processes related to sub-aerial exposure under tropical conditions (Cotten et al., 1995). Multi-element patterns for each of the GDVC effusive phase (Fig. 7c to f) permit to identify lavas of very close chemistry. Our oldest GDV cone lava, GU08, is significantly different from the two 113 ka lavas, 01GU55 and 04GW22, which are identical. Others lavas,

such as 04GW37 and 04GW31, and 01GU66 and 01GU60 for the 70-45 ka phase, also display very similar patterns (Fig. 7d). Similarly, 01GU63 and 04GW05 from the 45-15 ka and the <15 ka phase, respectively, clearly differ from others lavas from these phases (Fig. 7f and g).

4.3. Volume modeling results

After analysis of the landforms of the different temporal units inferred from our simplified interpretative geochronological map (Fig. 3), and using the sea level and the present-time topographic surfaces, five temporal three-dimensional surfaces could be modeled (Fig. 8). These picture the five main and successive steady states that can be assessed from our temporal data. Each modeled surface is presented from the oldest to the youngest, i.e. from the less well constrained to the best documented: the basement at 250 ka before the GDVC building, the landform surface at 70 ka when most of the GDV cone had built and the TRMC activity had started with the Trois-Rivières lava flow ensemble, one at 45 ka when most of the TRMC had built, one after at around 42 ka after the formation of the Grande-Découverte caldera on the GDV, and one between 15 ka and present-time after the last effusive phases had occurred. For each landform reconstruction we present hereafter the elements selected and used as constraints.

The basement of the GDVC can be considered as the steady-state surface of the southern part of the Axial Chain just before GDVC began to build up around 250 ka (Fig. 8A1). It has been modeled assuming that altitudes at the base of the South-Eastern, Southern and South-Western flanks of the last Axial Chain volcanoes (IcV, CV and STV respectively) were significant to the northern basal level of the GDVC. In the same way, we assume that the North-Eastern basis of the Monts Caraïbes volcanoes constrains the southern basis of the

GDVC. We then aim at estimating the maximal volume amplitude of the GDVC at 70 ka. Its landform has been constrained by the use of the older well-preserved topographic surfaces that outcrop regularly over large areas (i.e. 250 – 150 ka and 100 – 70 ka). This nevertheless excludes the North-Eastern 150 – 100 ka unit surfaces that show evidences of intense dismantling processes (Fig. 8A2). A good interpolation has been enabled for the surfaces now covered by the post 70 ka units (i.e. TRMC and > 15 ka units), as they present an elongated shape that allows good estimations of the surrounding altitudes. The third stage of this work focuses on the GDVC after emplacement of the MPA (70 - 45 ka, Fig. 8A3). Because there is no part of the MPA overlaid by younger units, the creation of this third landform simply consists in adding the topographic surface of the MPA to the previous landform modeling (Fig. 10A3). Fourth stage is a representation of the GDVC after its partial destruction by the Pintade eruption. We use here all but post-15 ka GDV unit topographic surfaces, plus the TRMC surface topography (Fig. 10A4). Finally the present-time topography illustrates the additional volume provided by the last <15 ka phase (Fig. 10A5). As altitudes and volumes are changing along with the successive stages, their calculation simply requires a one to one subtraction of the several landforms modelled. Finally, we determine extrusion rates by dividing the estimated volume by the duration of the corresponding stage, deduced from our age data (Fig. 2 and 3). Table 2 presents the volumes obtained for the main units. We compare them to some of the most characteristic volcanic phases of the earlier building of the island of Basse-Terre. In Table 3 are listed the volumes for each of the post 70 ka events.

5. Discussion

On the basis of the twenty-nine K-Ar ages now available for effusive phases (Fig. 3), together with previous geological constraints (Boudon et al., 1988), we present in Fig. 9 the succession of effusive stages encountered by the GDVC since 400 ka.

5.1. The GDVC area prior to 250 ka

The three most recent volcanic edifices of the AC (Icaques Volcano IcV, Capesterre Volcano CV and Sans Toucher Volcano STV) mark the northern morphological border of the GDVC and limit its extension to the north. It has been proposed that the IcV and CV emplaced subsequently to major flank collapses affecting southern AC, while STV emplaced latter within an erosional depression (Samper et al., 2007). Located beneath the western part of the GDV, the lava flow dated at 445 ± 6 ka (GU14 (Fig. 1 and 9a); (Carlut et al., 2000)) has been attributed to the STV (Samper et al., 2007). This is fully supported by geochemical data, as shown for K_2O and SiO_2 (Fig. 4a), for instance.

The GDVC is thus built over the southern end of the AC. Nevertheless, a gap of 200 kyr is present in our age data set, between the end of the AC activity and the oldest age of the GDV, 205 ± 28 ka (Carlut et al., 2000), which has been obtained towards the top, on the northern rim of the GDV. This can be due to the lack of access to lava flows of the GDV basement, which prevents us from constraining the age of the onset of its activity. We can propose the emplacement of a pre-GDVC (pGDVC, Fig. 9a) contemporaneously with older than 250 ka Morne Laffite and Petite Montagne domes (04GW14 and 04GW 04, Fig. 1), which have been dated at 314 ± 12 ka and 261 ± 7 ka, respectively. Note that such ages are in conflict with the hypothesis that these two lava domes have a coeval origin with the 0.6-0.4 Ma (Blanc, 1983) Mt Caraïbes (Fig. 1), as it has been suggested previously on the basis of petrographic similarities (Boudon et al., 1988).

The nature of the pre-GDVC is hypothetic. The Morne Laffite and Petite Montagne domes attest for effusive activity to have been set in the Grande Découverte area during the 445 – 250 ka interval, hence it is likely that the eruptive locus that gave birth to the GDV has been active since this period. However, it is difficult to say if the GDV started to build since then, or if it lately emplaced around 250 ka over former edifices such as a first proto-GDV cone or lava domes similar to the ones of the 445 – 250 ka interval. As we made it clear before, the lower bound of the GDVC has been defined at 250 ka to distinguish the former and less constrained effusive activity from the youngest for which our data set is much more complete.

5.2. GDV effusive activity from 250 to 34 ka

The diameter of the composite cone of the 250-200 ka GDV can be estimated to about seven to nine kilometers (Fig. 1). The destruction of the volcano summit during the Pintade eruption at 42 ka led to the formation of the Grande Découverte caldera (Komorowski et al., 2005) at a mean altitude of about 1000 m. The following phases of the GDV, the Carmichaël and Soufrière phases, have remained constrained within the caldera since 42 ka until present time. Effusive phases older than 42 ka (250 - 150 ka, 150 – 100 ka, 100 - 70 ka, 70 - 45 ka, Fig. 2) are distributed on various altitudes from the bottom of the edifice to the top of the preserved rims of the caldera. Remnants of the oldest lava flows are restricted to the northern slopes of the GDV (Fig. 9b). Most lava flows within the 150-100 ka interval (01GU55, 04GW22) are found on the northwestern slopes although a lone age of 129 ± 5 ka is obtained for a lava flow located to the southeast (Fig. 1 and 9c). Lava flows from the 100-70 ka interval (N1105, SAM58, 04GW30, 00GU53, GU29, 04GW32b, GU02, GU04, 01GU61, 98GU32; Fig.1, 9d and 9e) are found on eastern slopes, and appear beneath the <15 ka

volcano of La Citerne, which is associated to the Soufrière phase (Boudon et al., 1988; Komorowski et al., 2005). Whereas most products of the 70-45 ka period have been recognized within the TRMC, a lone age within this time interval has been identified on the southwestern slope of the GDV (04GW31, 65 ± 3 ka; Fig. 1 and 9e). The age of 34 ± 4 ka (Table 1) obtained for the Nez Cassé (01GU63; Fig. 1 and 9f), a remnant part of the rim of the Carmichaël Volcano, fully supports the hypothesis that this volcano emplaced within the Grande Découverte caldera formed by the 42 ka plinian eruption of Pintade (Komorowski et al., 2005).

5.3. The TRMC activity: 100 ka - present

The basement of the TRMC is composed of the 100-70 ka Trois-Rivières thick lava flows ending to the south coast, for which we obtained two undistinguishable ages of 87 ± 5 and 80 ± 3 ka (00GU53 and 04GW32b; Table 1 and Fig. 9d). North of this Trois-Rivières lava flow ensemble, three discrete edifices and their related lava flows emplaced during the 100-70 and 70-45 ka phases. From East to West, La Madeleine dome, the Gros Fougas and the Palmiste complexes (Fig. 1) design an E-W trending lineament. La Madeleine dome is a complex of several lava domes (Boudon et al., 1988). Two undistinguishable ages for basal lavas of 76 ± 12 ka and 75 ±14 ka (01GU61 and 98GU32, respectively) and the age of 58 ± 3 ka obtained on top of the dome suggest that building of the Madeleine lava dome started during the 100-70 ka phase and continued through the 70-45 ka phase. The Gros Fougas complex consists of a pile of thick lava flows dated at 60 ± 4 ka (04GW37) and covered by the strombolian edifice of Gros Fougas. The Palmiste complex is a thick andesitic lava flow (67 ± 3 ka, 01GU66) that may originate from an eruptive vent located to the east (Fig. 1). Both volcanic complexes emplaced during the 70-45 ka period (Fig. 9e). Fig. 9g shows that

three samples located close to the Madeleine dome display ages lower than 15 ka: 01GU65 (6 ± 6 ka) and 04GW22 (0 ± 1 ka) lava flows, and the andesitic dome of Morne Laffite 04GW05 (0 ± 20). Note that, as further discussed below, this is the first time that such recent volcanic activity is shown to have occurred within the TRMC. Note that only one age from the 45-15 ka phase (04GW26, 29 ± 6 ka) has been identified in the TRMC (Fig. 9f) for a lava flow located below the 6 ± 6 ka La Coulisse lava flow (01GU65; Fig. 9g).

5.4. Coeval activity from 100 ka to present

The four kilometers long Trois-Rivières lava flows (00GU53 and 04GW32b, Fig. 1), which we considered as the initial stage of the TRMC, emplaced within the 100-70 kyr interval, when effusive activity was also taking place on the GDV (Fig. 9d). They display basaltic-andesite compositions, slightly distinct than coeval lavas from the GDV (Fig. 2c). The main argument to support the hypothesis that these flows were not emitted from the GDV, situated six kilometers to the north, is based on morphological considerations. Fig. 10 shows three profiles of the southern part of the GDV. Two of them (S-N and NW-SE, A-D and A-C in Fig. 10, respectively) get across the La Madeleine-Le Palmiste alignment (MPA; Fig. 1). They can be compared with the W-E profile (A-B in Fig. 10) realized across the GDV 100-70 ka lava flows, which has been used as a reference profile for the GDV cone slope. The 100-70 ka Trois-Rivières lava flows and the 100-45 ka MPA appear clearly as a positive relief superimposed over the GDV reference slope. On the contrary the NW-SE profile (A-C, Fig. 10a) clearly shows that the younger than 15 ka Soufrière dome, L'Echelle and La Citerne edifices that have emplaced within the Carmichaël caldera, integrate regularly the slope of the cone. Thus, we suggest that both the Trois-Rivières lava flows and the MPA did not originate

from one of the main eruptive locus of the GDV, but rather from a different one located on its southern slope, most likely, a fissure vent presently covered by the MPA.

As pointed above, multi-elements diagrams (Fig. 6f-i) show relatively homogeneous compositions with significant differences between samples over the most mobile elements. However, within each time interval, lava groups from TRMC and GDV cannot be distinguished. For instance, within the 100-70 ka interval (Fig. 7f), SAM98, GU29 and 04GW30, and 04GW32b, display strikingly identical patterns while the former three are from the GDV and the latter from the TRMC (Fig. 1). Similarly, within the 70–45 ka time interval, 04GW31 and 04GW37 (Fig. 7g), from the GDV and TRMC, respectively, and within the 45-15 ka interval, GU05 and 04GW26 (Fig. 7h), from the GDV and TRMC, respectively, show similar patterns. Such undifferentiated behavior of coeval lavas between distinct centers can be interpreted as reflecting a single magma source for both GDV and TRMC. Such hypothesis is supported by the homogeneity of major and trace elements signatures (Fig. 6 and 7) and by very close Sr, Nd and Pb isotopic ratio (Samper et al., 2005) displayed by lavas from these massifs. Slight changes through time for both volcanic complexes lavas in the more mobile elements can then be explained in terms of crustal contamination within superficial reservoirs, prior to eruption.

5.5. Recent (< 10 ka) effusive activity

Our new age determination allows the identification of very recent effusive activity in the Trois Rivières-La Madeleine area. La Coulisse lava flow (01GU65; Fig. 1 and 9g) is of specific interest, as it seems to originate from La Madeleine dome (Boudon et al., 1988), which is dated at 58 ± 3 ka (01GU60; Fig. 1). We have obtained an age of 6 ± 6 ka for this

flow (Table 1), clearly in conflict with the hypothesis that this massive lava flow of 0.232 km^3 is a basal flow from La Madeleine. We then propose the source to be a vent located at the base of La Madeleine dome. Several arguments support our radiometric age determination. First, another flow (04GW26; Fig. 1) located underneath La Coulisse lava flow, has been dated at 29 ± 6 ka (Fig. 1 and 3). Second, Blanc (Blanc, 1983) did not succeed in dating this andesitic lava flow by K/Ar, but at a different sampling location than ours, she obtained an older bound of 15 ka. Third, based on a well-defined high paleointensity determination, an age within the 0-5 or 8-10 ka intervals was proposed for this flow (Carlut et al., 2000), in full agreement with our radiometric determination. Moreover, a very well defined age of 0 ± 1 ka (04GW02; Table 1) obtained on the lower east side of La Madeleine (Fig. 1), reinforce our interpretation that a very recent magmatic activity took place in this area considered previously at a low risk level (Komorowski et al., 2005). Finally, the presence of well-preserved levées, under tropical conditions, on both sides of La Coulisse lava flow (01GU65) supports its young age (Fig. 1).

Unfortunately, due to a very high atmospheric argon contamination, no radiometric constraints could be obtained in this study for lava flows located between the southern slopes of the Grande Découverte cone and the Trois Rivières-La Madeleine alignment (Fig. 1), and previously attributed to the La Madeleine phase (Boudon et al., 1988). However, Ar radiometric measurements close to the detection limit (Blanc, 1983) on the l'Habituée lava flow (Fig. 3.) provide an older bound of 10 ka. It is important to note that, close to this large volume flow, the Morne Liquin edifice (04GW05; Fig. 1 and 3) yields here a very recent age of 0 ± 20 ka (Table 1).

A recent age of 6 ± 2 ka has been obtained in the bed of Rivière Noire (04GW24; Table 1) on the GDV western flank (04GW24; Fig 1). Such young age, together with the morphology of this area (Fig. 1 and 4), and the age of 113 ± 2 ka (04GW22; Table 1) obtained

for a flow located higher in the massif (Fig. 1) suggest that 04GW24 is a valley flow originated from the GDV summit area, prior to the emplacement of the Soufrière dome.

5.6. The GDVC story

The GDVC area can be considered through three main stages along time: First stage before the GDV growth; Second stage, growth of the cone from 250 to 100 ka prior to the TRMC emplacement; Third and last stage, coeval activity set on both volcanic complexes from 100 ka to present-time. Nevertheless as the 200 ka lava flows, the oldest identified, are located on the top of the volcano, it can be assumed that around 200 ka most of the GDV cone had built. Then, the distribution of the later effusive phases leads to the assumption that after 70 ka there is no stage significant to cone growth. The summit was destructed at 42 ka, and the Carmichaël phase followed in the new-formed caldera. It has to be pointed out again that we have no clue about the story of the building of the cone before 200 ka (Fig. 9a and 9b). Lava flows from 200 to 70 ka, distributed all over the slopes of the volcano, can be considered as covering the 200 ka already-built cone. In this case, the 200 – 70 ka time interval represents a testimony of the eruptive episodes that occurred after most of the episode of aggradation had produced, during a lifetime of the volcano named the Grande Découverte phase. Whether it is plausible to consider the period from 250 to 200 ka as long enough to extrude most of the volume of the cone is a topic of debate, as 50 ka can be considered as a rather short time for the building of a volcano of such a size. Nevertheless we will keep 250 ka as the lower bound of the cone building-stage and develop our discussion from this statement.

Thus GDVC can also be temporally divided into an early stage from 250 to 70 ka and a latter one from 70 ka to present time. Each of those stages that we will further name Early GDVC and Late GDVC, respectively, includes three temporal units based on our age results. Early

GDVC can be subdivided in the 250-150, 150-100, and 100-70 ka phases. Whereas the 250-150 and 150-100 ka phases concern only the GDV, the TRMC started to emplace with the Trois-Rivières thick lava flows during the 100-70 ka phase. Late GDVC consists of a 70-45 ka phase that concerns mainly the TRMC through the emplacement of the MPA alignment, a 45-15 ka phase mainly set on the GDV with the building and then destruction of the Carmichaël Volcano, and the last < 15 ka phase that produced on both volcanic complexes through the emplacement of edifices of smaller scale on the GDV, and thick lava flows and small lava domes within the TRMC.

5.7. Volumes extruded through time within the GDVC

With 16.1 km^3, GDV represents 87% of the total volume of GDVC, the remnant 13% hence 2.4 km^3, belong to the TRMC. The important contrast of volumes existing between each of the two main volcanic complexes can be related to their lifetime. When weighted between 250 ka and present-time, the GDV extrusion rate reaches 6.4 10^{-5} km^3/yr. In the same fashion, extrusion rate for the whole TRMC over 100 ka is of 2.4 10^{-5} km^3/yr (Table 2).

Early GDVC: 250 – 70 ka

Although the GDVC steady-state at 70 ka is easy to model, volumetric contributions from each of the three first construction stages (250-150, 150-100, 100-70 ka) cannot be distinguished. We calculated an integrated volume of 13.7 km^3 for the whole Early GDVC which gives an average extrusion rate of 7.6 10^{-5} km^3/yr for the 250 – 70 ka time interval (Table 2, Fig. 8A2 and Fig. 11). The contribution of the 100-70 ka TRMC to these 13,7 km^3 can be neglected, which makes this extrusion rate significant to the GDV growth. The major part of Early GDVC is still preserved, which corresponds to 11.1 km^3, hence 81% of its

volume, and 73% of this latter volume (8.1 km^3) still outcrops, the other 27% being hidden under younger products. The total volume of the upper part of the cone removed by the 42 ka caldera-forming Pintade eruption (Fig. 8A4) reaches 2.5 km^3 (hence 19% of the Early GDVC), which is of the same order than the volume deduced for the pumice and scoria flow deposits from field studies (Komorowski et al., 2005).

Late GDVC: 70 ka - present

The overall Late GDVC corresponds to a volume of 4.7 km^3 and an emission rate of 6.9 10^{-5} km^3/yr between 70 ka and present-time. Late GDVC offers higher time and landform resolutions, as it is possible to isolate and quantify each phase: MPA volcanic alignment, 45 – 15 ka, and > 15 ka phases display respectively volumes of 1.7 km^3 (37 %), 1.1 km^3 (23 %), 1.9 km^3 (40 %) and emission rates of 7.0 10^{-5}, 3.7 10^{-5}, 1.310^{-4} km^3/yr. An estimate based on the residual slopes of the Carmichaël volcano (Nez Cassé, 01GU63, Fig. 1 and 9f) emplaced within the Grande Découverte caldera gives 1 km^3 for the volume of the whole edifice, which represents 90 % of the total volume of the 45 – 15 ka phase. In the same way, the dome of Amic, that contributes to the > 15 ka phase (Komorowski et al., 2005), is assumed to reach half a cubic kilometer, hence 25 % of the total volume of that phase.

Finally, we propose detailed volumes for the lava flows and lava domes of the 70 – 45 ka and > 15 ka phases (Table 3 and Fig. 8e). La Madeleine dome (0.77 km^3, Table 3) constitutes almost half the volume of the MPA (1.7 km^3, Table 2). During the last phase, L'Echelle (0.23 km^3, Table 3) and La Citerne (0.23 km^3, Table 3) edifices extruded over the GDV southern slope (Fig. 8A5 and 8B) and the lava flows of Dongo (0.21 km^3, Table 3) and La Coulisse (0.25 km^3, Table 3) are the most voluminous of the TRMC area (2.4 km^3, Table 2). La Coulisse lava flows displays a volume of about a quarter of cubic kilometres, which corresponds to an average thickness of 50 meters, in agreement with its surrounding levee.

Although La Soufrière dome is the apex of Basse Terre Island, it does not constitute a major unit (0.09 km^3, Table 3), but was extruded on the highest point of the GDV.

5.8 Significance of GDVC volumes and extrusion rates

For the building story of the GDVC

The integrated volume of construction of GDVC is shown on figure 12A. At each stage of reconstruction, we assign the entire overlying volume between the GDVC basement surface (Fig. 10A1) and the topographic surface of the stage considered. The red and blue lines connect cumulative volumes of GDVC and GDV respectively, from their onset to present-time. The slope of each line transcribes the average extrusion rates. Note that the GDVC cumulated volume curve (heavy line) is better fitted by its average cumulative curve (red line) than the GDV one (blue dotted line) by its average cumulative curve (blue line). Cumulative volumes for the GDVC are aligned at 70 ka, 45 ka and present-time, which corresponds to a mean rate of 7.4 10^{-5} km^3/yr (red line). This supports the hypothesis of a continuous construction of the GDVC through several pulses of activity since at least 70 ka. For example, the MPA (1.7 km^3), which corresponds to 70,8% of the whole volume of the TRMC (2.4 km^3), was mostly extruded through one effusive phase over 25 ka at most, at a mean rate of 7.0 10^{-5} km^3/yr (Fig. 2 and Table 2). For the last phase a similar volume (1.9 km^3) was extruded in 15 ka at most, which gives a higher extrusion rate of 1.3 10^{-4} km^3/yr (Table 2, Fig. 11). Thus, if the building of the Late GDVC occurred through pulses of activity of variable intensity and duration, the magmatic productivity stayed rather constant. The GDV alone, with a total volume of 16.1 km^3 yields a rate of 6.4 10^{-5} km^3/yr when weighted over 250 ka, which is similar to the extrusion rate of the whole Late GDVC, as well as those of several phases of this 70 – 0 ka time interval (Table 2, Fig. 11). Nevertheless, for the period of

construction of the Early GDVC before 70 ka, the contribution of the several phases identified are difficult to determine, as cumulative volumes are underestimated, as shown on figure 12. We only have access to a total estimation of the volume of the GDV cone at 70 ka. Though, as exposed previously in this discussion, we consider it to be almost built at 200 ka. For all these reasons, it seems rather irrelevant to consider a regular and smooth cone-building episode for the 250-70 ka period. It seems more probable to consider that an important decrease of the extrusion rate occurred during this period (Fig. 12B, green line), with additional volumes being extruded through the several phases identified at about 130, 110 and 80 ka (Fig. 2). Either most of the GDV cone was built over a short time e.g. 50 kyr from 250 to 200 ka (Fig. 12B, thin green dotted line), either its construction required much more time. In the latter case, it thus would have started to build during the 400 - 200 ka interval (Fig. 9a). These two extreme cases would correspond to extrusion rates comprised between about 7.0 10^{-5} km^3/yr (heavy green dotted line) and 2.7 10^{-4} km^3/yr (thin green dotted line). Note that in the former case the extrusion rate is thus the same than for the whole Late GDVC (Table 2, Fig. 11), and in the latter case it is similar to the value proposed for the Icaques Volcano, emplaced in 30 kyr after a flank-collapse event that affected the Southern Axial Chain (Samper et al., 2007) (Table 2, Fig. 11).

The estimates we realized for the extrusion rates of the overall GDVC, and GDV and TRMC volcanic complexes, suggest that magmatic extrusions have been rather continuous, and produced at a more or less constant rate, at least for the 70 ka – present time period. With the onset of the TRMC at 100 ka, a second important locus of eruption opened in the GDVC. Since then, it appears that from one pulse to another, eruptions have been set either simultaneously on both eruptive loci, either mainly on only one of them. This is to be linked to the magma plumbing system beneath the overall GDVC. Note that since 15 ka new sites of eruption have opened on both GDV and TRMC areas (Fig. 2, Fig. 9g, Fig. 10B).

In the whole Basse Terre story

The whole GDVC area consists of 56,5 km^3 above sea level. 69 % of this volume, i.e. 38 km^3, corresponds to its basement, that we consider to have been extruded between 650 and 250 ka at a rate of 0.95 10^{-4} km^3/yr (Table 2, Fig. 11) through contributions of the Axial Chain and pre-GDVC volcanic activities (Fig. 9a). The GDVC massif *s.s.* represents only 18.5 km^3 (31%), this volume taking into account an estimate of the dismantled material through erosion and the main destructive stages. The assumption that the GDVC started to emplace at about 250 ka leads to a rate of 0.74 10^{-4} km^3/yr, which appears to be very similar to its basement (Table 2, Fig. 11). Note that the rate for the extrusion of the overall GDVC area asl. represents a mean value of 0.85 10^{-4} km^3/yr.

With 1.8 10^{-4} km^3/yr over the last 1.8 Ma, the whole Basse Terre activity appears to be twice more efficient. It is due to the northern Axial Chain contribution, during which lifetime (1 Ma - 640 ka), 180 km^3 were extruded at a rate of 4.5 10^{-4} km^3/yr ((Samper et al., 2007)). This represents ten times more than the whole GDVC volume. When considering that the mean extrusion rate of the whole less than 1 Ma Southern Basse Terre reaches 2.8 x 10^{-4} km^3/yr (Table 2), it is likely that the building of the Axial Chain represents an important stage of higher magmatic production in the eruptive story of the island, and that since then a general decrease of magmatic production has been occurring. Comparison with volcanoes of the Southern Axial Chain such as the post flank-collapse event Icaques Volcano that was built in 30 ka, allows to mitigate the importance of the present-time emission rates. Indeed, with a value of 2.7.10^{-4} km^3/yr, extrusion of the 8 km^3 Icaques Volcano is twice more efficient than the higher rate of GDVC, the post 15 ka one. It confirms the influence of flank-collapse phenomenon as triggering factors of a raise of magmatic emission, as it has been described through the Axial Chain story (Samper et al., 2007) or in other well-documented volcanoes

(Quidelleur et al., 2005). If the GDVC differs from the Axial Chain volcanoes by very low extrusion rates, which signifies in this case much smaller volumes extruded, this volcanic complex and especially the GDV cone differs also by its remarkable longevity.

5.9. Geodynamic control

Based on the significant differences between La/Sm ratios measured on lava flows throughout Basse-Terre, the higher values observed for SC and GDVC massifs have been associated with increased partial fusion of their magmatic source (Samper et al., 2007). These authors proposed that such increase was related to the contribution of E-W propagating rifts, the La Désirade graben during the 1.8-1.15 Ma SC activity, and the Marie-Galante active rift during the GDVC activity, superimposed on the en-échelon Dominica–Basse-Terre–Montserrat normal faults system. The latter system controls the southward volcanic propagation of Basse-Terre, by accommodating a left-lateral component of slip along the arc (Feuillet et al., 2002).

The close ages of 67 ± 3, 60 ± 4 and 58 ± 3 ka, obtained here for Le Palmiste, Gros Fougas, and La Madeleine, respectively, (Table 1 and Fig. 1), constrained the emplacement of the E-W MPA, and hence, the on-land propagation of the Marie-Galante rift, at a mean age of about 62 ± 5 ka. In this area, the occurrence of ages lower than 10 ka (Fig. 9g) suggests that this rift has been active recently, and that a renewed propagation might be a triggering factor for future effusive volcanism in this area. In a go-stop-go rifting propagation context, these two clusters of ages suggest a recurrence time of about 50 ka, similar to the ones observed in other similar rift-propagation contexts (Audin et al., 2004; Manighetti et al., 1998).

6. Conclusions

The long-lived system of GDVC has been active over a period of at least 0.2 Ma. It is the most recent complex within the Basse-Terre island, where ongoing volcanism has been occurring since 2.8 Ma with a north to south overall migration (Samper et al., 2007). The GDVC experienced at least six main effusive stages, which contribute to shape the present day GDV and the TRMC, to the north and south of the GDVC, respectively. Already built since at least 205 ± 28 ka, the cone of the GDV has continued to grow, with an important construction phase between about 130 and 80 ka, which leads to the assumption that at 70 ka it had attained about 14 km^3, the maximum of its volume. At 42 ka, the caldera forming eruption of Pintade occurred (Komorowski et al., 2005). Subsequent effusive construction resumed within the depression with the emplacement of the Carmichaël volcano dated here at 34 ± 4 ka.

Lava flows of the GDVC display very close compositions between andesite and basaltic-andesite. A lone basalt, from the volcanic cone of Morne Liquin has been sampled. Major elements show a very slight tendency for a decreasing level of differentiation and La/Yb ratios suggest that, relative to the earlier Axial Chain magmatism, an increase in the partial fusion of the source could have occurred.

We have shown here that coeval effusive activity has been present in both GDV and TRMC massifs since the onset of the Trois Rivières lava flows eruption at about 87 ± 2 ka. Trace elements display strikingly similar signature, which we interpret as due to a common magmatic source, the location of eruptive vents being controlled by tectonic activity. Morphological investigations allowed us to suggest that the whole TRMC volcanism was emitted from vents distinct from the GDV, most probably a large E-W fissure network linked

to the Marie Galante rift. Tectonic activity probably contributed to extend the whole feeding magma-plumbing system beneath the GDVC massif. The mean age of 62 ± 5 ka, obtained for Le Palmiste, Gros Fougas, and La Madeleine, E-W alignment (MPA, 1.7 km^3) suggests that an important phase of the on-land propagation of the Marie-Galante active rift occurred at that time.

A less than 10 kyr volcanic activity is now described for both massifs, with ages as young as only a few kyr reported for lava flows and domes located east of the La Madeleine lava dome. Our new data suggest that volcanic risk evaluation, which was mainly based on past geological records of La Soufrière dome activity, needs to be now revised to account for this active area. Although, it should be kept in mind that the risk associated with such effusive volcanism is far lower than the one represented by the potential collapse of the Soufrière dome, for instance. However, emplacement of a relatively large volume (0.25 km^3) of lava flows, such as La Coulisse dated here at 6 ± 6 ka, would have important economic consequences.

Finally, the occurrence of large volume volcanism in both GDV and TRMC within the GDVC is tectonically controlled by the combined influence of the E-W Marie Galante on-land propagating rift and the NW-SE en-échelon Dominica–Basse-Terre–Montserrat normal faults system.

Acknowledgments

We would like to thank all the staff from the OVSG volcanic observatory of Houëlmont for assistance and discussion. Gilbert Hammouya is also thanked for providing us with sample SAM58. Precious help from Damien Mollex during field sampling and mineralogical

preparation was greatly appreciated. This study was funded by EU Exploris and CNRS-INSU DyETI programs. This is LGMT contribution XX and IPGP contribution XXXX.

References

Audin, L. et al., 2004. Paleomagnetism and K-Ar and 40Ar/39Ar ages in the Ali Sabieh area (Republic of Djibouti and Ethiopia): constraints on the mechanism of Aden ridge propagation into southeastern Afar during the last 10 Myr. Geophys. J. Int., 158: 327-345.

Blanc, F., 1983. Corrélations chronologiques et géochimiques des formations volcaniques du sud de la Basse-Terre de Guadeloupe (Petites Antilles). Début du cycle récent. 3e cycle Thesis Thesis, Univ. Sci. Medic. Grenoble, 171 p pp.

Boudon, G., Dagain, J., Semet, M.P. and Westercamp, D., 1988. Carte géologique1/20000e du massif volcnique de la Soufrière (Département de la Guadeloupe, Petites Antilles). BRGM, Orléans.

Boudon, G., Semet, M.P. and Vincent, P.M., 1987. Magma and hydrothermally driven sector collapses: the 3100 and 11,500 y.b.p. eruptions of La Grande Découverte (La Soufrière) volcano, Guadeloupe, French West Indies. J. Volc. Geotherm. Res., 33: 317-323.

Boudon, G., Semet, M.P. and Vincent, P.M., 1989. The Evolution of la Grande Découverte (la Soufrière) volcano, Guadeloupe (F.W. I.). In: J. Latter (Editor), Volcanic hazards: assessment and monitoring. IAVCEI Proceedings in Volcanology, Berlin: 86-109.

Boudon, G., Semet, M.P. and Vincent, P.M., 1992. Les éruptions à écroulement de flanc sur le volcan de la Grande-Découverte (La Soufrière) de Guadeloupe: implications sur le risque volcanique. Bull. Soc. Géol. France, 163(2): 159-167.

Carlut, J., Quidelleur, X., Courtillot, V. and Boudon, G., 2000. Paleomagnetic directions and K/Ar dating of 0-1 Ma lava flows from La Guadeloupe Island (French West Indies) : Implications for time averaged field models. J. Geophys. Res., 105: 835-849.

Cassignol, C. and Gillot, P.-Y., 1982. Range and effectiveness of unspiked potassium-argon dating: Experimental groundwork and applications. Numerical Dating in Stratigraphy. John Wiley, New York, 159-179 pp.

Cotten, J. et al., 1995. Origin of anomalous rare-earth element and yttrium enrichments in subaerially exposed basalts: Evidence from French Polynesia. Chem. Geol., 119: 115-138.

Davidson, J. and De Silva, S., 2000. Composite Volcanoes. In: H. Sigurdsson H., B., McNutt, and R. S.P., H., Stix, J. (Editors) (Editors), Encyclopedia of Volcanoes. Academic Press, San Diego, London, pp. 663-681.

Deino, A. and Potts, R., 1992. Age-probability spectra for examination of single-crystal $^{40}Ar/^{39}Ar$ dating results: examples from Olorgesailie, Southern Kenya Rift. Quaternary Int., 13/14: 47-53.

Feuillet, N., Manighetti, I. and Tapponnier, P., 2002. Arc parallel extension and localization of volcanic complexes in Guadeloupe, Lesser Antilles. J. Geophys. Res., 107(B12): 1-29.

Gill, J.B., 1981. Orogenic Andesites and Plate Tectonics. Springer-Verlag, New York, 390 pp pp.

Gillot, P.Y. and Cornette, Y., 1986. The Cassignol technique for potassium-argon dating, precision and accuracy: examples from late Pleistocene to recent volcanics from southern Italy. Chem. Geol., 59: 205-222.

Gillot, P.Y., Cornette, Y., Max, N. and Floris, B., 1992. Two reference materials, trachytes MDO-G and ISH-G, for argon dating (K-Ar and $^{40}Ar/^{39}Ar$) of Pleistocene and Holocene rocks. Geostandards Newsletter, 16: 55-60.

Guérin, G. and Samper, A., 2007. Aberrant thermoluminescence dates obtained from primary volcanic quartz. Rad. Measurements, in press.

Harford, C.L., Pringle, M.S., Sparks, R.S.J. and Young, S.R., 2002. The volcanic evolution of Montserrat using $^{40}Ar/^{39}Ar$ geochronology. Geological Society, London, Memoirs, 21(The Geological Society of London, 2002): 93-113.

Hofmann, A., 1988. Chemical differentiation of the Earth: the relationship between mantle, continental crust, and oceanic crust. Earth Planet. Sci. Lett., 90: 297-314.

Komorowski, J.C. et al., 2005. Guadeloupe. In: S.R. Unit (Editor), Volcanic hazard atlas of the Lessser Antilles. University of the West Indies, St Augustine, Trinidad , W.I., pp. 67-104.

Macdonald, R., Hawkesworth, C.J. and Heath, E., 2000. The lesser Antilles volcanic chain : a study in arc magmatism. Earth-Sci. Rev., 49: 1-76.

Manighetti, I. et al., 1998. Propagation of rifting along the Arabia-Somalia plate boundary: Into Afar. J. Geophys. Res., 103(B3): 4947-4974.

Odin, G.S. and al., e., 1982. Interlaboratory standards for dating purposes. In: G.S. Odin (Editor), Numerical dating in stratigraphy. John Wiley and Sons, Chichester, pp. 123-150.

Quidelleur, X., Gillot, P.-Y., Filoche, G. and Lefèvre, J.C., 2005. Fast geochemical changes and rapid lava accumulation at Stromboli Island (Italy) inferred from K-Ar dating and paleomagnetic variations at 60 and 40 ka. J. Volc. Geotherm. Res., 141: 177-193.

Quidelleur, X., Gillot, P.Y., Soler, V. and Lefèvre, J.C., 2001. K/Ar dating extended into the last millennium: Application to the the youngest effusive episode of the Teide volcano (Spain). Geophys. Res. Lett., 28: 3067-3070.

Samper, A., Chauvel, C. and Quidelleur, X., 2005. Geochemical and isotopic study of K-Ar dated volcanics from Basse Terre, Guadeloupe, Lesser Antilles Arc. In: Geophys. Res. Abs. (Editor), EGU 2005 Meeting, Vienna.

Samper, A., Quidelleur, X., Lahitte, P. and Mollex, D., 2007. Timing of effusive volcanism and collapse events whithin an oceanic arc island: Basse Terre, Guadeloupe archipelago (Lesser Antilles Arc). Earth Planet. Sci. Lett., 258: 175-191.

Semet, M., Vatin-Pérignon, N., Vincent, P.-M. and Joron, J.-L., 1981. L'éruption volcanique du XVIème siècle de la Soufrière de Guadeloupe, mélanges de magmas et dynamisme éruptif. Bull. PIRPSEV, CNRS-INAG, Paris, France, 60: 1-63.

Steiger, R.H. and Jäger, E., 1977. Subcommission on Geochronology: convention on the use of decay constants in Geo and Cosmochronology. Earth Planet. Sci. Lett., 36: 359-362.

White, S.M., Crisp, J.A. and Spera, F.J., 2006. Long-term volumetric eruption rates and magma budgets. Geochem. Geophys. Geosyst., 7.

Figure captions

Fig. 1. Top right: localization of the Guadeloupe archipelago within the Lesser Antilles Arc. Center: Basse-Terre Island shaded digital elevation model (light from NE; data from IGN). Timing of the main volcanic massifs of the island. Geochronological data from (Samper et al., 2007, Blanc, 1983 #1). Beneath: close up of the GDVC. Localization of the 29 K-Ar ages available on lava flows and lava domes (twenty ages from this study, three from (Blanc, 1983), seven from (Carlut et al., 2000)). Note that the GDVC is located between the 600-400 ka Southern Axial Chain and the Monts Caraïbes Massif.

Fig. 2. (a) Age probability density (Deino and Potts, 1992) outlining effusive phases maxima and maximum duration length for the GDVC over the last 350 ka. Twenty ages from this study, six from (Carlut et al., 2000) and three from (Blanc, 1983). (b) Close up of the 150 – 0 ka interval. Five main periods of effusive activity can be defined: 150 – 100, 100 – 70, 70 – 45, 45 – 15 and <15 ka. Note that within stages 150 – 100 ka and 100 – 70 ka, most ages concentrate within the 120 –100 ka and the 85 –70 ka time intervals, respectively.

Fig. 3. Interpretative map of the GDVC. (Basse-Terre Island digital elevation model from IGN). Geological interpretation based on the new age data set from this study and on the pre-existing geological map (Boudon et al., 1988). Ages from the southern Axial Chain and Monts Caraïbes volcanoes from (Blanc, 1983; Samper et al., 2007).

Fig. 4. K_2O versus SiO_2 diagram for lavas of each of the seven effusive phase of the Grande Découverte – Soufrière Massif. Fields from (Gill, 1981), and analyses from this study, (Carlut et al., 2000) and (Blanc, 1983). (a) 2.8 Ma – 0.435 ka: Grey areas for Northern Basse-Terre

volcanic massifs: BC for Basal Complex, SC for Septentrional Chain, AC for Axial Chain, STV for Sans Toucher Volcano (Southern Axial Chain), data from (Samper et al., 2007). Black star for the 445 ± 6 ka Axial Chain lava flow of Cascade Vauchelet (GU14; (Carlut et al., 2000; Samper et al., 2007)); white stars for edifices of Morne Laffite (04GW04) and Petite Montagne (04GW14) of the Trois-Rvières area (Fig. 1). For the next phases, grey symbols are for GDVC lavas, white symbols for TRM lavas. (b) 250 – 150 ka: Black cross for GU08 (205 ± 28 ka, (Carlut et al., 2000)), hexagons for 150 – 100 ka lavas. (c) 100 – 70 ka: Triangles. (d) 70 – 45 ka: squares. (e) 45 – 15 ka: diamonds. (f) <15 ka: circles. Note that the only basalt sampled (04GW05) belongs to the TRM area.

Fig. 5. Major elements evolution of GDVC lava flows as a function of time (in ka).

Fig. 6. (a) MgO versus time (in ka), (b) Chondrite normalized (Hofmann, 1988) La/Yb ratio versus time (in ka), (c) SiO_2 versus Mg#, (d) Chondrite normalized (Hofmann, 1988) La/Yb ratio versus Mg#.

Fig. 7. (a) GDV Rare Earth Elements (REE) patterns, chondrite normalized (Hofmann, 1988). (b) Same as (a) for TRMC. (c) GDV multi-element patterns, normalized to the primitive mantle (Hofmann, 1988). (d) Same as (c) for TRMC. (e) to (i) Trace-element patterns for each of the GDVC effusive phases, respectively (e) 250-100 ka, (f) 100-70 ka, (g) 70-45 ka, (h) 45-15 ka, (i) <15 ka.

Fig. 8. Several GDVC landform steady states through time. A) Three dimensional views of the five main phases of construction: A1. pre-GDVC (200ka), A2. end of the Early GDV phase (70 ka), A3. end of the Early MPA construction stage (45 ka), A4. after the 42 ka

Grande Découverte caldera forming-eruption, and A5. present-time. Red curves: profile of Fig. 8B. Grey color display for the surrounding topography. The green and pinks pins locate the highest points of Early GDVC and present GDVC, respectively. Unit colours are as in Fig. 3. Darkened colours display still outcropping. Lightened colours display each part of phases nowadays overlaid by latter products. B) Characteristic topographic profiles for each construction phase. Main morphological volcanic units are named. Dotted line for the profile of the GDV before the destruction of its summit at 42 ka.

Fig. 9. Evolution of the GDVC from 450 ka to present day: main effusive phases. (a) 450-250 ka pre-GDV (pGDV) and pre-TRMC; (b) 250-150 ka; (c) 150-100 ka; (d) 100-70 ka, onset of activity south of the GDV with the emplacement of the Trois Rivières lava flows; (e) 70-45 ka emplacement of the La Madeleine - Le Palmiste alignment (MPA); (f) 45-15 ka Carmichaël Volcano phase; (g) <15 ka edifices and lava flows associated to the La Soufrière phase and the Trois Rivières Volcanic Complex activity.

Fig. 10. Topographic profiles of the southern slopes of the GDVC (see insert for location). All profiles are from the Soufrière dome (A),the present-day highest point of the GDV. (a) East-West (AB) profile, used as a GDV slope reference, and NW-SE profile (AC) across the La Madeleine dome and the 6 ± 6 ka La Coulisse lava flow. (b) AB profile (see a) and North-South (AD) profile across the 100-70 ka Trois Rivières lava flows and the La Madeleine - Le Palmiste alignment (MPA).

Fig. 11. Extrusion rates for the main episodes of construction of southern Basse-Terre (km^3/yr). For early GDVC, the two hypothesis are shown: a continuous and regular growth over 180 ka between 250 and 70 ka, or a short-time growth over 50 ka from 250 to 200 ka.

Fig. 12. Cumulative extruded volume vs. time for GDVC. Colors of dots are as in Fig. 7. Heavy black line: cumulative emission volume of the overall remnant units of GDVC. Doted line integrated emission volume of the units of GDVC (including the collapsed sectors of Grande Découverte, Carmichaël and Amic crater). Dashed green line cumulative emission volume of the units of GDV (including also collapsed sectors). Red and green thin lines: integrated emission rates of GDVC and GDV, respectively. Explication in text

Table 1. New K-Ar ages from the GDVC. GDV: Grande Découverte Volcano *s. s.*, TRMC: Trois Rivières – Madeleine Complex. 40Ar*: radiogenic argon. Mean: mean age obtained by weighted each age determination by its radiogenic argon content (^{40}Ar*).

Sample	Site	Massif	Longitude	Latitude	K (%)	^{40}Ar* (%)	^{40}Ar* x10^{12} (atom/g)	Age (ka)	Mean (ka)
04GW04	Morne Laffite	TRMC	61°38.07'	16°02.68'	0.614	3.1	20.40	318 ± 11	314 ± 12
						2.6	19.90	310 ± 13	
04GW14	Petite Montagne	TRMC	61°36.85'	16°0.04'	0.476	4.6	13.10	264 ± 7	261 ± 7
						4.4	12.90	259 ± 7	
01GU55	Ravine Malanga	GDV	61°40.74'	16°2.60'	1.198	2.7	14.28	112 ± 4	113 ± 4
						3.7	14.26	114 ± 4	
04GW22	Rivière Noire 3	GDV	61°40.51'	16°02.28'	1.321	14.5	15.49	112 ± 2	113 ± 2
						2.5	16.37	119 ± 5	
SAM58	Savane à Mulet	GDV	61°39.91'	16°2.33'	0.900	0.6	8.62	92 ± 16	94 ± 16
						0.6	8.95	95 ± 15	
04GW30	Bassin Bleu	GDV	61°40.5'	16°01.13'	0.985	7.2	9.28	90 ± 2	89 ± 2
						1.9	8.94	87 ± 5	
00GU53	Roches gravées	TRMC	61°38.53'	15°58.21	0.547	1.6	4.81	84 ± 5	87 ± 5
						1.8	4.95	87 ± 5	
04GW32b	Petit Carbet	TRMC	61°38.07'	15°58.61'	0.800	2.5	7.09	85 ± 4	80 ± 3
						2.8	6.36	76 ± 3	
01GU61b	Fond-Graine W	TRMC	61°38.89'	15°59.99'	0.249	0.7	2.22	85 ± 12	76 ± 12
01GU61a					0.280	0.5	1.84	63 ± 12	
98GU32	Fond-Graine E	TRMC	61°38.75'	16°0.13'	0.335	0.5	2.50	72 ± 15	75 ± 14
						0.6	2.70	77 ± 14	
01GU66	Le Palmiste	TRMC	61°41.65'	15.59.88'	1.073	2.4	7.70	69 ± 3	67 ± 3
						2.4	7.23	65 ± 3	
04GW31	Morne Joseph	GDV	61°40.07'	16°0.19'	0.991	2.3	6.66	64 ± 3	65 ± 3
						1.6	6.84	66 ± 4	
01GU60	Piton Tarare	TRMC	61°38.64'	16°0.70'	0.560	2.1	3.38	58 ± 3	58 ± 3
						1.9	3.45	59 ± 3	
04GW37	L'étang	TRMC	61°49.46'	16°0.00'	1.011	1.5	6.94	66 ± 5	60 ± 4
						1.5	5.83	55 ± 4	
01GU63	Nez Cassé	GDV	61°40.28'	16°2.97'	0.712	0.8	2.41	32 ± 4	34 ± 4
						0.9	2.60	35 ± 4	
04GW26	Anse Duquery	TRMC	61°37.72'	15°58.26'	0.834	0.4	2.49	29 ± 7	29 ± 6
						0.5	2.50	29 ± 6	
01GU65	La Coulisse	TRMC	61°37.92'	15°58.53'	0.593	0.1	0.45	7 ± 6	6 ± 6
						0.0	0.14	2 ± 7	
04GW24	Rivière Noire 5	GDV	61°41.27'	16°1.59'	0.847	0.3	0.29	3 ± 1	6 ± 2
						0.5	0.73	8 ± 2	
04GW02	Racoon	TRMC	61°37.95'	16°16.61'	1.151	-0.2	-0.40	-3 ± 1	0 ± 1
						0.0	0.07	1 ± 1	
04GW05	Morne Liquin	TRMC	61°36.44'	16°00.80'	0.724	0.0	0.09	1 ± 20	0 ± 20
						-0.1	-0.018	-24 ± 23	

Table 2. Extrusion rates for the main construction phases of southern Basse-Terre (km^3/yr)

	Delay (Myr)	Begin (Myr)	End (Myr)	Volume (km^3)			Emission rate (km^3/yr)
BT previous effusive activity							
Basse-Terre (since1.8 Ma)	1.8	1.8	0.00	**328**			**$1.8\ 10^{-4}$**
AC+GDVC+MC (1- 0 Ma)	1	1.02	0.00	**284**			**$2.8\ 10^{-4}$**
AC before major flank-collapses	0.38	1.02	0.64	**179**			**$4.7\ 10^{-4}$ ***
Icaques Volcano (AC after 1st flank-collapse)	0.03	0.630	0.600	**8**			**$2.7\ 10^{-4}$**
Southern BT							
Overall GDVC area (a.s.l.)	0.400	0.650	0.000	**53**			**$8.5\ 10^{-5}$**
AC beneath GDVC	0.400	0.650	0.250	**38**	67%		**$9.5\ 10^{-5}$**
GDVC s.s. (250 - 0 ka)	0.250	0.250	0.000	**18.5**	33%		**$7.4\ 10^{-5}$**
GDVC: main volcanic complexes							
GDV (250 - 0 ka)	0.250	0.250	0.000	**16.1**	87%		**$6.4\ 10^{-5}$**
TRMC (100 - 0 ka)	0.100	0.100	0.000	**2.4**	13%		**$2.4\ 10^{-5}$**
Early GDVC (250 - 70 ka)	0.180	0.250	0.070	**13.7**			**$7.6\ 10^{-5}$**
still preserved	0.180	0.250	0.070	11.1	66%		$6.2\ 10^{-5}$
outcropping (73% of vol.)				8.1			
hidden by younger products (27% of vol.)				3.0			
eroded or collapsed				2.5	15%		
Late GDVC (70 - 0 ka)	0.070	0.070	0.000	**4.7**			**$6.9\ 10^{-5}$**
still preserved (68 %)				3.3	17%		$6.2\ 10^{-5}$
eroded or collapsed (32 %)				1.4	8%		
MPA (70 - 45 ka)	0.025	0.070	0.045	**1.7**		37%	**$7.0\ 10^{-5}$**
45 - 15 ka (Carmichaël Volcano)	0.030	0.045	0.015	**1.1**		23%	**$3.7\ 10^{-5}$**
still preserved (10 %)				0.1			$3.3\ 10^{-6}$
eroded or collapsed (90 %)				1.0			
< 15 ka	0.015	0.015	0.000	**1.9**		40%	**$1.3\ 10^{-4}$**
still preserved				1.4			$9.3\ 10^{-5}$
eroded or collapsed (Amic Volcano)				0.5			

* (Samper et al., 2007)

Table 3. Volume of the main units of the 70 – 45 ka and > 15 ka phases

Unit	volume (km^3)	%
> 15 ka		
La Coulisse	0,25	18%
L Echelle	0,23	17%
La Citerne	0,23	17%
Dongo	0,21	15%
L'Habituée	0,14	10%
La Soufrière	0,09	7%
Morne Boudoute	0,09	6%
Crete a Racoon	0,06	5%
Grande Chasse	0,05	4%
Morne Liquin	0,02	1%
Fond Gravois	0,01	1%
Total	1,39	100 %
70 - 15 ka		
La Madeleine dome	0,77	44%
Le Palmiste lava flow	0,47	27%
Plateau Gros Fougas	0,46	26%
Gros Fougas lava flow	0,02	1%
Gros Fougas cone	0,02	1%
Fond Graine lava flow	0,02	1%
Total	1,74	100 %

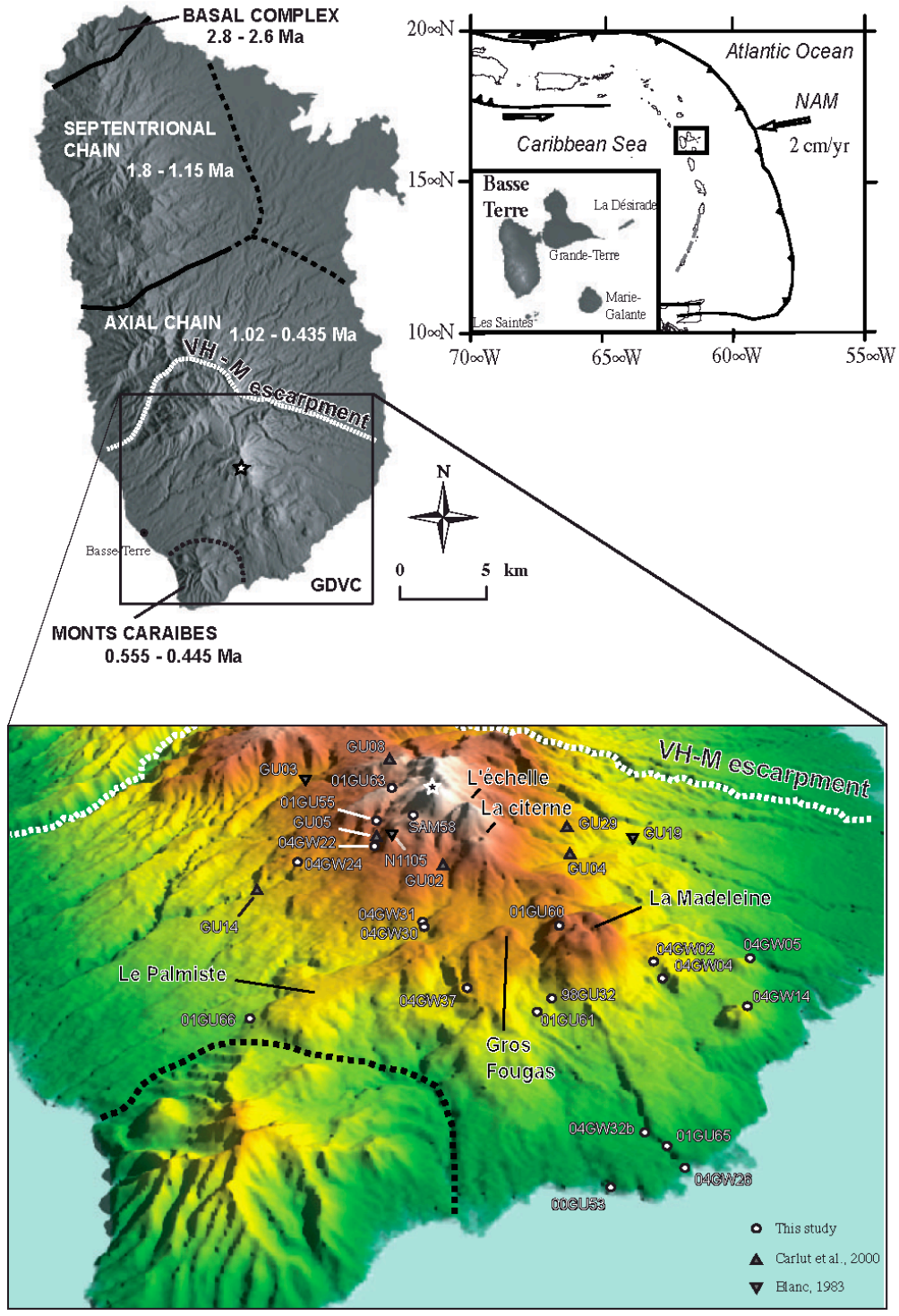

Fig. 1. (Samper et al., 2007)

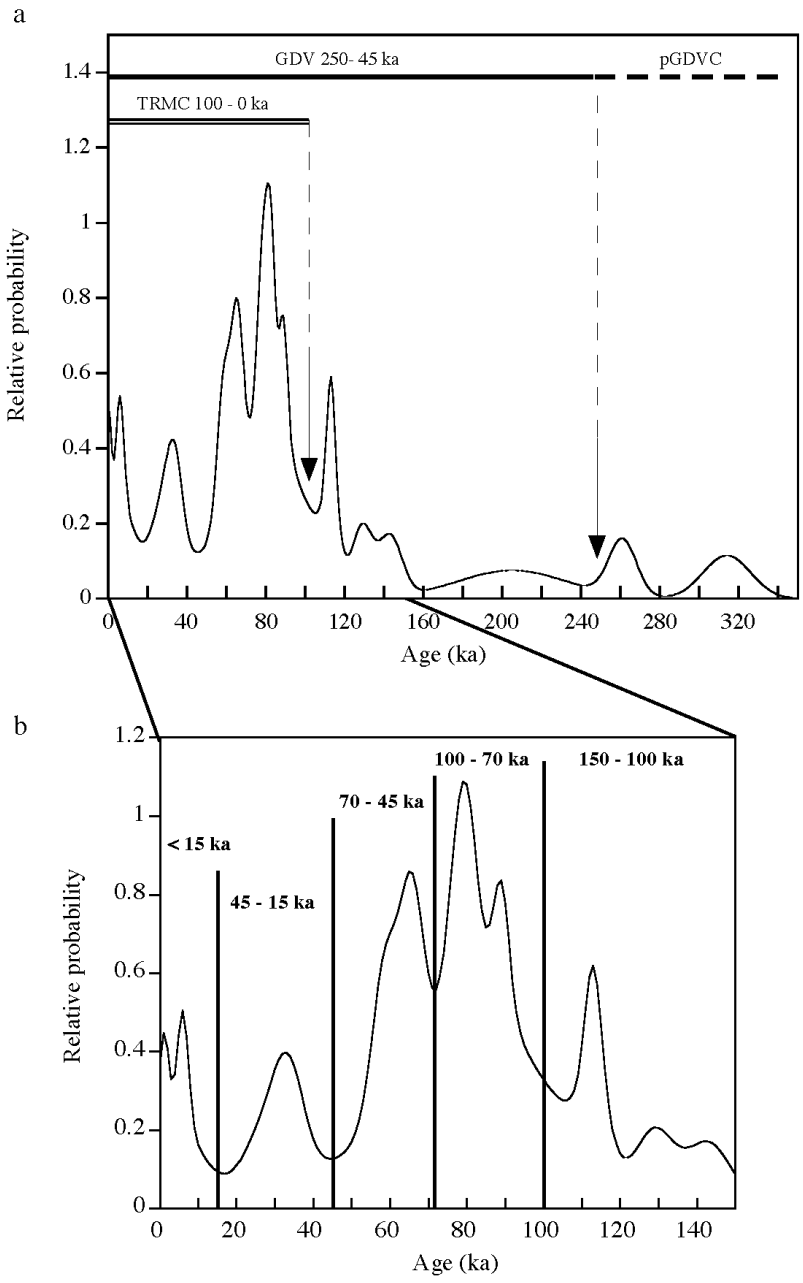

Fig. 2. (Samper et al., 2007)

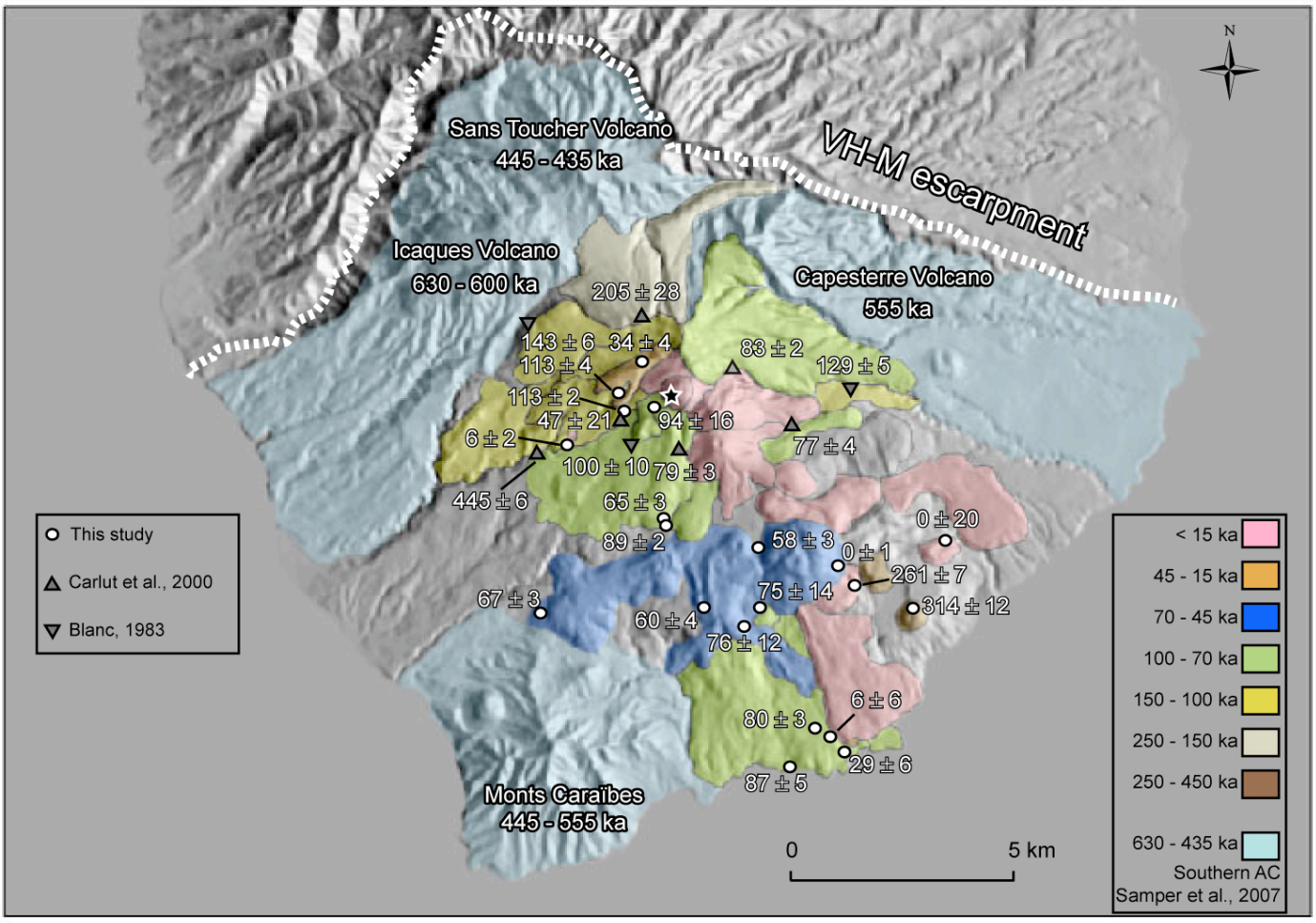

Fig. 3 (Samper et al., 2007)

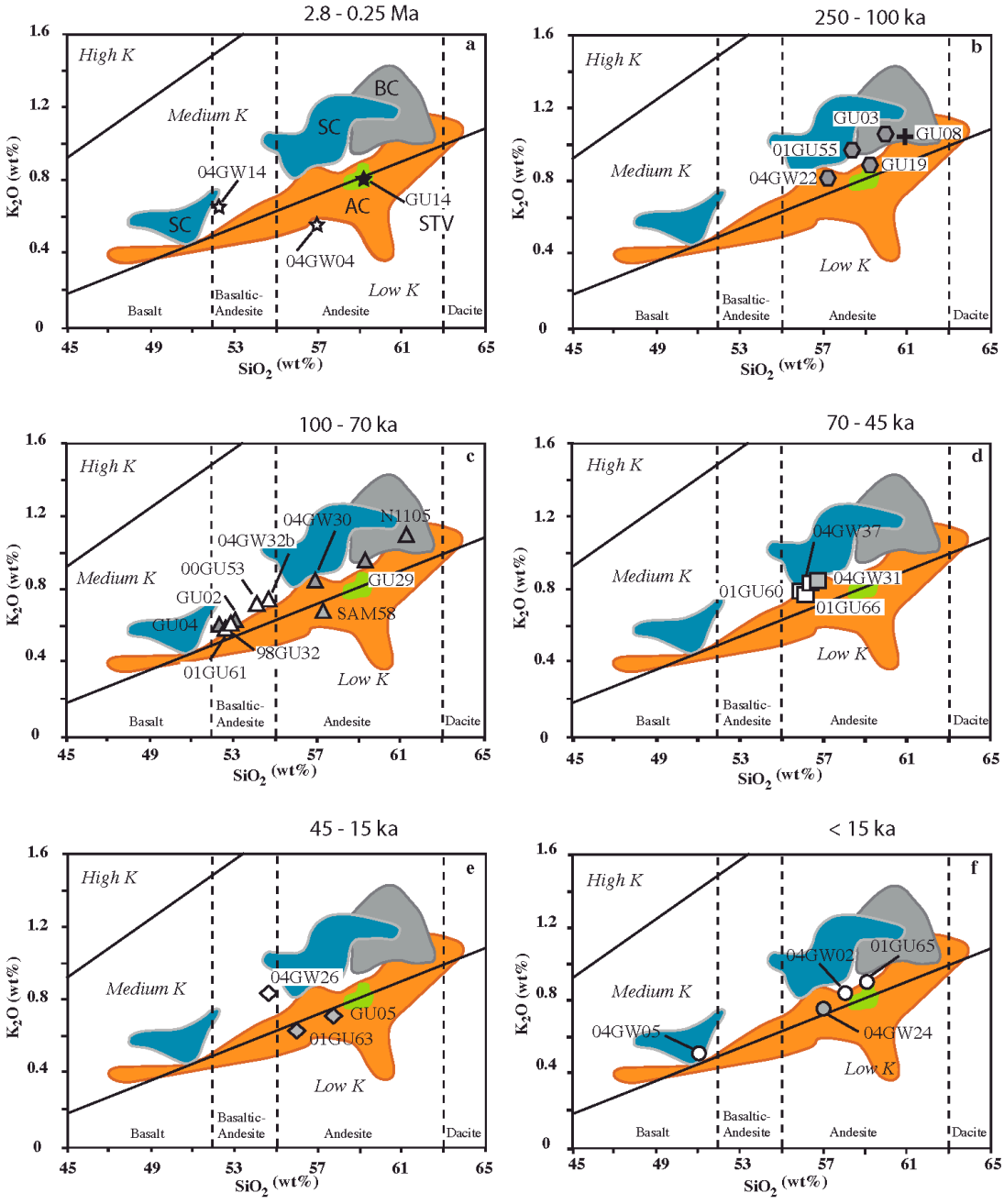

Fig. 4. (Samper et al., 2007)

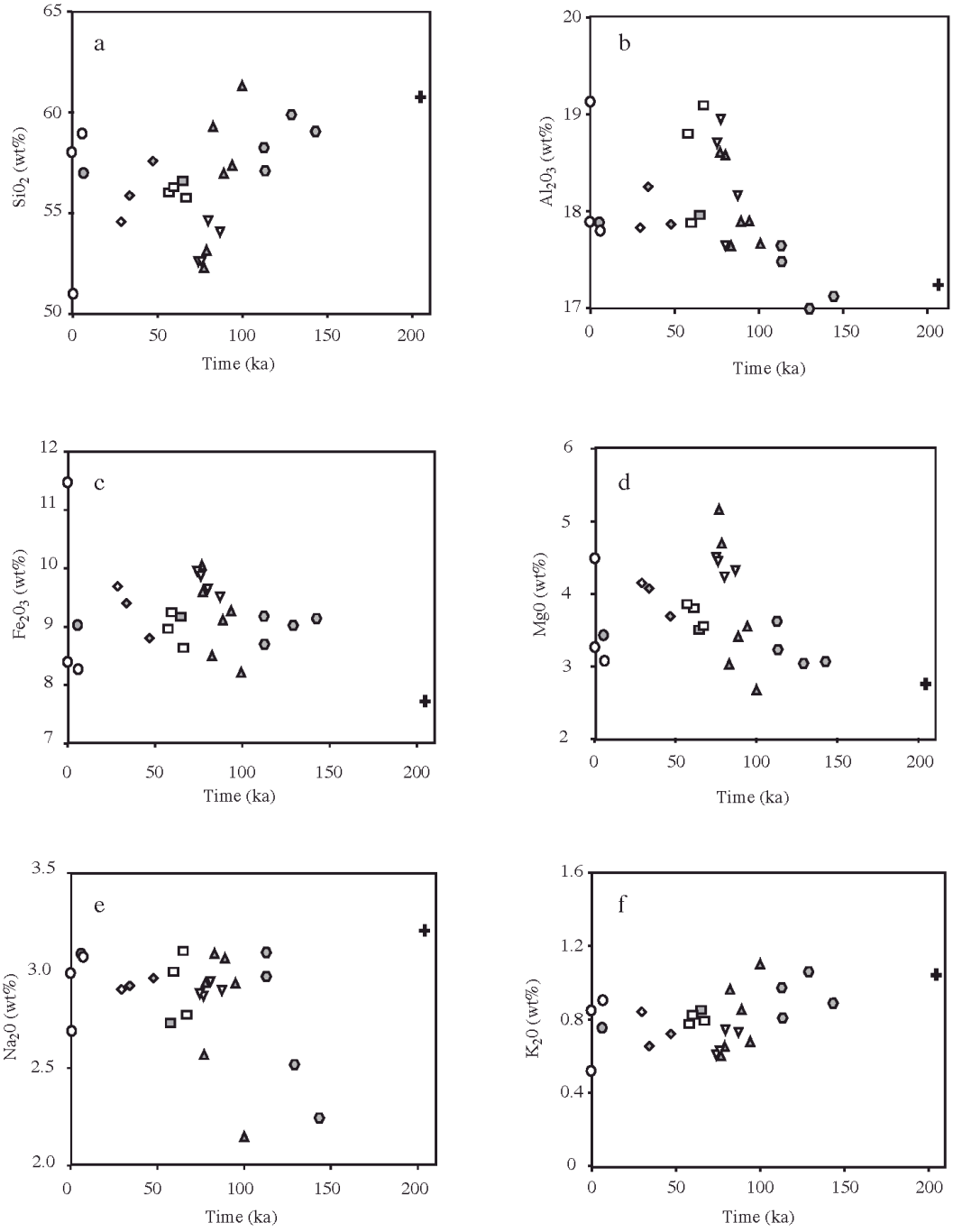

Fig. 5 (Samper et al., 2007)

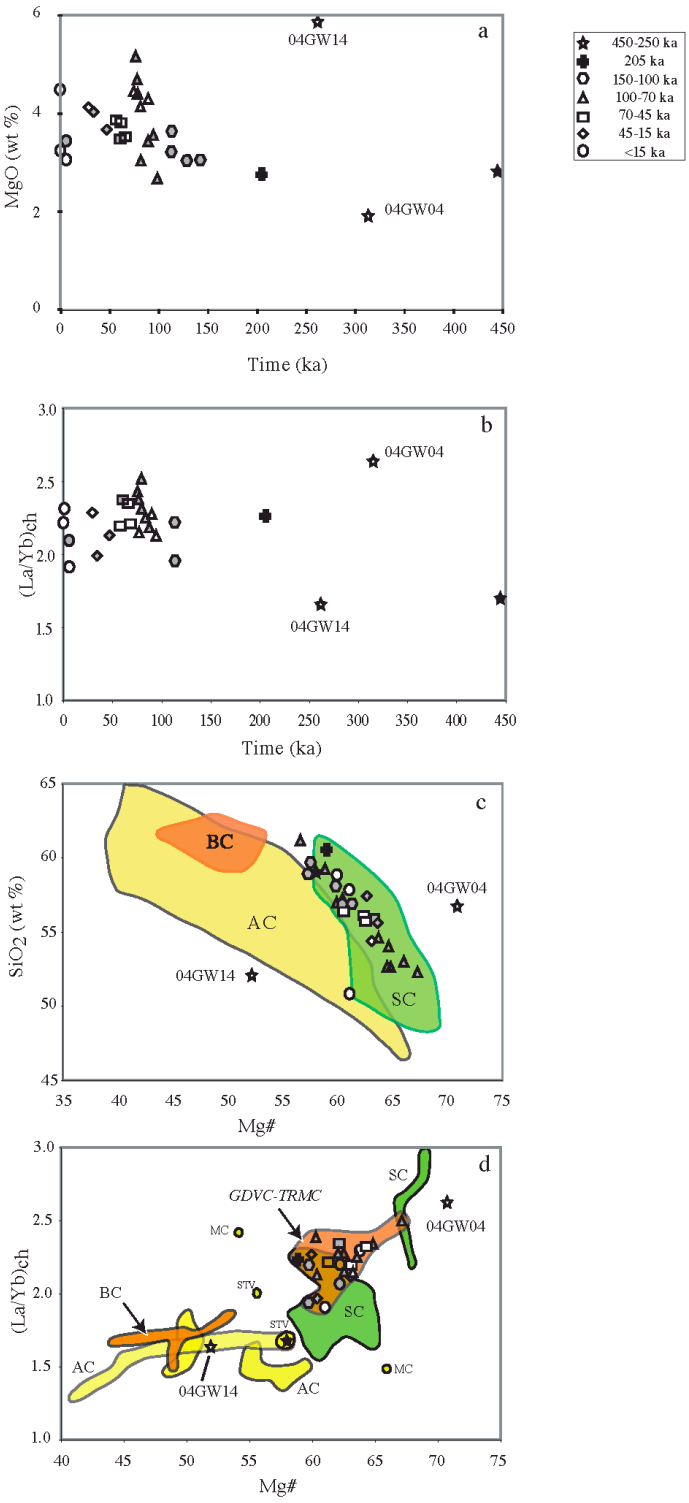

Fig. 6. (Samper et al., 2007)

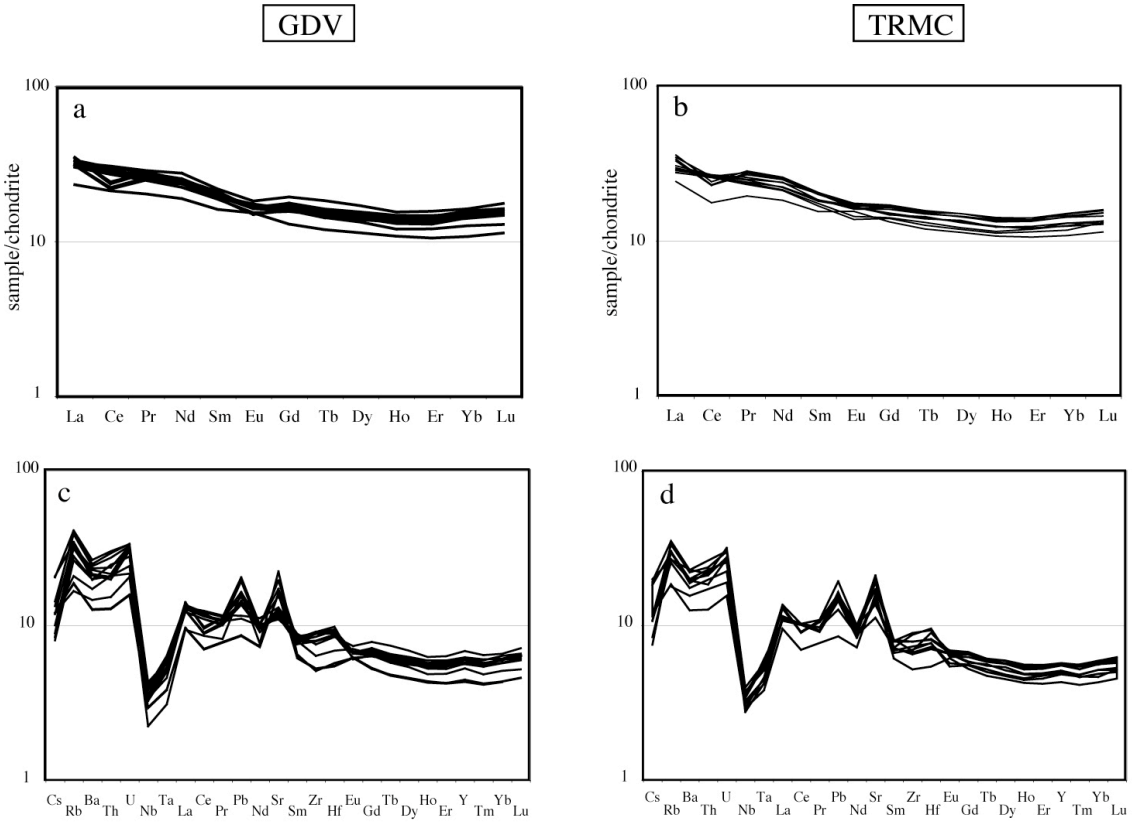

Fig. 7. (Samper et al., 2007)

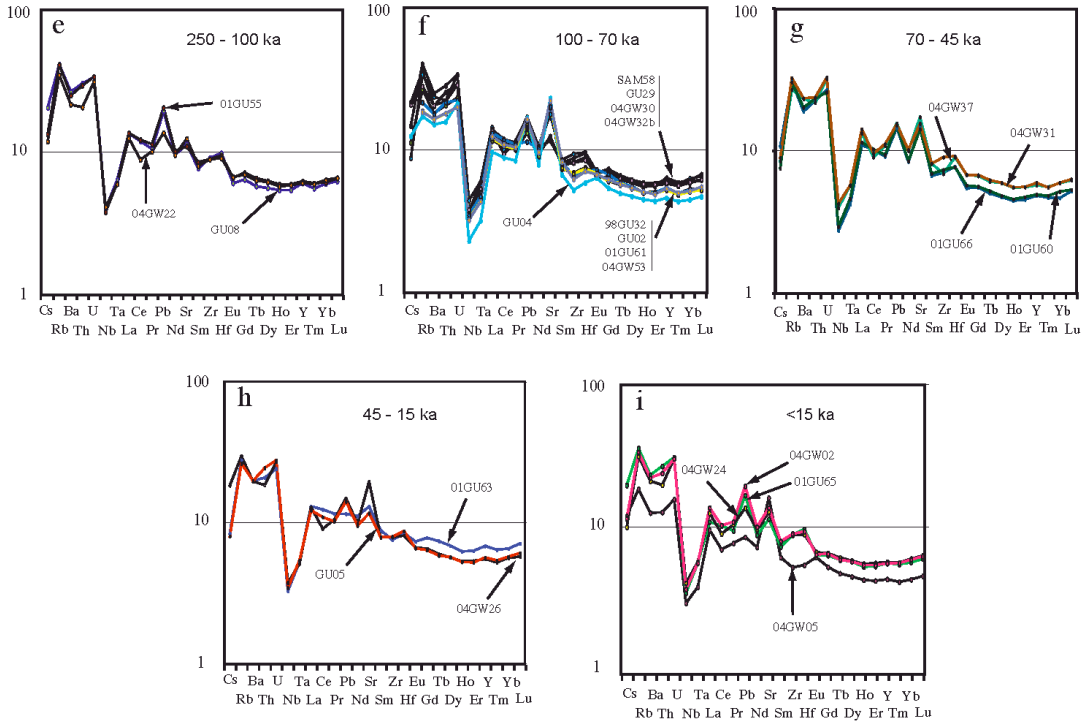

Fig. 7. (Samper et al., 2007)

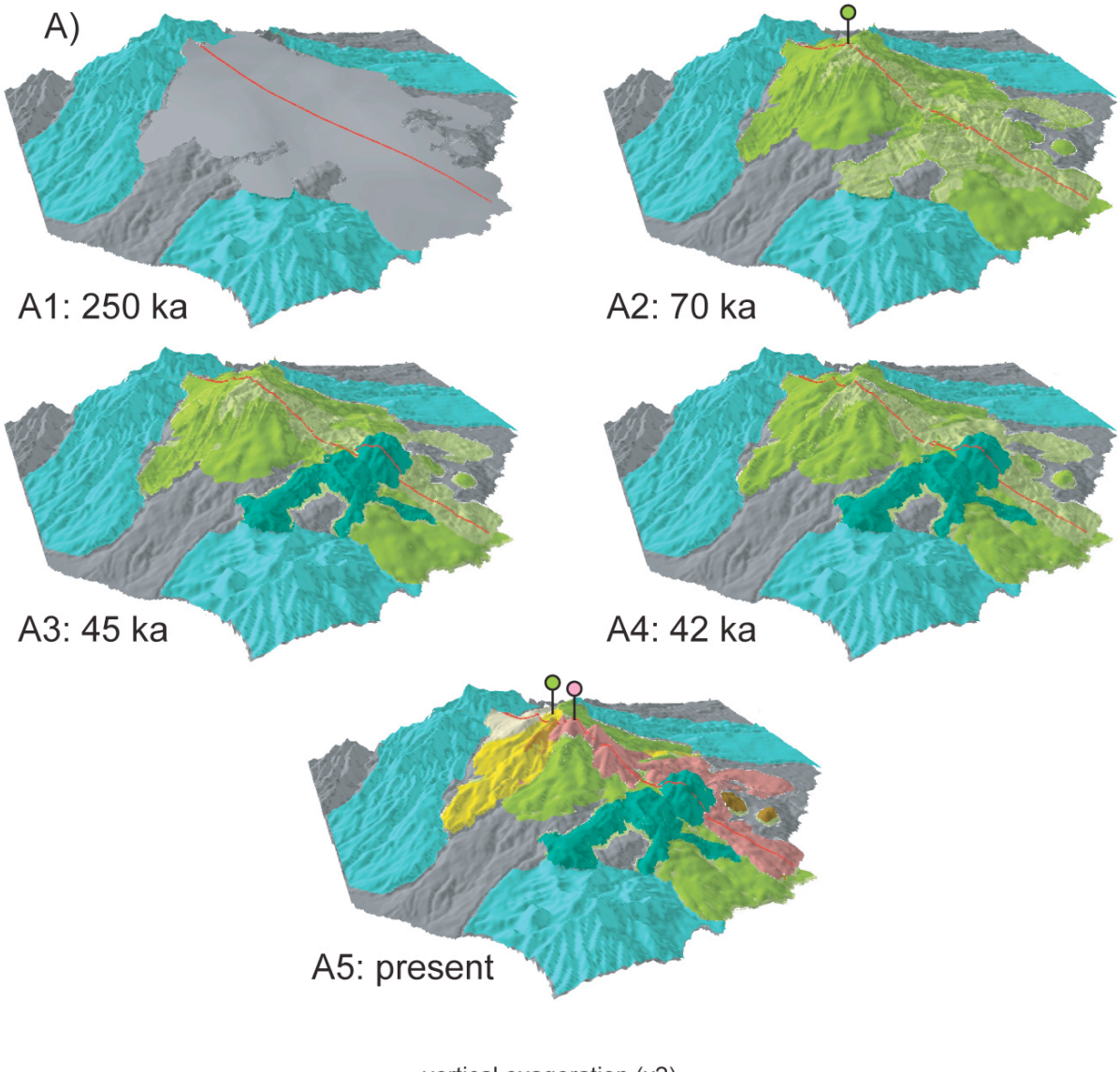

Fig. 8. (Samper et al., 2007)

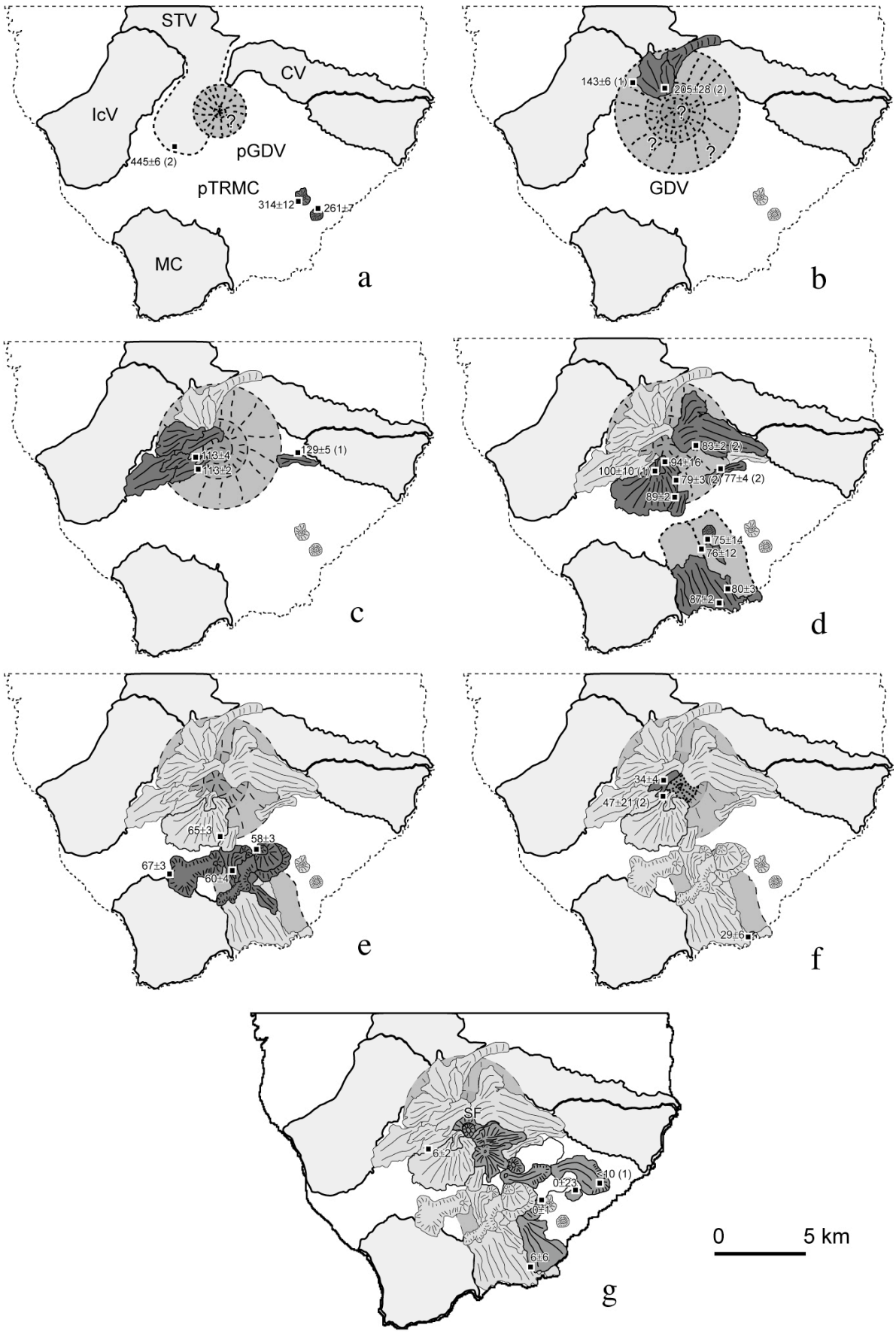

Fig. 9 (Samper et al., 2007)

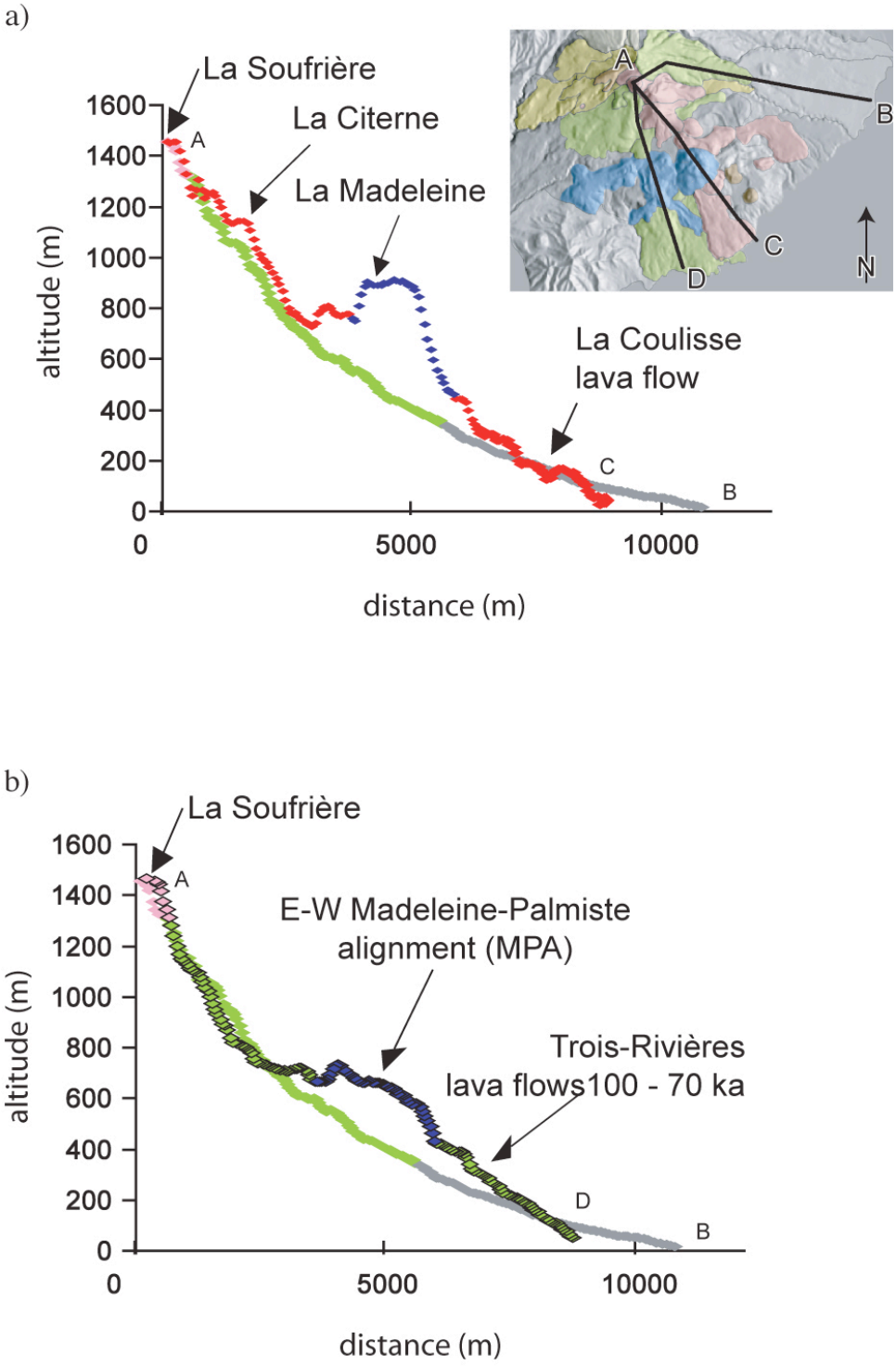

Fig. 10 (Samper et al., 2007)

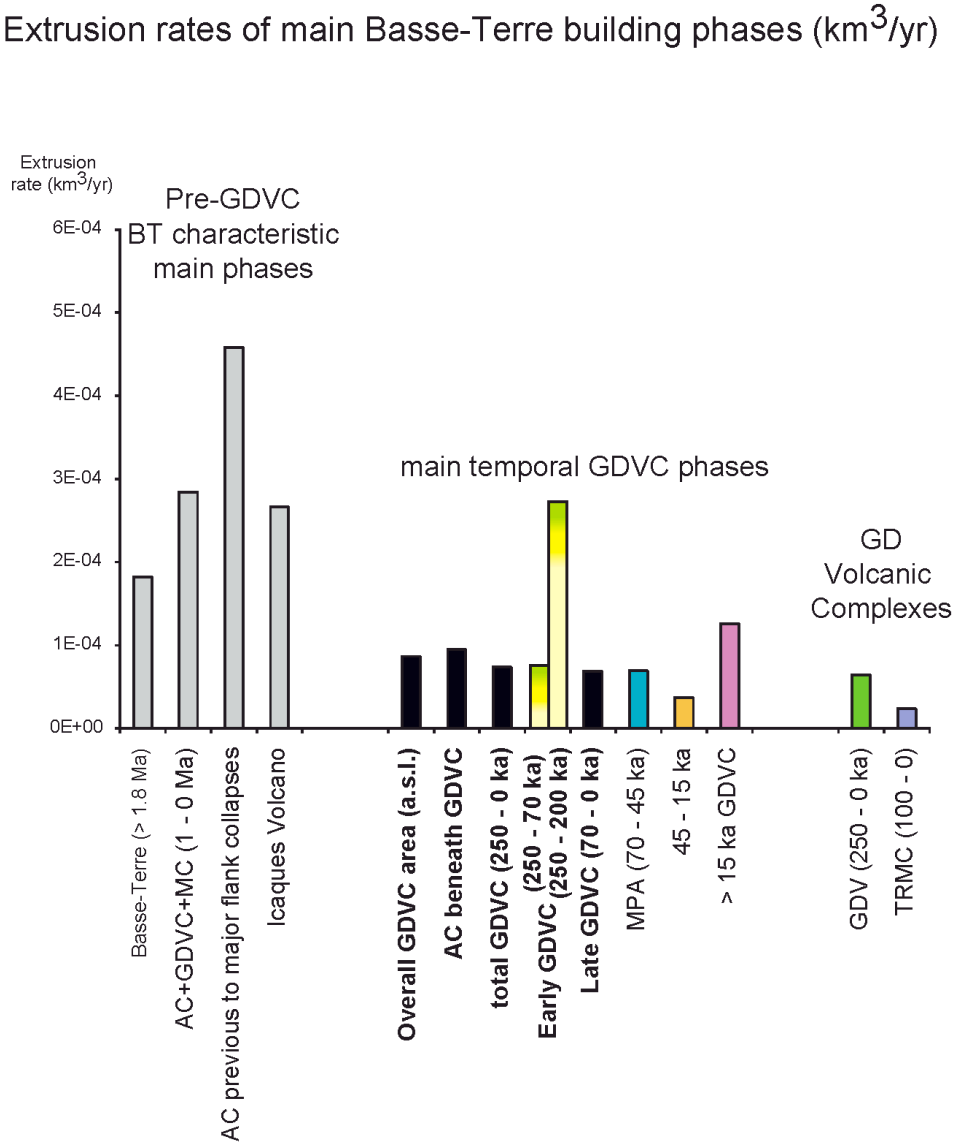

Fig. 11 (Samper et al., 2007)

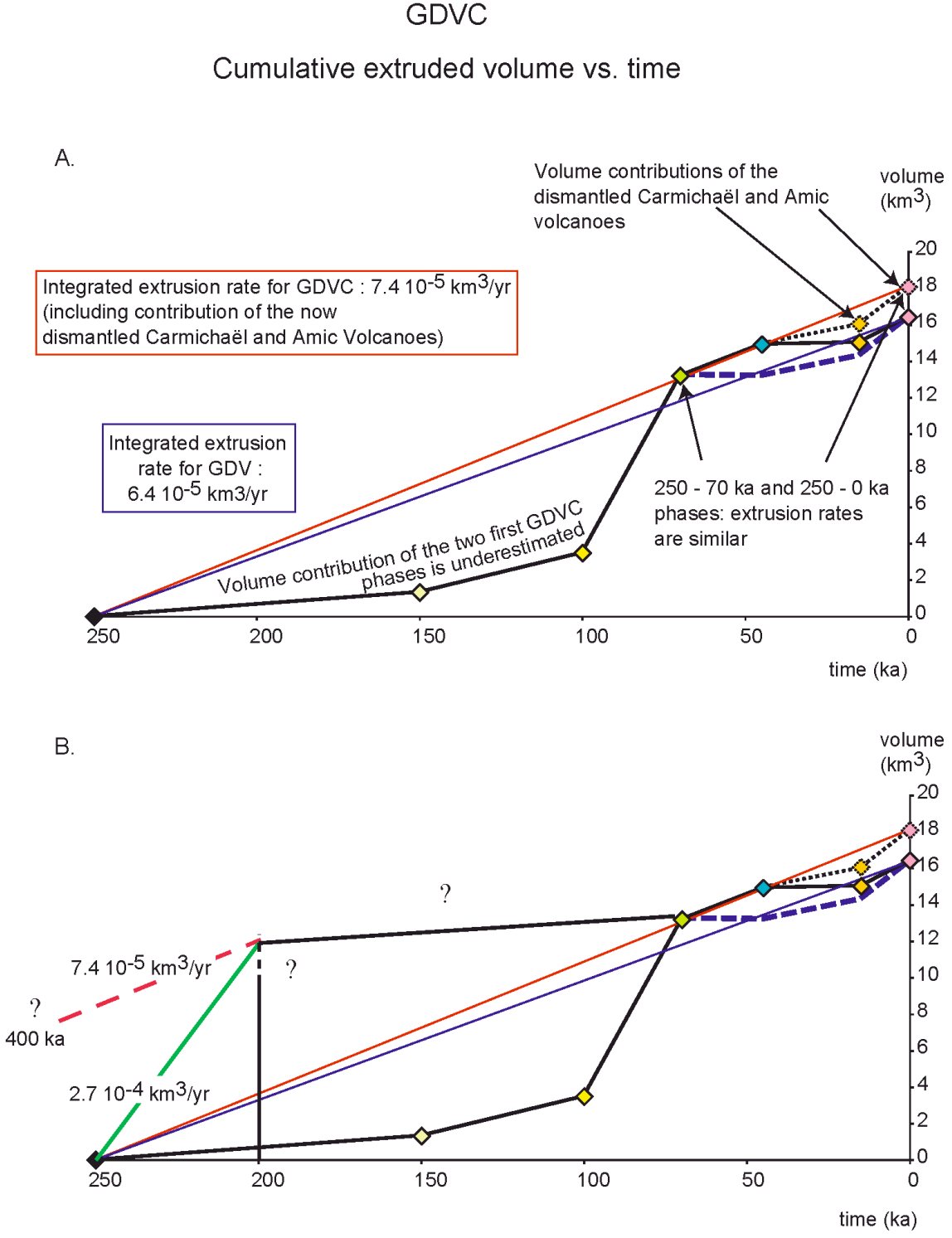

Fig. 12 (Samper et al., 2007)

Partie II

Apports géochronologiques à la caractérisation des phénomènes d'effondrement de flanc majeurs de l'Arc des Petites Antilles

Application aux îles de La Dominique, Martinique, Sainte-Lucie, et Basse-Terre

Radiometric Dating of Three Large Volume Flank-collapses in The Lesser Antilles Arc

A. Samper[1], X. Quidelleur[1,*], G. Boudon[2], A. Le Friant[2], J.C. Komorowski[2]

[1] Laboratoire de Géochronologie Multi-Techniques
UMR IDES 8148 CNRS-UPS, Dpt. Sciences de la Terre
Université Paris Sud 11, Bât. 504, 91405 Orsay (France)

[2] Institut de physique du Globe de Paris, CNRS UMR 7154, Equipe de Volcanologie, 4 place Jussieu, 75252 Paris Cedex 05 (France)

* Corresponding author; email: xavier.quidelleur@u-psud.fr

To be submitted to JVGR

Word counts. Text: 5658; Abstract: 195

References: 48; Table: 1; Fig.: 4

Abstract: It is now admitted that flank-collapses are a recurrent process of the evolution of the Lesser Antilles arc volcanoes. Large magnitude debris avalanche deposits have been identified off the coast of Dominica, Martinique and St. Lucia, with associated volumes up to 20 km^3 (Deplus et al., 2001). We present new radiometric dating of three old major events using the K-Ar Cassignol-Gillot technique. In the Qualibou depression of St. Lucia, the collapse has been constrained by dome emplacement prior to 95 ± 2 ka. In Dominica, where repetitive flank-collapse events occurred (Le Friant et al., 2002), the Plat-Pays event probably occurred after 96 ± 2 ka. Inside the inherited depression, Scotts Head, which is interpreted as a proximal pluri-kilometric megabloc from the Soufrière avalanche, has been dated at 14 ± 1

ka, providing an older bound for this event. In Martinique Island, three different domes within the Carbets structure dated at 337 ± 5 ka constrain the age of this high magnitude event. Finally, these results obtained from three of the most voluminous flank-collapses provide constraints to estimate the recurrence of these events, which represent one of the major hazards associated with volcanoes of the Lesser Antilles Arc.

Keywords: Lesser Antilles, flank-collapse, radiometric dating, K/Ar, Quaternary

Flank-collapse events are recognized as a recurrent process in the lifetime of active oceanic volcanoes. The most voluminous events have been reported around intra-plate oceanic islands (Hawaii, Canary Islands and Tahiti; (Carracedo et al., 1999; Clouard et al., 2001; Hildenbrand et al., 2004; Moore et al., 1994)), but large flank-collapse deposits have also been related to subduction arc volcanism. Recent bathymetric investigations performed along the Lesser Antilles volcanic arc, highlighted the occurrence of large-scale west directed flank-collapse events (Deplus et al., 2001; Le Friant, 2001), which have affected most islands. Imaging of the morphological signatures of the large-scale debris avalanche deposits on the slopes of the Grenada Basin allowed to identify the largest events. They have been reported off the southern islands of the arc with deposit areas of 3500 km^2 for Dominica (Plat Pays Volcanic Complex), 2000 km^2 for St. Lucia (Qualibou Structure) and 800 km^2 for Martinique (Montagne Pelée Volcano). Based on the size of the horseshoe-shaped structures recognized on-land, the volume of material involved has been estimated to about 20 km^3 for the largest event identified off southern Dominica (Le Friant et al., 2002) and 30-40 km^3 for the old flank-collapse event of Pitons des Carbets, Martinique (Boudon et al., 2007; Boudon et al., 1992; Le Friant and Boudon, 2003). These volumes are one or two orders of magnitude lower than the volume of shield volcanoes destabilized during flank-collapse events for intra plate oceanic islands such as Hawaii or the Canary Islands. Nevertheless flank-collapse represents one of the major hazards associated with volcanism in the Lesser Antilles (Boudon et al., 2006). Smaller edifice collapses affecting only the summit of composite volcanoes of the Lesser Antilles have been shown to be a recurrent process of volcanic activity. For instance, the Grande Découverte Composite Volcano in Basse Terre (Guadeloupe) experienced at least 11 flank-collapse events within the last 42 kyr, with volume of each lower than 0.5 km^3 (Boudon et al., 1984; Boudon et al., 1987; Komorowski et al., 2005; Komorowski et al.,

2002). Similarly, the ongoing dome construction and collapse sequences observed at Montserrat climaxed during the "Boxing Day" event in December 1997, when 0.05 km^3 of material were involved in a destructive debris avalanche (Sparks et al., 2002; Voight et al., 2002; Young et al., 2002). Besides their relatively high frequency, such events remain limited in volume compared to the large flank-collapse events of the southern part of the arc and their associated offshore debris-avalanche deposits (Boudon et al., 2007).

Chronologic data on volcanic edifices and lava flows are needed to constrain through time the sequence of collapse events in order to better assess the volcanological evolution of eruptive location. Effectively, well-marked amphitheater structures have long been identified as the scars of collapsed volcanoes, such as at Montagne Pelée Volcano (Vincent et al., 1989) or in southern Dominica (Roobol et al., 1983). More recently, from on-land continuation of superimposed debris-avalanche deposits observed off-shore (Deplus et al., 2001; Le Friant, 2001), multiple collapse events have been related to imbricate collapse structures. On Martinique and Dominica, the volumes of such structures decrease, with the more recent events being less voluminous (Le Friant and Boudon, 2003; Le Friant et al., 2002). However, since the sedimentation rate around the central islands of the Lesser Antilles arc can amount to 25 cm/kyr (Reid et al., 1996), deposits older than 200 kyr cannot be identified by sea floor bathymetry (Deplus et al., 2001). Hence, high-resolution age data coupled to on-land geological studies are the only valid approach to constrain the older events through time, and assess a possible recurrence time of these events.

For this purpose, the present study focuses on the volcanic structures of southern Dominica and within the Qualibou depression in Saint Lucia, which were the sources of the largest debris avalanche identified in the Grenada Basin (Boudon et al., 2006; Deplus et al., 2001; Le Friant, 2001; Le Friant et al., 2002). We have also investigated the large horseshoe-shaped structure of the Piton des Carbets (Martinique), for which only on-land debris

avalanche deposits have been recognized. These three devastating events each involved volumes of several tens of cubic kilometers. Prior to this study, no well-constrained timing was available.

Geologic setting

Dominica

The Plat Pays Volcanic Complex occupies the south-western part of the island of Dominica. It is considered as having experienced successive episodes of lateral flank-collapse events and post-collapse lava dome emplacement (Le Friant et al., 2002; Roobol et al., 1983; Wadge, 1985). Off-shore, recent studies identified the most widespread submarine debris-avalanche deposits of the Lesser Antilles, which cover an area of 3500 km^2 (Deplus et al., 2001; Le Friant, 2001). At least two flank-collapse events were inferred from these deposits, but on-land investigations coupled with submarine morphological extension of terrestrial horse-shoe-shaped structures led Le Friant et al. (2002) to propose that three flank-collapse events occurred. The older and larger one, the Plat Pays event, generated the main part of the debris-avalanche deposits identified offshore and on-land including the Loubière area. Le Friant et al. (2002) suggested on the basis of the sedimentary covering of the offshore debris-avalanche an age older than 100 ka. The rims of the horseshoe-shaped structure disappear under the more recent products of the Plat Pays volcanic complex. A second flank-collapse occurred on this volcanic complex and produced the Soufrière amphitheater associated with a hummocky debris-avalanche deposit with large blocks including the Scott's Head peninsula. On the basis of ^{14}C dates obtained on charcoal included in pyroclastic deposits, Le Friant et al. (2002) proposed an age comprised between 6600 ± 50 and 2380 ± 75 years BP. A more recent and smaller flank-collapse occurred between 2380 and 675 years BP. However, such interpretation has been challenged by Lindsay et al. (2003), who suggested that the Soufrière

depression resulted from a combination of flank-collapse and caldera, associated with the Grand Bay ignimbrite emplacement dated about 39 kyr by ^{14}C (Lindsay et al., 2003). Fig. 2 shows the location of the three samples analyzed here in order to constrain the timing of the collapse events.

Saint Lucia

Located on the south west side of Saint Lucia, The Qualibou depression was first interpreted as a gravity collapse structure related with the explosive emplacement of the ash-and-pumice flows of Choiseul and Belfond (Tomblin, 1965; Wohletz et al., 1986). Based on both the morphology of the structure characterized by a steep wall arcuate depression open to the west towards the Grenada Basin, and on the offshore continuation of the depression rims, the Qualibou depression was then associated with a large flank-collapse event (Mattioli et al., 1995; Roobol et al., 1983). This episode is thought to be independent of the ash-and-pumice flow deposits, which probably originated from the centre of the island (Wright et al., 1984). Recent marine geophysical data carried during the Aguadomar cruise permitted to recognize extended debris avalanche deposits off the south-western part of the island (Deplus et al., 2001). Le Friant (2001) demonstrated by a combined marine and on-land study that the Qualibou depression has a sector collapse origin. Offshore megablocks have been identified up to 25 km off the coast. A part of the debris avalanche deposits, which cover more than 2000 km^2 into the Grenada Basin, can be associated to the Qualibou depression. Within the depression, basalt lava flows found near the coast are remnants of the pre-collapse volcanic basement, while some andesite and dacite lava domes, including the two lava domes of Petit Piton and Gros Piton, were probably emplaced following the flank-collapse. Fig. 3 shows the location of the samples dated in the present study.

Martinique

In Martinique, the Pitons du Carbet volcano is located south of Montagne Pelée and west of the Morne Jacob volcano. It has experienced a large flank-collapse event followed by the emplacement of several andesitic domes, the Pitons du Carbets *s.s.*, within the resulting horseshoe-shaped structure (Boudon et al., 2007; Boudon et al., 1992). The large arcuate structure is open towards the Caribbean Sea to the west, limited by a steep wall to the north, but its southern limit is not well constrained yet. Associated debris-avalanche deposits are found on the west side, inside the structure and all along the shoreline, forming cliffs more than a hundreds meters high in some places. The collapsed volume has been estimated around 30-40 km^3 (Boudon et al., 1992). No clear evidence has been found offshore (Deplus et al., 2001), probably because of the relatively old age of this event and the high sedimentation rate within the basin (Le Friant and Boudon, 2003; Reid et al., 1996). Within the structure, pronounced river incisions and the formation of relatively deep valleys radially distributed from the Piton des Carbets domes suggest that the hydrologic network was reorganized after the lateral collapse and the following lava dome emplacement. As a result, intense erosion has exposed basaltic lava flows from the pre-collapse basement.

Dating methodology and sampling strategy

In order to constrain the timing of these large-scale events, we followed a sampling strategy consisting in choosing carefully the most meaningful sampling sites. Hence, we have dated within each collapsed structure remnants of volcanic edifices, such as basal lava flows, and lava domes emplaced after the flank-collapses. As already applied for other geochronological studies of collapsed structures from volcanic islands such as Tahiti Island (Hildenbrand et al., 2004), and in Basse Terre Island (Guadeloupe) (Samper et al., 2006), we have used the K-Ar Cassignol-Gillot technique (Cassignol and Gillot, 1982; Gillot and Cornette,

1986) on samples selected on the basis of a careful thin section examination. All samples showing alteration were discarded. After sieving in the 125 - 250 μm size fraction, phenocrysts of plagioclase, clinopyroxene and amphibole were removed using heavy liquids. The groundmass selected for dating was obtained in a narrow density range in order to eliminate possible undetected trace of weathering. Then, magnetic separation was applied to remove residual phenocrysts. Note that the remaining selected fraction for dating typically represents less than 10% in volume from the initial whole-rock material. It was used for both K and Ar measurements. K was measured by flame emission spectroscopy and compared with standards MDO-G and ISH-G (Gillot et al., 1992), and Ar was measured with a mass spectrometer identical to the one described by Gillot and Cornette (Gillot and Cornette, 1986). Because of the stability of the measuring conditions, the mass spectrometer is especially suitable for very young dating. The ^{40}Ar signal calibration is obtained from air pipette measurements calibrated from repeated analyses of the inter-laboratory standard GL-O with the recommended value of 6.679×10^{14} at/g of ^{40}Ar* (Odin and al., 1982). The atmospheric correction, performed after each sample analysis, is achieved by comparison of the ^{40}Ar/^{36}Ar ratio of the sample with the ^{40}Ar/^{36}Ar ratio of an air-pipette measured in the same pressure conditions. Note that, therefore, no assumption regarding the true value of the atmospheric ^{40}Ar/^{36}Ar ratio is needed. Typical uncertainties of 1% are achieved for the ^{40}Ar signal calibration and for the K determination. The uncertainty on the ^{40}Ar* determination is a function of the radiogenic content of the sample, the detection limit of our system being presently of 0.1% of ^{40}Ar* (Quidelleur et al., 2001). Decay constants and isotopic ratios of Steiger and Jäger (Steiger and Jäger, 1977) have been used. All uncertainties quoted herein are given at the 1 sigma confidence level.

Results

Four samples from Plat Pays volcanic complex of southern Dominica passed our petrological selection, but only three could be dated. A lava dome sampled at La Sorcière (south of Pointe Guignard; Fig. 2) yielded very high argon signal due to intense contamination, probably caused by post crystallization hydrothermal fluid circulation. From the remaining three ages, two were obtained from massive fractured lavas interpreted as megablocks from debris-avalanche deposits (Le Friant et al., 2002), which both show characteristic jigsaw cracks structures. Lava from Loubière quarry (01DQ01), located within the Plat Pays complex yielded a well-defined age of 96 ± 2 ka (Table 1). The Scotts Head (01DQ02), a prominent lava dome, interpreted either as in-situ (Lindsay et al., 2003), or as a submerged megablock from the debris-avalanche deposit associated to the Soufrière flank-collapse event (Le Friant et al., 2002), yielded an age of 14 ± 1 ka (Table 1). Plagioclase minerals, separated within a narrow density range (2.65 - 2.74) from the same sample, show a much older age of 50 ± 3 ka, which confirms that a strong concern exists for plagioclase dating in the Lesser Antilles, as previously observed for recent lavas on Monsterrat (Harford et al., 2002). Finally, the third sample dated belongs to the Bois d'Inde lava dome (01DQ06), which is located within the presumed first Plats Pays flank-collapse structure (Le Friant et al., 2002), yielded a rather poorly defined age of 31 ± 10 ka (Table 1). The relatively large uncertainty can be explained by the low radiogenic yield due to a high atmospheric argon contamination of this sample.

All samples from Saint Lucia dated here are from within the Qualibou depression. Dacite lava domes have been associated with post-collapse magmatic activity, while basalt lava flows are remnant of the pre-collapse activity. An age of 3 ± 3 ka has been obtained for the Terre Blanche dacite lava dome (01SL08; Table 1). The radiogenic argon yield is only 0.1%, our present limit of detection (Quidelleur et al., 2001), which explains the large relative

uncertainty for this sample. The Petit Piton and Gros Piton dacite lava domes have been dated at 95 ± 2 and 77 ± 2 ka, respectively (Table 1). The latter (01SL03) was obtained by averaging two indistinguishable ages (Table 1) performed on different size fractions (63 – 125 and 125 – 250 μm), which provides additional confidence in the result. In the same fashion than for 01DQ02, the plagioclase separates from 01SL03 yield a much older age of 161 ± 7 ka, which suggests the presence of inherited crystals or magmatic ^{40}Ar in excess. These results are in conflict with earlier age determinations of 0.26 ± 0.04 Ma (Briden et al., 1979) for Petit Piton, and 0.23 ± 0.1 and 0.26 ± 0.1 Ma (Aquater, 1982 in; Lindsay, 2005), for Gros Piton. Two basalt lava flows have been analyzed here. The aphyric lava flow of Malgrétoute (01SL01), sampled along the coast, south of Soufrière village, has been dated at 6.64 ± 0.12 Ma (Table 1). A previous determination of 5.61 ± 0.25 (Briden et al., 1979) is not concordant, but the aphyric nature of this flow makes the identification and removal of possible weathered fraction problematic. An age of 1.10 ± 0.02 Ma (Table 1) has been obtained for the porphyric basaltic flow of Jalousie (01SL04) sampled along the coast in-between the Petit and Gros Piton. Very different ages of 6.1 ± 0.6 and 6.5 ± 0.6 Ma (Aquater, 1982 in; Lindsay, 2005) were previously reported for this lava flow.

In Martinique, three indistinguishable ages of 331 ± 5, 338 ± 5 and 341 ± 5 ka (04MT02, ALMA and 04MT07, respectively; Table 1) constrain the timing of emplacement of the andesitic lava domes of Pitons des Carbets at 337 ± 5 ka. An older age of 0.86 ± 0.05 Ma was previously obtained by whole rock K-Ar dating for Piton Dumauzé (Westercamp et al., 1990). Outside the scar, the pre-collapse Piton Gelé lava dome (04MT06) is dated at 770 ± 11 ka, and the lava flow of Bellevue (04MT01) at 1.69 ± 0.02 Ma (Table 1). An older age of 1.06 ± 0.05 Ma was previously obtained for Piton Gelé (Westercamp et al., 1990). Within the amphitheatre structure, two basalt lava flows from the basement were sampled on the northern (04MT08) and southern (04MT04) sides. Ages of 2.27 ± 0.03 and 1.86 ± 0.03 Ma were

obtained for the former and the latter, respectively (Table 1). An older age of 2.60 ± 0.07 Ma (Westercamp et al., 1990) was previously obtained for 04MT04.

Discussion

Age results

The K-Ar Cassignol Gillot technique applied to groundmass samples, coupled to a coherent and valuable sampling strategy, both on the samples location and selection, has been shown to be a very accurate dating tool for Lesser Antilles lavas. It provided strong timing constraints regarding the paleomagnetic field variations (Carlut et al., 2000) and the magmatic and volcanologic evolution of the whole island of Basse Terre (Guadeloupe) (Samper et al., 2006). Earlier studies were shown to have provided incorrect ages because they used ^{38}Ar spiked K-Ar from whole-rock samples. Due to undetected xenocryst contamination in whole rock analyses and, most probably, in addition with un-removed weathered phases, unreliable excessively old ages were obtained, as demonstrated at La Guadeloupe (Carlut et al., 2000) and Montserrat (Harford et al., 2002). The need for careful mineralogical preparation has been highlighted here for samples 01DQ02 and 01SL03 (Table 1) from the joint analyses of plagioclase separates and groundmass. We have shown here that excess radiogenic ^{40}Ar yield from plagioclase crystals, and/or late accumulation of plagioclase xenocrysts within the magma chamber, which prevented the total reset of the K-Ar system, provide ages that are too old. In addition with undetected K-loss during weathering, such contamination demonstrates that whole rock dating should never be performed, neither by K-Ar nor $^{40}Ar/^{39}Ar$ dating, and probably explains the anomalously excessively old ages previously obtained from whole rock samples throughout the Lesser Antilles. Hence, all earlier results obtained by whole rock K-Ar dating are not further considered in the following discussion.

The use of the K-Ar Cassignol Gillot technique applied on selected samples enabled to settle the age of several different volcanic edifices present within the structures, and to bracket the age of those flank-collapse events.

Dominica

Only three new age determinations are available for Dominica (Table 1), but they provide strong constraints regarding the timing of the successive edifice collapses recorded in the Grenada Basin bathymetry (Deplus et al., 2001; Le Friant et al., 2002). A lava block (01DQ01) sampled in the Loubière Quarry interpreted by (Le Friant et al., 2002) as a megablock belonging to the debris-avalanche of the Plat Pays flank-collapse event has been dated at 96 ± 2 ka (Fig. 2). This lava was alternatively interpreted by (Lindsay et al., 2003) as fragmental deposits from the post-collapse lava dome of La Falaise, which erupted between ~39 and 28.5 ka (Lindsay et al., 2003). Our age clearly discards the latter hypothesis and rather shows that 01DQ01 was not sampled from a post Soufrière collapse lava dome. On the other hand, if its attribution to a debris-avalanche deposit is correct, it provides an older bound for the timing of the Plats Pays flank-collapse (1; (Le Friant et al., 2002)), which has been proposed as the main event affecting southern Dominica.

The in-situ lava dome of Bois d'Inde (01DQ06) located outside the Soufrière depression and emplaced between flank-collapses 1 and 2, Plat Pays and Soufrière flank-collapses, respectively (Le Friant et al., 2002), has been dated at 31 ± 10 ka (Table 1). Within the uncertainty, this age is compatible with the stratigraphic relationship between the Bois d'Inde dome and the overlying Grand Bay Ignimbrite, which is dated at about 39 ka (Lindsay et al., 2003). Our age of 31 ± 10 ka thus provides a younger bound for the first flank-collapse (Plat Pays; (Le Friant et al., 2002)).

We obtained an age of 14 ± 1 ka for Scotts Head (01DQ02; Table 1), which is in agreement with the ^{14}C age of 2.380 ± 75 years B.P. obtained for pyroclastic fallout deposits covering it. This peninsula (Fig. 1a) has been either interpreted as a debris-avalanche megablock on the basis of characteristic jigsaw crack structures (Le Friant et al., 2002) or as an in situ post-Soufrière collapse lava dome (Lindsay et al., 2003). Our age is thus in agreement with the age of the Soufrière flank-collapse proposed to be between 6600 ± 50 and 2380 ± 75 years BP on the basis of ^{14}C dates (Le Friant et al., 2002). On the other hand, our age is in conflict with the hypothesis of (Lindsay et al., 2003), which proposed that the Soufrière depression resulted from the combination of a flank-collapse event and a caldera resulting from the emission of the Grand Bay ignimbrite at ~39 ka. Effectively, our age is not compatible with the model proposed by (Lindsay et al., 2003) in which growth of the Scotts Head lava dome is related to rapid lava dome emplacement following superficial magma chamber depressurization due to collapse de-loading, that would have occurred about 25 kyr earlier (Lindsay et al., 2003).

Following the three successive flank-collapses hypothesis (Le Friant et al., 2002), our ages from Dominica constrained the first event (Plat Pays Event collapse) between 96 ± 2 and 31 ± 10 ka. Assuming a sedimentation rate of 25 cm/kyr over the submarine deposits, Le Friant et al. (2002) proposed an age of 100 ka for this event. Our age suggests that it is probably towards the older end of this interval. We have dated the Scotts Head megablock, interpreted by Le Friant et al. (Le Friant et al., 2002) and Boudon et al. (Boudon et al., 2007) as a proximal relict avalanche plurikilometric megablock relied to the Soufrière Event, at 14 ± 1 ka. Unfortunately, our study does not provide any age constraint regarding the more recent flank-collapse of Morne Rouge. However, it adds further strength to the hypothesis of Le Friant et al. (2002).

Saint Lucia

The age of formation of the Qualibou depression can be significantly revised from our new age data (Table 1). Based on the erroneous previous ages of Petit and Gros Pitons, it was estimated at about 300 ka (Lindsay, 2005).

Inside the Qualibou structure two basal lava flows have been dated at 1.10 ± 0.02 (01SL04) and 6.62 ± 0.12 Ma (01SL01). Probably remnants of older edifices that most likely were related to the volcanic massif surrounding the Qualibou depression, such as Mounts Tabac and Gimie, they were exposed subsequently to removal of superficial lavas during the Qualibou flank-collapse. Note that the 1.10 ± 0.02 Ma lava flow presents characteristic jigsaw cracks and therefore has been displaced consequently to the collapse. However, as no detailed geochronological record of the several volcanic phases is available, and as no age data within the 6 Ma – 300 ka interval were previously obtained for lavas of the Qualibou area, our age of 1.10 ± 0.02 Ma provides a new time constraint on the eruptive story prior to the formation of the Qualibou depression.

On the western coast, the dacite lava domes of Petit Piton and Gros Piton yield respectively 95 ± 2 ka and 77 ± 2 ka, whereas the lava dome of Terre Blanche, associated with a modern fumarolic activity, provides a zero-age test for our technique with an age of 3 ± 3 ka. Hence, the Qualibou flank-collapse event took place between 1.10 ± 0.02 Ma and 95 ± 2 ka, probably slightly before 95 ± 2 ka, age of the Petit Piton dome emplacement. About 10 meters of sediments cover the debris avalanche deposits related to the Qualibou flank-collapse (Le Friant, 2001). Given an averaged sedimentation rate of about10 cm/kyr (Reid et al., 1996), the crude age estimate is about 100 kyr, which is in agreement with our estimate for the Qualibou collapse.

Magmatic activity within the depression, mostly characterized by andesite and dacite dome forming, started after the flank-collapse dated here at about 100 kyr and has continued

until the present day (Lindsay, 2005), with emplacement of the dome of Terre Blanche for which we provide a new age estimation of 3 ± 3 ka.

Martinique

We have dated basal basaltic lava flows and andesitic lava domes inside and outside the amphitheater structure of Pitons des Carbets. Our results bracket the collapse event between 770 ± 11 and 341 ± 5 ka. However, it can be considered that the age of the flank-collapse is not much older than the mean age of 337 ± 5 ka, calculated for the Pitons des Carbets domes emplacement. Effectively, it has been observed at Ohau (Hawaii) (Presley et al., 1997), La Palma (Canary Islands) (Carracedo et al., 1999; Hildenbrand et al., 2003), Tahiti (Society Islands) (Hildenbrand et al., 2004) and Montagne Pelée (Boudon et al., 2007), for instance, that volumetric partial-collapse of volcanic islands are often rapidly followed by a period of enhanced magma production and new edifice construction such as volcanic domes. Models support such observations (Pinel and Jaupart, 2000), where mass de-loading due to the collapse of the overlying edifice induces a significant release of pressure within the magma chamber, thus favouring a new eruptive cycle. In the same fashion, we propose that fast emplacement of voluminous lava domes within a few kyr as demonstrated by the homogeneity of our K-Ar ages (Table 1), has been favoured by the sudden change in the superficial lithostatic pressure conditions following edifice collapse. At Oahu and Tahiti, it has been shown that mass wasting increased partial melting conditions at the source, thus triggering renewed volcanism (Hildenbrand et al., 2004; Presley et al., 1997). Note that, due to the relatively high sedimentation rate (Reid et al., 1996), this relatively old age obtained here for the collapse is consistent with the lack of evidence on the seismic profiles for debris avalanches deposits in the Grenada Basin (Boudon et al., 2007; Deplus et al., 2001; Le Friant and Boudon, 2003).

Occurrence of mass wasting events in the Lesser Antilles

Together with reliable geochronological data and field constraints (Boudon et al., 2007) previously available on several islands, the ages obtained in this study provide additional constraints on the timing of large-scale flank-collapse events along the Lesser Antilles arc.

In Martinique, we have dated a single flank-collapse event involving removal of about 30-40 km^3 of material in the Piton des Carbets structure, at 337 ± 5 ka, which is significantly younger than previously supposed. Former structures such as the andesitic lava flows of 04MT08 and 04MT04 which respectively yield ages of 2.27 ± 0.03 and 1.86 ± 0.03 Ma are present within the structure (Fig. 4) and have been exhumed by the flank-collapse event and the following 300 kyr long superficial erosion. As they show no evidence of displacement, we suppose that the basal level of the single stage flank-collapse was situated on land, and that the event did not affect the submarine flanks of the island as it may be the case for the islands of Dominica and Saint Lucia. These flows can be related either to the Morne Jacob Complex located immediately north east of the structure, either to a former Pitons des Carbets Volcanic Complex (Westercamp et al., 1990). Note that the lava flow 04MT01 located northwest of the northern rim of the structure, dated at 1.69 ± 0.02 Ma, may also belong to the former volcanic complex affected by the flank-collapse. Debris-avalanche deposits are numerous within the depression (Westercamp et al., 1990) and have not yet been recognized at sea. It can be supposed that most part of materials have been driven away from the coast into the Grenada Basin through the numerous channels located west of the structure, similarly than observed on the west shore of Basse Terre (Deplus et al., 2001; Samper et al., 2006). Following subsequent emplacement in the depression, magmatic activity is now localized northwards, within the Montagne Pelée volcano area. From deposits recognized at sea (Deplus et al., 2001; Le Friant and Boudon, 2003), and morphological evidences on-land, it has been shown that

the latter edifice experienced three successive collapses at about 200-100, 25 and 9 ka (Le Friant and Boudon, 2003).

In Saint Lucia remnants of the previous volcanic complex are found in the collapsed area. For the first time a younger stage of pre-collapse activity is identified around 1 Ma within the area. Post-collapse magmatic activity is characterized by lava dome growth with a relatively low rate of eruption, and has been concentrated within the depression for at least 100 kyr, as attested by several geothermal fields within the structure and the presently on-going fumarolic activity of the Dome of Terre Blanche for which we provide the age of 3 ± 3 ka (Table 1). This is the youngest time constraint available for a volcanic edifice located within the depression and it attests, unlike what was previously assumed, that the Qualibou structure has undergone very recent magmatic activity.

In Dominica, up to three successive flank-collapses have been identified over the last 100 ka (Le Friant et al., 2002). Similarly than previously observed at different settings, such as at La Réunion (Indian Ocean) (Gillot et al., 1994) or at La Martinique for the Montagne Pelée volcano (Le Friant and Boudon, 2003), a decreasing volume and recurrence time are inferred between the successive flank-collapse events of Dominica (Le Friant et al., 2002).

An extensive study of effusive magmatism within Basse-Terre island (Guadeloupe) also using the K-Ar Cassignol-Gillot technique allowed dating of a major flank-collapse affecting the southern part of northern Basse Terre between 659 ± 11 and 629 ± 13 ka (Samper et al., 2006). Then, magmatic activity migrated southwards to build the Grande-Découverte Composite Volcano during the last 200 kyr (Boudon et al., 1989; Carlut et al., 2000; Komorowski et al., 2005). Forty-five thousand years ago, the summit part of the volcanic edifice has been affected by a large caldera collapse event associated with voluminous ash-and-pumice fall and flow deposits (Boudon et al., 1988; Boudon et al., 1989; Boudon et al., 1992; Komorowski et al., 2005; Komorowski et al., 2002). Since, the activity

resumed at the same location and has been characterized by a succession of reconstructions of the volcanic edifice and its destruction by flank-collapse events, nine of them occurring during the last 15 kyr (Komorowski et al., 2005; Komorowski et al., 2002). In the same fashion, the 130 ka old South-Soufrière Hills massif at Montserrat presents at least four sector-collapse scars on its summit area (Harford et al., 2002; Le Friant et al., 2004). The on-going eruption at Soufrière Hills takes place within the most recent scar, the English's Crater sector-collapse area, which formed 2 kyr ago (Boudon et al., 2007). The ~100 ka and youngest events dated here in Dominica and Saint Lucia, as well as those identified in the Montagne Pelée massif, are localized within still active volcanic complexes. Alternatively, in Basse Terre and Martinique, no evidences for younger flank-collapse events are found within the oldest (> 300 ka) horseshoe-shaped structures. After having rapidly filled in these areas with new edifices, volcanic activity has migrated southwards and northwards, in Guadeloupe and Martinique, respectively.

Thus, through an appropriated sampling methodology and the use of the K-Ar Cassignol-Gillot technique, major flank-collapse events have been identified over the last 650 kyr around 650, 335 ka, and many of them in the best documented 0-100 kyr interval. Boudon et al. (2006) discussed the fact that apparent increasing recurrence rates are an artefact due to erosion processes, hence that only the largest events can be recognized for volcanoes of several hundred thousand years old, while more can be identified in the 0-100 kyr interval. However there is no striking recurrence timescale for the collapse events in the Lesser Antilles. (Boudon et al., 2007) discussed the abundance and origin of flank-collapses in the Lesser Antilles Arc on the basis of the evolution of active volcanoes. Thus, they distinguish two main zones: the northern islands Montserrat (Soufrière Hills volcano) and Basse-Terre (La Soufrière volcano, Guadeloupe), and the southern islands from Dominica to Grenada. On the northern islands flank-collapses appear to be repetitive, limited to the summit part of the

edifices thus involving low volumes <1 km^3 and occurring either along different directions or affecting repetitively the same flank of the edifice (Boudon et al., 2007). On the southern islands flank-collapses are less frequent, systematically directed towards the Caribbean Basin and involving more important volumes up to several km^3 to tens of km^3. However, the two oldest large flank-collapses identified in the Lesser Antilles occurred on the island of Basse-Terre towards two different directions, and likely involved several km^3 of material (Samper et al., 2006). Thus we think that the subsequent original eruption rate and the volcanic migration logic within each island has also to be taken into account in order to complete the understanding of flank-collapse phenomena in Lesser Antilles.

Conclusions

The K-Ar Cassignol-Gillot technique applied to the groundmass phase is a powerful technique for dating Lesser Antilles lavas. Analyses on plagioclase crystals showed radiogenic ^{40}Ar excess that yielded excessively old ages, demonstrating that whole rock dating should never be performed. As inferred from previous studies, which identified large magnitude debris-avalanche deposits offshore the islands of Dominica, Saint Lucia and Martinique, flank-collapse is a recurrent process affecting the Lesser Antilles arc volcanoes (Boudon et al., 2007). Although strong tropical erosion does not allow their systematic identification, correlations with on land collapse scars together with dating of key volcanic stages allowed us to constrain through time some of the major regional collapse events (Boudon et al., 2007; Boudon et al., 1987; Le Friant and Boudon, 2003; Le Friant et al., 2002). Our K-Ar ages span from 337 ± 5 ka to present time. Flank-collapse events are a common process in the evolution of Lesser Antilles volcanoes (Boudon et al., 2007; Deplus et al., 2001; Le Friant, 2001). Together with other reliable ages (Samper et al., 2006), our data

give support to the characterization of this phenomenon through time and its recurrence, at least for the last 650 ka.

In Dominica radiometric ages on lavas from the imbricate structures showed that the first of the three flank-collapses identified by (Le Friant et al., 2002) occurred around 100 ka, each new event being of lesser volume and extent than the previous one, as observed on Montagne Pelée in Martinique (Le Friant and Boudon, 2003), for instance. In Saint Lucia, our study revises the formation of the Qualibou depression to about 100 ka, from a new age (95 ± 2 ka) obtained on the post-collapse Petit Piton lava dome. Magmatic activity characterized by dacitic lava dome recurrent growths has continued up to the present. No evidence of younger flank-collapse events has been identified, neither at sea nor on land in St Lucia. In Martinique, the formation of the structure of the Pitons des Carbets is probably not much older than 337 ± 5 ka on the basis of three indistinguishable ages obtained on three different post-collapse lava domes.

Finally, the horse-shoe shaped structures within Dominica, Saint Lucia and Martinique are all open towards the Grenada Basin and located close to its steep eastern slopes. Local tectonic control coupled with favourable global conditions, such as low sea level associated with global temperature decrease (Le Friant and Boudon, 2003), or alternatively, during the rapid onset of a warm climate following cold conditions (Quidelleur et al., 2006), could favour volcanoes instability. Therefore, the recurrence time of flank-collapses events in the Lesser Antilles is linked to tectonic activity, magma production rate and favourable climatic conditions. It can be as high as a few 10^4 years (Komorowski et al., 2005) and extend to several 10^5 years (Samper et al., 2006), probably depending on the combination of these three dominating triggering factors.

Acknowledgments: We thank M. Semet for discussion and for providing us with the ALMA sample from Martinique. We are also grateful to the staff of the Volcanological and Seismological Observatories of Martinique for logistical help. This study was partly supported by a PNRN-INSU program. We thank S. Carrette, C. Schillingford, D. Williams and the Ministry of Agriculture and Environment for assistance and for providing us with the authorization to sample in National Parks of Dominica. This is LGMT contribution No. 67.

References

Aquater, 1982. Exploration of St. Lucia's geothermal ressources, Annex A, Ministry of Finance and Planning.

Boudon, G., Dagain, J., Semet, M.P. and Westercamp, D., 1988. Carte géologique à 1/20000e du massif volcanique de la Soufrière (Département de la Guadeloupe, Petites antilles). BRGM, Orléans.

Boudon, G., Le Friant, A., Komorowski, J.-C., Deplus, C. and Semet, M., 2007. Volcano flank instability in the Lesser Antilles Arc: Diversity of scale, processes, and temporal recurrence. J. Geophys. Res., 112, B08205, doi:10.1029/2006JB004674.

Boudon, G., Semet, M.P. and Vincent, P.M., 1984. Flank failure-directed blast eruption at Soufrière, Guadeloupe, French West Indies: A 3,000-year-old Mt. St. Helens ? Geology, 12: 350-353.

Boudon, G., Semet, M.P. and Vincent, P.M., 1987. Magma and hydrothermally driven sector collapses: the 3100 and 11,500 Y. B.P. eruptions of La Grande-Découverte (La Soufrière) volcano, Guadeloupe, French West Indies. J. Volcanol. Geotherm. Res., 33: 317-323.

Boudon, G., Semet, M.P. and Vincent, P.M., 1989. The Evolution of la Grande Découverte (la Soufrière) volcano, Guadeloupe (F.W. I.). In: J. Latter (Editor), Volcanic hazards: assessment and monitoring. IAVCEI Proceedings in Volcanology, Berlin, pp. 86-109.

Boudon, G., Semet, M.P. and Vincent, P.M., 1992. Major flank collapse at Pitons du Carbet volcano, Martinique: one of the largest similar structure in the Lesser Antilles arc, 29th International Geological Congress, Kyoto, Japan, pp. 505.

Briden, J.C., Rex, D.C., Fallar, A.M. and Tomblin, J.F., 1979. K-Ar geochronology and palaeomagnetism of volcanic rocks from the Lesser Antilles Island Arc. Phil. Trans. R. Soc. Lond. Ser. A, 291: 485-258.

Carlut, J., Quidelleur, X., Courtillot, V. and Boudon, G., 2000. Paleomagnetic directions and K/Ar dating of 0-1 Ma lava flows from La Guadeloupe Island (French West Indies) : Implications for time averaged field models. J. Geophys. Res., 105: 835-849.

Carracedo, J.C., Day, S.J., Guillou, H. and Torrado, F.J.P., 1999. Giant Quaternary landslides in the evolution of La Palma and El Hierro, Canary Islands. J. Volcanol. Geotherm. Res., 94(1-4): 169-190.

Cassignol, C. and Gillot, P.-Y., 1982. Range and effectiveness of unspiked potassium-argon dating: Experimental groundwork and applications. Numerical Dating in Stratigraphy. John Wiley, New York, 159-179 pp.

Clouard, V., Bonneville, A. and Gillot, P.Y., 2001. A giant landslide on the southern flank of Tahiti Island, French Polynesia. Geophys. Res. Lett., 28: 2253-2256.

Deplus, C. et al., 2001. Submarine Evidence for Large-scale Debris Avalanches in the Lesser Antilles Arc. Earth Planet. Sci. Lett., 192: 145-157.

Feuillet, N., Manighetti, I., Tapponnier, P. and Jacques, E., 2002. Arc parallel extension and localization of volcanic complexes in Guadeloupe, Lesser Antilles. J. Geophys. Res., 107(B12): 2331, doi:10.1029/2001JB000308.

Gillot, P.-Y. and Cornette, Y., 1986. The Cassignol technique for potassium-argon dating, precision and accuracy: examples from late Pleistocene to recent volcanics from southern Italy. Chem. Geol., 59: 205-222.

Gillot, P.-Y., Lefèvre, J.-C. and Nativel, P.-E., 1994. Model for the structural evolution of the volcanoes of Réunion Island. Earth Planet. Sci. Lett., 122(3-4): 291-302.

Gillot, P.Y., Cornette, Y., Max, N. and Floris, B., 1992. Two reference materials, trachytes MDO-G and ISH-G, for argon dating (K-Ar and 40Ar/39Ar) of Pleistocene and

Holocene rocks. Geostandards Newsletter, 16(1): 55-60.
Harford, C.L., Pringle, M.S., Sparks, R.S.J. and Young, S.R., 2002. The volcanic evolution of Montserrat using $^{40}Ar/^{39}Ar$ geochronology. Geological Society, London, Memoirs, 21: 93-113.
Hildenbrand, A., Gillot, P.-Y. and Le Roy, I., 2004. Volcano-tectonic and geochemical evolution of an oceanic intra-plate volcano : Tahiti-Nui (French Polynesia). Earth Planet. Sci. Lett., 217: 349-365.
Hildenbrand, A., Gillot, P.Y., Soler, V. and Lahitte, P., 2003. Evidence for a persistent uplifting of La Palma (Canary Islands), inferred from morphological and radiometric data. Earth Planet. Sci. Lett., 210: 277-289.
Komorowski, J.C. et al., 2005. Guadeloupe. In: S.R. Unit (Editor), Volcanic hazard atlas of the Lesser Antilles. University of the West Indies, St Augustine, Trinidad , W.I., pp. 67-104.
Komorowski, J.C., Boudon, G., Semet, M., Villemant, B. and Hammouya, G., 2002. Recurrent flank-collapses at Soufrière of Guadeloupe volcano: implications of acid hydrothermal fluids on edifice stability Mount Pelée 1902-2002, Explosive volcanism in subduction zones, IPGP-INSU-IAVCEI Internatinal Congress, Martinique, 12-16 mai 2002.
Le Friant, A., 2001. Les déstabilisations de flanc des volcans actifs de l'arc des Petites Antilles : origines et conséquences. Thèse de Doctorat Thesis, Université Paris 7 - Denis Diderot, 378 pp.
Le Friant, A. and Boudon, G., 2003. Large-scale flank collapse events during the activity of Montagne pelée, Martinique, Lesser Antilles. J. Geophys. Res., 108: 2055.
Le Friant, A., Boudon, G., Komorowski, J.-C. and Deplus, C., 2002. L'île de la Dominique, à l'origine des avalanches de débris les plus volumineuses de l'arc des Petites Antilles. C.R. Geoscience, 334: 235-243.
Le Friant, A. et al., 2004. Geomorphological evolution of Montserrat (West Indies): importance of flank collapse and erosional processes. J. Geol. Soc. London, 161: 147-160.
Lindsay, J.M., 2005. Saint Lucia. In: S.R. Unit (Editor), Volcanic hazard atlas of the Lessser Antilles. University of the West Indies, St Augustine, Trinidad , W.I., pp. 218-238.
Lindsay, J.M., Stasiuk, M.V. and Shepherd, J.B., 2003. Geological history and potential hazards of the late-Pleistocene to Recent Plat Pays volcanic complex, Dominica, Lesser Antilles. Bull. Volcanol., 65(2-3): 201-220.
Mattioli, G.S., Jansma, P.E., Jaramillo, L. and Smith, A.L., 1995. Sector collapse in island arc volcanoes: a digital topographic and bathymetric investigation of the Qualibou depression, St. Lucia, Lesser Antilles. Carribean Journal of Science, 31: 163-173.
Moore, J.G., Normark, W.R. and Holcomb, R.T., 1994. Giant Hawaiian landslides. Ann. Rev. Earth Planet. Sci., 22: 119-144.
Odin, G.S. and al., e., 1982. Interlaboratory standards for dating purposes. In: G.S. Odin (Editor), Numerical dating in stratigraphy. John Wiley and Sons, Chichester, pp. 123-150.
Pinel, V. and Jaupart, C., 2000. The effect of edifice load on magma ascent beneath a volcano. Phil. Trans. R. Soc. Lond., 358: 1515-1532.
Presley, T.K., Sinton, J.M. and Pringle, M., 1997. Postshield volcanism and catastrophic mass wasting of the Waianae volcano, Oahu, Hawaii. Bull. Volcanol., 58: 597-616.
Quidelleur, X., Gillot, P.Y., Soler, V. and Lefèvre, J.C., 2001. K/Ar dating extended into the last millennium: Application to the the youngest effusive episode of the Teide volcano (Spain). Geophys. Res. Lett., 28: 3067-3070.
Quidelleur, X., Hildenbrand, A. and Samper, A., 2006. Link between quaternary

paleoclimatic changes and volcanic oceanic islands evolution. Quaternary Geochronology: submitted.
Reid, R.P., Carey, S.N. and Ross, D.R., 1996. Late quaternary sedimentation in the Lesser Antilles island arc. Geol. Soc. Am. Bull., 108: 78-100.
Roobol, M.J., Wright, J.V. and Smith., A.L., 1983. Calderas or gravity-slide structures in the Lesser Antilles island arc ? J. Volcanol. Geotherm. Res., 19: 121-134.
Samper, A., Quidelleur, X., Lahitte, P. and Mollex, D., 2006. Timing of effusive volcanism whithin the whole Basse Terre Island (Guadeloupe, F.W.I.) from new K-Ar Cassignol-Gillot Ages. Earth Planet. Sci. Lett.: submitted.
Smith, W.H.F. and Sandwell, D.T., 1997. Global sea floor topography from satellite altimetry and ship depth soundings. Science, 277(5334): 1956-1962.
Sparks, R.S.J. et al., 2002. Generation of a debris-avalanche and violent pyroclastic density current: the Boxing Day eruption of 26 december 1997 at the Soufrière Hills Volcano, Montserrat. In: T.H. Druitt and B.P. Kokelaar (Editors), The eruption of Soufrière Hills Volcano, Montserrat, from 1995 to 1999, London Geol. Soc., Memoirs, pp. 409-434.
Steiger, R.H. and Jäger, E., 1977. Subcommission on Geochronology: convention on the use of decay constants in Geo and Cosmochronology. Earth Planet. Sci. Lett., 36: 359-362.
Tomblin, J.F., 1965. The geology of the Soufrière volcanic centre, St. Lucia, Fourth Caribbean Geological Conference, Trinidad, pp. 367-376.
Vincent, P.M., Bourdier, J.L. and Boudon, G., 1989. The primitive volcano of Mount Pelée: its construction and partial destruction by flank collapse. J. Volcanol. Geotherm. Res., 38: 1-15.
Voight, B. et al., 2002. The 26 December (Boxing Day) 1997 sector collapse and debris-avalanche at Soufrière Hills Volcano, Montserrat. In: T.H. Druitt and B.P. Kokelaar (Editors), The eruption of Soufrière Hills Volcano, Montserrat, from 1995 to 1999. Geological Society, London, Memoirs, pp. 363-407.
Wadge, G., 1985. Morne Patates Volcano, Southern Dominica, Lesser Antilles. Geological Magazine, 122(3): 253-260.
Westercamp, D., Pelletier, B., Thibaut, P.M., Traineau, H. and Andreieff, P., 1990. Carte géologique de la France (1/50 000), feuille Martinique. BRGM, Orléans.
Wohletz, K. et al., 1986. The Qualibou Caldera, St-Lucia, West-Indies. J. Volcanol. Geotherm. Res., 27(1-2): 77-115.
Wright, J.V. et al., 1984. Late Quaternary Explosive Silicic Volcanism on St-Lucia, West-Indies. Geological Magazine, 121(1): 1-15.
Young, S. et al., 2002. Hazard implications of small-scale edifice instability and sector collapse: a case history from Soufrière Hills volcano, Montserrat. In: T.H. Druitt and B.P. Kokelaar (Editors), The eruption of Soufrière Hills Volcano, Montserrat, from 1995 to 1999. Geological Society, London, Memoirs, pp. 349-361.

Fig. captions

Fig. 1.: Geodynamic setting of the Lesser Antilles Arc (G. and M.: Guadeloupe and Montserrat islands, respectively). Bathymetry from (Smith and Sandwell, 1997) and localization of main faults from (Feuillet et al., 2002). Inserted bathymetric map localizes the three islands studied, as well as the morphological fronts of DADs taken from (Deplus et al., 2001), originating from the on-land horseshoe-shaped structures.

Fig. 2.: Simplified geological map of Plat Pays volcanic complex, Dominica from (Le Friant et al., 2002). Localization and ages of the three dated samples is shown. Black areas represent debris-avalanche deposits, grey areas represent post-collapse slided blocks, white areas represent dacitic domes. Escarpments delimit the collapsed structure.

Fig. 3.: Simplified geological map of the Qualibou Structure, St. Lucia from (Le Friant, 2001). Localization and ages of the four dated samples is shown.

Fig. 4.: Martinique Island shaded digital elevation model (horizontal and altitudinal resolution is 50 and 15 m, respectively; light from north; data IGN). Localization and ages of the seven dated samples is shown (in black: pre-collapse volcanic formations; in white: post-collapse volcanic formations).

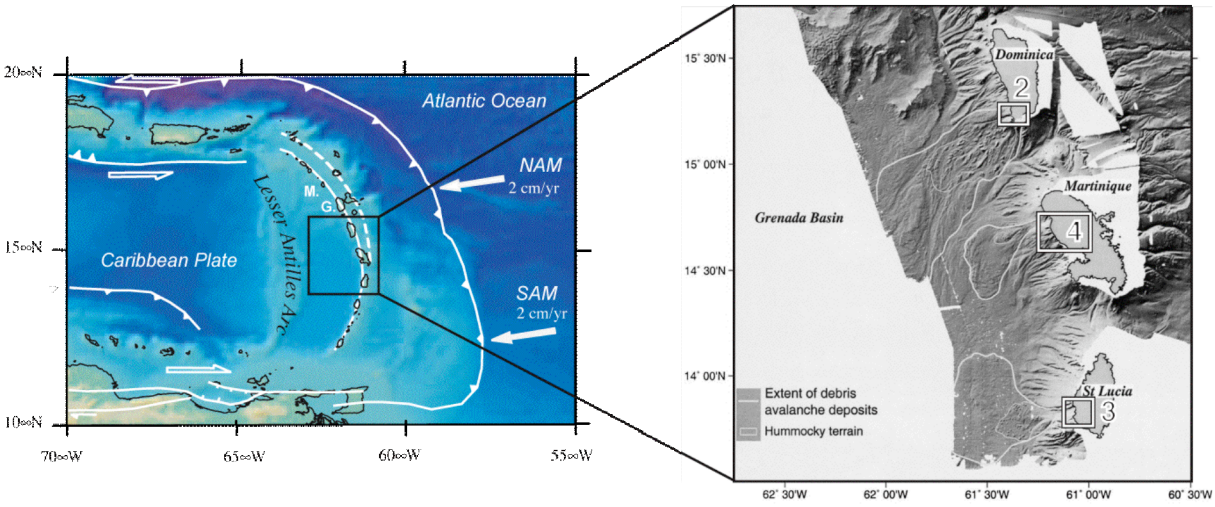

Figure 1 (Samper et al., 2007)

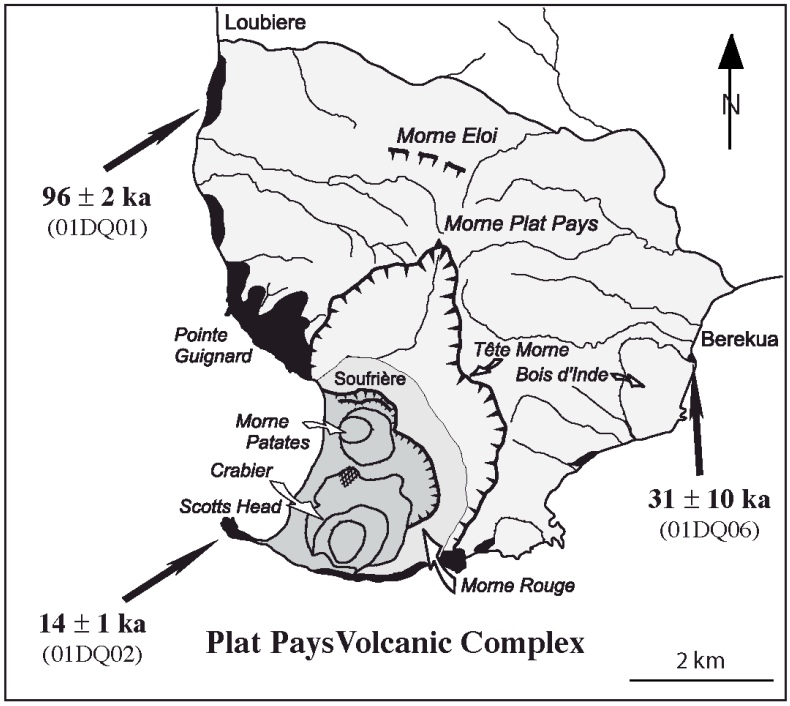

Figure 2 (Samper et al., 2007)

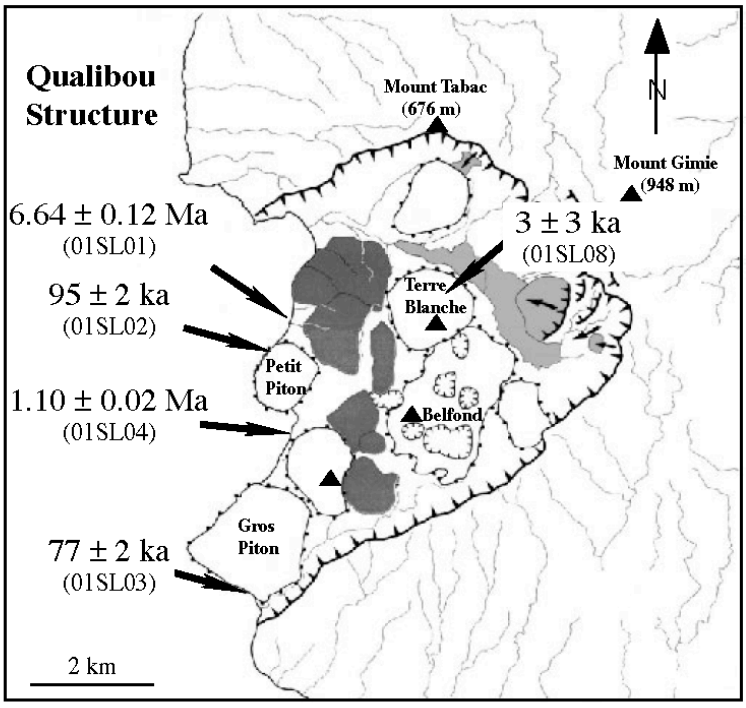

Figure 3 (Samper et al., 2007)

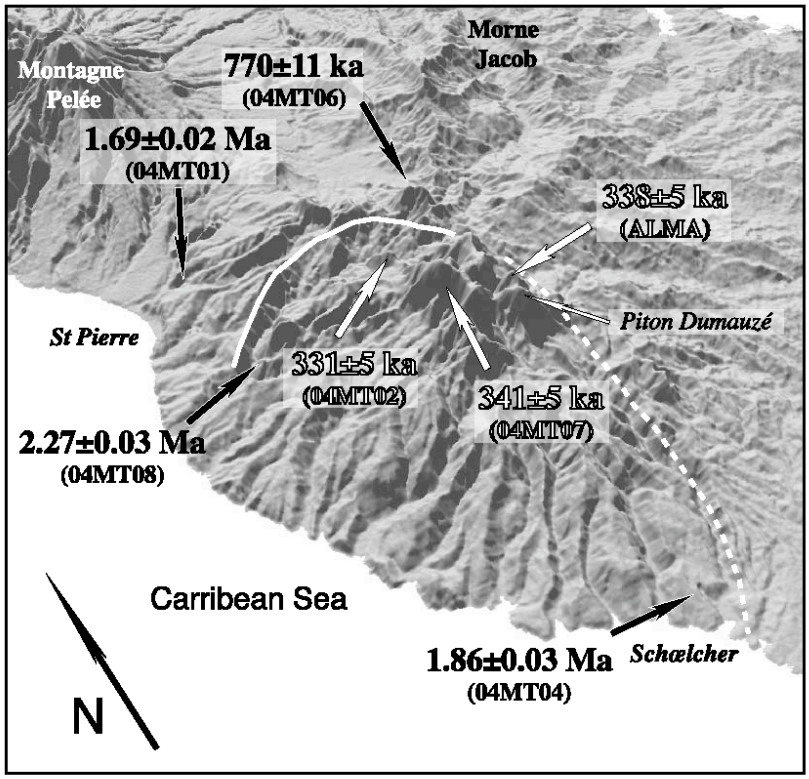

Figure 4 (Samper et al., 2007)

Causal link between Quaternary paleoclimatic changes and volcanic islands evolution

Quidelleur, X.*, Hildenbrand, A. and Samper, A.

Laboratoire IDES, UMR 8148 CNRS-UPS
Université Paris Sud 11, Bâtiment 504, 91405 Orsay cedex (France)

* Corresponding author; email: xavier.quidelleur@u-psud.fr

Submitted to Geophys. Res. Lett., August 2007

Words count (abstract+text+52 references): 4753

Abstract

Giant landslides and resulting tsunamis represent the main geologic hazards linked to volcanic island evolution [*McMurtry et al.*, 2004; *Moore et al.*, 1994; *Ward and Day*, 2001]. From bathymetric data and onland geological studies, flank failures have been identified around numerous volcanic islands, in most geodynamic contexts. However, the enabling and triggering conditions are still poorly understood and several internal and external causes may act simultaneously to reach a critical threshold [*McGuire*, 1996]. Here we show that most large volume (>10 km^3) landslides occur at glacial stages termination and we propose that a causal relationship between flank collapse of volcanic islands and global climatic changes has existed at least since 900 kyr. Moreover, ages reported here favour the hypothesis that major flank collapse events occurred during the onset of glacial to interglacial transitions when a sudden influx of melt water from polar ice caps causes rapid sea level rise. We propose that following a sub aerial erosion interval during low sea level stands, rapid sea level rise induces enhanced coastal erosion and sudden changes of pore pressure conditions within basal layers, which favour edifice failure. Finally, the effect of climate warming trough sea level changes revealed here will help to better appraise the geological hazard linked to oceanic island collapses.

Keywords: Quaternary, Sea level, Flank collapses, Volcanic islands

1. Introduction

Flank collapses events from volcanic islands have been reported for intraplate oceanic islands at Hawaii [*Moore et al.*, 1994], Canary Islands [*Carracedo et al.*, 1999; *Masson et al.*, 2002; *Watts and Masson*, 1995], Tahiti [*Clouard et al.*, 2001; *Hildenbrand et al.*, 2004], La Réunion [*Gillot et al.*, 1994; *Oehler et al.*, 2004] and Cape Verde Islands [*Day et al.*, 1999; *Elsworth and Day*, 1999], for instance, and in oceanic arcs [*Deplus et al.*, 2001; *Kokelaar and Romagnoli*, 1995; *Satake and Kato*, 2001]. They also affect volcanic edifices built on continental crust but usually with a volume far smaller than on oceanic island volcanoes. In the present study, only large volume (> 10 km^3) landslides, all of them from oceanic islands, are considered. Several internal and external causes have been proposed as the main triggering condition [*McGuire*, 1996]. Volcanic rift zones have been recognized in many oceanic islands and have been linked to edifice failures [*Siebert*, 1984]. They concentrate magma upwelling as dyke swarms, which can trigger instability by strength reduction through thermal or mechanical pressurization of pore fluids [*Elsworth and Day*, 1999], or by the growth of an anomalously high topographic load [*McGuire*, 1996]. Slope angle and gravitational instability certainly favour failure, but low-angle edifices such as shield volcanoes are also prone to large flank destabilizations. Asymmetric building onto a dipping basement can direct collapses towards a preferred direction. Such structural control of preferred landslide direction has been advocated in the Lesser Antilles [*Deplus et al.*, 2001]. Caldera collapse events can also be associated with flank collapses, and has even been proposed as the main triggering factor for the formation of the Las Cañadas depression at Tenerife [*Hürlimann et al.*, 1999]. However, the exact relationship between directed blast, caldera formation and flank failure remains difficult to establish [*Siebert*, 1984]. Instantaneous destabilization of weakened edifices can result from strong regional

earthquakes, or from seismicity along listric basement faults acting as decollement surfaces. Reduction of strength of the basal volcanic layers by hydrothermal alteration and/or increased pore fluid pressure during high rainfall periods can also favour instability.

A significant increase in explosive volcanism since the Early Miocene has been reported and was interpreted as a consequence of the rapidly changing climatic conditions which have characterized this interval [*Kennett and Thunell*, 1975]. This correlation has also been recognized over shorter time scales in the distribution of tephra layers within $\delta^{18}O$ changes recorded in Greenland GISP2 ice core [*Zielinski et al.*, 1996], and in the Mediterranean basin [*McGuire et al.*, 1997; *Paterne and Guichard*, 1993], during the last 110 kyr.

In order to investigate a possible relationship between global Quaternary climatic changes and catastrophic mass wasting affecting oceanic islands, high quality age determinations of these events are required. Two approaches are followed, but well dated events remain scarce.

The first dating approach [*McMurtry et al.*, 1999] is based on the $\delta^{18}O$ stratigraphy from below and above turbidite deposits, or directly, but with the danger of analysing reworked sediments, of pelagic sediments entrained into the turbidite during mass wasting events.

The second approach is based on radiometric dating, most often using the K/Ar Cassignol-Gillot technique [*Gillot and Cornette*, 1986], which is specially suitable to Quaternary volcanics [*Quidelleur et al.*, 2003] up to the last millennium [*Quidelleur et al.*, 2001]. This technique relies on severe sample selection followed by meticulous mineralogical separation of the fresh volcanic groundmass, the mineral phase which crystallized last, during sub-aerial lava flow emplacement. Any concern related to excess (mantle derived) argon, or Ar or K loss during weathering is therefore avoided. Furthermore, without the need for

artificial sample irradiation, no ^{39}Ar recoil, nor high isotopic interferences correction necessary with the $^{40}Ar/^{39}Ar$ technique for basalt and andesite samples [*McDougall and Harrison*, 1999] are required here. Accurate age determinations of flank failure are challenging because direct radiometric dating of these events is not feasible in most case, unless the collapse is associated with the emplacement of a pyroclastic blast, which can be dated if its mineralogical content is favourable. Alternatively, an age can be derived by bracketing the event using ages of the last volcanic flows emplaced before the collapse, as well as the post-collapse magmatism. However, due to the lack of age data, only a few events are well constrained by both pre and post-collapse magmatism. Furthermore, sparse post-collapse volcanism on the outer flanks outside the collapse scar can bias such approach. In the present study, we then rely only on the age of the volcanic edifice emplaced after the collapse. Physical modelling and field studies have shown that volcanoes collapse is generally immediately followed by renewed activity. This has been related to pressure released within the magma chamber subsequently to collapse deloading [*Pinel and Jaupart*, 2000]. At Tahiti, rapid in fill on the northern depression, caused by the northern flank collapse, was made with a rate of 5 km^3/kyr, while it was estimated to a maximum of 2 km^3/kyr before the collapse [*Hildenbrand et al.*, 2004]. A causal link between collapse events and renewed activity has also been evidenced at Oahu (Hawaii), where mass wasting triggered volcanism is associated with increased partial melting [*Presley et al.*, 1997]. The time interval between collapse and renewed volcanism is therefore probably short, and our interpretations for collapses dated by radiometric ages using post-collapse volcanism can then only be biased towards too young ages.

2. Ages of well constrained flank collapses

In the Canary archipelago large debris avalanches have been identified around the young volcanic islands of La Palma, El Hierro and Tenerife. At La Palma, the development of the 5 km wide erosion caldera de Taburiente has been linked with the Cumbre Nueva collapse of the northern shield, followed by the rapid emplacement of the Bejenado volcano within the collapse scar [*Carracedo et al.*, 1999]. The associated debris avalanche deposits observed on the ocean floor to the west of the island cover an area of 780 km^2, with an estimated volume of about 100 km^3 [*Masson et al.*, 2002]. The last construction stage of the northern shield on the rim of the Taburiente has been dated at 566±8 ka, while the earliest basal stage of the post-collapse Bejenado volcano is 537±8 ka old [*Guillou et al.*, 2001]. The later age is our best estimate for the Cumbre Nueva collapse. Several large-scale collapses have affected El Hierro, the westernmost Island of the archipelago [*Carracedo et al.*, 1999; *Gee et al.*, 2001; *Krastel et al.*, 2001; *Masson*, 1996; *Masson et al.*, 2002; *Mitchell et al.*, 2002]. The debris avalanche of El Golfo, with its clearly associated embayment onland, covers an area of 1500-2600 km^2, for a volume of about 150-180 km^3, while volume and extent of the underlying Tinor landslide are difficult to retrieve. The Tinor volcano developed between 1.12 Ma and 882 ka [*Guillou et al.*, 1996] and was then affected by a large-scale North West directed collapse after 882±10 ka [*Carracedo et al.*, 1999]. However, due to the lack of post-collapse volcanism, this event is not considered further here. Latter collapses of Las Playas and El Julan are not well dated enough, but the El Golfo event is better constrained, with a two stages landslide [*Carracedo et al.*, 1999], the first at 134±6 ka and the second at 15±2 ka, based on K-Ar dating of pre- and post collapse lavas, respectively [*Guillou et al.*, 1996]. From the lack of strong evidences in the debris avalanche deposits offshore, the two stages hypothesis has been questioned [*Masson et al.*, 2002]. However, on-land studies seem to argue for the two stages hypothesis [*Carracedo et al.*, 1999], which is considered here

(Table1). On the island of Tenerife, several horse-shoe shaped valleys located across the NE rift zone have been related to major flank collapse events [*Ablay and Hürlimann*, 2000; *Krastel et al.*, 2001; *Masson et al.*, 2002; *Watts and Masson*, 1995]. Orotava and Icod valleys are directed to the North West and Guimar to the South East. Only the Icod landslide, the youngest of these events is sufficiently well dated. Its offshore deposits extend to 1700 km^2 with a volume of 150 km^3. The Teide volcano emplaced subsequently to the landslide, on top of the resulting "Mortalon" breccia. Dating of the lowermost lava flow of the Teide, sampled within a water-recovery gallery at the contact with the landslide breccia, constrained the Icod landslide at 161 ± 5 ka [*Gillot et al.*, 2001]. This age is in good agreement with the Ar/Ar ages of 163 ± 1 ka [*van den Bogaard and Schirnick*, 2001] and 169 ± 1 ka [*Brown et al.*, 2003] obtained from sanidine separates from the plinian eruption of El Abrigo, which has been related to the Icod landslide.

Offshore bathymetry measurements have demonstrated that recurrent mass wasting events have affected most islands from the Lesser Antilles volcanic arc within the last 200-100 kyr, with associated volumes of about 30 and 20 km^3 reported off southern Dominica and Montagne Pelée (Martinique), respectively [*Deplus et al.*, 2001]. Unfortunately, no precise ages are available for these events [*Le Friant and Boudon*, 2003; *Le Friant et al.*, 2002]. Due to the relatively high sedimentation rate within the Grenada basin, older collapse events cannot be identified offshore, but on-land morphological studies coupled with precise K/Ar age determinations allowed the identification and dating of two major events on Guadeloupe and Martinique Islands. An age of 659±11 ka was obtained for the last construction phase of the pre-collapse Matéliane volcano (Guadeloupe Island), and a younger age of 629±13 ka, which therefore dates the collapse, was obtained for the Icaques volcano emplaced subsequently within the landslide depression [*Samper et al.*, 2007]. Large debris avalanche deposits found on-land within a large horseshoe-shaped depression demonstrated that a major

flank collapse event, with a volume estimated around 30-40 km^3, occurred on Martinique, and was followed by the rapid emplacement of the Pitons du Carbet at 337±5 ka [*Quidelleur et al.*, 2004], which represents the best age estimate for this collapse.

Catastrophic mass wasting events have been imaged around all the islands of the Hawaiian archipelago. Submarine areas covered by the deposits typically range from 2,000 to 15,000 km^2, and estimated volumes amount to 5000 km^3 [*Moore et al.*, 1994]. As many as 68 major landslides were reported along the Hawaiian stretch, from Midway to the island of Hawaii, with an average rate of one major landslide every 350 kyr [*Moore et al.*, 1994], estimate recently revised to a much shorter recurrence time [*Garcia et al.*, 2006]. Unfortunately, only the Alika phase 1 collapse from the Mauna Loa volcano (Big Island) is well dated with an age of 127±5 ka derived from the correlation between high $\delta^{18}O$ values measured from planktonic foraminiferal assemblages, sampled within turbidite deposits, and the global reference curves [*McMurtry et al.*, 1999]. Unfortunately, probably because of the low K content of shield building tholeiiic basalts, none of the Hawaiian collapses is accurately dated by the K-Ar method.

Following the construction of a first shield volcano, between 1.37 ± 0.02 Ma and 0.87 ± 0.02 Ma [*Hildenbrand et al.*, 2004], Tahiti Island (French Polynesia) experienced two major flank collapses directed south and north, respectively. The former, identified offshore, has an estimated volume of 300 km^3 onshore with a total debris volume of 1150 km^3 [*Clouard et al.*, 2001]. The latter left an onland depression volume of 400-450 km^3 and offshore debris volume of about 800 km^3 [*Hildenbrand et al.*, 2006]. Both landslides have been related to the E-W rift zone developed during the subaerial growth of the main shield. The subsequent emplacement of the second shield volcano within the northern collapse depression started at 872 ± 10 ka [*Hildenbrand et al.*, 2004], which then can be used as the accurate dating of the northern collapse (Table 1).

Bathymetric investigations of the surrounding sea floor have shown that mass wasting events are common features of Réunion Island (Indian Ocean) [*Oehler et al.*, 2004]. Onland studies associated with K-Ar dating demonstrated that recurrent flank collapses have affected the whole island since 2 Ma [*Gillot et al.*, 1994]. The three last lateral collapses of Caldera des Remparts, Caldera des Sables and Enclos Fouqué are constrained to 250 ± 30 ka, 35 ± 8 ka and 5 ± 1 ka, respectively [*Gillot et al.*, 1994]. Unfortunately, the relatively large age uncertainty, due to the lack of sampling of the base of post-collapse lava flows, associated with the oldest and most important one prevents the use of these results here.

3. Discussion

All major flank collapses affecting volcanic islands with well-constrained timing control, most often obtained using the K-Ar Cassignol Gillot technique [*Gillot and Cornette*, 1986] are reported in Table 1. Figure 1 shows the correlation of these events with Quaternary climate changes as described by a global stack of benthic $\delta^{18}O$ records [*Lisiecki and Raymo*, 2005]. It is striking to note that most collapses occurred within a glacial to interglacial termination. As previously suggested for the onset of interglacial stage 5.5 (about 125 ka) [*Carracedo et al.*, 1999; *McMurtry et al.*, 1999], we show here that a direct link between climatic change and long-term evolution of oceanic volcanoes prevailed during the last 900 kyr (Fig. 1).

To a first order, $\delta^{18}O$ variations can be considered as a good proxy for sea level changes resulting from glacial-interglacial cycles, with an inverse relationship between $\delta^{18}O$ values and relative sea level [*Lambeck et al.*, 2002]. In order to further identify the causal link between climate change and volcanic collapse, it is necessary to discriminate if volcanic collapses occur during high sea level intervals, and are thus favoured by hot and humid climatic conditions, or, alternatively, if they occur during drier climate under low sea level

stand. Figure 1 shows that most events are rather located towards the onset of the rapid climatic changes, except Tenerife collapse, which occurred during a secondary minimum of a glacial interval. Within uncertainty, they all include the coldest intervals (high value of $\delta^{18}O$, i.e. minima in Fig. 1). In addition, since the dating approach followed here is mainly based on the age of the post-collapse volcanic emplacement, the age of the collapse itself can only be biased towards younger ages and the ages reported here (Table 1 and Fig. 1) must be considered as strict younger bounds.

The youngest collapse of El Hierro (Table 1) has been related with a volcanoclastic turbidite emplaced on the Madeira abyssal plain during the last deglaciation, between oxygen isotopic stages 2 and 1 [*Masson*, 1996]. Similarly, the intermediate values of $\delta^{18}O$ recorded within the associated turbidite [*McMurtry et al.*, 1999] demonstrate that the Alika 2 giant landslide occurred during the fast glacial-interglacial climatic change, between isotopic stages 6 and 5.

All the above lines of evidence allow us to propose a model in which large scale flank collapses of volcanic islands occurred during rapid sea-level rise associated with deglaciation. However, this is not exclusive and collapses, although with a much smaller volume than those reported here (Table 1), have occurred within the last interglacial stage, at Stromboli [*Gillot and Keller*, 1993; *Kokelaar and Romagnoli*, 1995], Martinique Island [*Le Friant and Boudon*, 2003], or La Réunion [*Gillot et al.*, 1994], for instance. Furthermore, flank collapses involving a few km^3 of material took place during the historic period in Japan (Oshima-Oshima island; [*Satake and Kato*, 2001]) and in New Guinea (Ritter island; [*Ward and Day*, 2003]), in 1741 and 1888 A.D., respectively. These events can be interpreted as delayed collapses of weakened edifices, but are, in any case, one or several order of magnitude of those investigated here (Table 1).

Our hypothesis is apparently in contradiction to the suggestion that large failures are related to increased retention of groundwater during wet and warm climates characterizing interglacial periods [*McMurtry et al*., 2004]. However, the detailed patterns of sea level rise and rainfall at the transition between glacial to interglacial at tropical latitude needs further investigations.

Paleo-sea level determinations, inferred from the direct dating of Barbados corals by U-Th, showed that the last deglaciation occurred with several surges in melt water [*Bard et al*., 1990]. Moreover, rapid flux of fresh water over 100 to 500 years through partial collapse of ice sheets has been reported at the onset of the deglaciation, around 19 ka [*Clark et al*., 2004]. One can suppose that at the end of glacial periods, when the ice sheet growth is high, the onset of the deglaciation process and the subsequent rapid sea level rise affect the stability of volcanic edifices and can trigger large flank collapses, such as those reported here for the last 900 kyr.

Several mechanisms can be proposed. During the low sea level stands, the equilibrium level of oceanic island rivers is lowered, producing an important vertical deepening of submarine canyons, which significantly alters the edifice stability. Then, when sea level rapidly rises, marine coastal erosion is strongly enhanced [*Hapke and Green*, 2006] and can destabilize the weakened volcanic edifice. In a similar fashion, it can also be proposed that the rapid sea level rise strongly changes the pore pressure conditions of porous layers such as soils and/or pyroclastic deposits, which were subaerial during low sea level stages and then previously dried due to a lowered basal water table. Such surfaces would act as the main decollement layers where the collapse initiates during rapid sea level rise.

4. Conclusions

Large volume (>10km^3) flank failures have been identified in several volcanic islands, but direct dating of these events remains rarely available. We present here the compilation of all available ages that constrain the timing of these events. Most of them were acquired using the K-Ar radiometric method with analytical uncertainty of about 1-2 %. Our approach is mainly based on dating of post magmatism emplaced subsequently to collapse, within the scar, and therefore represents a younger bound for the timing of collapse events. The comparison between these ages and sea level changes allow s us to propose a causal link between flank collapse of volcanic islands and global climatic changes during late Quaternary (i.e. during the last 900 kyr). Effectively, most collapses occurred within a glacial to interglacial termination. Moreover, we propose that major flank collapse events took place at the older bounds of these intervals, during the onset of glacial to interglacial transitions, when sudden influx of melt water from polar ice caps causes rapid sea level rise. However, our conclusions, based on a still limited database, need to be reinforced by additional ages of flank collapses, when these will become available. Finally, this study highlights the need for high precision ages from Quaternary volcanic edifices to infer any mutual influences of global changes and volcanic eruptions.

References

Ablay, G., and M. Hürlimann, Evolution of the north flank of Tenerife by recurrent giant landslides, *J. Volcanol. Geotherm. Res.*, *103*, 135-159, 2000.

Bard, E., B. Hamelin, and R.G. Fairbanks, U-Th ages obtained by mass spectrometry in corals from Barbados: sea level during the past 130,000 years, *Nature*, *346*, 456-458, 1990.

Brown, R.J., T.L. Barry, M.J. Branney, M.S. Pringle, and S.E. Bryan, The Quaternary pyroclastic succession of southeast Tenerife, Canary Islands: explosive eruptions, related caldera subsidence, and sector collapse, *Geological Magazine*, *140* (3), 265-288, 2003.

Carracedo, J.C., S.J. Day, H. Guillou, and F.J.P. Torrado, Giant Quaternary landslides in the evolution of La Palma and El Hierro, Canary Islands, *J. Volcanol. Geotherm. Res.*, *94* (1-4), 169-190, 1999.

Clark, P.U., A.M. McCabe, A.C. Mix, and A.J. Weaver, Rapid rise of sea level 19,000 years ago and its global implications, *Science*, *304* (5674), 1141-1144, 2004.

Clouard, V., A. Bonneville, and P.Y. Gillot, A giant landslide on the southern flank of Tahiti Island, French Polynesia, *Geophys. Res. Lett.*, *28*, 2253-2256, 2001.

Day, S.J., S.I.N. Heleno da Silva, and J.F.B.D. Fonseca, A past giant lateral collapse and present-day flank instability of Fogo, Cape Verde Islands, *J. Volcanol. Geotherm. Res.*, *94*, 191-218, 1999.

Deplus, C., A. Le Friant, G. Boudon, J.-C. Komorowski, B. Villemant, C. Harford, J. Ségoufin, and J.-L. Cheminée, Submarine Evidence for Large-scale Debris Avalanches in the Lesser Antilles Arc, *Earth Planet. Sci. Lett.*, *192*, 145-157, 2001.

Elsworth, D., and S.J. Day, Flank collapse triggered by intrusion: the Canarian and Cape Verde Archipelagoes, *J. Volcanol. Geotherm. Res.*, *94*, 323-340, 1999.

Garcia, M.O., S.B. Sherman, G.F. Moore, R. Goll, I. Popova-Goll, J.H. Nathland, and G. Acton, Frequent landslides from Ko'olau volcano: results from ODP hole 1223A, *J. Volcanol. Geotherm. Res.*, *151*, 251-268, 2006.

Gee, M.J.R., A.B. Watts, D.G. Masson, and N.C. Mitchell, Landslides and the evolution of El Hierro in the Canary Islands, *Marine Geology*, *177* (3-4), 271-293, 2001.

Gillot, P.-Y., and Y. Cornette, The Cassignol technique for potassium-argon dating, precision and accuracy: examples from late Pleistocene to recent volcanics from southern Italy, *Chem. Geol.*, *59*, 205-222, 1986.

Gillot, P.-Y., J.-C. Lefèvre, and P.-E. Nativel, Model for the structural evolution of the volcanoes of Réunion Island, *Earth Planet. Sci. Lett.*, *122* (3-4), 291-302, 1994.

Gillot, P.Y., and J. Keller, Radiochronological dating of Stromboli, *Acta Vulcanologica*, *3*, 69-77, 1993.

Gillot, P.Y., V. Soler, and X. Quidelleur, Piling rate and magmatic evolution through time of the Teide volcano (Tenerife, Canary islands), in *EUG XI meeting*, edited by E.U.o. Geosciences, pp. 803, Terra Abstracts, Strasbourg, 2001.

Guillou, H., J.C. Carracedo, and R.A. Duncan, K-Ar, 40Ar/39Ar ages and magnetostratigraphy of Brunhes and Matuyama lava sequences from La Palma Island, *J. Volcanol. Geotherm. Res.*, *106*, 175-194, 2001.

Guillou, H., J.C. Carracedo, F.J.P. Torrado, and E.R. Badiola, K-Ar ages and magnetic stratigraphy of a hotspot-induced, fast grown oceanic island: El Hierro, Canary Islands, *J. Volcanol. Geotherm. Res.*, *73* (1-2), 141-155, 1996.

Hapke, C.J., and K.R. Green, Coastal landslide material loss rates associated with severe climatic events, *Geology*, *34*, 1077-1080, 2006.

Hildenbrand, A., P.-Y. Gillot, and I. Le Roy, Volcano-tectonic and geochemical evolution of an oceanic intra-plate volcano : Tahiti-Nui (French Polynesia), *Earth Planet. Sci. Lett.*,

217, 349-365, 2004.

Hildenbrand, A., P.Y. Gillot, and A. Bonneville, Off-shore evidence for a huge landslide of the northern flank of Tahiti-Nui (French Polynesia), *Geochem. Geophys. Geosyst.*, *7*, Q03006, doi:10.1029/2005GC001003., 2006.

Hürlimann, M., E. Turon, and J. Martì, Large landslides triggered by caldera collapse events in Tenerife, Canary Islands, *Phys. Chem. Earth*, *24*, 921-924, 1999.

Kennett, J.P., and R.C. Thunell, Global increase in Quaternary explosive volcanism, *Science*, *187*, 497-503, 1975.

Kokelaar, P., and C. Romagnoli, Sector collapse, sedimentation and clast population evolution at an active island-arc volcano: Stromboli, Italy, *Bull. Volcanol.*, *57*, 240-262, 1995.

Krastel, S., H.U. Schmincke, C.L. Jacobs, R. Rihm, T.P. Le Bas, and B. Alibes, Submarine landslides around the Canary Islands, *J. Geophys. Res.*, *106*, 3977-3997, 2001.

Lambeck, K., T.M. Esat, and E.-K. Potter, Links between climate and sea levels for the past three million years, *Nature*, *419*, 199-206, 2002.

Le Friant, A., and G. Boudon, Large-scale flank collapse events during the activity of Montagne pelée, Martinique, Lesser Antilles, *J. Geophys. Res.*, *108*, 2055, 2003.

Le Friant, A., G. Boudon, J.C. Komorowski, and C. Deplus, L'île de la Dominique, à l'origine des avalanches de débris les plus volumineuses de l'arc des Petites Antilles, *C. R. Acad. Sci., Geosci.*, *334*, 235–243, 2002.

Lisiecki, L.E., and M.E. Raymo, A Pliocene-Pleistocene stack of 57 globally distributed benthic $\delta^{18}O$ records, *Paleoceanography*, *20*, PA1003, doi: 10.1029/2004PA001071, 2005.

Masson, D.G., Catastrophic collapse of the volcanic island of Hierro 15 ka ago and the history of landslides in the Canary Islands, *Geology*, *24*, 231-234, 1996.

Masson, D.G., A.B. Watts, M.J.R. Gee, R. Urgeles, N.C. Mitchell, T.P. Le Bas, and M. Canals, Slope failures on the flanks of the western Canary Islands, *Earth-Science Reviews*, *57*, 1-35, 2002.

McDougall, I., and T.M. Harrison, *Geochronology and thermochronology by the 40Ar/39Ar method*, 269 pp., Oxford Univ. Press, New York, 1999.

McGuire, W.J., Volcano instability: a review of comtemporary themes, in *Volcano Instability on Earth and Other Planets*, edited by W.J. McGuire, W.J. Jones, and A.P. Neuberg, pp. 1-23, Gological Society Special Publication, London, 1996.

McGuire, W.J., R.J. Howarth, C.R. Firth, A.R. Solow, A.D. Pullens, S.J. Saunders, I.S. Stewart, and C. Vita-Finzi, Correlation between rate of sea-level change and frequency of explosive volcanism in the Mediterranean, *Nature*, *389*, 473-476, 1997.

McMurtry, G.M., E. Herrero-Bervera, M.D. Cremer, J.R. Smith, C. Sherman, and M.E. Torresan, Stratigraphic constraints on the timing and emplacement of the Alika 2 giant Hawaiian submarine landslide, *J. Volcanol. Geotherm. Res.*, *94*, 35-58, 1999.

McMurtry, G.M., P. Watts, G.J. Fryer, J.R. Smith, and F. Imamura, Giant landslides, mega-tsunamis, and paleao-sea level in the Hawaiian Islands, *Marine Geology*, *203*, 219-233, 2004.

Mitchell, N.C., D.G. Masson, A.B. Watts, M.J.R. Gee, and R. Urgeles, The morphology of the submarine flanks of volcanic ocean islands - A comparative study of the Canary and Hawaiian hotspot islands, *Journal of Volcanology and Geothermal Research*, *115* (1-2), 83-107, 2002.

Moore, J.G., W.R. Normark, and R.T. Holcomb, Giant Hawaiian landslides, *Ann. Rev. Earth Planet. Sci.*, *22*, 119-144, 1994.

Oehler, J.F., P. Labazuy, and J.F. Lenat, Recurrence of major flank landslides during the last 2-Ma-history of Reunion Island, *Bulletin of Volcanology*, *66* (7), 585-598, 2004.

Paterne, M., and F. Guichard, Triggering of volcanic pulses in the Campanian area, south Italy, by periodic deep magma influx, *J. Geophys. Res.*, *98*, 1861-1873, 1993.

Pinel, V., and C. Jaupart, The effect of edifice load on magma ascent beneath a volcano, *Phil. Trans. R. Soc. Lond.*, *358*, 1515-1532, 2000.

Presley, T.K., J.M. Sinton, and M. Pringle, Postshield volcanism and catastrophic mass wasting of the Waianae volcano, Oahu, Hawaii, *Bull. Volcanol.*, *58*, 597-616, 1997.

Quidelleur, X., J. Carlut, V. Soler, J.-P. Valet, and P.-Y. Gillot, The age and duration of the Matuyama-Brunhes transition from new K-Ar data from La Palma (Canary Islands) and revisited 40Ar/39Ar ages, *Earth Planet. Sci. Lett.*, *208*, 149-163, 2003.

Quidelleur, X., P.Y. Gillot, V. Soler, and J.C. Lefèvre, K/Ar dating extended into the last millennium: Application to the the youngest effusive episode of the Teide volcano (Spain), *Geophys. Res. Lett.*, *28*, 3067-3070, 2001.

Quidelleur, X., A. Samper, G. Boudon, A. Le Friant, and J.C. Komorowski, Radiometric Dating of Large Volume Flank Collapses in The Lesser Antilles Arc., in *Fall Meet. Suppl.*, edited by E.T. AGU, pp. Abstract V41B-1397, San Fransisco, 2004.

Samper, A., X. Quidelleur, P. Lahitte, and D. Mollex, Timing of effusive volcanism and collapse events whithin an oceanic arc island: Basse Terre, Guadeloupe archipelago (Lesser Antilles Arc), *Earth Planet. Sci. Lett.*, *258*, 175-191, 2007.

Satake, K., and Y. Kato, The 1741 Oshima-Oshima eruption: Extent and volume of submarine debris avalanche, *Geophys. Res. Lett.*, *28*, 427-430, 2001.

Siebert, L., Large volcanic debris avalanches: characteristics of source areas, deposits, and associted eruptions, *J. Volcanol. Geotherm. Res.*, *22*, 163-197, 1984.

van den Bogaard, P., and C. Schirnick, The Diego Hernadez crisis: 40Ar/39Ar dating of the youngest higly explosive eruption cycle on Tenerife, in *26th assembly*, edited by E.G. Society, Geophy. Res. Abs., Nice, 2001.

Ward, S.N., and S. Day, Cumbre Vieja Volcano - Potential collapse and tsunami at La Palma, Canary Islands, *Geophysical Research Letters*, *28*, 3397-3400, 2001.

Ward, S.N., and S. Day, Ritter Island Volcano-lateral collapse and the tsunami of 1888, *Geophys. J. Int.*, *154*, 891-902, 2003.

Watts, A.B., and D.G. Masson, A giant landslide on the north flank of Tenerife, Canary Islands, *J. Geophys. Res.*, *100*, 24,487-24,498, 1995.

Zielinski, G.A., P.A. Mayewski, L.D. Meeker, S. Whitlow, and M.S. Twickler, A 110,000-yr record of explosive volcanism from the GISP2 (Greenland) ice core, *Quaternary Res.*, *45*, 109-118, 1996.

Figure legend:

Figure 1: Ages of well-dated oceanic island flank collapses (red diamond) compared with Quaternary climatic changes as shown by a stack of 57 globally distributed $\delta^{18}O$ records ([*Lisiecki and Raymo*, 2005]; deep blue continuous curve). Analytical age uncertainties (1σ) are shown with light blue areas.

Table 1

Well-dated oceanic island collapses with volume larger than 10 km^3. Age is given with an analytical uncertainty of 1 sigma. K/Ar pre-col. and K/Ar post-col.: age derived from K/Ar dating of pre-, or post-collapse, volcanism, respectively. $\delta^{18}O$ strat.: age derived from oxygen isotopes stratigraphy.

Location	Collapse	Volume (km^3)	Age (ka)	Dating method	Reference
La Palma	Cumbre Nueva	100-200	537±8	K/Ar post-col.	[*Guillou et al.*, 2001]
El Hierro	El Golfo 1	150-180	134±6	K/Ar pre-col.	[*Carracedo et al.*, 1999]
	El Golfo 2	250-350	15±2	K/Ar post-col.	[*Masson*, 1996]
Tenerife	Icod	150	161±5	K/Ar post-col.	[*Gillot et al.*, 2001]
Guadeloupe	Icaques	10-20	629±13	K/Ar post-col.	[*Samper et al.*, 2007]
Martinique	Carbets	30-40	337±5	K/Ar post-col.	[*Quidelleur et al.*, 2004]
Hawaii	Alika 2	200-800	127±5	$\delta^{18}O$ strat.	[*McMurtry et al.*, 1999]
Tahiti	North	400-450	872±10	K/Ar post-col.	[*Hildenbrand et al.*, 2004]

Figure1

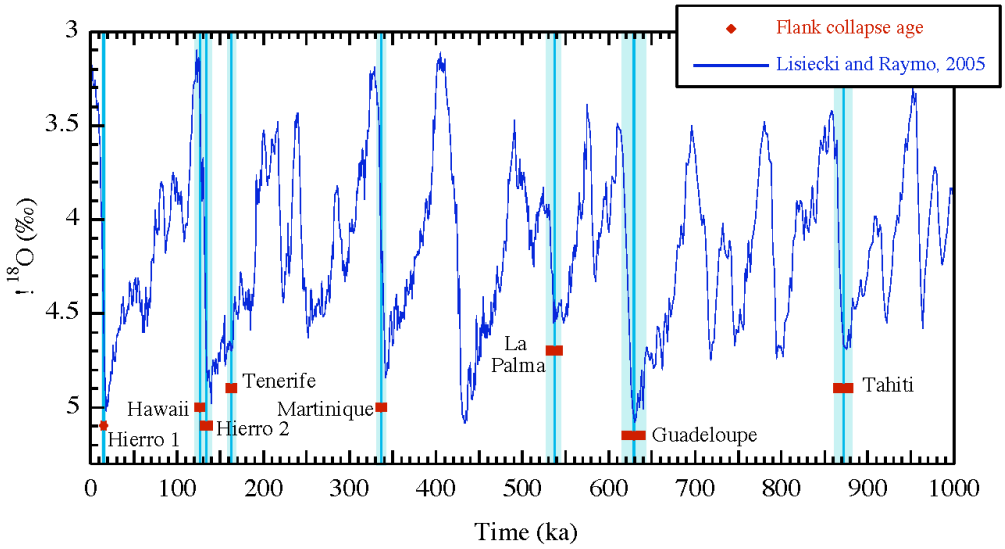

Figure 1 (Quidelleur et al., 2007)

Synthèse et Conclusions

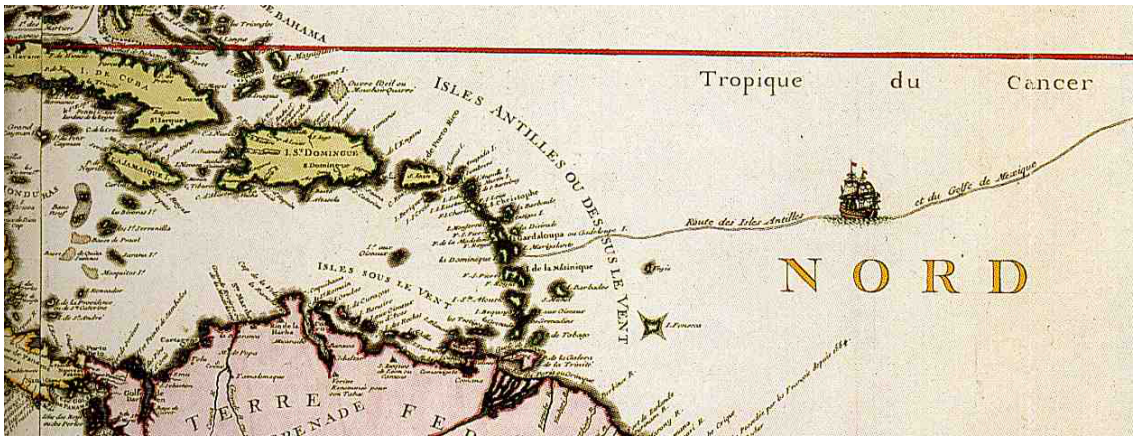

Les conclusions de ce travail de thèse reposent principalement sur l'analyse et la synthèse des données géochronologiques obtenues sur les roches volcaniques de l'île de Basse-Terre, grâce à la technique de datation ^{40}K-^{40}Ar Cassignol-Gillot. Cette approche fut combinée à la reconnaissance des morphologies volcaniques caractéristiques. Lorsque ce fut possible et nécessaire à l'étude, furent également réalisés l'individualisation de ces morphologies, le calcul de leur volume, et la reconstruction des volumes manquants.

Ce chapitre a pour but de synthétiser les connaissances apportées par ce travail de thèse, ainsi que les questionnements inhérents restants. Nous commencerons donc par une réflexion générale sur les données obtenues afin de mettre en perspective leur signification.

I La construction de l'île de Basse-Terre depuis 3 Ma : une interprétation

Le volcanisme sub-aérien de l'île de Basse-Terre s'est initié il y a 2,8 Ma. Quatre massifs volcaniques se sont répartis depuis au sein de cet espace temporel. Ils couvrent une surface totale de 860 km^2 environ, la surface totale de l'île étant de 950 km^2. Nos données géochronologiques obtenues sur l'ensemble de ces quatre massifs nous permettent de proposer une histoire cohérente de la construction de l'île de Basse-Terre, et de contraindre des durées minimum d'activité pour chacun de ces massifs.

Le Complexe Basal 2,8 – 2,7 Ma

Le Complexe Basal est contraint entre 2,79 ± 0,04 et 2,68 ± 0,04 Ma. Sa faible extension géographique (18,4 km^2) et son faible volume (1,5 km^3) extrudé en 110 ka au

minimum, indiqueraient que son activité temporelle fut courte, ou bien que les produits d'une activité plus prolongée auraient été recouverts et donc masqués par l'ensemble volcanique qui suivit. Le taux d'extrusion " brut " pouvant être calculé est de 1,36 10^{-5} km^3/an.

La Chaîne Septentrionale 1,8 – 1,15 Ma

La Chaîne Septentrionale, qui se localise immédiatement au Sud du complexe Basal, se distingue de celui-ci par une durée d'activité beaucoup plus longue, de l'ordre de 660 ka, entre 1,81 ± 0,03 et 1,15 ± 0,02 Ma. Cette chaîne volcanique présente une extension géographique bien supérieure à celle du Complexe Basal, de l'ordre de 247 km^2, ainsi qu'un volume de 64 km^3 préservés (initialement estimé à 74 km^3 au minimum) soit équivalent à quarante fois celui du Complexe Basal. Le taux d'extrusion caractérisant la Chaîne Septentrionale est donc de 9,68 10^{-5} km^3/an.

La Chaîne Axiale 1 Ma – 435 ka

La Chaîne Axiale prend le relais de l'activité entre 1023 ± 25 et 435 ± 8 ka. Bien que la Chaîne Axiale soit localisée immédiatement au Sud de la Chaîne Septentrionale, ces deux chaînes volcaniques ne se recouvrent pas, leur morphologie les distinguant très bien l'une de l'autre. La période d'activité de la Chaîne Axiale s'étend sur une durée comparable à celle de la Chaîne Septentrionale soit 640 ka. Nous avons reconstruit l'étendue de la Chaîne Axiale avant effondrement de sa partie sud et estimé son volume à 179 km^3. Nous montrons que la Chaîne Axiale, composée d'une succession d'édifices composites imbriqués et alignés suivant une direction NW-SE, s'étendait vraisemblablement jusqu'à hauteur de l'actuel cône de Grande Découverte, soit une surface totale de 355 km^2, un tiers supérieur à celle de la Chaîne Septentrionale. Le taux d'extrusion estimé est de 4.5 10^{-4} km^3/yr, ce qui est le plus fort taux obtenu pour l'île de Basse-Terre. Après effondrement de sa partie Sud il y a à peu près 640 ka

pour le premier épisode et probablement autour de 550 ka pour le second, l'activité de la Chaîne s'est poursuivie pendant près de 200 ka par la mise en place de trois édifices. Le Volcan des Icaques (629 ± 13 – 600 ± 17 ka), le Volcan de Capesterre (autour de 554 ± 8 ka) et le Volcan du Sans-Toucher (447 ± 6 – 435 ± 8 ka) délimitent la bordure nord de l'actuel massif de Grande-Découverte.

La période 435 – 205 ka

Bien que jouxtant la terminaison sud de la Chaîne Axiale, nous ne disposons pour le complexe volcanique de la Grande-Découverte que de données comprises entre 205 ± 28 ka et l'actuel. Un manque de données temporelles significatives souligne la transition entre le volcanisme terminal de la Chaîne Axiale et celui, déjà initié, du Massif de la Grande-Découverte, soit une transition longue de 200 ka. Trois hypothèses ont été soulevées par ce travail. La datation à 445 ± 6 ka d'une coulée de la base du cône de Grande Découverte, qui présente un chimisme permettant de la rattacher sans équivoque à l'activité du volcan du Sans Toucher, dernier édifice témoin de l'activité de la Chaîne Axiale, permet de supposer une activité prolongée de celle-ci au-delà de 435 ka. Une seconde possibilité réside en la croissance du cône de Grande-Découverte dès 400 ka environ, ou au cours de ce laps de temps de 200 ka ; une troisième en l'existence d'un complexe volcanique antérieur à la construction du cône, un complexe hypothétique que nous avons nommé " pré-GDV ". Nous rappelons ici que cette troisième hypothèse a été formulée à la suite de l'identification au Sud-Est du volcan de Grande Découverte des deux dômes de Morne Laffite (261 ± 7 ka) et Petite Montagne (314 ± 12 ka) construits pendant l'intervalle de temps qui nous intéresse ici. Nous ferons remarquer cependant que ces deux édifices présentent un chimisme constrasté, l'édifice le plus ancien présentant une signature proche des laves de la Chaîne Axiale, tandis que celle du plus récent se rapprocherait des roches de Grande-Découverte. Une quatrième hypothèse

pourrait être envisagée, celle d'une période de repos longue de 200 ka. Cette dernière semble peu probable au vu de la continuité temporelle de l'activité volcanique de l'île Basse-Terre, illustrée par les données géochronologiques de ce travail.

Un taux d'extrusion minimal de 9,5 10^{-5} km^3/yr peut être déduit pour cette phase volcanique longue de 400 ka, soit un volume résiduel de 38 km^3 environ.

Le complexe volcanique de la Grande-Découverte 205 ka - actuel

Ce massif débute par la construction de l'édifice composite de Grande-Découverte (GDV), à la terminaison de l'axe NW-SE de la Chaîne Axiale. Le taux d'extrusion du volume total du cône (16,1 km^3) est de 6,4 10^{-5} km^3/yr pour une durée de construction moyennée sur 250 ka. Un second locus éruptif s'initie au Sud du cône de GDV il y a 100 ka environ. La persistance jusqu'à l'actuel de l'activité sur ce second site aboutit à la construction du complexe de Trois-Rivières Madeleine (TRMC). Son volume total atteint 2,4 km^3, soit un taux d'extrusion de 6,4 10^{-5} km^3/yr. Néanmoins, la majeure partie du volume du cône composite de Grande-Découverte se met en place au cours de trois phases effusives majeures dont la dernière s'achève il y a 70 ka, tandis que le TRMC connaît une seule phase majeure entre 70 et 45 ka, qui voit l'extrusion des volumes de l'alignement La Madeleine – Le Palmiste (MPA - 1,7 km^3).

Bien que la longévité du Complexe de Grande-Découverte soit de l'ordre de 250 ka au minimum, soit un tiers de la durée totale des Chaînes Septentrionales et Axiales, les volumes extrudés (18,5 km^3) sont comparativement ici bien moindres. Le GDV est un cône composite de durée de vie remarquable et de volume semble-t-il supérieur d'un ordre 2 à celui des édifices composites terminaux de la Chaîne Axiale comme par exemple le Volcan des Icaques de volume estimé à 8 km^3.

II Directions structurales et front volcanique

Nos données chronologiques couplées à une observation simple des directions structurales des chaînes volcaniques de l'île de Basse-Terre nous permettent de proposer que l'extraction des magmas et leur disposition spatiale soient contrôlées depuis au moins 2,8 Ma par le réseau de failles normales découpant l'archipel guadeloupéen. Nous confirmons ainsi l'hypothèse de relation spatio-temporelle entre volcanisme et déformation active superficielle émise par (Feuillet, 2000; Feuillet et al., 2001; Feuillet et al., 2002). Nous suggérons ainsi que le graben de la Désirade ait joué un rôle dans l'extraction des magmas des massifs orientés N-S du Nord Basse-Terre (Complexe Basal et Chaîne Septentrional) et qu'il ait donc été actif depuis trois millions d'années environ. Cette hypothèse est concordante avec (Feuillet et al., 2002) qui proposent une initiation de sa formation antérieurement à 2 Ma. Ce graben de direction E-W ne s'est cependant pas propagé à l'île de Basse-Terre et l'alignement N-S du volcanisme du Nord Basse-Terre lui est perpendiculaire.

Le système de failles normales en échelon à composante sénestre de Basse-Terre – Montserrat a été relié à l'extraction des magmas composant le Sud Basse-Terre (Chaîne Axiale et Complexe Volcanique de Grande-Découverte). Sa propagation à terre remonterait ainsi à l'initiation du volcanisme de la Chaîne Axiale, soit il y a 1 Ma environ. Les volcans du Directeur et les petits édifices immergés de la Chaîne de Bouillante se situent sur le trajet de propagation de ce système de failles (Figure 2, Introduction). Nous proposons que tout comme pour le volcanisme de la Chaîne Axiale, l'extrusion de ces édifices sous-marins soit liée à un segment du Système de Basse-Terre – Montserrat. L'âge de ces édifices serait ainsi de l'ordre de 1 Ma au minimum. Des hauts fonds sous-marins cartés comme des édifices

volcaniques par (Feuillet, 2000) (Figure 2, Introduction) entre les îles de Montserrat et le Nord de Basse-Terre présentent un alignement NW-SE parallèle à celui du Système de Basse-Terre – Montserrat. Cette ligne volcanique pourrait être liée à des segments de ce système, mais situés plus à l'Est.

Bien que les morphologies du Complexe Basal et de la Chaîne Septentrionale soient plus émoussées que celles de la Chaîne Axiale, car plus anciennes que ces dernières, il semble cependant qu'un changement de la nature du volcanisme se soit produit. Les édifices de la Chaîne Axiale, ainsi que le volcan de Grande-Découverte, sont des volcans composites d'extension et volume à priori supérieurs aux édifices du Nord Basse-Terre > 1 Ma. Une analogie partielle avec la zone volcanique transtensive de Taupo, arc de Taupo-Hikurangi, Nouvelle-Zélande, peut être proposée. En effet dans ce système, des édifices composites de nature andésitique (volcans de Tongariro, Ruapehu) se localisent sur les relais transtensifs associés à une zone principale de rifting. Les zones transtensives sont situées dans l'axe de celle-ci mais à l'extérieur, au niveau de ses terminaisons Nord et Sud ; tandis que des calderas, associées à un volcanisme plus acide, rhyolitique, se développent au centre du rift (Spinks et al., 2005). Dans le cas de Basse-Terre seul le développement de volcans composites associés à des relais transtensifs peut être identifié, et la nature des laves principalement andésitique à andésitique-basaltique est relativement homogène et stable au cours du temps.

Si une migration globale du volcanisme peut être décrite depuis 2,8 Ma entre les extrémités Nord et Sud de l'île de Basse-Terre, suivant des vitesses de 18 à 25 km/Ma, nous n'avons pas identifié de propagation nette du volcanisme au sein de la Chaîne Septentrionale. Une activité contemporaine et continue le long de son axe, ou le long de segments de cet axe

est observable. Néanmoins, la majorité des édifices et coulées les plus jeunes a été identifiée au Sud, ce qui suggère que l'activité terminale de cette chaîne se soit produite à sa terminaison Sud. En ce qui concerne la Chaîne Axiale, les édifices les plus jeunes se situent à mesure que l'on se déplace vers le Sud de son axe NW-SE. Les données chronologiques indiquent cependant une contemporanéité de l'activité pour plusieurs des édifices alignés sur cet axe.

Nos contraintes temporelles et observations morphologiques permettent de préciser la période de propagation à terre du rift de Marie-Galante. Le déclenchement des deux phénomènes de déstabilisation de flanc qui ont affecté la terminaison Sud de la Chaîne Axiale, peut en effet être associés à cette propagation, l'âge du premier effondrement ayant été contraint à 640 ka. Les trois édifices postérieurs à ces épisodes d'effondrements, le Volcan des Icaques, de Capesterre, et du Sans-Toucher sont ainsi vraisemblablement situés dans une zone d'intersection des deux systèmes. Cependant ces édifices et le cône de Grande-Découverte sont alignés avec les édifices anciens de la Chaîne Axiale, ce qui suggère que la direction NW-SE serait restée un axe majeur de construction et de migration du volcanisme entre 1 Ma et 200 ka. Notons de même que cet axe aurait permis une extrusion plus abondante de magma, la Chaîne Axiale enregistrant les taux d'extrusion les plus importants de l'île. Au Sud du cône de Grande-Découverte, la propagation d'un segment du rift de Marie-Galante est identifiée par la mise en place des coulées de Trois-Rivières à 87 ± 2 ka. Depuis, la persistance de l'activité au niveau de ce linéament jusqu'à l'actuel, a conduit à la construction du complexe volcanique de Trois Rivières – Madeleine dont un épisode majeur s'est produit autour de 62 ± 5 ka par la mise en place de l'alignement de La Madeleine-Le Palmiste (MPA).

Enfin, malgré une homogénéité générale de la nature des laves de l'île de Basse-Terre, caractéristiques des îles du Centre de l'arc des Petites Antilles, nous notons une variabilité cyclique des signatures géochimiques au cours du temps. En effet, les laves du Complexe Basal et de la Chaîne Axiale d'une part, et les laves de la Chaîne Septentrionale et du Complexe de Grande-Découverte d'autre part, constituent deux groupes à comportement distinct, semblerait-il lié à une différenciation ou contamination superficielle des magmas, celle-ci pouvant être contrôlée par les systèmes de failles superficielles affectant Basse-Terre.

En conclusion, les trois systèmes de failles superficielles qui découpent l'archipel guadeloupéen contrôlent l'extraction et la variabilité spatio-temporelle des magmas de la zone de l'archipel recoupée par l'actuel front volcanique, soit les îles de Basse-Terre et des Saintes, appartenant à la branche de l'arc récent. Il est à noter que la vitesse de migration du volcanisme à Basse-Terre est de l'ordre de 18 km/Ma au cours des derniers 2,8 Ma et augmente à 25 km/Ma sur 1,8 Ma, ce qui correspond à une vitesse moyenne de 1,8 à 2,5 cm/an, vitesses équivalentes à celle de la convergence entre les plaques Nord-Américaine et Caraïbes. L'ouverture du rift NE-SE d'Anegada au Pliocène soit il y a 5 Ma environ, aurait marqué un changement du régime de contraintes générales affectant la frontière des plaques Nord-Américaine et Caraïbes (Mann et al., 2005). Cette modification du contexte tectonique général aurait conduit à l'initiation dans toute la partie Nord de l'arc de systèmes de rifting de direction E-W en position avant-arc, perpendiculaires au mouvement de subduction, ainsi que de systèmes transtensifs N-S situés en arrière-arc. La propagation de ces systèmes vers le Sud de l'arc aurait atteint l'archipel de la Guadeloupe il y a 3 Ma environ.

III Conclusions et perspectives

Les échelles de temps, interprétation et utilisation des données K-Ar

La construction sub-aérienne de l'île de Basse-Terre s'est réalisée suivant une migration Nord-Sud sur une période couvrant 3 Ma. En raison de l'âge et de l'érosion subie par chacun des quatre massifs volcaniques, nous n'avons pas accès au même degré de résolution temporelle et morphologique pour tous. Si les couvertures temporelles de chacun des complexes volcaniques de l'île sont très bien contraintes à l'échelle de la centaine de milliers d'années avec une précision atteignant la dizaine de milliers d'années, une information plus affinée, soit sur 10^4 et 10^3 ans ne peut être atteinte que dans le cas des massifs d'âge inférieur au million d'années. En ce qui concerne les morphologies, nous sommes également limités dans notre étude et nos interprétations par les effets de l'érosion. Il en est de même pour les observations de terrain. Une étude approfondie et complémentaire des affleurements disponibles serait d'ailleurs nécessaire et utile à une meilleure compréhension des épisodes de destruction de la Chaîne Axiale, et de construction du complexe volcanique de la Grande-Découverte, notamment des phases les plus récentes d'âge inférieur à dix mille ans. En particulier, une investigation de la rivière Classe qui longe la partie Est de l'escarpement de Vieux-Habitants – Matéliane et un échantillonnage des coulées de remplissage donnerait, tout d'abord, une contrainte affinée de l'âge du second effondrement de flanc. D'autre part, cela nous aiderait à déterminer si la formation de cet escarpement est principalement d'origine tectonique. En effet, il serait essentiel de préciser si la présence d'une coulée perchée bordant cet escarpement est due à un surcreusement lié à l'érosion, ou bien à une surrection tectonique liée à la propagation à terre du graben de Marie-Galante. Il devrait être entrepris également de définir s'il existe un lien entre les activités récentes du cône de Grande-Découverte et du complexe de Trois-Rivières – Madeleine. Le

cas échéant, caractériser et comprendre la nature de cette relation aiderait à mieux estimer l'aléa volcanique dans le massif de la Grande-Découverte.

En ce qui concerne les massifs les plus anciens de Basse-Terre, une étude de terrain aussi affinée que dans le Sud Basse-Terre serait en revanche malheureusement difficile, et s'avèrerait probablement peu complémentaire au degré de résolution temporelle K-Ar à notre disposition. Dans le cas des structures d'effondrement de flanc des îles de la Dominique, de la Martinique et de Sainte-Lucie, il serait intéressant de procéder à des études de terrain à terre et à des échantillonnages à but géochronologique afin d'essayer d'affiner la caractérisation temporelle de cette alternance d'épisodes de destruction et de construction.

Il apparaît ainsi de grande importance d'être clair sur la signification et la limite de toute donnée géochronologique obtenue, tant dans l'identification et la caractérisation des divers processus géologiques que dans l'établissement de conclusions.

Références Bibliographiques

Ablay, G., and M. Hürlimann, Evolution of the north flank of Tenerife by recurrent giant landslides, *J. Volcanol. Geotherm. Res.*, *103*, 135-159, 2000.

Andreieff, P., Bizon, G. and Bouysse, P., 1981. Révision de l'âge des formations sédimentaires de l'île de Saint-Martin; implications sur la chronologie du volcanisme de l'arc insulaire des Petites Antilles. C.R. Acad. Sci., II, 292: 79-82.

Andreieff, P., Bonneton, J.R., Vila, J.M. and Westercamp, D., 1984. Découverte du Paléocène supérieur à Anguilla, à l'extrémité nord de l'arc des Petites Antilles. 10è Réunion Annuelle Sciences de la Terre, Bordeaux, France: 15.

Aquater, 1982. Exploration of St. Lucia geothermal ressources, Annex A, Ministry of Finance and Planning.

Audin, L. et al., 2004. Paleomagnetism and K-Ar and 40Ar/39Ar ages in the Ali Sabieh area (Republic of Djibouti and Ethiopia): constraints on the mechanism of Aden ridge propagation into southeastern Afar during the last 10 Myr. Geophys. J. Int., 158: 327-345.

Bard, E., B. Hamelin, and R.G. Fairbanks, U-Th ages obtained by mass spectrometry in corals from Barbados: sea level during the past 130,000 years, *Nature*, *346*, 456-458, 1990.

Blanc, F., 1983. Corrélations chronologiques et géochimiques des formations volcaniques du sud de la Basse-Terre de Guadeloupe (Petites Antilles). Début du cycle récent. 3e cycle Thesis Thesis, Univ. Sci. Medic. Grenoble, 171 pp.

Boudon, G., Dagain, J., Semet, M.P. and Westercamp, D., 1988. Carte géologique à 1/20000e du massif volcanique de la Soufrière (Département de la Guadeloupe, Petites antilles). BRGM, Orléans.

Boudon, G., Le Friant, A., Komorowski, J.-C., Deplus, C. and Semet, M. P., 2007. Volcano flank instability in the Lesser Antilles Arc: Diversity of scale, processes, and temporal recurrence. J. Geophys. Res., 112, B08205, doi : 10.1029/2006JB004674.

Boudon, G., Le Friant, A., Villemant, B. and Viode, J.P., 2005. Martinique. In: S.R. Unit (Editor), Volcanic hazard atlas of the Lessser Antilles. University of the West Indies, St Augustine, Trinidad , W.I., pp. 126-145.

Boudon, G., Semet, M.P., Komorowski, J.C., Villemant, B. and Michel, A., 2003. Was the last magmatic eruption of la Soufrière, Guadeloupe, in 1440 AD, triggered by partial collapse of the volcano?, EGS-AGU-EUG Joint Assembly, Nice, France, pp. 10398.

Boudon, G., Semet, M.P. and Vincent, P.M., 1984. Flank failure-directed blast eruption at Soufrière, Guadeloupe, French West Indies: A 3,000-year-old Mt. St. Helens ? Geology, 12: 350-353.

Boudon, G., Semet, M.P. and Vincent, P.M., 1987. Magma and hydrothermally driven sector collapses: the 3100 and 11,500 Y. B.P. eruptions of La Grande-Découverte (La Soufrière) volcano, Guadeloupe, French West Indies. J. Volcanol. Geotherm. Res., 33: 317-323.

Boudon, G., Semet, M.P. and Vincent, P.M., 1989. The Evolution of la Grande Découverte (la Soufrière) volcano, Guadeloupe (F.W. I.). In: J. Latter (Editor), Volcanic hazards: assessment and monitoring. IAVCEI Proceedings in Volcanology, Berlin, pp. 86-109.

Boudon, G., Semet, M.P. and Vincent, P.M., 1992a. Les éruptions à écroulement de flanc sur le volcan de la Grande-Découverte (La Soufrière) de Guadeloupe: implications sur le risque volcanique. Bull. Soc. Géol. France, 163(2): 159-167.

Boudon, G., Semet, M.P. and Vincent, P.M., 1992b. Major flank collapse at Pitons du Carbet volcano, Martinique: one of the largest similar structure in the Lesser Antilles arc, 29th International Geological Congress, Kyoto, Japan, pp. 505.

Bouysse, P., 1979. Caractères morphostructuraux et évolution géodynamique de l'arc insulaire des Petites Antilles (Campagne Arcante 1). Bull. Bur. Rech. Geol. Min. Fr, 2: 185-210.

Bouysse, P. et al., 1985. Aves Swel and Northern Lesser Antilles ridge: rock-dredging results from Arcante 3 Cruise, Géodynamique des Caraïbes. Editions Technip, pp. 65-76.
Bouysse, P. and Garrabe, F., 1984. Neogene Tectonic Evolution of the Limestone Caribbees in the Guadeloupe Archipelago. Comptes Rendus De L Academie Des Sciences Serie Ii, 298(17): 763-766.
Bouysse, P. and Guennoc, P., 1983a. Data on the Structure of the Insular Arc in the Lesser-Antilles, between St-Lucia and Anguilla. Marine Geology, 53(1-2): 131-166.
Bouysse, P. and Guennoc, P., 1983b. Données sur la structure de l'arc insulaire des Petites Antilles : Entre St Lucie et Anguilla. Mar. Geol., 53: 131-166.
Bouysse, P. et al., 1988. Submarine Tectonic and Volcanic Structures of the Lesser Antilles Recent Arc (Kickem Jenny, Qualibou, Mount Pelee, Northwest Guadeloupe). Marine Geology, 81(1-4): 261-287.
Bouysse, P., Mascle, A., Mauffret, A., Mercier de lépinay, B., Jany., Leclere-Vanhoeve, A., Montjaret, M-C.,, 1988. Reconnaissance de structures tectoniques et volcaniques sous-marines de l'arc récent des Petites Antilles (kick'em Jenny, Qualibou, Montagne Pelée, Nord-ouest de la Guadeloupe). Marine Geology, 81: 261-287.
Bouysse, P. and Westercamp, D., 1990. Subduction of Atlantic aseismic ridges and late Cenozoic evolution of the Lesser Antilles Island Arc. Tectonophysics, 175: 349-380.
Bouysse, P., Westercamp, D., Andreieff, P., Baubron, J.C. et Scolari, G.,, 1985. Le volcanisme sous-marin néogène récent au large des côtes Caraïbes des Antilles françaises. Relations avec le volcanisme à terre et évolution du front volcanique. Géol. Fr.,, 1: 101-114.
Briden, J.C., Rex, D.C., Fallar, A.M. and Tomblin, J.F., 1979. K-Ar geochronology and palaeomagnetism of volcanic rocks from the Lesser Antilles Island Arc. Phil. Trans. R. Soc. Lond. Ser. A, 291: 485-258.
Brown, R.J., T.L. Barry, M.J. Branney, M.S. Pringle, and S.E. Bryan, The Quaternary pyroclastic succession of southeast Tenerife, Canary Islands: explosive eruptions, related caldera subsidence, and sector collapse, *Geological Magazine*, *140* (3), 265-288, 2003.
Cande, S. and Kent, D., 1995. Revised calibration of the geomagnetic polarity time scale. J. Geophys. Res., 100(B4): 6093-6095.
Carlut, J. and Quidelleur, X., 2000. Absolute paleointensities recorded during the Brunhes chron at La Guadeloupe Island. Phys. Earth. Planet. Int., 120: 255-269.
Carlut, J., Quidelleur, X., Courtillot, V. and Boudon, G., 2000. Paleomagnetic directions and K/Ar dating of 0-1 Ma lava flows from La Guadeloupe Island (French West Indies) : Implications for time averaged field models. J. Geophys. Res., 105: 835-849.
Carracedo, J.C., Day, S.J., Guillou, H. and Torrado, F.J.P., 1999. Giant Quaternary landslides in the evolution of La Palma and El Hierro, Canary Islands. J. Volcanol. Geotherm. Res., 94(1-4): 169-190.
Cassignol, C. and Gillot, P.-Y., 1982. Range and effectiveness of unspiked potassium-argon dating: Experimental groundwork and applications. Numerical Dating in Stratigraphy. John Wiley, New York, 159-179 pp.
Chiarabba, C., Amato, A. and Delaney, P.T., 1997. Crustal structure, evolution, and volcanic unrest of the Alban Hills, Central Italy. Bull. Volcanol., 59(3): 161-170.
Clark, P.U., A.M. McCabe, A.C. Mix, and A.J. Weaver, Rapid rise of sea level 19,000 years ago and its global implications, *Science*, *304* (5674), 1141-1144, 2004.
Clouard, V., Bonneville, A. and Gillot, P.Y., 2001. A giant landslide on the southern flank of Tahiti Island, French Polynesia. Geophys. Res. Lett., 28: 2253-2256.
Coles, D. et al., 2004. Spatial decision analysis of geothermal resource sites in the Qualibou Caldera, Saint Lucia, Lesser Antilles. Geothermics, 33(3): 277-308.

Cotten, J. et al., 1995. Origin of anomalous rare-earth element and yttrium enrichments in subaerially exposed basalts: Evidence from French Polynesia. Chem. Geol., 119: 115-138.

Crisp, J.A., 1984. Rates of Magma Emplacement and Volcanic Output. J. Volcanol. Geotherm. Res., 20(3-4): 177-211.

Dagain, J., 1981. La mise en place du massif volcanique Madeleine-Soufriere, Basse-Terre de Guadeloupe, Antilles. 3e cycle Thesis, Université Paris Sud, Orsay: 156.

Davidson, J. and De Silva, S., 2000. Composite Volcanoes. In: H. Sigurdsson H., B., McNutt, and R. S.P., H., Stix, J. (Editors) (Editors), Encyclopedia of Volcanoes. Academic Press, San Diego, London, pp. 663-681.

Day, S.J., S.I.N. Heleno da Silva, and J.F.B.D. Fonseca, A past giant lateral collapse and present-day flank instability of Fogo, Cape Verde Islands, *J. Volcanol. Geotherm. Res.*, *94*, 191-218, 1999.

De Reynal de St Michel, M., 1966. Carte géologique détaillée de la France. Département de la Guadeloupe au 1/50000. Feuilles de Basse Terre et des Saintes. Imprimerie Nationale, Ministère de l'industrie Paris.

Deino, A. and Potts, R., 1992. Age-probability spectra for examination of single-crystal $^{40}Ar/^{39}Ar$ dating results: examples from Olorgesailie, Southern Kenya Rift. Quaternary Int., 13/14: 47-53.

DeMets, C. et al., 2000. GPS geodetic constraints on Caribbean-North America plate motion. Geophys. Res. Lett., 27: 437-440.

Deng, J. and R., S.L., 1995. Determination of Euler pole for contemporary relative motion of Caribbean and North America plates using slip vectors of intraplate earthquakes. Tectonics, 14: 39-53.

Deplus, C., A. Le Friant, G. Boudon, J.-C. Komorowski, B. Villemant, C. Harford, J. Ségoufin, and J.-L. Cheminée, Submarine Evidence for Large-scale Debris Avalanches in the Lesser Antilles Arc, *Earth Planet. Sci. Lett.*, *192*, 145-157, 2001.

Elsworth, D., and S.J. Day, Flank collapse triggered by intrusion: the Canarian and Cape Verde Archipelagoes, *J. Volcanol. Geotherm. Res.*, *94*, 323-340, 1999.

Feuillet, N., 2000. Sismotectonique des Petites Antilles. Liaison entre activité sismique et volcanique, Thèse de Doctorat de l'Université Paris 7 - Denis Diderot. UFR Sciences Physiques de la Terre, Paris, 283 pp.

Feuillet, N., Manighetti, I. and Tapponier, P., 2001a. Active arc-transverse normal faulting in Guadeloupe (French Lesser Antilles). Earth Planet. Sci. Lett., 333 (2001): 583-590.

Feuillet, N., Manighetti, I. and Tapponnier, P., 2001b. Extension active perpendiculaire à la subduction dans l'arc des Petites Antilles (Guadeloupe, Antilles françaises). C. R. Acad. Sci., 333: 583–590.

Feuillet, N., Manighetti, I., Tapponnier, P. and Jacques, E., 2002. Arc parallel extension and localization of volcanic complexes in Guadeloupe, Lesser Antilles. J. Geophys. Res., 107(B12): 2331, doi:10.1029/2001JB000308.

Feuillet, N., Tapponnier, P., Manighetti, I., Villemant, B. and King, G., 2004. Differential uplift and tilt of Pleistocene reef platforms and Quaternary slip rate on the Morne-Piton normal fault (Guadeloupe, French West Indies). J. Geophys. Res., 109(B2).

Fink, L.K., 1972. Bathymetric and geologic studies of the Guadeloupe region, Lesser Antilles Arc. Mar. Geol., 12: 267-288.

Gadalia, A., Gstalter, N. and Westercamp, D., 1988. La chaîne volcanique de Bouillante, Basse-Terre de Guadeloupe, (Petites Antilles) : Identité pétrographique, volcanologique et géodynamique. C. R. Acad. Sci. Paris, Earth and Planetary Sciences, Géologie de la France, n°2-3: 101-130.

Gadalia, A. and Westercamp, D., 1984. Prospection géothermique de la zone de Bouillante-

Vieux Habitants, Guadeloupe. Exploitation géologique. Rap. Interne BRGM, Orléans, 84 SGN 063 GTH: 54.
Garcia, M.O., S.B. Sherman, G.F. Moore, R. Goll, I. Popova-Goll, J.H. Nathland, and G. Acton, Frequent landslides from Ko'olau volcano: results from ODP hole 1223A, *J. Volcanol. Geotherm. Res.*, *151*, 251-268, 2006.
Garrabé, F., 1983. Evolution sédimentaire et structurale de la Grande-Terre de Guadeloupe, Thèse de Doctorat de l'Université Paris-Sud, 171 pp.
Gee, M.J.R., A.B. Watts, D.G. Masson, and N.C. Mitchell, Landslides and the evolution of El Hierro in the Canary Islands, *Marine Geology*, *177* (3-4), 271-293, 2001.
Gill, J.B., 1981. Orogenic Andesites and Plate Tectonics. Springer-Verlag, New York, 390 pp pp.
Gillot, P.-Y. and Cornette, Y., 1986. The Cassignol technique for potassium-argon dating, precision and accuracy: examples from late Pleistocene to recent volcanics from southern Italy. Chem. Geol., 59: 205-222.
Gillot, P.-Y., Lefèvre, J.-C. and Nativel, P.-E., 1994. Model for the structural evolution of the volcanoes of Réunion Island. Earth Planet. Sci. Lett., 122(3-4): 291-302.
Gillot, P.Y., Cornette, Y., Max, N. and Floris, B., 1992. Two reference materials, trachytes MDO-G and ISH-G, for argon dating (K-Ar and 40Ar/39Ar) of Pleistocene and Holocene rocks. Geostandards Newsletter, 16(1): 55-60.
Gillot, P.Y., and J. Keller, Radiochronological dating of Stromboli, *Acta Vulcanologica*, *3*, 69-77, 1993.
Gillot, P.Y., V. Soler, and X. Quidelleur, Piling rate and magmatic evolution through time of the Teide volcano (Tenerife, Canary islands), in *EUG XI meeting*, edited by E.U.o. Geosciences, pp. 803, Terra Abstracts, Strasbourg, 2001.
Gstalter, N., 1986. Les formations ponceuses à quartz de la région sud de Basse-Terre (Guadeloupe), Pétrologie, géochimie, thermobarométrie et chimie des inclusions vitreuses. Thèse de l'Université de Paris-Sud, Orsay., n°92: 296 pp.
Guérin, G. and Samper, A., 2007. Aberrant thermoluminescence dates obtained from primary volcanic quartz. Rad. Measurements, in press.
Guillou, H., J.C. Carracedo, F.J.P. Torrado, and E.R. Badiola, K-Ar ages and magnetic stratigraphy of a hotspot-induced, fast grown oceanic island: El Hierro, Canary Islands, *J. Volcanol. Geotherm. Res.*, *73* (1-2), 141-155, 1996.
Gunn, B.M., Roobol, M.J. and Smith, A.L., 1980. Geochemistry of the volcanoes of Basse Terre, Guadeloupe - An example of intra-island variation. Bull. Volcanol.(43-2): 403-411.
Hapke, C.J., and K.R. Green, Coastal landslide material loss rates associated with severe climatic events, *Geology*, *34*, 1077-1080, 2006.
Harford, C.L., Pringle, M.S., Sparks, R.S.J. and Young, S.R., 2002. The volcanic evolution of Montserrat using $^{40}Ar/^{39}Ar$ geochronology. Geological Society, London, Memoirs, 21(The Geological Society of London, 2002): 93-113.
Hawkesworth, C.J. and Powell, M., 1980. Magma genesis in the Lesser Antilles island arc. Earth Planet. Sci. Lett., 51: 297-308.
Heuret, A. and Lallemand, S., 2005. Plate motions, slab dynamics and back-arc deformation. Phys. Earth Planet. Int., 149(1-2): 31-51.
Hildenbrand, A., Gillot, P.-Y. and Le Roy, I., 2004. Volcano-tectonic and geochemical evolution of an oceanic intra-plate volcano : Tahiti-Nui (French Polynesia). Earth Planet. Sci. Lett., 217: 349-365.
Hildenbrand, A., Gillot, P.Y., Soler, V. and Lahitte, P., 2003. Evidence for a persistent uplifting of La Palma (Canary Islands), inferred from morphological and radiometric data. Earth and Planetary Science Letters, 210: 277-289.

Hildreth, W. and Lanphere, M.A., 1994. Potassium-Argon Geochronology of a Basalt-Andesite-Dacite Arc System - the Mount Adams Volcanic Field, Cascade Range of Southern Washington. Geological Society of America Bulletin, 106(11): 1413-1429.

Hofmann, A., 1988. Chemical differentiation of the Earth: the relationship between mantle, continental crust, and oceanic crust. Earth Planet. Sci. Lett., 90: 297-314.

Hürlimann, M., Garcia-Piera, J.O. and Ledesma, A., 2000. Causes and mobility of large volcanic landslides: application to Tenerife, Canary Islands. J. Volcanol. Geotherm. Res., 103: 121-134.

Jacques, D., Maury, R.C.,, 1988. L'archipel des Saintes (Guadeloupe, petites Antilles) : géologie et pétrologie., Géologie de la France, n°2-3,: 89-99.

Jordan, T.H., 1975. The present-day motion of the Caribbean plate. J. Geophys. Res.,, 80: 4433-4439.

Kirschvink, J., 1980. The least-squares line and plane and the analysis of paleomagnetic data: examples from Siberia and Morocco. Geoph. J. Royal Astr. Soc., 62: 699-718.

Kennett, J.P., and R.C. Thunell, Global increase in Quaternary explosive volcanism, *Science*, *187*, 497-503, 1975.

Kokelaar, P., and C. Romagnoli, Sector collapse, sedimentation and clast population evolution at an active island-arc volcano: Stromboli, Italy, *Bull. Volcanol.*, *57*, 240-262, 1995.

Krastel, S., H.U. Schmincke, C.L. Jacobs, R. Rihm, T.P. Le Bas, and B. Alibes, Submarine Komorowski, J.C. et al., 2005a. Guadeloupe. In: S.R. Unit (Editor), Volcanic hazard atlas of the Lessser Antilles. University of the West Indies, St Augustine, Trinidad , W.I., pp. 67-104.

Komorowski, J.C. et al., 2005b. Guadeloupe. In: S.R. Unit (Editor), Volcanic hazard atlas of the Lesser Antilles. University of the West Indies, St Augustine, Trinidad , W.I., pp. 67-104.

Komorowski, J.C., Boudon, G., Semet, M., Villemant, B. and Hammouya, G., 2002. Recurrent flank-collapses at Soufrière of Guadeloupe volcano: implications of acid hydrothermal fluids on edifice stability Mount Pelée 1902-2002, Explosive volcanism in subduction zones, IPGP-INSU-IAVCEI Internatinal Congress, Martinique, 12-16 mai 2002.

Lambeck, K., T.M. Esat, and E.-K. Potter, Links between climate and sea levels for the past three million years, *Nature*, *419*, 199-206, 2002.

Le Friant, A., 2001. Les déstabilisations de flanc des volcans actifs de l'arc des Petites Antilles : origines et conséquences. Thèse de Doctorat de l'Université Paris 7 - Denic Diderot. UFR Sciences Physiques de la Terre.: 378 p.

Le Friant, A. and Boudon, G., 2003. Large-scale flank collapse events during the activity of Montagne pelée, Martinique, Lesser Antilles. J. Geophys. Res., 108: 2055.

Le Friant, A., Boudon, G., Komorowski, J-C., Deplus, C.,, 2002. L'île de la Dominique, à l'origine des avalanches de débris les plus volumineuses de l'arc des Petites Antilles. C.R. Geoscience, 334: 235-243.

Le Friant, A. et al., 2004. Geomorphological evolution of Montserrat (West Indies): importance of flank collapse and erosional processes. J. Geol. Soc. London, 161: 147-160.

Le Guen de Kerneizon, M., Bellon, H., Carron, J.P. and Maury, R., 1983. L'île de Sainte-Lucie (Petites Antilles): distinction de sprincipales sséries magmatiques à partir des données pétrochimiques et géochronologiques. Bull. Soc. géol. France, 6: 845-853.

Léticée, J.L. et al., 2005. Mise en évidence d'une discontinuité émersive majeure au sein de la plate-forme récifale plio-pléistocène de l'avant-arc des Petites Antilles. C.R. Geoscience, 337: 617-624.

Lindsay, J.M., 2005. Saint Lucia. In: S.R. Unit (Editor), Volcanic hazard atlas of the Lessser Antilles. University of the West Indies, St Augustine, Trinidad , W.I., pp. 218-238.
Lindsay, J.M., Smith, A.L., Roobol, M.J. and Stasiuk, M.V., 2005a. Dominica. In: S.R. Unit (Editor), Volcanic hazard atlas of the Lessser Antilles. University of the West Indies, St Augustine, Trinidad , W.I., pp. 1-46.
Lindsay, J.M., Stasiuk, M.V. and Shepherd, J.B., 2003. Geological history and potential hazards of the late-Pleistocene to Recent Plat Pays volcanic complex, Dominica, Lesser Antilles. Bull. Volcanol., 65(2-3): 201-220.
Lindsay, J.M., Trumbull, R.B. and Siebel, W., 2005b. Geochemistry and petrogenesis of late Pleistocene to recent volcanism in Southern Dominica, Lesser Antilles. Journal of Volcanology and Geothermal Research, 148(3-4): 253-294.
Lisiecki, L.E. and Raymo, M.E., 2005. A Pliocene-Pleistocene stack of 57 globally distributed benthic d^{18}O records. Paleoceanography, 20.
Masson, D.G., Catastrophic collapse of the volcanic island of Hierro 15 ka ago and the history of landslides in the Canary Islands, *Geology*, *24*, 231-234, 1996.
Masson, D.G., A.B. Watts, M.J.R. Gee, R. Urgeles, N.C. Mitchell, T.P. Le Bas, and M. Canals, Slope failures on the flanks of the western Canary Islands, *Earth-Science Reviews*, *57*, 1-35, 2002.
Macdonald, R., Hawkesworth, C.J. and Heath, E., 2000. The Lesser Antilles volcanic chain : a study in arc magmatism. Earth-Sci. Rev., 49: 1-76.
Manighetti, I. et al., 1998. Propagation of rifting along the Arabia-Somalia plate boundary: Into Afar. J. Geophys. Res., 103(B3): 4947-4974.
Mann, P., Hippolyte, J.-C., Grindlay, N.R. and Abrams, L.J., 2005. Neotectonics of southern Puerto Rico and its offshore margin. Active tectonics
and seismic hazards of Puerto Rico, the Virgin Islands, and offshore areas: Geological Society of America Special Paper, 385, 173–214 pp.
Martin-Kaye, P.H.A., 1969. A summary of the geology of the Lesser Antilles. Overseas Geology and Mineral Ressources, 10: 172-206.
Mascle, A. and Westercamp, D., 1983. Géologie d'Antigua, Petites Antilles. Bull. Soc. Geol. Fr., Sér. 7, t. 15, no. 6: 855-866.
Mattioli, G.S., Jansma, P.E., Jaramillo, L. and Smith, A.L., 1995. Sector collapse in island arc volcanoes: a digital topographic and bathymetric investigation of the Qualibou depression, St. Lucia, Lesser Antilles. Carribean Journal of Science, 31: 163-173.
Maury, R.C., Westbrook, G.K., Baker, P.E., Bouysse, P. and Westercamp, D., 1990. Geology of the Lesser Antilles. The Geology of North America, vol. H, The Caribbean Region: 141-166.
McCann, W.R. and Sykes, L.R., 1984. Subduction of aseismic ridges beneath the Caribbean plate; implications for the tectonics and seismic potential of the nrtheastern Caribbean. J. Geophys. Res., 89: 4493-4519.
McDougall, I., and T.M. Harrison, *Geochronology and thermochronology by the 40Ar/39Ar method*, 269 pp., Oxford Univ. Press, New York, 1999.
McGuire, W.J., 1996. Volcano instability: a review of comtemporary themes. In: W.J. McGuire, W.J. Jones and A.P. Neuberg (Editors), Volcano Instability on Earth and Other Planets. Geological Society Special Publication, London, pp. 1-23.
McMurtry, G.M., E. Herrero-Bervera, M.D. Cremer, J.R. Smith, C. Sherman, and M.E. Torresan, Stratigraphic constraints on the timing and emplacement of the Alika 2 giant Hawaiian submarine landslide, *J. Volcanol. Geotherm. Res.*, *94*, 35-58, 1999.
McMurtry, G.M., P. Watts, G.J. Fryer, J.R. Smith, and F. Imamura, Giant landslides, mega-tsunamis, and paleao-sea level in the Hawaiian Islands, *Marine Geology*, *203*, 219-233, 2004.

Minster, J.B. and H., J.T., 1978. Present-day plate motions. J. Geophys. Res.,, 83: 5331-5354.
Mitchell, N.C., D.G. Masson, A.B. Watts, M.J.R. Gee, and R. Urgeles, The morphology of the submarine flanks of volcanic ocean islands - A comparative study of the Canary and Hawaiian hotspot islands, *Journal of Volcanology and Geothermal Research*, *115* (1-2), 83-107, 2002.
Moore, J.G., Normark, W.R. and Holcomb, R.T., 1994. Giant Hawaiian landslides. Ann. Rev. Earth Planet. Sci., 22: 119-144.
Odin, G.S. and al., e., 1982. Interlaboratory standards for dating purposes. In: G.S. Odin (Editor), Numerical dating in stratigraphy. John Wiley and Sons, Chichester, pp. 123-150.
Oehler, J.F., P. Labazuy, and J.F. Lenat, Recurrence of major flank landslides during the last 2-Ma-history of Reunion Island, *Bulletin of Volcanology*, *66* (7), 585-598, 2004.
Paterne, M., and F. Guichard, Triggering of volcanic pulses in the Campanian area, south Italy, by periodic deep magma influx, *J. Geophys. Res.*, *98*, 1861-1873, 1993.
Pinel, V. and Jaupart, C., 2000. The effect of edifice load on magma ascent beneath a volcano. Phil. Trans. R. Soc. Lond., 358: 1515-1532.
Presley, T.K., Sinton, J.M. and Pringle, M., 1997. Postshield volcanism and catastrophic mass wasting of the Waianae volcano, Oahu, Hawaii. Bull. Volcanol., 58: 597-616.
Quidelleur, X., Carlut, J., Soler, V., Valet, J.-P. and Gillot, P.-Y., 2003. The age and duration of the Matuyama-Brunhes transition from new K-Ar data from La Palma (Canary Islands) and revisited 40Ar/39Ar ages. Earth Planet. Sci. Lett., 208: 149-163.
Quidelleur, X., Gillot, P.-Y., Filoche, G. and Lefèvre, J.C., 2005. Fast geochemical changes and rapid lava accumulation at Stromboli Island (Italy) inferred from K-Ar dating and paleomagnetic variations at 60 and 40 ka. J. Volc. Geotherm. Res., 141: 177-193.
Quidelleur, X., Gillot, P.Y., Soler, V. and Lefèvre, J.C., 2001. K/Ar dating extended into the last millennium: Application to the the youngest effusive episode of the Teide volcano (Spain). Geophys. Res. Lett., 28: 3067-3070.
Quidelleur, X., A. Samper, G. Boudon, A. Le Friant, and J.C. Komorowski, Radiometric Dating of Large Volume Flank Collapses in The Lesser Antilles Arc., in *Fall Meet. Suppl.*, edited by E.T. AGU, pp. Abstract V41B-1397, San Fransisco, 2004.
Quidelleur, X., Hildenbrand, A. and Samper, A., 2007. Link between Quaternary paleoclimatic changes and volcanic oceanic islands evolution. Geophys. Res. Lett, submitted.
Rad, S., J., A.C. and Gaillardet, J., 2006a. Time scale of erosion and weathering processes in tropical volcanic islands: Guadeloupe, Martinique and Réunion. in prep.
Rad, S., Louvat, P., Gorge, C., Gaillardet, K. and Allegre, C.J., 2006b. River dissolved and solid loads in the Lesser Antilles: New insight into basalt weathering processes. J. Geochem. Exploration, 88(1-3): 308-312.
Reid, R.P., Carey, S.N. and Ross, D.R., 1996. Late quaternary sedimentation in the Lesser Antilles island arc. Geol. Soc. Am. Bull., 108: 78-100.
Roobol, M.J., Wright, J.V. and Smith., A.L., 1983. Calderas or gravity-slide structures in the Lesser Antilles island arc ? J. Volcanol. Geotherm. Res., 19: 121-134.
Samper, A., Chauvel, C. and Quidelleur, X., 2005. Geochemical and isotopic study of K-Ar dated volcanics from Basse Terre, Guadeloupe, Lesser Antilles Arc. In: Geophys. Res. Abs. (Editor), EGU 2005 Meeting, Vienna.
Samper, A., Quidelleur, X., Boudon, G., Le Friant, A. and Komorowski, J.C., 2007a. Radiometric Dating of Large Volume Flank Collapses in The Lesser Antilles Arc. J. Geol. Soc. London, submitted.
Samper, A., Quidelleur, X., Komorowski, J.C., Lahitte, P. and Boudon, G., 2007b. Geochronological study of the Grande Découverte Volcano effusive phases, Basse

Terre, Guadeloupe, FWI. in prep.
Samper, A., Quidelleur, X., Lahitte, P. and Mollex, D., 2007c. Timing of effusive volcanism and collapse events whithin an oceanic arc island: Basse Terre, Guadeloupe archipelago (Lesser Antilles Arc). Earth Planet. Sci. Lett., 258: 175-191.
Satake, K., and Y. Kato, The 1741 Oshima-Oshima eruption: Extent and volume of submarine debris avalanche, *Geophys. Res. Lett.*, *28*, 427-430, 2001.
Semet, M., Vatin-Pérignon, N., Vincent, P.-M. and Joron, J.-L., 1981. L'éruption volcanique du XVIème siècle de la Soufrière de Guadeloupe, mélanges de magmas et dynamisme éruptif. Bull. PIRPSEV, CNRS-INAG, Paris, France, 60: 1-63.
Siebert, L., Large volcanic debris avalanches: characteristics of source areas, deposits, and associted eruptions, *J. Volcanol. Geotherm. Res.*, *22*, 163-197, 1984.
Smith, W.H.F. and Sandwell, D.T., 1997. Global sea floor topography from satellite altimetry and ship depth soundings. Science, 277(5334): 1956-1962.
Sparks, R.S.J. et al., 2002. Generation of a debris-avalanche and violent pyroclastic density current: the Boxing Day eruption of 26 december 1997 at the Soufrière Hills Volcano, Montserrat. In: T.H. Druitt and B.P. Kokelaar (Editors), The eruption of Soufrière Hills Volcano, Montserrat, from 1995 to 1999, London Geol. Soc., Memoirs, pp. 409-434.
Spinks, K.D., Acocella, V., Cole, J.W. and Basset, K.N., 2005. Structural control of volcanism and caldera development in the transtensional Taupo Volcanic Zone, New Zealand. J. Volcanol. Geotherm. Res., 144: 7–22.
Steiger, R.H. and Jäger, E., 1977. Subcommission on Geochronology: convention on the use of decay constants in Geo and Cosmochronology. Earth Planet. Sci. Lett., 36: 359-362.
Tomblin, J.F., 1965. The geology of the Soufrière volcanic centre, St. Lucia, Fourth Caribbean Geological Conference, Trinidad, pp. 367-376.
Tovish, A. and Schubert, G., 1978. Island arc curvature, velocity of convergence, and angle of subduction. Geophys. Res. Lett., 5(4): 329-332.
Turner, S., George, R., Jerram, D.A., Carpenter, N. and Hawkesworth, C., 2003. Case studies of plagioclase growth and residence times in island arc lavas from Tonga and the Lesser Antilles, and a model to reconcile discordant age information. Earth Planet. Sci. Lett., 214(1-2): 279-294.
Vincent, P.M., Bourdier, J.L. and Boudon, G., 1989. The primitive volcano of Mount Pelée: its construction and partial destruction by flank collapse. J. Volcanol. Geotherm. Res., 38: 1-15.
van den Bogaard, P., and C. Schirnick, The Diego Hernadez crisis: 40Ar/39Ar dating of the youngest higly explosive eruption cycle on Tenerife, in *26th assembly*, edited by E.G. Society, Geophy. Res. Abs., Nice, 2001.
Voight, B. et al., 2002. The 26 December (Boxing Day) 1997 sector collapse and debris-avalanche at Soufrière Hills Volcano, Montserrat. In: T.H. Druitt and B.P. Kokelaar (Editors), The eruption of Soufrière Hills Volcano, Montserrat, from 1995 to 1999. Geological Society, London, Memoirs, pp. 363-407.
Wadge, G., 1984. Comparison of volcanic production rates and subduction rates in the Lesser Antilles and Central America. Geology, 12: 555-558.
Wadge, G., 1985. Morne Patates Volcano, Southern Dominica, Lesser Antilles. Geological Magazine, 122(3): 253-260.
Wadge, G., 1986. The dykes and structural setting of the volcanic front in the Lesser Antilles Island Arc. Bull. Volcanol., 48: 349-372.
Wadge, G. and Shepherd, J.B., 1984. Segmentation of the Lesser Antilles subduction zone. Earth Planet. Sci. Lett., 71: 297-304.

Ward, S.N., and S. Day, Cumbre Vieja Volcano - Potential collapse and tsunami at La Palma, Canary Islands, *Geophysical Research Letters*, *28*, 3397-3400, 2001.

Ward, S.N., and S. Day, Ritter Island Volcano-lateral collapse and the tsunami of 1888, *Geophys. J. Int.*, *154*, 891-902, 2003.

Watts, A.B., and D.G. Masson, A giant landslide on the north flank of Tenerife, Canary Westercamp, D., Pelletier, B., Thibaut, P.M., Traineau, H. and Andreieff, P., 1990. Carte géologique de la France (1/50 000), feuille Martinique. BRGM, Orléans.

Westercamp, D. and Tazieff, H., 1980. Martinique, Guadeloupe, Saint-Martin, La Désirade. Guide Géologique, Paris, 136 pp.

White, S.M., Crisp, J.A. and Spera, F.J., 2006. Long-term volumetric eruption rates and magma budgets. Geochem. Geophys. Geosyst., 7.

Wohletz, K. et al., 1986. The Qualibou Caldera, St-Lucia, West-Indies. J. Volcanol. Geotherm. Res., 27(1-2): 77-115.

Wright, J.V. et al., 1984. Late Quaternary Explosive Silicic Volcanism on St-Lucia, West-Indies. Geological Magazine, 121(1): 1-15.

Young, S. et al., 2002. Hazard implications of small-scale edifice instability and sector collapse: a case history from Soufrière Hills volcano, Montserrat. In: T.H. Druitt and B.P. Kokelaar (Editors), The eruption of Soufrière Hills Volcano, Montserrat, from 1995 to 1999. Geological Society, London, Memoirs, pp. 349-361.

Zielinski, G.A., P.A. Mayewski, L.D. Meeker, S. Whitlow, and M.S. Twickler, A 110,000-yr record of explosive volcanism from the GISP2 (Greenland) ice core, *Quaternary Res.*, *45*, 109-118, 1996.

Zijderveld, J.D.A., 1967. A.C. demagnetization of rocks: Analysis of results. In: D.W. Collinson, K.M. Creer and S.K. Runcorn (Editors), Methods in paleomagnetism. Elsevier, New York, pp. 254-286.

Annexes

ARTICLE IN PRESS

Available online at www.sciencedirect.com

ScienceDirect

Radiation Measurements ▮▮▮ (▮▮▮▮) ▮▮▮–▮▮▮

Radiation Measurements

www.elsevier.com/locate/radmeas

Aberrant thermoluminescence dates obtained from primary volcanic quartz

Gilles Guérin[a,*], Agnès Samper[b]

[a]*Laboratoire des Sciences du Climat et de l'Environnement, CEA-CNRS, avenue de la Terrasse, 91191 Gif-sur-Yvette, France*
[b]*Laboratoire de géochronologie multitechnique (UPS-IPGP), Université de Paris-Sud Orsay, 91405 Orsay Cedex, France*

Received 19 October 2006; received in revised form 2 March 2007; accepted 26 March 2007

Abstract

This study deals with the dating by thermoluminescence (TL) of quartz from six volcanic formations of the Saint Lucia Island (Lesser Antilles Arc). Quartz microcrystals up to one millimetre in size were extracted from dacites and pumice flows and prepared in a way similar to the well-known inclusion technique. The TL properties of these quartz were used to estimate apparent palaeodoses using the multi-aliquot protocol. The quartz TL was studied in three different spectral domains: red, green and ultraviolet/blue. The calculated annual dose-rates yielded a set of 18 age-estimates. For some samples complementary dates were obtained using high temperature TL (HTTL) of plagioclase feldspars. These latter dates combined with previously determined radiocarbon and unspiked K–Ar dates were used to explore the validity of ages computed from the TL of quartz. Individual values for quartz appear to be scattered and do not match ages deduced from ^{14}C, unspiked K–Ar or HTTL on plagioclase dates. These results indicate that when conventional TL methodologies derived from the inclusion method are applied to volcanic quartz major dating problems are to be expected.

1. Introduction

Quartz is a very abundant mineral, and it has been used as a dosimeter from the earliest days of thermoluminescence (TL) (e.g. Kaul et al., 1966; Fleming, 1970, 1972; Aitken, 1985) and more recently in the OSL dating of sediments (e.g. Aitken, 1985, 1992, 1998; Wintle, 1997). Though quartz has been rarely used for the study of volcanic activity (Fattahi and Stokes, 2003), some luminescence dating work has been done on detrital quartz extracted from sediments heated by volcanic lava flows (Pilleyre et al., 1992) or extracted from granite xenoliths (Valladas, 1978; Miallier et al., 1984, 1994), and less often on quartz from the volcanic rock itself (Hashimoto et al., 1991; Fattahi and Stokes, 2000). For detrital quartz, as well as for primary volcanic quartz, the dating has been generally done using red TL (RTL). For volcanic quartz (Hashimoto et al., 1987, 1991, 1996; Fattahi and Stokes, 2000; Stokes and Fattahi, 2003; Ganzawa et al., 2005) the estimated ages agreed with geological expectations. These results provided initial evidence of the suitability of volcanic quartz for TL dating, but they represent a limited data set that has not been tested by other dating methods. However, such cross-comparisons would be very useful because one might expect the thermal and radiation dose histories of quartz of different origins (from sediment baked by a lava flow, or primary volcanic quartz) to have an impact on their TL behaviour and on the calculated dates.

As quartz is very common in some geological contexts, such as volcanic arcs where few dating methods are available for young ages, we decided to examine the properties of volcanic quartz to see if it is suitable for TL dating. A geological and chronological study, currently in progress on the Saint Lucia Island in the West Indies, allowed us to test the validity of quartz TL ages obtained on volcanic units by comparing them to ^{14}C ages or recent unspiked K–Ar dates (Quidelleur et al., 2004).

2. Geological setting and sampling

The island of Saint Lucia is one of the major centres of late Quaternary silicic volcanism in the Lesser Antilles Arc (Robson and Tomblin, 1966). Since the mid 1960s, various authors have studied the geology and stratigraphy of the volcanic

* Corresponding author. Current address: Département des sciences de la Terre, Université de Paris-Sud Orsay, 91405 Orsay Cedex, France.
Tel.: +33 1 69 15 67 68; fax: +33 1 69 15 48 91.
E-mail address: gilles.guerin@u-psud.fr (G. Guérin).

1350-4487/$ - see front matter © 2007 Elsevier Ltd. All rights reserved.
doi:10.1016/j.radmeas.2007.03.006

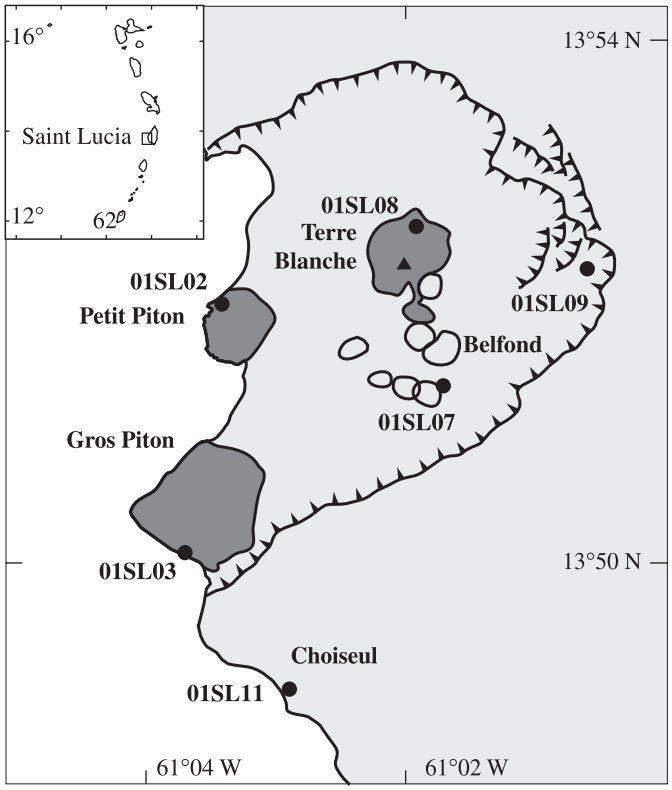

Fig. 1. Simplified map of the south-west corner of the Saint Lucia island and sample locations related to main volcanic formations (after Lindsay et al., 2005).

units of this island (Tomblin, 1964, 1979; Martin-Kaye, 1969; Le Guen de Kerneizon et al., 1983; Vatin-Pérignon and Chevallier, 1983; Wright et al., 1984; Vatin-Pérignon et al., 1985). This volcanism is represented by widespread aprons and fans of pumice flow and ash flow deposits radiating around the central highlands as well as young dacite domes extruded in volcano-tectonic depressions. Petit Piton and Gros Piton domes within the Qualibou depression are representative of this structure. The pumice succession can be divided into older quartz-poor deposits forming the Choiseul Pumice and a younger crystal-rich deposit called the Belfond Pumice in which quartz is abundant. The latter is the product of several eruptions of high silicic magma. Within the main southwest Qualibou depression, the Terre Blanche dome is still an active zone of fumaroles and is the most recent area of volcanic activity of the island (Tomblin, 1979) with a recent (1782) phreatic activity (Sulphur Springs). Among these formations six outcrops of known age containing quartz-bearing rocks were selected (Fig. 1). The calculated ages of these units are summarised in Table 1 (unless mentioned otherwise, only the statistical uncertainty is quoted at 1σ in all the tables and figures).

3. Thermoluminescence measurements

3.1. Sample preparation

Samples (average size 20–25 cm) were collected in the field with no special precautions against exposure to sunlight. Pure quartz as well as a plagioclase feldspar fraction were prepared to make up six samples. Once in the laboratory, the samples were manipulated under low intensity sodium halogen lamps. The over all preparation was done in a way close to the inclusion method (Fleming, 1970). After the outer first cm of each sample was removed using a diamond circular saw the remaining core was crushed in a jaw crusher and then sieved to remove the finer fractions.

Table 1
Sample provenience and age estimates (1σ uncertainties)

Sample	Location	Rock type	Estimated age (ka)
01SL02	Petit Piton	Massive dacite	95.0 ± 2.0 (a)
01SL03	Gros Piton	Massive dacite	77.0 ± 2.0 (a)
01SL07	Etang Belfond	Massive dacite	
01SL08	Terre Blanche	Pumice	3 ± 3 (b)
01SL09	Belfond Pumice deposit	Pumice	20–29 (c)
01SL11	Choiseul Pumice deposit	Pumice	34.5 ± 0.4 (c)

(a) Ages measured by unspiked K–Ar method (Quidelleur et al., 2004; Samper et al., 2007), (b) Geological evidence (young sub-active zone with fumaroles activity) and K–Ar determination, (c) BP uncalibrated ^{14}C based on multiple determinations on charcoals (Wright et al., 1984; Roobol et al., 1983; Lindsay et al., 2005).

Quartz grains in the three pumice samples, 01SL08, 01SL09 and 01SL11, were big enough to allow the 0.5 mm fraction to be handpicked. For the three remaining samples, the 0.5–1 mm fraction was submitted to a separation in a Franz magnetic separator, which yielded an almost pure quartz fraction. All six samples were then etched for 20 min in 40% hydrofluoric acid, which dissolved the outer part of quartz crystals and minimised the effects of alpha radiation. The etching also eliminated any remaining volcanic glass and feldspar. This fraction was then gently hand crushed in an agate mortar and sieved to obtain a 90–125 μm fraction, which was etched again for a few minutes with hydrofluoric acid in order to eliminate any residual feldspar. The final fraction was then thoroughly washed with acetone in an ultrasonic bath and dried at 40 °C in total darkness.

The feldspar fraction was treated in a different manner. Once freed of its outer part and crushed, the 90–125 μm fraction of each sample was separated into two parts by the use of bromoform (tribromomethane) of 2.80 density. The lighter fraction, containing both some quartz and feldspar was then divided in two fractions using a Franz separator. The slightly magnetic fraction being almost free of quartz and composed of feldspars was kept for TL measurements.

3.2. Palaeodose measurements

TL measurements were made using a 36 position automatic TL-OSL reader designed and built in our laboratory. This apparatus was equipped with a 9235QSA photomultiplier tube. Light was filtered with the help of different glass filter combinations. To measure RTL we used a long pass filter RG610 (cut-off: 610 nm; passband limit: 660 nm) combined with a short pass IR cut-off filter TA-I 2 mm (cut-off about 700 nm).

Please cite this article as: Guérin, G., Samper, A., Aberrant thermoluminescence dates obtained from primary volcanic quartz. Radiat. Meas. (2007), doi: 10.1016/j.radmeas.2007.03.006

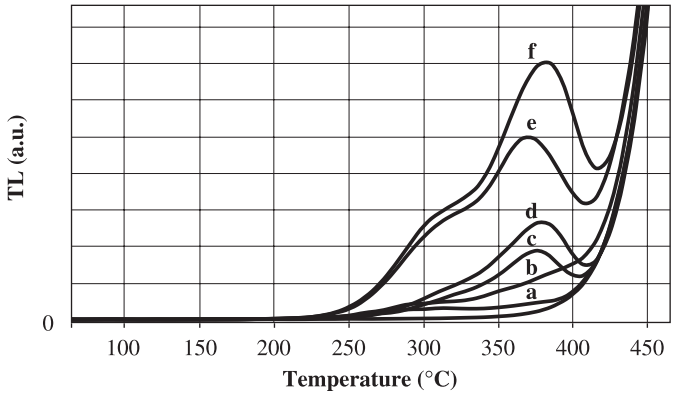

Fig. 2. Natural thermoluminescence glow-curves of quartz from Saint Lucia volcanic rocks (green TL at 531 nm, 5 °C/s, no preheat).

Green TL (GTL) was measured using the same short pass filter and a DA531c filter (centre wavelength: 530 nm, full width at half max: 75 nm). Ultraviolet/blue luminescence, henceforth referred to simply as "blue" (BTL), was measured with the help of a DH380c filter (centre wavelength: 380 nm, full width at half max: 100 nm). The high temperature TL of feldspars was studied using two stacked H326c filters (resulting a 325 nm centre wavelength and a full width at half max of about 50 nm). All these glass filters, except for the standard RG610 (Schott), were supplied by the former MTO company (Sagem).

The processed samples consisting of a 90–125 μm powder were divided into aliquots of constant volume of about 4 mg each, then placed on individual stainless steel disks before measurements. The ^{90}Sr beta source integrated in our reader delivers a 3.4 Gy/min radiation dose. TL glow-curves are measured in a nitrogen flux with a 5 °C/s heating rate. The natural TL glow-curves of the six dated samples plotted in Fig. 2 are all very similar and resemble those of non-volcanic quartz. The so-called 325 °C as well as the 375 °C peaks are well defined. The second-glow (not shown here) displays a strong 110 °C peak and glow-curves of primary volcanic quartz do not seem to be very different from those of non-volcanic quartz.

A standard multiple aliquot protocol (Aitken, 1985) was used to determine palaeodoses. For each sample, at least two added doses were delivered to sets of natural TL aliquots (generally 6–8 in each set). This made it possible to obtain an apparent dose by extrapolation (using a linear model of TL growth vs. radiation dose). Plateau tests were systematically performed and a linearity correction was applied to the apparent dose. This correction was evaluated using sets of aliquots bleached by heating for 10 s at 600 °C in nitrogen atmosphere in the case of quartz and for 5 s at 760 °C in the case of feldspars. The bleached aliquots were used to determine the growth curves of TL with the radiation dose which allowed us to estimate the non-linearity effects (supralinearity) on apparent dose extrapolations. TL measurements of aliquot sets were inter-crossed to minimise the effects of possible variations in the photomultiplier gain. Each aliquot was preheated before TL measurements. For quartz, this preheating is slightly dependent on the spectral domain used to measure the TL (Table 2). For the RTL the preheating parameters are close to those used for non-volcanic quartz (Pilleyre et al., 1992). In the case of feldspars, preheating protocols are those which give flat plateau tests (Guérin, 2006) in high temperature dating (Guérin and Valladas, 1980).

Table 2
Preheat parameters used for measurements of quartz and feldspar

	Type of TL	Temperature (°C)	Duration (s)
Quartz	Red TL	320	30 or 10
	Green TL	250	30
	Blue TL	270	30
Feldspars	HTTL	560 or 570	40

Table 3
Apparent palaeodoses in grays estimated in different spectral domains for quartz and feldspar

Sample	Apparent palaeodose (Gy)			
	Quartz			Feldspar
	RTL 610 nm	GTL 531 nm	BTL 380 nm	HTTL 325 nm
01SL02	63.0 ± 1.8*	62.6 ± 1.8*	6.2 ± 0.5*	445.00 ± 42.00
01SL03	51.7 ± 4.0	40.9 ± 1.5*	24.5 ± 1.0	325.00 ± 15.00
01SL07	12.0 ± 1.4	18.7 ± 1*	3.0 ± 0.2*	50.40 ± 7.90
01SL08	9.8 ± 0.9	10.2 ± 0.5	4.3 ± 0.7*	58.00 ± 3.50
01SL09	15.4 ± 0.7	15.4 ± 0.6	9.8 ± 0.3	nd
01SL11	18.3 ± 1.1	18.7 ± 0.7	18.6 ± 4.1	nd

(nd): not determined, (*): plateau test is not satisfied (1σ uncertainties).

Results of equivalent dose measurements for quartz and feldspars are summarised in Table 3. In the case of feldspar samples 01SL09 and 01SL11 no palaeodoses were extrapolated because there was no TL emission at high temperature, a common phenomenon in this type of rocks (Guérin and Petit, 1983). For quartz or feldspar, measurements were fairly reproducible (and even better in the case of quartz RTL) and extrapolations of palaeodoses were done under good conditions of linearity of TL growth with dose. In most cases, the plateau test is satisfied as shown in Fig. 3 and extrapolations can be made within the flat zone. When the plateau test is not satisfied, extrapolations are made using the maximum of TL peak around 370 °C.

3.3. Annual dose-rate evaluation

Uranium, thorium and potassium concentrations were measured by high-resolution gamma spectrometry on a representative sub-sample of the whole rock of about 100 g counted for at least 24 h on a coaxial HPGe detector. The post-radon values (mainly ^{214}Bi for the U series and ^{208}Tl for the Th series) as well as pre-radon values were taken into account in the concentration calculations. We found no evidence of any major disequilibrium within the radioactive decay chains. The spectrometer was calibrated with the IAEA standards RGU-1, RGTh-1 and IAEA-375. The concentrations and their

Please cite this article as: Guérin, G., Samper, A., Aberrant thermoluminescence dates obtained from primary volcanic quartz. Radiat. Meas. (2007), doi: 10.1016/j.radmeas.2007.03.006

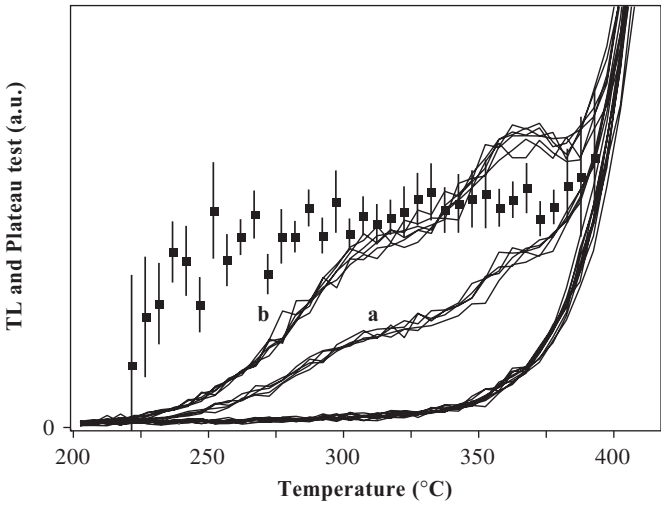

Fig. 3. Plateau test obtained for 01SL08. (a): NTL (Natural TL), (b): NTL + 10.64 Gy (TLD). Quartz green TL (531 nm), 5 °C/s, preheating: 30 s, 250 °C. Only a few glow-curves are plotted to show the reproducibility of aliquot measurements, plateau test on Y-axis is a value proportional to NTL/(TLD-NTL).

Table 4
U, Th and K concentrations of the whole rocks measured by gamma spectrometry (1σ uncertainties)

Sample	U (ppm)	Th (ppm)	K (%)
01SL02	2.14 ± 0.04	6.47 ± 0.14	1.39 ± 0.02
01SL03	2.40 ± 0.05	6.30 ± 0.14	1.50 ± 0.03
01SL07	2.37 ± 0.05	7.05 ± 0.15	1.47 ± 0.02
01SL08	1.98 ± 0.04	7.19 ± 0.15	1.28 ± 0.02
01SL09	2.76 ± 0.05	8.52 ± 0.16	1.73 ± 0.03
01SL11	2.53 ± 0.05	8.11 ± 0.16	1.67 ± 0.03

uncertainties (estimated from the counting statistics and the standards) are listed in Table 4.

In the case of quartz microcrystals, external alpha contribution to the annual dose-rate was neglected by assuming that the HF etching had removed their outer parts. We also chose, as a first approximation, to neglect the internal alpha dose contribution, as alpha efficiency to generate TL in quartz is low (Valladas and Valladas, 1982) and because the concentrations of U or Th in quartz are always very low. For the beta dose-rate evaluation, the macroscopic size of the quartz in the rock had been taken into account by applying the appropriate attenuation factors (Mejdahl, 1979).

In the case of feldspars, alpha radiation was the major contributor to the annual dose-rate. This contribution was computed using the omnidirectional flux system (Valladas and Valladas, 1982; Valladas, 1988). Standard values for the dose-rate conversion factor of the alpha flux were used (Bell, 1979). For each sample, an equivalence factor was calculated by taking the ratio of the beta dose to the omnidirectional alpha flux (at 3.25 MeV) that creates the same TL intensity. This factor was measured on bleached single-layer 90–125 μm aliquots using a ^{241}Am alpha source and a ^{90}Sr beta source. Another multiplicative factor was applied to take into account the size of the feldspar in the rock and the internal contribution of U and Th to the alpha dose (Guérin and Valladas, 1980). The actual internal U and Th concentrations within the feldspars have not been measured. The way in which the feldspars were prepared produced fractions highly representative of the whole rock. In such silica-rich lavas and pumices, besides quartz phenocrysts and few femic and opaque minerals, up to 80% of the rock is composed of feldspars. This is why we chose to estimate dose-rates assuming a uniform distribution of U and Th with no partition of these elements between the whole rock and the feldspars. This hypothesis probably slightly overestimates the annual alpha dose-rate.

Table 5
Annual dose-rate estimates for quartz in mGy/yr (1σ uncertainties) deduced from the values of U, Th and K concentrations (Table 4) and attenuation factor deduced from the estimated grain diameter in the rock (Mejdahl, 1979)

Sample	Beta attenuation	Beta dose rate	Gamma dose rate	Annual dose rate
01SL02	0.67	1.06 ± 0.01	0.89 ± 0.01	2.03 ± 0.02
01SL03	0.67	1.13 ± 0.02	0.94 ± 0.01	2.15 ± 0.02
01SL07	0.67	1.18 ± 0.02	0.96 ± 0.01	2.17 ± 0.02
01SL08	0.45	0.67 ± 0.02	0.88 ± 0.01	1.63 ± 0.02
01SL09	0.45	0.90 ± 0.02	1.14 ± 0.01	2.12 ± 0.02
01SL11	0.45	0.86 ± 0.02	1.08 ± 0.01	2.02 ± 0.02

For both quartz and feldspars, cosmic ray contribution has been estimated at 0.080 ± 0.005 mGy/yr (Prescott and Hutton, 1994), by taking into account the fact that samples were taken from at least 5 m below the surface. Gamma and beta dose-rates were computed using the conversion factors derived from the energies given by the ENSDF (Adamiec and Aitken, 1998). The estimated dose-rates for quartz are listed in Table 5 and the dose-rates for feldspars in Table 6.

4. Discussion

Palaeodoses measured under different conditions and estimated annual dose-rates allowed us to calculate the set of apparent ages listed in Table 7. The most striking fact is the scatter of the sub-set of ages obtained for quartz. Sample 01SL11 is the only one for which the red, green and blue TL gave the same value for the apparent palaeodose. For all the other samples, the extrapolated BTL values were smaller than those of RTL or GTL. In four cases, however, red and green TL gave the same estimates for the apparent palaeodose (differences are significant for 01SL03 and 01SL07). The lack of internal coherence of TL results for quartz is puzzling, as one would have expected apparent dose extrapolations to be independent of the colour of the TL. Thus, it is not surprising that the TL ages do not agree with the ages estimated by other means. Results for 01SL11 are even more puzzling because while plateau tests are satisfied in the three spectral domains and the three extrapolated apparent palaeodoses match, the computed TL ages do not agree with the ^{14}C ages. It would seem that age-estimates calculated from quartz are systematically underestimated,

Please cite this article as: Guérin, G., Samper, A., Aberrant thermoluminescence dates obtained from primary volcanic quartz. Radiat. Meas. (2007), doi: 10.1016/j.radmeas.2007.03.006

Table 6
Annual dose-rates (mGy/yr) for feldspars using concentrations of Table 4 (1σ uncertainties)

Sample	Alpha efficiency	$D\alpha$	$D\beta$	$D\gamma$	Total
01SL02 F	5.1 ± 0.4	2.25 ± 0.21	1.58 ± 0.02	0.89 ± 0.01	4.80 ± 0.21
01SL03 F	3.5 ± 0.3	1.66 ± 0.17	1.70 ± 0.02	0.94 ± 0.01	4.38 ± 0.17
01SL07 F	8.7 ± 0.9	4.27 ± 0.47	1.69 ± 0.02	0.96 ± 0.01	7.00 ± 0.47
01SL08 F	11.4 ± 1.2	5.15 ± 0.60	1.49 ± 0.02	0.88 ± 0.01	7.60 ± 0.60

Alpha efficiency (nGy cm^2/alpha yr) was measured on bleached aliquots and alpha dose rate is computed using a 6.0 ± 0.3 geometry factor equivalent to a quasi-uniform repartition of U and Th. Contribution of cosmic rays has been uniformly set to 0.080 ± 0.005 mGy/yr.

Table 7
Apparent ages and dose-rates obtained on quartz using red, green and blue TL emissions

Sample		Palaeodose (Gy)	Annual Dose rate (mGy/an)	Apparent age (ka)	Other age (ka)	Method
01SL02	RTL (610 nm)	63.0 ± 1.8	2.11 ± 0.02	29.9 ± 0.9	92.7 ± 9.7	HTTL
	GTL (531 nm)	62.6 ± 1.8		29.7 ± 0.9		
	BTL (380 nm)	6.2 ± 0.5		2.9 ± 0.2	95.0 ± 2.0	K–Ar
01SL03	RTL (610 nm)	51.7 ± 4.0	2.24 ± 0.02	23.1 ± 1.8	74.2 ± 4.2	HTTL
	GTL (531 nm)	40.9 ± 1.5		18.2 ± 0.7		
	BTL (380 nm)	24.5 ± 1.0		10.9 ± 0.5	77.0 ± 2.0	K–Ar
01SL07	RTL (610 nm)	12.5 ± 1.0	2.27 ± 0.02	5.5 ± 0.4	7.6 ± 1.2	HTTL
	GTL (531 nm)	18.7 ± 1.0		8.3 ± 0.4		
	BTL (380 nm)	3.0 ± 0.2		1.3 ± 0.1		
01SL08	RTL (610 nm)	9.8 ± 0.9	1.69 ± 0.02	5.8 ± 0.5	7.6 ± 0.8	HTTL
	GTL (531 nm)	10.2 ± 0.5		6.0 ± 0.3	3.0 ± 3.0	K–Ar
	BTL (380 nm)	4.3 ± 0.7		2.5 ± 0.4		
01SL09	RTL (610 nm)	15.4 ± 0.7	2.21 ± 0.02	7.0 ± 0.3	20–29	^{14}C
	GTL (531 nm)	15.4 ± 0.6		7.0 ± 0.3		
	BTL (380 nm)	9.8 ± 0.3		4.4 ± 0.1		
01SL11	RTL (610 nm)	18.3 ± 1.1	2.09 ± 0.02	8.8 ± 0.5	34.5 ± 0.4	^{14}C
	GTL (531 nm)	18.7 ± 0.7		9.0 ± 0.3		
	BTL (380 nm)	18.6 ± 4.1		8.9 ± 2.0		

Other age values are based either on plagioclase thermoluminescence (HTTL), K–Ar or uncalibrated ^{14}C (all figures are quoted with 1σ uncertainties).

with the RTL results being closest to those obtained by other methods. Nevertheless, even with red TL, the age can be underestimated by as much as a factor of 3 and only one sample, 01SL07, had a RTL age close to that obtained by HTTL.

Several explanations, some very implausible, can be suggested to account for these differences. The first one could be a partial bleaching of the sample due to light exposure in the field, but as we noted above the samples were extracted from large rocks not transparent to light beyond a fraction of an mm. Moreover, the outer layer (about 1 cm) of each sample was discarded during the initial phase of laboratory treatment and we verified the harmlessness of light emitted by our Na–halogen lamps by exposing sample aliquots to these lamps for about 1 h. Though this exposure was longer and more intense than that experienced by our samples during the laboratory processing, no detectable TL bleaching was observed. Furthermore, some plateau tests (see Fig. 3) encompass both the 325 and 375 °C TL peaks known to have different sensitivities to light bleaching (e.g. Franklin et al., 2000). Thus, it is unlikely that unintentional exposure to light during the preparation of our samples was responsible for the age underestimates.

Another explanation could be a contribution of feldspar to the TL in a range of temperatures where the minerals are affected by thermal or anomalous fading (Wintle, 1977). Visual examination of all our samples revealed no evidence of contamination by feldspars. Checks by X-ray analysis done with a PanAnalytical X′Pert Pro MPD diffractometer revealed the presence of feldspars (3.22 Å peak) in 01SL02, 01SL07 and 01SL09 but at levels below 0.5%. Such concentrations were found to have no impact on the TL measurements of quartz when the relative TL sensitivity of quartz and feldspars from the host rock were compared.

Still another reason could be that the samples dated by ^{14}C were attributed to the wrong geological formation, or that age estimates obtained by other methods are incorrect. Wrong attribution is unlikely, because the formations of Choiseul and Belfond are very characteristic and extend over a large geographical area. The ^{14}C ages are unlikely to be wrong because they come from several independent measurements on charcoal from different places and are coherent (Wright et al., 1984; Lindsay et al., 2005). Concerning the K–Ar ages, the unspiked method associated with specific protocols for sample

Please cite this article as: Guérin, G., Samper, A., Aberrant thermoluminescence dates obtained from primary volcanic quartz. Radiat. Meas. (2007), doi: 10.1016/j.radmeas.2007.03.006

preparation has been shown to be well-adapted to the measurement of young ages (Gillot and Cornette, 1986; Quidelleur et al., 2001). However, in K–Ar datings a contribution of inherited radiogenic ^{40}Ar cannot be totally excluded and this would yield overestimated ages. Such a contribution must be negligible, judging by the good agreement between K–Ar and plagioclase HTTL ages for 01SL02 and 01SL03 and an acceptable agreement in the case of 01SL08. A detailed discussion of anomalous fading and alpha dose-rate contribution to the feldspar annual dose calculations is beyond the scope of this paper. As a safety precaution, we used an overestimating calculation for alpha dose-rate contribution, and if there were to be some fading, the computed feldspar TL ages should be taken as the lower limits of the true ages. Under this conservative approach the impact of any inherited radiogenic ^{40}Ar on the calculated K–Ar ages can be ruled out (in other words, K–Ar calculated ages cannot have been strongly overestimated). On the whole, only GTL of 01SL07 and RTL and GTL of 01SL08 appear to give correct ages compatible with those obtained by other methods.

The last explanation could be that the calculated annual dose-rates were off by as much as a factor of 2 or 3. Radioactive disequilibrium (due to a continuous loss of radon for instance) would yield an actual annual dose-rate lower than our present estimate. Once again, it is difficult to plead for such an effect, particularly when a factor of 2 is involved, because it should have affected all the samples, including feldspars, which could not have witnessed the high apparent palaeodoses that were measured (in other words, feldspar and quartz palaeodoses are not compatible whatever the actual annual dose-rate is). Moreover, such a major problem would have been detected by gamma spectrometry.

5. Conclusions

The scatter of estimated TL ages calculated for primary volcanic quartz is puzzling and provides evidence for the unusual luminescence behaviour of this mineral. Ages appear to be inaccurate even though the plateau test is satisfied or when apparent palaeodoses are independent of the spectral domain of measurements while quartz samples extracted from volcanic and sedimentary rocks are undoubtedly mineralogically identical, one may argue that they might exhibit different TL behaviour as they contain different trace element impurities, and as they were not formed in the same manner, they experienced different crystallisation rates and were not exposed to the same radiation and temperature fluctuations in the past. Dose-rate effects have been identified in very pure filonian quartz (Valladas and Ferreira, 1980) as well as in some other types of quartz (Chawla et al., 1998). This may be part of the explanation for the results reported here. One could also question the sample preparation itself (HF etching and crushing) though this would be a radical criticism of the inclusion technique used successfully for more than 30 years on "standard" quartz. The long term fading and dose-rate experiments and dose recovery tests currently being done on these volcanic samples may provide some clues to explain the anomalies presented here.

Undoubtedly, this set of age inter-comparisons is too small for anyone to conclude that volcanic quartz is unsuitable for TL dating. Even though satisfactory explanations for the physics of the luminescence behaviour are lacking, this is a case showing that conventional methodology and standard procedures used in TL dating are no guarantee that reliable ages will be obtained. This unexpected drawback suggests that TL dates of quartz from volcanic environments should be accepted with caution when no external age controls are performed. One should keep in mind that red TL ages, if taken as a stand-alone set, could have been considered, although a bit young, to be compatible with geological data.

Acknowledgements

We are grateful to Dr. Ph. Bonté of the LSCE (CEA-CNRS, Gif-sur-Yvette) for kindly providing gamma spectrometry analysis, Ph. Pradel (IDES, UPS-Orsay) for providing X-rays diffraction diagrams.

References

Adamiec, G., Aitken, M.J., 1998. Dose-rate conversion factors: update. Ancient TL 16 (2), 37–50.
Aitken, M.J., 1985. Thermoluminescence Dating. Academic Press, London.
Aitken, M.J., 1992. Optical dating. Quat. Sci. Rev. 11, 127–131.
Aitken, M.J., 1998. An Introduction to Optical Dating. Oxford University Press, Oxford.
Bell, W.T., 1979. Thermoluminescence dating: radiation dose-rate data. Archaeometry 21 (2), 243–245.
Chawla, S., Gundu Rao, T.K., Singhvi, A.K., 1998. Quartz thermoluminescence: dose and dose-rate effects and their implications. Radiat. Meas. 29, 53–63.
Fattahi, M., Stokes, S., 2000. Extending the time range of luminescence dating using red TL (RTL) from volcanic quartz. Radiat. Meas. 32 (5–6), 479–485.
Fattahi, M., Stokes, S., 2003. Dating volcanic and related sediments by luminescence methods: a review. Earth Sci. Rev. 62, 229–264.
Fleming, S.J., 1970. Thermoluminescence dating: refinement of the quartz inclusion method. Archaeometry 12, 133–147.
Fleming, S.J., 1972. Thermoluminescence authenticity testing of ancient ceramics using radiation-sensitivity changes in quartz. Naturwissenschaften 59, 145–151.
Franklin, A.D., Prescott, J.R., Robertson, G.B., 2000. Comparison of blue and red TL from quartz. Radiat. Meas. 32 (5–6), 633–639.
Ganzawa, Y., Furukawa, H., Hashimoto, T., Sanzelle, S., Miallier, D., Pilleyre, Th., 2005. Single grains dating of volcanic quartz from pyroclastic flows using Red TL. Radiat. Meas. 39, 479–487.
Gillot, P.-Y., Cornette, Y., 1986. The Cassignol technique for potassium–argon dating, precision and accuracy: examples from late pleistocene to recent volcanics from southern Italy. Chem. Geol. 59, 205–222.
Guérin, G., 2006. Some aspects of phenomenology and kinetics of high temperature thermoluminescence of plagioclase feldspars. Radiat. Meas. 41, 936–941.
Guérin, G., Valladas, G., 1980. Thermoluminescence dating of volcanic plagioclases. Nature 286, 697–699.
Guérin, G., Petit, R.-H., 1983. Datation par thermoluminescence des laves de la Guadeloupe: quelques problèmes. C.R. Ac. Sci. 296 (II), 1791–1794.
Hashimoto, T., Yokosaka, K., Habuki, H., 1987. Emission properties of thermoluminescence from natural quartz. Blue and red response to absorbed dose. Nucl. Tracks Radiat. Meas. 13 (1), 57–66.
Hashimoto, T., Kojima, M., Sakai, T., 1991. Age determination of prehistorical sites in Japan using red thermoluminescence measurements from quartz grains. Archaeol. Nat. Sci. 23, 13–25.

Please cite this article as: Guérin, G., Samper, A., Aberrant thermoluminescence dates obtained from primary volcanic quartz. Radiat. Meas. (2007), doi: 10.1016/j.radmeas.2007.03.006

Hashimoto, T., Notoya, S., Komura, K., Shiral, N., 1996. Red thermoluminescence dating of some volcanic-ash and pyroclastic-flow layers related to Takamori pre-historical sites using quartz inclusion method. Archaeol. Nat. Sci. 33, 1–15.

Kaul, I.K., Bhattacharya, P.K., Tolpadi, S., 1966. Age determination by study of the thermoluminescence of smoky quartz. J. Geophys. Res. 71 (4), 1275–1282.

Le Guen de Kerneizon, M., Bellon, H., Carron, J.-P., Maury, R.C., 1983. L'Ile de Ste-Lucie (Petites Antilles): distinction des principales séries magmatiques à partir des données pétrochimiques et géochronologiques. Bull. Soc. Géol. de France 7 (5), 773–781.

Lindsay, J.M., Smith, A.L., Roobol, M.J., Stasiuk, M.V., 2005. Volcanic Hazard Atlas of the Lesser Antilles. Seismic Research Unit, The University of West Indies, Trinidad and Tobago. ISBN 976-95142-0-9, 279pp.

Martin-Kaye, P.H.A., 1969. A summary of the geology of the Lesser Antilles. Overseas Geol. Miner. Resour. 10, 172–806.

Mejdahl, V., 1979. Thermoluminescence dating: beta-dose attenuation in quartz grains. Archaeometry 21 (1), 61–72.

Miallier, D., Faïn, J., Sanzelle, S., Raynal, J.-P., Daugas, J.-P., Paquereau M.-M., 1984. Datation du volcanisme quaternaire du Massif Central français par la méthode des inclusions de quartz en thermoluminescence et comparaison avec d'autres approches. Xe RAST, 396–396.

Miallier, D., Faïn, J., Sanzelle, S., Pilleyre, Th., Montret, M., Soumana, S., Falguères, C., 1994. Attempts at dating pumice deposits around 580 ka by use of red TL and ESR of xenolithic quartz inclusions. Radiat. Meas. 23 (2–3), 399–404.

Pilleyre, Th., Montret, M., Faïn, J., Miallier, D., Sanzelle, S., 1992. Attempts at dating ancient volcanoes using the red TL. Quartz Quat. Sci. Rev. 11, 13–17.

Prescott, J.R., Hutton, J.T., 1994. Cosmic ray contributions to dose rates for luminescence and ESR dating: large depths and long term time variation. Radiat. Meas. 23 (2–3), 497–500.

Quidelleur, X., Gillot, P.-Y., Soler, V., Lefèvre, J.-C., 2001. K–Ar dating extended into the last millennium: application to the youngest effusive episode of the Teide volcano (Canary Islands, Spain). Geophys. Res. Lett. 28, 3067–3070.

Quidelleur, X., Samper, A., Boudon, G., Le Friant, A., Komorowski, J., 2004. Radiometric dating of large volume flank collapse in the Lesser Antilles. Eos Trans. AGU 85 (47), (Fall Meet Suppl.).

Robson, G.R., Tomblin, J.F., 1966. Catalogue of active volcanoes of the world including Solfatara fields: Part 20, West Indies: Rome. International Association of Volcanologists. 56 pp.

Roobol, M.J., Wright, J.V., Smith, A.L., 1983. Calderas or gravity-slide structures in the Lesser Antilles island arc? J. Volcanol. Geotherm. Res. 19, 121–134.

Samper, A., Quidelleur, X., Boudon, G., Le Friant, A., Komorowski, J., 2007. Radiometric dating of large volume flank collapses in the Lesser Antilles arc J. Geol. Soc. London, submitted for publication.

Stokes, S., Fattahi, M., 2003. Red emission luminescence from quartz and feldspar for dating applications: an overview. Radiat. Meas. 37 (4–5), 383–395.

Tomblin, J.F., 1964. The volcanism history and petrology of the Soufrière region, St Lucia. University of Oxford, England. 213pp.

Tomblin, J.F., 1979. Le volcanisme récent et les éruptions historiques dans la partie centrale de l'arc insulaire des petites antilles, Saint-Lucia, Saint-Vincent. Bull. BRGM 2 (IV 3/4), 307–315.

Valladas, G., 1978. A problem encountered in dating Quartz by thermoluminescence. Eighteenth International Symposium on Archaeometry and Archaeological Prospection, pp. 499–504.

Valladas, G., 1988. Stopping power and range of alpha particles in SiO_2. Ancient TL (6), 7–8.

Valladas, G., Ferreira, J., 1980. On the dose-rate dependence of the thermoluminescence of quartz. Nucl. Instrum. Methods 175, 216–218.

Valladas, G., Valladas, H., 1982. Effet de l'irradiation alpha sur des grains de quartz. PACT 6, 171–178.

Vatin-Pérignon, N., Chevallier, L., 1983. St-Lucia, West Indies: new interpretation of the last eruptive event. Terra Cognita 3, 154.

Vatin-Pérignon, N., Chevallier, L., Blanc, F., 1985. Les événements dacitiques récents de la Soufrière de Sainte Lucie, Petites Antilles. Bull. PIRPSEV, CNRS-INAG (90), 32.

Wintle, A.G., 1977. Detailed study of a thermoluminescent mineral exhibiting anomalous fading. J. Lumin. 15, 385–393.

Wintle, A.G., 1997. Luminescence dating: laboratory procedures and protocols. Radiat. Meas. 27, 385–393.

Wright, J.V., Roobol, M.J., Smith, A.L., Sparks, R.S.J., Brazier, A., Rose, W.I., Sigurdsson, H., 1984. Late quaternary explosive silicic volcanism on St Lucia, West Indies. Geol. Mag. 121, 1–15.

Please cite this article as: Guérin, G., Samper, A., Aberrant thermoluminescence dates obtained from primary volcanic quartz. Radiat. Meas. (2007), doi: 10.1016/j.radmeas.2007.03.006

Available online at www.sciencedirect.com
SCIENCE DIRECT®
Lithos 74 (2004) 167–198
LITHOS
www.elsevier.com/locate/lithos

The Tethyan plume: geochemical diversity of Middle Permian basalts from the Oman rifted margin

H. Lapierre[a,*], A. Samper[a], D. Bosch[b], R.C. Maury[c], F. Béchennec[d], J. Cotten[c], A. Demant[e], P. Brunet[f], F. Keller[a], J. Marcoux[g]

[a] *Laboratoire Géodynamique des Chaînes Alpines, UMR-CNRS 5025, Université Joseoh Fourier, Géosciences, B.P. 53, 15 rue Gignoux, 38041 Grenoble cedex, France*
[b] *Laboratoire de Tectonophysique, UMR-CNRS 5568, Institut des Sciences de la Terre, de l'Eau et de l'Espace de Montpellier, Université Montpellier 2, Place E. Bataillon, 34095 Montpellier cedex, 05, France*
[c] *Laboratoire Domaines Océaniques, UMR-CNRS 6538, Université de Bretagne Occidentale, Place Nicolas Copernic, 29280 Plouzané, France*
[d] *Bureau de Recherches Géologiques et Minières, SGR Pays de Loire, B.P. 92342, 44323 Nantes cedex 3, France*
[e] *Laboratoire de Pétrologie Magmatique, Faculté des Sciences de St Jérôme, Université Aix-Marseille III, CC 441, 13397 Marseille cedex 20, France*
[f] *Laboratoire Mécanismes de Transfert en Géologie, UMR-CNRS 5563, Université P. Sabatier, 38 rue des trente-six ponts, 31400 Toulouse, France*
[g] *UMR-CNRS 7578, Institut de Physique du Globe de Paris, Université Paris VII, 4 Place Jussieu, 75252 Paris, France*

Received 18 June 2003; accepted 11 February 2004

Available online 26 April 2004

Abstract

According to palinspastic reconstructions, the Neo-Tethys opening took place during the Permian between the Cimmerian fragments in the north and the Indo-Arabian margin in the south. Igneous remnants of this opening are exposed in Oman within either the Hawasina nappes or the para-autochtonous Arabian platform exposed in the Saih Hatat tectonic window. They consist predominantly of pillowed basaltic flows among which three groups have been distinguished. Group 1 is tholeiitic and characterized by low TiO_2 and incompatible trace element contents, and a large range of εNd_i values. Group 1 basalts are associated with distal sediments and plot near the boundary of or within the MORB field in the Pb–Pb correlation diagrams and between the MORB and Bulk Silica Earth (BSE) fields in $\varepsilon Nd_i - (^{206}Pb/^{204}Pb)_i$ diagram. Group 2 basalts are alkaline and differ from Group 1 ones by their higher TiO_2, La and Nb contents, and lower and more homogeneous εNd_i values (+3 to +5). Group 2 volcanics are similar to alkali basalts from oceanic islands and share with Group 1 similar initial Pb ratios. Group 3 consists of tholeiitic and alkali basalts which are interbedded either with carbonate-platform sediments from the Saih Hatat window or with distal sediments from the Hawasina Nappes. This group differs from Groups 1 and 2 by its low to negative εNd_i (+1.6 to −2). Group 1 likely derived from the mixing of depleted and enriched sources while Group 2 derived exclusively from an enriched source. There is no indication that continental crust was involved in the genesis of both Groups 1 and 2. In contrast, the low to negative εNd_i values of Group 3 suggest that the magmas of this group were contaminated by the Arabian continental crust during their ascent. The geochemical features of the Middle Permian plume-related basalts suggest thus that

* Corresponding author.
E-mail address: lapierre@ujf-grenoble.fr (H. Lapierre).

0024-4937/$ - see front matter
doi:10.1016/j.lithos.2004.02.006

the basement of the Hawasina basin was not genuine oceanic crust but either the thinned Arabian rifted continental margin or the continent–ocean transition zone of the Neo-Tethys.

Keywords: Plume-related basalts; Middle Permian; Neo-Tethys; Arabian rifted margin; Hawasina Nappes; Oman; Isotopic chemistry

1. Introduction

The Permo-Triassic transition coincides with the breakup of Pangea, the Neo-Tethyan ocean opening, the development of continental rifts, and changes in the Earth's environment that are held responsible for a major mass extinction. This major lithospheric reorganization is accompanied by the extrusion of voluminous flood basalts which is attributed to the upwelling of large scale mantle plumes (super plumes) which rise from the core–mantle boundary and impinge the lithosphere (Coffin and Eldholm, 1992, 1994; Kent et al., 1992; Wilson and Guiraud, 1998; Courtillot et al., 1999).

According to different palinspastic reconstructions (Scotese and Golonka, 1993; Matte, 2002; Stampfli et al., 2001; Nikishin et al., 2002) the Neo-Tethys opening began during the Mid to Late Permian and took place between the Cimmerian continental fragments in the north and the Indian–Arabian margin in the south. Igneous remnants of this opening are exposed in the Himalayas (Vannay and Spring, 1993; Acharyya, 1992; Gaetani and Garzanti, 1991; Garzanti et al., 1994, 1996a, 1996b, 1999; Garzanti and Sciunnach, 1997; Robertson, 1998, 2000; Corfield et al., 1999), Iran (Berberian and King, 1981; Sengör et al., 1993), Zagros (Sëngor, 1990; Sengör et al., 1993), and Oman (Béchennec et al., 1988, 1991; Rabu et al., 1990; Robertson and Searle, 1990; Robertson et al., 1990; Sengör et al., 1993) (Fig. 1). During the Late Triassic, the opening of a Neo-Tethys southern basin took place farther west, north of the African margin and south of the Menderes continental block. This opening is well documented in southern Turkey (Marcoux, 1987; Robertson and Waldron, 1990), NW Syria (Parrot, 1974; Al-Riyami et al., 2000), and SW Cyprus (Lapierre and Rocci, 1976; Malpas et al., 1993; Lapierre et al., submitted for publication).

In order to reconstruct the different stages of the development of the Neo-Tethyan ocean, one must study the remnants of this ocean and its margins which are generally preserved in nappes or sheets thrusted onto the continental margins or incorporated within the Alpine folded chains. The only preserved remnants of the Middle to Late Permian incipient stage of the Neo-Tethys development are those of its rifted southern margin, now exposed in the Himalayas and Oman (Fig. 1). They consist of Middle to Upper Permian volcanics associated either with platform carbonates or with shallow to deep marine sediments. They usually occur as sheets thrusted on the Indian (Indian Himalayas) and Arabian (Oman) plate margins. These nappes are tectonically overlain by the Jurassic Spontang ophiolites (Ladakh) and Cretaceous Samail ophiolite (Oman).

In Oman, the remnants of the southern margin of the Neo-Tethyan ocean belong to the Hawasina nappes (Fig. 2) which consist of imbricated sedimentary and volcanic units. The latter document the Late Paleozoic and Mesozoic evolution of the Neo-Tethys and the rifted passive Arabian continental margin. The common occurrence of Middle Permian pillowed basaltic flows at the base of the Hawasina Nappes led many authors (Glennie et al., 1974; Blendinger et al., 1990, 1992; Stampfli et al., 1991; Pillevuit et al., 1992, 1997; Stampfli and Pillevuit, 1993) to consider that the Neo-Tethys was already floored by oceanic crust at the end of the Paleozoic. Alternatively, others proposed that the Middle Permian volcanism was plume-related and accompanied the breakup and rifting of the Arabian platform (Lippard et al., 1986; Béchennec et al., 1988, 1991; Maury et al., 2001, 2003).

The goal of this paper is to discuss the trace element and Nd and Pb isotopic chemistry of faunistically well-dated Middle Permian basaltic lavas located within either the Hawasina Nappes (Al Ajal, Rustaq, Wadi Wasit and Buday'ah localities; Fig. 3) or within the para-autochtonous Arabian margin (Wadi

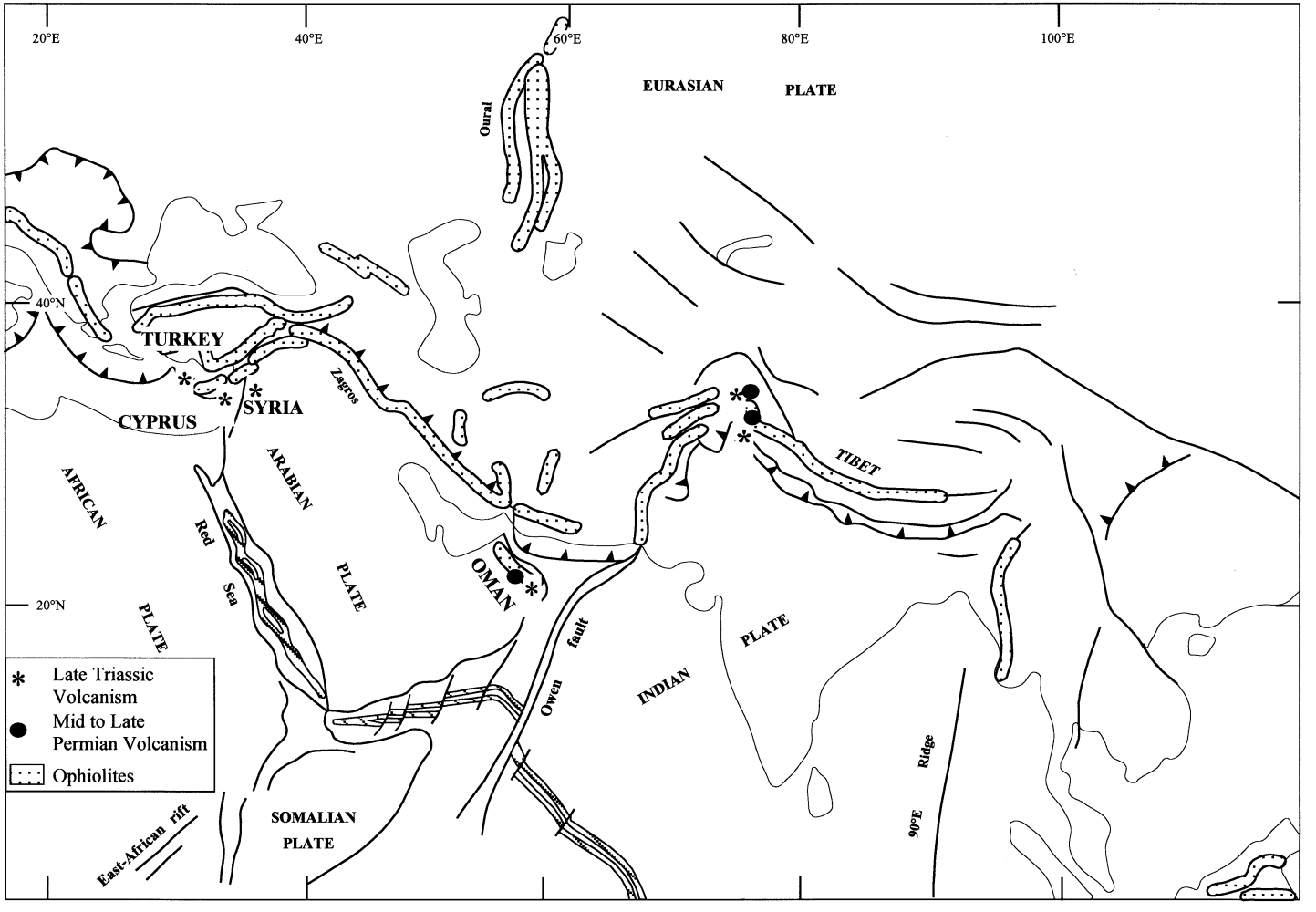

Fig. 1. Sketch map of the Tethyan ophiolites and the Permian–Triassic volcanic sequences (after Searle, 1983).

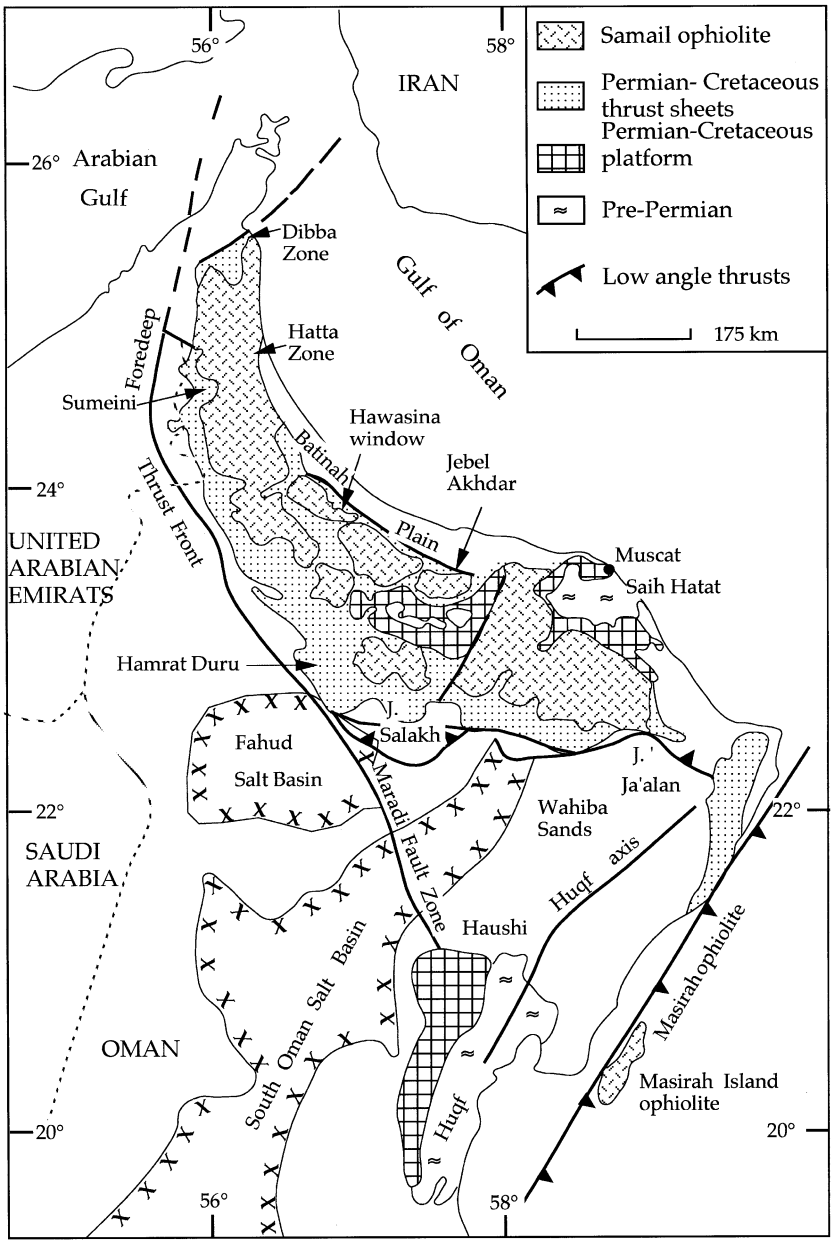

Fig. 2. Structural sketch map of the Oman Mountains showing the main tectonic units (after Robertson and Searle, 1990).

Aday, Saih Hatat window, Fig. 3). These geochemical data will help to (i) determine the nature of the sources involved in the genesis of this volcanism, (ii) precise its geodynamic setting, and (iii) constrain the evolution of the Arabian margin at the end of Paleozoic times.

2. Geologic setting

The Oman Mountain Ranges consist of (1) the autochthonous–parautochthonous Late Proterozoic–Palaeozoic basement and Permian–Cretaceous Arabian platform, (2) the allochthonous sedimentary

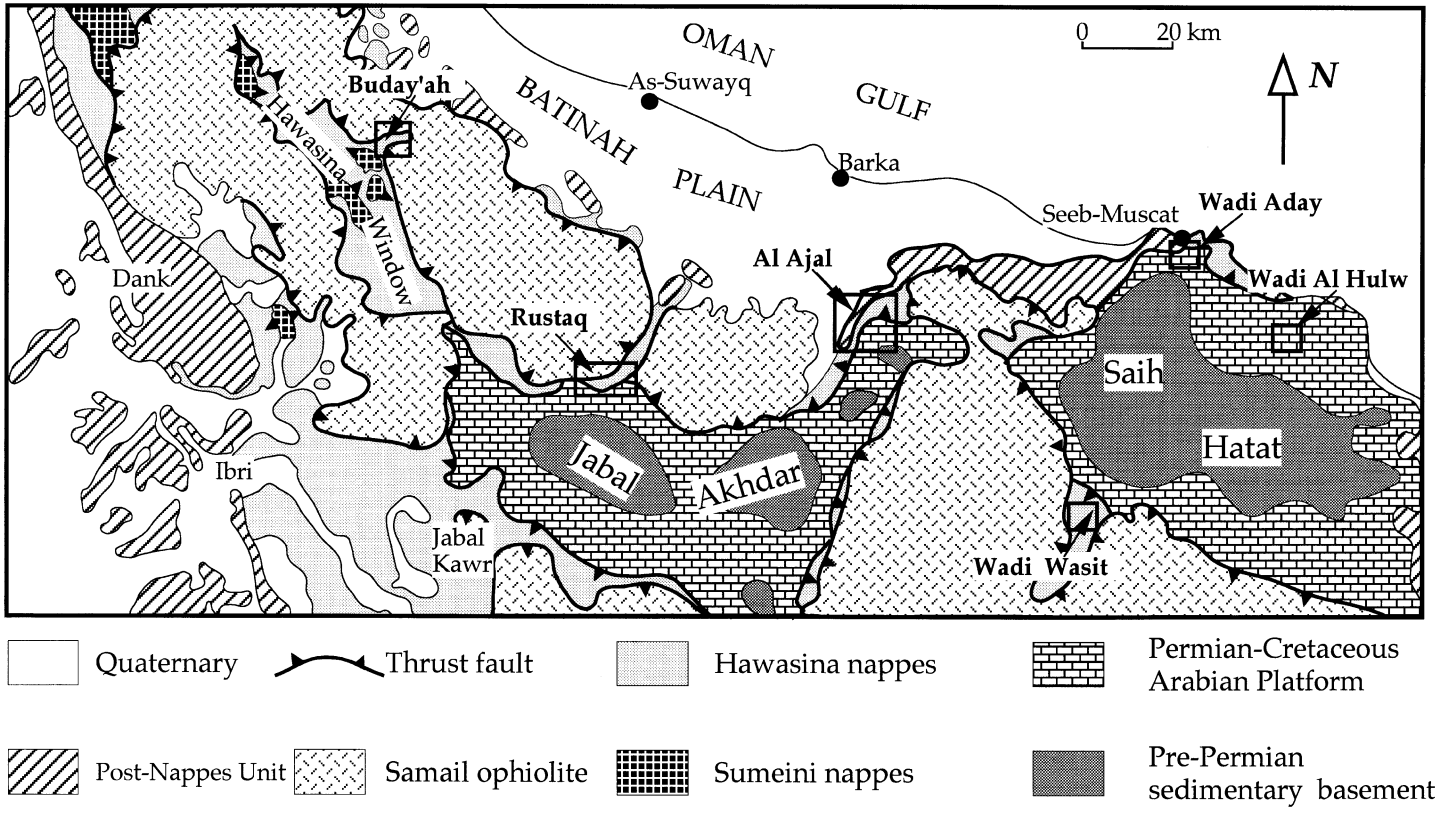

Fig. 3. Geologic map of the Hawasina nappes and the Arabian platform showing the locations of the Permian volcanic rocks (after Béchennec et al., 1988; Maury et al., 2003).

Table 1
Major and trace element chemistry of the Permian volcanic rocks from Oman

(a)

Group 1 +11.1 < εNd < +3.8 Low TiO_2 LREE-depleted (A)	Olivine cpx + feldspar Basalt		Olivine + Cr-spinel Basalt		Olivine cpx + feldspar Basalt		Olivine cpx + feldspar Basalt	
Sample number	OM07		OM123		OM237		OM13	
SiO_2%	47.7	49.81	46.9	48.93	47.5	49.79	51.50	53.72
TiO_2	0.82	0.86	0.76	0.79	0.74	0.78	0.90	0.94
Al_2O_3	15.05	15.72	15.3	15.96	16.4	17.19	13.75	14.34
Fe_2O_3	9.4	9.82	9.04	9.43	9.07	9.51	7.78	8.12
MnO	0.15	0.16	0.14	0.15	0.14	0.15	0.14	0.15
MgO	8.05	8.41	7.75	8.09	7.85	8.23	7.24	7.55
CaO	11.2	11.70	13.05	13.61	10.05	10.54	13.45	14.03
Na_2O	3.05	3.19	2.78	2.90	2.86	3.00	0.98	1.02
K_2O	0.27	0.28	0.06	0.06	0.72	0.76	0.02	0.02
P_2O_5	0.08	0.08	0.08	0.08	0.07	0.07	0.10	0.10
LOI	3.82		4.4		4.01		4.19	
Sc (ppm)	38		35		36		36.00	
Ti	5347		4951		4846		5864.00	
V	255		237		230		240.00	
Ni	106		210		132		125.00	
Co	43.209		42.156		34.69		38.84	
Cr	328		450		415		360.00	
Cs	0.130		0.160		0.450		2.17	
Rb	4.290		0.84		10.29		0.30	
Ba	34.230		23.91		37.1		12.00	
Th	0.090		0.18		0.07		0.28	
U	0.060		0.04		0.03		0.12	
Nb	1.150		2.15		0.71		3.05	
Ta	0.080		0.13		0.051		0.18	
Pb	0.310		0.53		0.26		0.46	
Sr	182.180		126.2		125.11		51.00	
Zr	45.100		46.49		38.91		53.45	
Hf	1.250		1.24		1.15		1.46	
Y	23.210		18.5		18.3		20.50	
Zr/Hf	36.080		37.492		33.835		36.61	
La (ppm)	1.500		2.07		1.11		2.78	
Ce	4.670		5.74		3.67		7.38	
Pr	0.840		0.934		0.68		1.13	
Nd	4.680		4.84		3.81		5.87	
Sm	1.780		1.71		1.45		1.95	
Eu	0.700		0.68		0.6		0.74	
Gd	2.780		2.4		2.26		2.72	

Group 1 +11.1 < εNd < +3.8 Low TiO_2 Flat REE (B)	Olivine Feldspar Cpx				Olivine + feldspar		Olivine cpx + feldspar		Olivine + feldspar	
Sample number	Dolerite		Basalt		Basalt		Basalt		Basalt	
	OM109		OM125		OM135		OM138		OM141	
SiO_2%	45.65	47.81	46.75	49.00	43.90	46.96	49.80	51.66	45.80	48.46
TiO_2	1.14	1.19	1.02	1.07	1.02	1.09	1.13	1.17	1.32	1.40
Al_2O_3	16.25	17.02	16.05	16.82	18.75	20.06	14.60	15.15	16.55	17.51
Fe_2O_3	9.85	10.32	10.00	10.48	9.54	10.21	10.38	10.77	11.52	12.19
MnO	0.17	0.18	0.16	0.17	0.18	0.19	0.18	0.19	0.16	0.17
MgO	8.07	8.45	8.10	8.49	7.48	8.00	8.28	8.59	8.25	8.73
CaO	11.20	11.73	9.23	9.67	9.30	9.95	8.25	8.56	5.91	6.25
Na_2O	2.92	3.06	2.79	2.92	3.15	3.37	3.16	3.28	4.48	4.74
K_2O	0.11	0.12	1.19	1.25	0.04	0.04	0.48	0.50	0.35	0.37
P_2O_5	0.13	0.14	0.12	0.13	0.12	0.13	0.14	0.15	0.17	0.18
LOI	4.25		4.14		6.61		3.43		4.95	
Sc (ppm)	38.00		38.00		39.00		40.00		43.00	
Ti	7456.00		6677.00		6815.00		7321.00		8725.00	
V	255.00		265.00		260.00		287.00		295.00	
Ni	180.00		170.00		162.00		101.00		205.00	
Co	44.70		46.57		39.69		39.96		48.28	
Cr	415.00		460.00		410.00		235.00		480.00	
Cs	0.40		1.48		0.46		0.60		0.27	
Rb	1.47		25.10		0.48		5.86		6.97	
Ba	26.18		104.40		49.87		85.37		48.01	
Th	0.49		0.46		0.46		0.53		0.74	
U	0.12		0.11		0.11		0.13		0.17	
Nb	5.70		4.99		4.72		5.93		8.44	
Ta	0.34		0.30		0.29		0.36		0.49	
Pb	0.60		0.49		1.30		0.33		0.77	
Sr	92.76		144.14		101.63		151.60		123.58	
Zr	79.63		68.51		64.47		75.12		95.59	
Hf	1.97		1.69		1.69		1.96		2.34	
Y	24.50		19.00		23.00		25.00		24.00	
Zr/Hf	40.40		40.58		38.08		38.30		40.94	
La (ppm)	4.59		4.06		3.98		5.26		5.06	
Ce	11.94		9.92		9.66		12.65		13.39	
Pr	1.76		1.45		1.41		1.82		1.96	
Nd	8.48		7.08		6.83		8.77		9.42	
Sm	2.64		2.24		2.25		2.69		3.00	
Eu	0.93		0.83		0.86		0.90		1.05	
Gd	3.44		2.90		3.07		3.52		3.68	

Tb	0.510	0.44	0.42	0.50	Tb	0.62	0.52	0.58	0.63	0.65
Dy	3.490	2.94	2.9	3.22	Dy	3.99	3.40	3.74	4.07	4.23
Ho	0.790	0.67	0.64	0.73	Ho	0.89	0.73	0.84	0.91	0.90
Er	2.280	1.95	1.9	2.06	Er	2.60	2.13	2.42	2.69	2.60
Yb	2.200	1.82	1.83	2.02	Yb	2.42	2.15	2.22	2.44	2.41
Lu	0.340	0.29	0.29	0.32	Lu	0.38	0.32	0.35	0.37	0.36
$(La/Yb)_N$	0.489	0.816	0.435	0.99	$(La/Yb)_N$	1.36	1.35	1.29	1.55	1.50
Mg#	66.8	66.9	67.1	68.7	Mg#	65.84	65.59	64.85	65.24	62.76

(b)

Group 1 +11.1 < εNd < +3.8 Low TiO_2 Flat REE (B)	Cr-spinel Olivine Basalt OM232		Cr-spinel Olivine Basalt OM235		Cr-spinel Olivine Basalt OM236		Group 1 +11.1 < εNd < +3.8 Low TiO_2 L REE-enriched (C)	Olivine Feldspar Cpx Dolerite OM115		cpx OM115	Cr-spinel Olivine Basalt OM117		Olivine cpx + feldspar Basalt OM140		Olivine + feldspar Basalt OM227	
SiO_2%	46.80	49.59	44.50	47.33	47.8	49.77	SiO_2%	47.00	49.19		47.00	48.86	43.5	48.40	44.5	47.88
TiO_2	1.06	1.12	1.11	1.18	1.01	1.05	TiO_2	1.26	1.32		1.39	1.45	1.59	1.77	1.37	1.47
Al_2O_3	14.80	15.68	17.65	18.77	15.16	15.79	Al_2O_3	16.20	16.96		15.45	16.06	13.85	15.41	17.05	18.35
Fe_2O_3	10.48	11.10	11.50	12.23	9.56	9.95	Fe_2O_3	9.50	9.94		9.10	9.46	10.85	12.07	10.25	11.03
MnO	0.14	0.15	0.16	0.17	0.16	0.17	MnO	0.15	0.16		0.15	0.16	0.26	0.29	0.16	0.17
MgO	4.80	5.09	4.18	4.45	8.45	8.80	MgO	8.14	8.52		6.60	6.86	1.37	1.52	5.25	5.65
CaO	11.20	11.87	10.90	11.59	9.95	10.36	CaO	9.60	10.05		12.80	13.31	11	12.24	10.2	10.98
Na_2O	4.94	5.23	3.85	4.10	2.97	3.09	Na_2O	3.07	3.21		3.46	3.60	6.7	7.45	3.22	3.47
K_2O	0.04	0.04	0.03	0.03	0.86	0.90	K_2O	0.47	0.49		0.04	0.04	0.53	0.59	0.75	0.81
P_2O_5	0.12	0.13	0.14	0.15	0.12	0.13	P_2O_5	0.15	0.16		0.20	0.21	0.23	0.26	0.19	0.20
LOI	5.82		5.83		3.85		LOI	4.25			3.97		10.09		7.02	
Sc (ppm)	41.00		46.00		38		Sc (ppm)	37.00			34.00		28		40.50	
Ti	7013.00		7376.00		6570		Ti	8236.00			9025.00		10,605		9206.00	
V	300.00		340.00		260		V	260.00			259.00		388		270.00	
Ni	132.00		205.00		150		Ni	115.00			152.00		66		142.00	
Co	44.27		42.15		38.1528		Co	36.62			40.34		29.614		49.66	
Cr	410.00		565.00		420		Cr	380.00			382.00		175		425.00	
Cs	0.04		0.31		0.60		Cs	1.36		0.21	0.46		0.41		3.19	
Rb	0.51		0.29		12.60		Rb	6.39		1.65	0.43		9.30		9.01	
Ba	45.02		48.15		42.03		Ba	41.83		9.63	28.01		88.71		38.87	
Th	0.35		0.38		0.40		Th	0.66		0.11	1.09		0.68		0.76	
U	0.17		0.24		0.10		U	0.18		0.05	0.24		0.38		0.18	
Nb	3.77		4.41		4.31		Nb	7.17		1.71	11.64		8.21		8.94	
Ta	0.22		0.28		0.26		Ta	0.44		0.11	0.68		0.50		0.51	
Pb	0.71		0.70		0.41		Pb	0.50		0.20	0.87		1.42		0.98	
Sr	255.91		93.87		154.62		Sr	172.24		36.56	163.88		194.53		124.85	
Zr	68.79		67.66		58.49		Zr	86.40		44.02	111.47		112.24		104.51	
Hf	1.74		1.79		1.53		Hf	2.24		1.67	2.60		2.51		2.52	
Y	24.00		27.50		23.00		Y	23.50		25.37	24.50		21.00		22.50	

(continued on next page)

Table 1 (*continued*)

(b)

Group 1 +11.1 < εNd < +3.8 Low TiO_2 Flat REE (B)	Cr-spinel Olivine Basalt OM232	Cr-spinel Olivine Basalt OM235	Cr-spinel Olivine Basalt OM236	Group 1 +11.1 < εNd < +3.8 Low TiO_2 L REE-enriched (C)	Olivine Feldspar Cpx Dolerite OM115	cpx OM115	Cr-spinel Olivine Basalt OM117	Olivine cpx + feldspar Basalt OM140	Olivine + feldspar Basalt OM227
Zr/Hf	39.53	37.86	38.33	Zr/Hf	38.50	26.30	42.82	44.65	41.47
La (ppm)	3.20	4.27	3.46	La (ppm)	6.17	1.45	9.09	8.38	6.53
Ce	8.45	10.26	8.59	Ce	14.66	4.20	19.84	21.11	15.60
Pr	1.35	1.54	1.29	Pr	2.09	0.80	2.73	2.88	2.20
Nd	6.82	7.91	6.28	Nd	9.70	4.86	12.28	13.43	10.38
Sm	2.33	2.69	2.03	Sm	2.87	2.14	3.45	3.65	3.07
Eu	0.84	0.93	0.73	Eu	0.98	0.78	1.21	1.35	1.11
Gd	3.14	3.46	2.75	Gd	3.59	3.39	4.02	4.47	3.72
Tb	0.58	0.64	0.50	Tb	0.62	0.60	0.70	0.67	0.69
Dy	3.78	4.20	3.21	Dy	3.85	4.13	4.47	3.86	4.14
Ho	0.88	0.91	0.73	Ho	0.86	0.89	0.90	0.79	0.90
Er	2.51	2.74	2.08	Er	2.47	2.57	2.61	2.01	2.55
Yb	2.35	2.25	1.98	Yb	2.28	2.36	2.38	1.76	2.30
Lu	0.36	0.35	0.30	Lu	0.36	0.37	0.35	0.27	0.34
$(La/Yb)_N$	0.98	1.36	1.25	$(La/Yb)_N$	1.94	0.44	2.74	3.42	2.03
Mg#	51.87	46.10	67.53	Mg#	66.84		63.05	22.90	54.65

(c)

Group 2 +5 < εNd < +3 High TiO_2 L REE-enriched	Dolerite Intrusive OM05	Feldspar Laths Ti-oxides Basalt OM09	Feldspar Laths Ti-oxides Basalt OM118	Alkali Basalt OM121	Olivine Feldspar Ti-rich Cpx Dolerite OM131	Feldspar Laths Ti-oxides Basalt OM143	Feldspar Laths Ti-oxides OM210	Alkali Basalt OM243
SiO_2%	43.40	47.08	43.90	47.37	48	50.27	44.5	46.97	45	47.20	43.7	46.11	48.8	51.52	46.60	48.19
TiO_2	2.33	2.52	3.23	3.49	3.68	3.85	3.38	3.57	2.86	3.00	3.95	4.17	3.46	3.65	3.67	3.79
Al_2O_3	15.20	16.49	13.30	14.35	14.96	15.67	15.7	16.57	16.75	17.57	16.5	17.41	16.58	17.50	14.55	15.04
Fe_2O_3	10.40	11.28	14.25	15.38	13.05	13.67	14.05	14.83	11.65	12.22	13.7	14.46	12.35	13.04	15.50	16.03
MnO	0.33	0.35	0.16	0.17	0.09	0.09	0.16	0.17	0.17	0.18	0.15	0.16	0.06	0.06	0.20	0.20

MgO	4.56	4.94	2.97	3.21	4.48	4.69	5.38	5.68	5.4	5.66	7	7.39	2.07	2.19	3.87	4.00
CaO	10.35	11.22	8.85	9.55	4.49	4.70	5.25	5.54	8	8.39	2.79	2.94	3.98	4.20	4.88	5.04
Na_2O	5.15	5.58	4.30	4.64	5.40	5.66	4.72	4.98	3.65	3.83	5.4	5.70	6.15	6.49	4.67	4.83
K_2O	0.06	0.06	1.02	1.10	0.14	0.15	0.05	0.05	1.27	1.33	0.14	0.15	0.69	0.73	2.13	2.20
P_2O_5	0.33	0.35	0.70	0.76	1.20	1.26	1.55	1.64	0.6	0.63	1.45	1.53	0.58	0.61	0.63	0.65
LOI	7.90		7.02		3.96		4.53		4.02		4.41		4.95		2.49	
Sc (ppm)	52.00		17.80		18.00		19.00		21.00		21.30		14.50		25.5	
Ti	15,120.00		21,766.00		24,068.00		22,281.00		18,733.00		26,030.00		22,814.00		22,740	
V	430.00		214.00		215.00		170.00		250.00		180.00		325.00		315	
Ni	38.00		27.00		15.00		5.00		51.00		9.00		39.00		27	
Co	45.00		32.59		23.67		31.77		33.89		39.77		44.51		48	
Cr	50.00		13.00		2.00		1.00		65.00		1.00		16.00		17	
Cs			0.54		0.13		0.26		0.57		0.18		0.82			
Rb	1.10		20.00		1.20		0.16		20.60		1.68		27.98		33	
Ba	28.00		92.00		67.26		203.18		158.02		56.77		92.39		239	
Th	2.80		3.62		3.85		5.00		4.48		4.82		3.39		3.2	
U			0.76		1.25		1.28		1.14		2.27		0.64			
Nb	17.00		47.82		53.25		67.32		54.76		60.47		39.33		33	
Ta			2.72		2.96		3.76		3.21		3.68		2.39			
Pb			2.54		2.80		3.36		2.75		2.83		4.50			
Sr	248.00		181.00		142.90		207.63		397.11		99.61		113.55		275	
Zr	75.00		270.43		358.63		456.97		280.30		424.24		275.13		99.000	
Hf			6.05		7.74		9.68		6.01		9.30		5.52			
Y	50.00		29.00		40.00		48.00		30.00		38.00		27.00		30	
Zr/Hf			44.71		46.36		47.22		46.66		45.60		49.81			
La (ppm)	17.40		36.57		44.20		52.08		36.00		43.94		19.13		31	
Ce	35.00		76.59		95.80		122.34		76.58		100.17		41.33		67	
Pr			9.88		12.76		16.24		9.53		13.02		5.37			
Nd	23.50		40.71		54.35		69.94		37.37		56.27		24.20		38	
Sm	6.20		8.80		12.10		15.43		7.53		12.33		6.46		8.2	
Eu	2.13		2.76		3.95		5.12		2.40		3.96		2.21		2.54	
Gd	8.20		8.03		11.49		14.50		6.94		11.51		6.59		7.6	
Tb			1.23		1.74		2.10		1.04		1.68		1.09			
Dy	8.90		6.81		9.31		11.08		5.76		9.05		6.08		6	
Ho			1.28		1.74		2.09		1.10		1.72		1.23			
Er	4.80		3.44		4.60		5.38		2.96		4.56		3.23		2.6	
Yb	4.28		2.92		3.91		4.01		2.51		3.26		2.66		1.92	
Lu			0.42		0.58		0.58		0.37		0.47		0.38			
$(La/Yb)_N$			8.98		8.12		9.31		10.28		9.66		5.15			
Mg#			32.90		44.68		47.40		52.17		54.59		28.28			

(continued on next page)

Table 1 (*continued*)

(d)

Group 3 +1.6 < εNd < −2 Low TiO_2 LREE-enriched	Dolerite Intrusive OM88		Basalt OM240		Dolerite Intrusive OM96		OM02		Olivine Feldspar Cpx phyric Basalt OM126		Feldspar Laths Ti-oxides Basalt OM216		Basalt OM241	
SiO_2%	55.25	56.60	55.60	57.11	45.15	46.68	52.40	53.69	46.5	49.91	50.2	52.84	46.20	48.29
TiO_2	1.75	1.79	1.57	1.61	3.18	3.28	2.15	2.2	1.95	2.09	2.38	2.51	3.54	3.7
Al_2O_3	12.10	12.39	15.30	15.73	15.35	15.87	14.70	15.06	15.8	16.96	16.05	16.90	18.70	19.54
Fe_2O_3	14.88	15.24	14.52	14.90	17.5	18.09	12.13	12.43	10.2	10.95	14.7	15.47	19.35	20.22
MnO	0.10	0.10	0.03	0.30	0.2	0.20	0.22	0.23	0.15	0.16	0.05	0.05	0.03	0.03
MgO	2.70	2.76	0.78	0.80	3.32	3.48	2.98	3.05	5.8	6.23	2.22	2.34	1.07	1.11
CaO	7.92	8.11	2.60	2.67	6.27	6.48	5.77	5.91	8.15	8.75	2.94	3.10	0.72	0.75
Na_2O	2.55	2.61	4.10	4.21	3.98	4.40	4.40	4.51	4.05	4.35	4.15	4.37	1.51	1.57
K_2O	0.13	0.13	2.25	2.31	1.26	1.30	1.92	1.96	0.23	0.25	1.11	1.17	4.46	4.66
P_2O_5	0.23	0.23	0.49	0.50	0.51	0.52	0.92	0.94	0.34	0.37	1.2	1.26	0.08	0.08
LOI	1.90				3.28		2.24		6.26		4.53		2.96	
Sc (ppm)	42.50		14		22.50		18.20		32.00		7.00		27.00	
Ti	10,740.00		9660.00		19,680.00		13,200.00		13,071.00		15,644.00		22,200.00	
V	307.00		90.00		305.00		125.00		280.00		120.00		225.00	
Ni	28.00		16.00		54.00		15.00		98.00		29.00		24.00	
Co	27.00	26.23	15.50	15.90	47.00	45.28	27.00	27.54	41.17		14.98		18.00	19.22
Cr	22.00		18.00		98.00		16.00		210.00		2.00		47.00	
Cs		0.99		1.77		0.99		1.30	0.53		1.42			3.56
Rb	3.50	3.05	48.50	47.61	19.60	18.08	41.00	42.02	4.55		30.52		82.50	78.51

Ba	20.00	18.18	540.00	529.54	235.00	217.04	382.00	360.42	68.31	389.06	850.00	791.78
Th	2.75	2.83	9.60	8.88	2.65	2.71	5.70	6.43	3.31	7.17	9.60	9.99
U		0.29		2.11		0.86		1.42	0.55	0.99		3.01
Nb	13.00	13.40	52.00	59.26	28.00	27.59	45.00	50.88	33.54	64.74	69.00	79.3
Ta		0.77		3.45		1.80		2.89	1.85	3.91		4.43
Pb		5.71		8.75		10.24		12.20	1.97	3.33		8.09
Sr	245.00	143.42	570.00	594.20	480.00	473.16	420.00	442.72	279.27	126.64	176.00	185.4
Zr	132.00	67.53	240.00	423.32	115.00	155.62	144.00	299.07	191.89	463.54	448.00	491.37
Hf		1.77		9.66		3.84		6.57	4.44	10.32		10.96
Y	43.50	43.82	49.00	55.12	22.00	23.89	41.00	47.20	28.00	38.00	38.50	40.45
Zr/Hf		38.21		43.82		40.55		45.49	43.23	44.90		44.84
La (ppm)	16.40	15.37	59.00	59.19	25.50	24.85	47.00	47.84	24.09	36.01	49.00	47.82
Ce	29.80	30.46	124.00	123.24	48.50	53.48	105.00	103.84	50.74	82.48	112.00	109.49
Pr		4.03		14.53		6.82		13.06	6.24	10.62		12.96
Nd	18.50	17.19	59.00	57.07	30.50	28.25	58.00	53.89	24.55	47.32	51.00	49.12
Sm	4.90	4.70	12.00	12.35	6.20	5.88	11.80	11.65	5.28	12.02	10.30	10.19
Eu	1.65	1.64	3.65	3.70	1.98	2.05	3.24	3.53	1.70	3.82	3.02	3.03
Gd	6.5	6.11	11.1	12.06	6.30	6.04	11.00	10.78	5.31	11.64	9.00	9.22
Tb		1.12		1.75		0.86		1.57	0.87	1.75		1.43
Dy	7.00	7.06	9.30	9.95	4.60	4.72	8.30	8.46	5.13	9.28	7.80	7.99
Ho		1.55		1.96		0.88		1.65	1.04	1.76		1.59
Er	4.10	4.56	4.00	5.37	2.00	2.34	3.70	4.13	2.93	4.35	3.80	4.37
Yb	3.48	3.71	3.10	4.38	1.37	1.81	2.47	3.21	2.64	3.19	3.50	3.67
Lu		0.51		0.59		0.25		0.45	0.39	0.43		0.53
$(La/Yb)_N$			13.60		13.35		13.65		6.55	8.09	10.04	
Mg#									57.23	26.22		

Samples location is indicated in Table 2.

Major and trace element chemistry of the Middle Permian mafic volcanics from Oman. Major and trace element contents were determined by ICP-AES and ICP-MS, respectively.

Sumeini–Hawasina and ophiolitic Samail nappes, and (3) the autochthonous Late Cretaceous–Tertiary post-nappe sedimentary cover.

The Sumeini and Hawasina nappes thrusted onto the Arabian platform during Late Cretaceous and sandwiched between the platform and the Samail ophiolite are interpreted as continental slope and ocean basin deposits originating from the southern Permian–Cretaceous Tethyan margin (Glennie et al., 1974). Especially, the lower Hawasina units (Hamrat Duru Gp.) and locally the Arabian platform series (Saiq Fm.) document an important Middle Permian igneous activity (Béchennec et al., 1988, 1991). These Permian volcanic rocks are mainly made of tubular pillow basalt with subordinate icelandite, hawaiite and trachyandesite usually associated with hyaloclastic breccias and tuffs.

The volcanics analyzed (Tables 1 and 2) in this work, which are associated with faunistically well dated sediments, were sampled either from the Hamrat Duru series (Al Jil Fm.) in four areas, Al Ajal, Wadi Wasit, Rustaq and Buday'ah or from the Saiq Formation along the Wadi Aday and Wadi Al Hulw in the Saih Hatat window (Fig. 3).

In the Al Ajal area, the Hamrat Duru units are exposed in five main stacked thrust sheets (Béchennec et al., 1992a; Maury et al., 2003). These sheets (HD1 to HD5) consist, from base to top, of (i) volcanic rocks, mainly basaltic pillow-lavas, capped by Permian red shales and radiolarian cherts (Maury et al., 2003), (ii) Early Triassic calciturbidite and siltstone (Al Jil Fm.), (iii) Middle-Late Triassic radiolarian chert and *Halobia-bearing* limestone, (iv) Early Jurassic turbiditic quartz sandstone (Matbat Fm.). The sedimentology of the turbiditic facies documents a piling up of the thrust sheets originating from proximal (HD1) to distal (HD4) paleogeographic settings (with respect to the adjacent Arabian platform). Because of tectonic overprint, the setting of the HD5 sheet cannot be identified.

In the Wadi Wasit area (Béchennec et al., 1992a) are exposed basaltic pillow-lavas capped first by Middle Permian red cephalopods-bearing carbonates (Blendinger et al., 1992; Cordey et al., 2001a), shales,

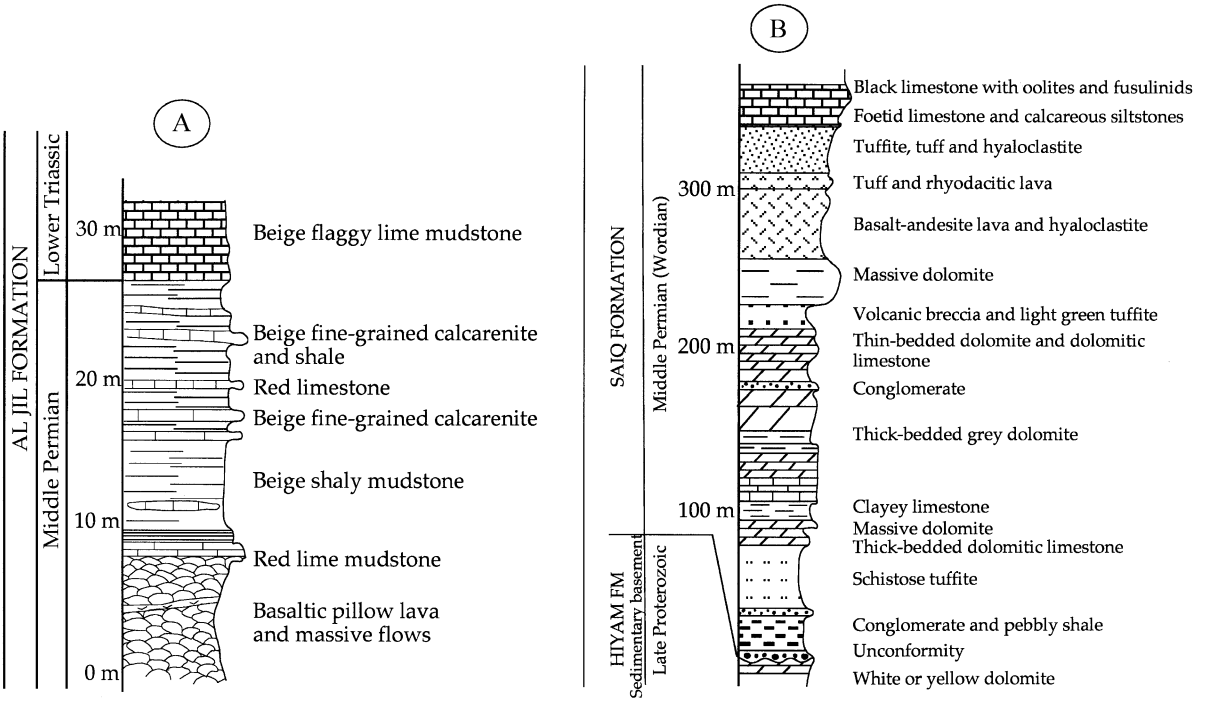

Fig. 4. Lithostratigraphic columns of the Al Jil (Buday'ah) and Saiq (Wadi Aday) Formations (after Béchennec et al., 1988; Maury et al., 2003).

calcarenites, and then by a calcirudite horizon and an Early Triassic calcilutite series (Al Jil Fm.); the clastic deposits have features of proximal turbidite.

Buday'ah (Figs. 3 and 4A) is the first locality where Middle Permian radiolarian cherts were described (Béchennec, 1988; De Wever et al., 1988; Béchennec et al., 1992b; Cordey et al., 2001b). Associated with shale and mudstone, they cap a thick pillowed basaltic pile and the whole thrust sheet is interpreted as an unit originating from a distal paleogeographic setting.

In Rustaq, a 60-m-thick basaltic pillow-lava sequence is capped by Hallstat-type red ammonoids-bearing well dated Middle Permian limestones (Blendinger et al., 1992; Pillevuit, 1993; Kozur et al., 2001). The paleogeographic setting of this section remains undetermined.

The second set of volcanic samples belongs to the Middle-Late Permian Arabian carbonate platform. It has been collected in the Saih Hatat window (Wadi Aday: OM121, OM125, OM240, OM241, OM243, and Wadi Al Hulw: OM96, OM88, Tables 1 and 2, Figs. 2, 3 and 4B). These samples are affected by a Late-Cretaceous subduction-related high pressure–low temperature metamorphism (Le Métour et al., 1990; Michard et al., 1994; Chemenda et al., 1996; Miller et al., 1998). Along the Wadi Aday (Fig. 4b), two main metavolcanic sequences are interbedded within the Middle-Late Permian shallow-marine carbonates of the Saiq Fm. (Le Métour, 1988; Le Métour et al., 1992). They include fine-grained metavolcaniclastic rocks, basaltic to dacitic metalavas and metatuffs. Likewise, in the Wadi Al Hulw (Fig. 3), metadolerites intrude the Middle-Late Permian platform carbonates.

In summary, the samples analyzed in this work were collected from two distinct paleogeographic settings: the Arabian platform and the proximal to distal parts of the adjacent Hamrat Duru basin, which belongs to the huge (several hundred kilometers wide, possibly 500 km according to Béchennec et al., 1988) Hawasina basin.

3. Analytical procedures

Major and compatible trace element were determined (Table 1) by ICP-optical spectroscopy at the Université de Bretagne occidentale in Brest, using the procedures of Cotten et al. (1995). Trace elements of selected 23 samples, including the REE (Table 1) were analyzed by ICP-MS at the Université Joseph Fourier in Grenoble, after acid dissolution of 100 mg sample, using the procedures of Barrat et al. (1996). Limits of detection for REE and Y = 003 ppm, U, Pb and Th = 0.5 ppm, Hf and Nb = 0.1 ppm, Ta = 0.03 ppm and Zr = 0.04 ppm. Standards used for the analyses were JB2, WSE, Bir-1 and JR1. Analytical errors are 1–3% for major elements and less than 3% for trace elements. All the samples were pulverised in an agate mill.

Sr (static acquisition) and Nd (dynamic acquisition) isotopic ratios (Table 2) were measured on 50 samples at the Laboratoire de Géochimie isotopique de l'Université Paul Sabatier de Toulouse on a Finnigan MAT261 multicollector mass spectrometer using the analytical procedures of Lapierre et al. (1997). Results on standards yielded $^{143}Nd/^{144}Nd = 0.511850 \pm 0.000017$ on 12 standards analyzed. Results on NBS 987 Sr standard yielded $^{87}Sr/^{86}Sr = 0.710250 \pm 0.000030$ on 11 standard determinations. $^{87}Sr/^{86}Sr$ and $^{143}Nd/^{144}Nd$ were normalized for mass fractionation relative to $^{86}Sr/^{88}Sr = 0.1194$ and $^{146}Nd/^{144}Nd = 0.7219$, respectively. εNd_i calculated with actual $(^{143}Nd/^{144}Nd)_{CHUR} = 0.512638$ and $(^{147}Sm/^{144}Nd)_{CHUR} = 0.1967$. εSr_i calculated with actual $(^{87}Sr/^{86}Sr)_{CHUR} = 0.70450$ and $(^{87}Rb/^{86}Sr)_{CHUR} = 0.084$ (McCulloch and Wasserburg, 1978). Before Nd and Sr separation, two leaching steps with 2.5 N HCL during 20 min at 100 °C were done before acid disgestion.

For lead separation, 26 powdered samples were weighted to obtain approximatively 100 to 200 ng of lead. A leaching step with 6 N HCl during 30 min at 65 °C was done before acid digestion. Samples were then dissolved during 36–48 h on a hotplate with a mixing of tridistilled Hf:HNO_3 concentrated acids. After evaporation to dryness, 1 ml of HNO_3 was added to the residue and kept at about 90 °C for 12–24 h. After complete evaporation, 0.5 ml of 8N HBr was added to the sample which was kept at 70 °C for 2–3 h before complete evaporation. The chemical separation of lead was done using 50 μl of l of anion exchange resin (AG1X8, 200–400 mesh) and samples were loaded and washed in 0.5 N HBr. Lead was then eluted in 6 N HCl. Pb blanks were

Table 2
Nd, Sr and Pb isotopic compositions of the Middle Permian volcanics

(a)

Location	Al Ajal	Al Ajal	Al Ajal	Al Ajal	Budayah	Location	Al Ajal	Al Ajal
Group 1						Group 1		
+11.1>εNd>+3.8						+11.1>εNd>+3.8		
Low TiO_2						Low TiO_2		
LREE-depleted (A)						Flat REE (B)		
Sample number	OM07	OM123	OM237	OM13	OM222	Sample number	OM109	OM125
Rb						Rb		
Sr						Sr		
$^{87}Sr/^{86}Sr$	0.705847 ± 10	0.705753 ± 8	0.705980 ± 10	0.705431 ± 25		$^{87}Sr/^{86}Sr$	0.705944 ± 36	0.706940 ± 11
$^{87}Rb/^{86}Sr$	0.068166	0.019346	0.237818	0.009085		$^{87}Rb/^{86}Sr$	0.045937	0.503698
$(^{87}Sr/^{86}Sr)_i$	0.705585	0.705679	0.705067	0.705396		$(^{87}Sr/^{86}Sr)_i$	0.705768	0.705005
$(\varepsilon Sr)_i$	+19.9	+21.3	+12.6	+17.2		$(\varepsilon Sr)_i$	+22.5	+11.7
Sm					3	Sm		
Nd					8.9	Nd		
$^{143}Nd/^{144}Nd$	0.513085 ± 8	0.512975 ± 4	0.51308 ± 6	0.512952 ± 9	0.513127 ± 5	$^{143}Nd/^{144}Nd$	0.512841 ± 6	0.51289 ± 3
$^{147}Sm/^{144}Nd$	0.229773	0.213325	0.230694	0.20055	0.203078	$(^{147}Sm/^{144}Nd)$	0.188462	0.191541
$(^{143}Nd/^{144}Nd)_i$	0.512679	0.5126	0.512672	0.512598	0.512667	$(^{143}Nd/^{143}Nd)_i$	0.512508	0.512551
$(\varepsilon Nd)_i$	+7.6	+6	+7.5	+6	+9.3	$(\varepsilon Nd)_i$	+4.3	+5.1
$(^{206}Pb/^{204}Pb)$	18.547	18.083	18.459	18.468		$(^{206}Pb/^{204}Pb)$	18.597	18.476
$(^{207}Pb/^{204}Pb)$	15.498	15.492	15.456	15.503		$(^{207}Pb/^{204}Pb)$	15.511	15.508
$(^{208}Pb/^{204}Pb)$	37.907	38.017	37.800	38.360		$(^{208}Pb/^{204}Pb)$	38.473	38.544
$(^{206}Pb/^{204}Pb)_i$	18.06	17.86	17.79	17.8		$(^{206}Pb/^{204}Pb)_i$	18.06	17.89
$(^{207}Pb/^{204}Pb)_i$	15.47	15.48	15.43	15,347		$(^{207}Pb/^{204}Pb)_i$	15.48	15.48
$(^{208}Pb/^{204}Pb)_i$	37.65	37.72	37.7	37.84		$(^{208}Pb/^{204}Pb)_i$	37.75	37.73

Location	Al Ajal	Al Ajal	Al Ajal	Al Ajal	Al Ajal	Al Ajal	Budayah	Budayah
Group 1								
+11.1>εNd>+3.8								
Low TiO_2								
Flat REE (B)								
Sample number	OM135	OM138	OM141	OM232	OM235	OM236	OM22	OM23
Rb							14.4	9.5
Sr							151	255
$^{87}Sr/^{86}Sr$	–	0.705982 ± 8	0.706757 ± 10	0.706805 ± 10	0.707724 ± 11	0.706384 ± 7	0.706171 ± 8	0.706269 ± 9
$^{87}Rb/^{86}Sr$	–	0.1118	0.163702	0.00579	0.008806	0.235712	0.275870	0.107772
$(^{87}Sr/^{86}Sr)_i$	–	0.705556	0.706128	0.706783	0.70769	0.705479	0.705111	0.705855

$(\varepsilon Sr)_i$	–	+19.6	+27.6	+36.9	+49.8	+18.4	+13.2	+23.8
Sm							2.9	2.4
Nd							9.4	7.5
$^{143}Nd/^{144}Nd$	0.512919 ± 6	0.512877 ± 5	0.512846 ± 6	0.513033 ± 6	0.512972 ± 6	0.512934 ± 7	0.513120 ± 6	0.513199 ± 5
$(^{147}Sm/^{144}Nd)$	0.199673	0.18544	0.192585	0.20684	0.205548	0.195677	0.186534	0.193484
$(^{143}Nd/^{143}Nd)_i$	0.512566	0.512549	0.512506	0.512667	0.512609	0.512588	0.512790	0.512857
$(\varepsilon Nd)_i$	+5.4	+5.1	+4.2	+7.4	+6.2	+5.8	+9.8	+11.1
$(^{206}Pb/^{204}Pb)$	18.582	19.281	18.531	18.741	18.152	17.071		
$(^{207}Pb/^{204}Pb)$	15.565	15.570	15.512	15.563	15.542	15.508		
$(^{208}Pb/^{204}Pb)$	38.568	39.213	38.703	38.581	38.504	38.572		
$(^{206}Pb/^{204}Pb)_i$	18.35	18.2	17.94	18.09	17.94	17.83		
$(^{207}Pb/^{204}Pb)_i$	15.55	15.51	15.48	15.53	15.49	15.48		
$(^{208}Pb/^{204}Pb)_i$	38.26	37.78	37.86	38.14	38.02	37.7		

(b)

Location	Al Ajal	Al Ajal	Al Ajal	Al Ajal	Al Ajal	Rustaq	Rustaq	Buday'ah
Group 1								
$+11.1>\varepsilon Nd>+3.8$								
Low TiO_2								
L REE-enriched (C)								
Sample number	OM115	cpx OM115	OM117	OM140	OM227	OM14	OM15	OM17
Rb						6.9	3.9	0.5
Sr						226	132	142
$^{87}Sr/^{86}Sr$	0.705452 ± 12	0.705258 ± 8	0.704969 ± 9	0.707937 ± 10	–	0.708050 ± 8	0.708070 ± 8	0.706500 ± 8
$^{87}Rb/^{86}Sr$	0.107387	0.130198	0.007537	0.138294	–	0.088336	0.085485	0.10186
$(^{87}Sr/^{86}Sr)_i$	0.70504	0.704758	0.70494	0.707406	–	0.707710	0.707741	0.70646
$(\varepsilon Sr)_i$	+12.2	+8.2	+10.8	+45.8	–	+50.1	+50.6	+32.4
Sm						3.65	3.7	4.1
Nd						14	13.2	16.5
$^{143}Nd/^{144}Nd$	0.512872 ± 5	0.51297 ± 5	0.512786 ± 5	0.512817 ± 5	0.512833 ± 5	0.512847 ± 5	0.512856 ± 6	0.512816 ± 7
$(^{147}Sm/^{144}Nd)$	0.17882	0.266488	0.1697	0.164122	0.178803	0.157625	0.169468	0.150230
$(^{143}Nd/^{144}Nd)_i$	0.512486	0.512499	0.512486	0.512527	0.512517	0.512568	0.512547	0.512550
$(\varepsilon Nd)_i$	+5.2	+4.1	+3.8	+4.6	+4.4	+5.4	+5.0	+5.1
$(^{206}Pb/^{204}Pb)$	18.960		18.639	18.794	18.552			
$(^{207}Pb/^{204}Pb)$	15.538		15.516	15.561	15.521			
$(^{208}Pb/^{204}Pb)$	38.783		38.939	38.615	38.677			
$(^{206}Pb/^{204}Pb)_i$	18.14		17.9	18.07	18.06			
$(^{207}Pb/^{204}Pb)_i$	15.5		15.48	15.52	15.5			
$(^{208}Pb/^{204}Pb)_i$	37.62		37.83	38.2	38			

(continued on next page)

Table 2 (*continued*)

(b)

Location	Buday'ah	Buday'ah	Location	Al Ajal	Al Ajal	Al Ajal	Al Ajal	Al Ajal
Group 1			Group 2					
+11.1>εNd>+3.8			+5>εNd>+3					
Low TiO_2			High TiO_2					
L REE-enriched (C)			L REE-enriched					
Sample number	OM19	OM18	Sample number	OM05	OM09	OM118	OM121	OM131
Rb	0.85	0.9	Rb					
Sr	400	270	Sr					
$^{87}Sr/^{86}Sr$	0.707027 ± 9	0.706635 ± 8	$^{87}Sr/^{86}Sr$	0.712009 ± 12	0.705145 ± 12	0.705503 ± 14	0.704877 ± 9	0.704219 ± 8
$^{87}Rb/^{86}Sr$	0.006147	0.009643	$^{87}Rb/^{86}Sr$	0.01283	0.31671	0.150054	0.002201	0.150035
$(^{87}Sr/^{86}Sr)_i$	0.707003	0.706597	$(^{87}Sr/^{86}Sr)_i$	0.711959	0.703928	0.704927	0.704869	0.703643
$(\varepsilon Sr)_i$	+40.1	+34.3	$(\varepsilon Sr)_i$	+110.4	−3.61	+10.6	+9.7	−7.6
Sm	5.1	4.1	Sm					
Nd	22	15.4	Nd					
$^{143}Nd/^{144}Nd$	0.512763 ± 7	0.512814 ± 5	$^{143}Nd/^{144}Nd$	0.512757 ± 6	0.512702 ± 5	0.512725 ± 5	0.51274 ± 5	0.512744 ± 5
$(^{147}Sm/^{144}Nd)$	0.140152	0.160962	$(^{147}Sm/^{144}Nd)$	0.15905	0.130671	0.134587	0.133388	0.121847
$(^{143}Nd/^{144}Nd)_i$	0.512515	0.512290	$(^{143}Nd/^{144}Nd)_i$	0.512475	0.512471	0.512487	0.512504	0.512529
$(\varepsilon Nd)_i$	+4.4	+4.5	$(\varepsilon Nd)_i$	+3.6	+3.5	+3.8	+4.2	+4.6
$(^{206}Pb/^{204}Pb)$			$(^{206}Pb/^{204}Pb)$		19.013	19.406	19.284	18.703
$(^{207}Pb/^{204}Pb)$			$(^{207}Pb/^{204}Pb)$		15.541	15.578	15.554	15.518
$(^{208}Pb/^{204}Pb)$			$(^{208}Pb/^{204}Pb)$		39.235	39.189	39.135	38.729
$(^{206}Pb/^{204}Pb)_i$			$(^{206}Pb/^{204}Pb)_i$		18.21	18.19	18.24	17.58
$(^{207}Pb/^{204}Pb)_i$			$(^{207}Pb/^{204}Pb)_i$		15.5	15.51	15.5	15.46
$(^{208}Pb/^{204}Pb)_i$			$(^{208}Pb/^{204}Pb)_i$		37.96	37.96	37.81	37.29

(c)

Location	Al Ajal	Al Ajal	Al Ajal	Wadi Wasit	Wadi Wasit	Wadi Wasit	Wadi Wasit	Wadi Wasit	Wadi Wasit
Group 2									
+5>εNd>+3									
High TiO_2									
L REE-enriched									
Sample number	OM143	OM210	OM243	OM30	OM31	OM36	OM37	OM40	OM204
Rb				30.5	54.5	14.7	8.4	20.5	29.5
Sr				405	148	275	350	830	268
$^{87}Sr/^{86}Sr$	0.705613 ± 7	0.709817 ± 7	0.705572 ± 8	0.705163 ± 10	0.705961 ± 10	0.705490 ± 13	0.704986 ± 8	0.705015 ± 9	0.705389 ± 8

$^{87}Rb/^{86}Sr$	0.048903	0.713165	0.347117	0.217823	1.06523	0.154623	0.069419	0.071440	0.318400
$(^{87}Sr/^{86}Sr)_i$	0.705425	0.707078	0.7042385	0.704326	0.702869	0.704896	0.704719	0.704740	0.704165
$(\varepsilon Sr)_i$	+17.6	+41.1	+0.8	+2.1	−32.9	+10.2	+7.6	+7.9	−0.23
Sm				12.8	12.6	9.6	10.4	8.2	10.7
Nd				66	62	47	51	40.5	50
$^{143}Nd/^{144}Nd$	0.512733 ± 4	0.512733 ± 5	0.512711 ± 5	0.512732 ± 5	0.512738 ± 5	0.512698 ± 5	0.512701 ± 6	0.512758 ± 5	0.512731 ± 11
$(^{147}Sm/^{144}Nd)$	0.132526	0.16132	0.130459	0.117250	0.122865	0.123486	0.123284	0.122408	0.129378
$(^{143}Nd/^{144}Nd)_i$	0.512499	0.512448	0.512325	0.512524	0.512520	0.512479	0.512483	0.512541	0.512502
$(\varepsilon Nd)_i$	+4.1	+3.1	+3.7	+4.6	+4.5	+3.7	+3.8	+4.9	+4.1
$(^{206}Pb/^{204}Pb)$	20.219	18.958							
$(^{207}Pb/^{204}Pb)$	15.612	15.652							
$(^{208}Pb/^{204}Pb)$	39.239	39.312							
$(^{206}Pb/^{204}Pb)_i$	17.99	18.57							
$(^{207}Pb/^{204}Pb)_i$	15.5	15.63							
$(^{208}Pb/^{204}Pb)_i$	37.79	38.64							

Location	Wadi Al Hulw	Wadi Al Hulw	Wadi Aday	Wadi Aday	Wadi Aday	Al Ajal	Al Ajal
Group 3							
$+1.6>\varepsilon Nd>-2$							
Low TiO_2							
LREE-enriched							
Sample number	OM88	OM96	OM240	OM02	OM241	OM126	OM216
Rb							
Sr							
$^{87}Sr/^{86}Sr$	0.706455 ± 9	0.705483 ± 10	0.706294 ± 10	0.705592 ± 13	0.707980 ± 8	0.706680 ± 9	0.708273 ± 7
$^{87}Rb/^{86}Sr$	0.041327	0.118115	0.246145	0.282377	1.356245	0.0470927	0.697403
$(^{87}Sr/^{86}Sr)_i$	0.706296	0.705029	0.705348	0.704507	0.70277	0.706499	0.705594
εSr	+30	+12	+16.56	+4.6	−20.1	+32.9	+20.1
Sm							
Nd							
$^{143}Nd/^{144}Nd$	0.512471 ± 13	0.512590 ± 5	0.512554 ± 5	0.512573 ± 6	0.512541 ± 7	0.512542 ± 5	0.512511 ± 5
$(^{147}Sm/^{144}Nd)$	0.160012	0.122892	0.122958	0.125152	0.122094	0.129906	0.153538
$(^{143}Nd/^{144}Nd)_i$	0.512188	0.512372	0.512336	0.512351	0.512325	0.512312	0.51224
$(\varepsilon Nd)_i$	−2.0	+1.6	+0.9	+1.2	+0.68	+0.4	−0.99
$(^{206}Pb/^{204}Pb)$	18.57395	18.5580	18.7688	18.6439	18.9087	18.498	18.103
$(^{207}Pb/^{204}Pb)$	15.6664	15.5842	15.5991	15.5857	15.6108	15.540	15.514
$(^{208}Pb/^{204}Pb)$	39.08868	38.7336	39.05265	38.8754	39.1565	39.089	38.923
$(^{206}Pb/^{204}Pb)_i$	18.44	18.33	18.11	18.39	17.89	17.75	17.29
$(^{207}Pb/^{204}Pb)_i$	15.67	15.57	15.56	15.57	15.56	15.5	15.47
$(^{208}Pb/^{204}Pb)_i$	38.65	38.50	38.15	38.41	38.05	37.6	38.02

Nd, Sr and Pb isotopic compositions of the Middle Permian mafic volcanics from Oman. Rb, Sr, Sm, Nd reported here were determined by ICP-AES.

less than 40 pg and are negligible for the present analyses.

Lead isotope analyses were made on a VG model Plasma 54 magnetic sector-inductively coupled plasma-mass spectrometer (MC-ICP-MS) at the Ecole Normale Supérieure de Lyon. Lead isotope compositions were measured using the Tl normalization method described by White et al. (2000). For Pb isotope analysis, samples were bracketed between NIST 981 standards and calculated with respect to the value reported for this standard by Todt et al. (1996). This technique yields internal precision of ca. 50 ppm (2σ and an external reproductibility of ca. 150 ppm (2σ or $^{206}Pb/^{204}Pb$ ratios determined on 20 NIST standards.

All the isotopic data (Table 2) have been corrected for in situ decay using an age of 270 Ma, based on that of the Middle Permian (Wordian to Capitanian) faunas found in the red shales and radiolarian cherts (De Wever et al., 1988; Blendinger et al., 1992).

4. Geochemistry of the Middle Permian volcanics and dolerites

4.1. Main rock types

Most of the studied volcanic rocks are subaphyric basalts with well-preserved pillow structures. The phenocrysts (usually less than 5 modal%) consist of millimeter-sized olivine with Cr-rich spinel inclusions. Olivine is systematically altered to smectites, chlorite and sometimes to calcite or quartz. The abundant chloritized groundmass consists of dendritic clinopyroxene associated with plagioclase microlites. A few olivine basalts are highly phyric with abundant and large (up to one centimeter) plagioclase and clinopyroxene phenocrysts. Finally, olvine-free basalts are aphyric and consist of abundant groundmass including plagioclase microlites and chlorite ± calcite-filled vesicles. Dolerites display sub-ophitic textures with preserved clinopyroxene and centimeter-sized plagioclase laths replaced by albite. Alkaline dolerite (Group 2, OM131, $TiO_2 = 3\%$, Table 1c) includes Ti-rich diopside while Ti-poor augite is present in the tholeiitic sample (Group, OM109, $TiO_2 = 1.19$, Table 1a).

In addition, samples from Saih Hatat window (OM121, OM125, OM240, OM241, OM243, OM96, OM88, Table 1) have experienced various degrees of high pressure metamorphism and contain epidote, actinolite, phengite and even garnet (in Wadi Al Hulw dolerites OM88 and OM96). Their Na_2O, K_2O and MgO contents have been likely modified during alteration and/or metamorphism (Maury et al., 2003). Especially, some MgO values which are much too low given the typical basaltic petrography of the corresponding samples are not considered as primary by these authors.

4.2. Effects of alteration on elemental mobility

The altered nature of the volcanic rocks and dolerites from Oman implies that before any petrogenetic and geodynamic inferences can be drawn from the chemistry of the rocks, the possible chemical effects of post-magmatic mobility of elements must be accounted for. Most of the analyzed rocks have an LOI $\leq 8\%$ (Table 1).

Thorium (Th) is considered as being immobile during low grade alteration and metamorphism of igneous rocks of mafic to intermediate composition interacting with hydrothermal fluids (Gibson et al., 1982). It has been plotted against major (TiO_2, Fe_2O_3), and incompatible (Nb, Rb) and compatible (Sr, Pb) trace elements in Fig. 5. TiO_2 and Nb display rather good correlations when plotted against Th, especially for the rocks with the lowest Th contents. Two groups can be distinguished on the basis of TiO_2, Nb and Th contents: (i) a group with low TiO_2 ($\leq 2\%$), Nb (≤ 20 ppm) and Th (≤ 2 ppm, Table 1) abundances, (ii) a group characterized by significantly higher levels in TiO_2 ($\geq 2\%$), Nb (≥ 20 ppm) and Th (≥ 2 ppm) (Maury et al., 2001; Samper, 2002; Maury et al., 2003). The latter authors have shown that both low-Ti and high-Ti groups display equivalent SiO_2 contents, a feature which seems to preclude the derivation of high-Ti magmas from low-Ti ones though fractionation-related processes. Rb and Sr display no correlation with Th. This feature suggests that the large ion lithophile elements (LILE) have been mobilised. Thus, the variations of the LILE will not be discussed further. On the contrary, the high field strength elements (HFSE), e.g., Ti, Nb, Th, Zr (not shown) and Pb correlate rather well with Th, suggesting their relative immobility during post-magmatic processes. High pressure metamorphism

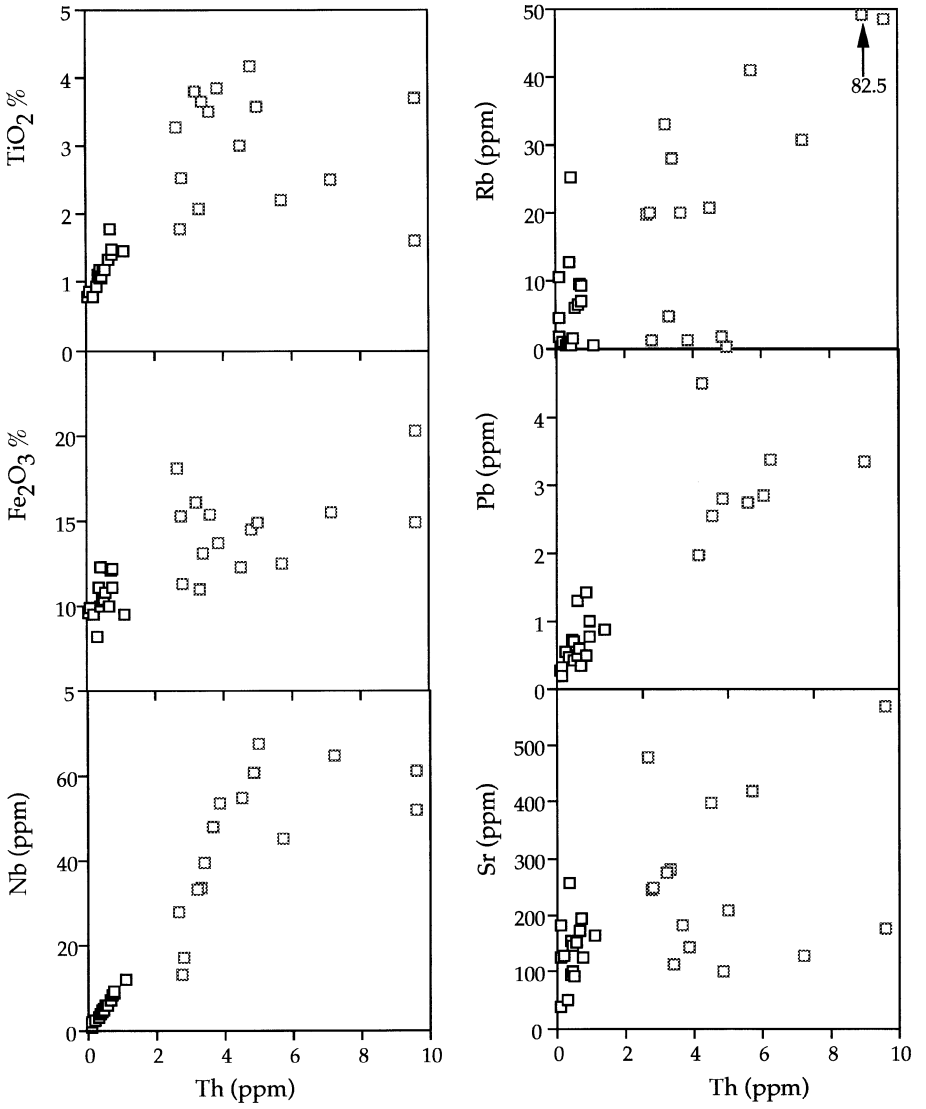

Fig. 5. TiO_2, Fe_2O_3, Nb, Rb, Sr and Pb vs. Th plots showing the mobility of LILE during the low grade metamorphism experienced by the Permian volcanics from Oman.

experienced by samples from the Saih Hatat window (Wadi Aday and Al Hulw) does not seem to have significantly affected their TiO_2 content and some incompatible trace element ratios, e.g., La/Yb and Th/Yb. Indeed, dolerites from Al Hulw and alkali basalts from Wadi Aday still display chemical features typical of low-Ti and high-Ti samples, respectively.

4.3. Main geochemical types

From major, trace element, and Nd isotopic compositions of the Middle Permian volcanics and dolerites, three groups of basaltic rocks can be distinguished.

Group 1 is characterized by low TiO_2 and incompatible (Th, La, Nb) (Table 1) trace element contents,

$(La/Yb)_N \leq 3.5$. These samples have positive εNd_i values ranging from +11.1 to +3.8 (Table 2). This group is composed of tholeiitic basalts and dolerites, three types (A, B and C) of which can be distinguished on the basis of their chondrite-normalized (Sun and McDonough, 1989) REE patterns and primitive mantle (Sun and McDonough, 1989) normalized multi-element plots (Fig. 6A). Type A is characterized by LREE-depleted patterns similar to N-MORB, rather flat multi-element spectra and gen-

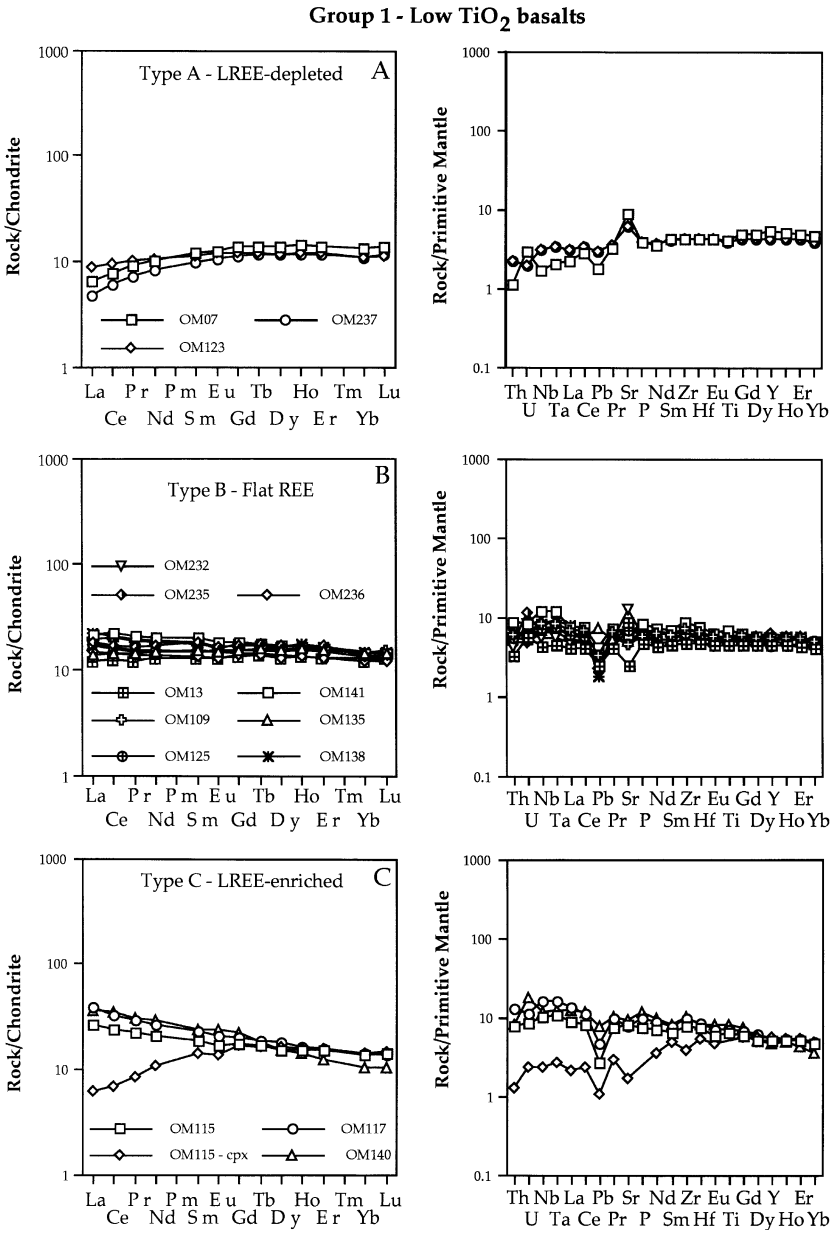

Fig. 6. Chondrite-normalized (Sun and McDonough, 1989) rare earth patterns and primitive mantle-normalized (Sun and McDonough, 1989) multi-element plots for the Middle Permian volcanics from Oman.

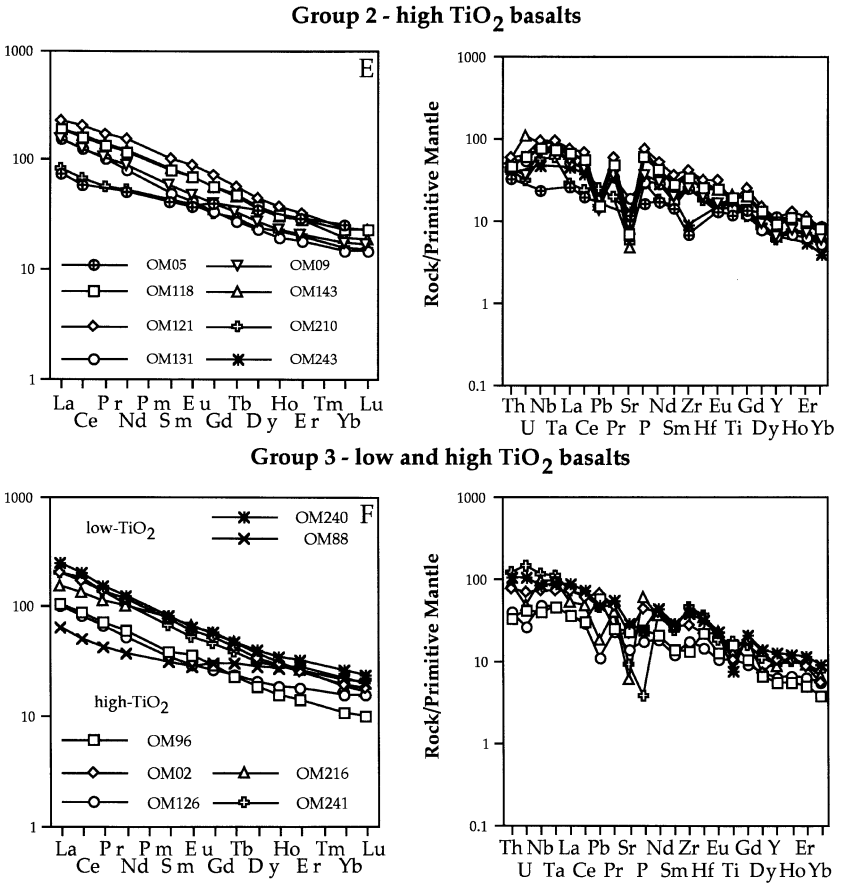

Fig. 6 (*continued*).

erally the highest εNd_i values (+9.3 to +6, Table 2, with the exception of sample OM23, (Type B, $(La/Yb)_N = 1.3$, $\varepsilon Nd = +11.1$, Table 2). Type A multi-element patterns exhibit also a marked positive Sr anomaly and a slight depletion in La, Nb, and Ta relative to Zr, Hf and HREE. Among Type A rocks, samples OM123 and OM237 differ from typical N-MORB by higher La/Nb ratios. Type B appears to be the most abundant. It has very homogeneous trace element features, i.e., flat REE patterns and multi-element plots slightly enriched in La, Nb, and Ta relative to Zr, Hf and HREE (Fig. 6B). Type B spans a large range of εNd_i values (+11.1 to +3.8, Table 2). The differences among Type B rocks lie in the presence of negative or positive Pb and Sr anomalies reflecting plagioclase removal or accumulation. Type C, compared to Type B, is enriched in Th, Nb, Ta and LREE (Fig. 6C). As a whole, Group 1 displays negative correlations in the εNd_i vs. Th, $(La/Yb)_N$, La, and Nb diagrams (Fig. 7). It plots in the $(^{207}Pb/^{204}Pb)_i$–$(^{206}Pb/^{204}Pb)_i$ correlation diagram (Fig. 8A) just above the North Hemisphere Reference Line (NHRL, Zingler and Hart, 1986) and overlaps the MORB field (Rollinson, 1993). Group 1 clusters between the MORB and Bulk Silica Earth (BSE) domains in the εNd_i–$(^{206}Pb/^{204}Pb)_i$ correlation diagrams, respectively (Fig. 8B).

Group 2 differs from Group 1 by higher TiO_2, La and Nb contents, higher $(La/Yb)_N$ ratio (≥ 5, Table 1, Fig. 6E) and lower and more homogeneous εNd_i values (+3.1 to +4.9, Table 2). This group is composed of alkali basalts characterized by LREE-enriched patterns, $La/Nb < 1$, and multi-element plots that show enrichments in Th, Nb and Ta,

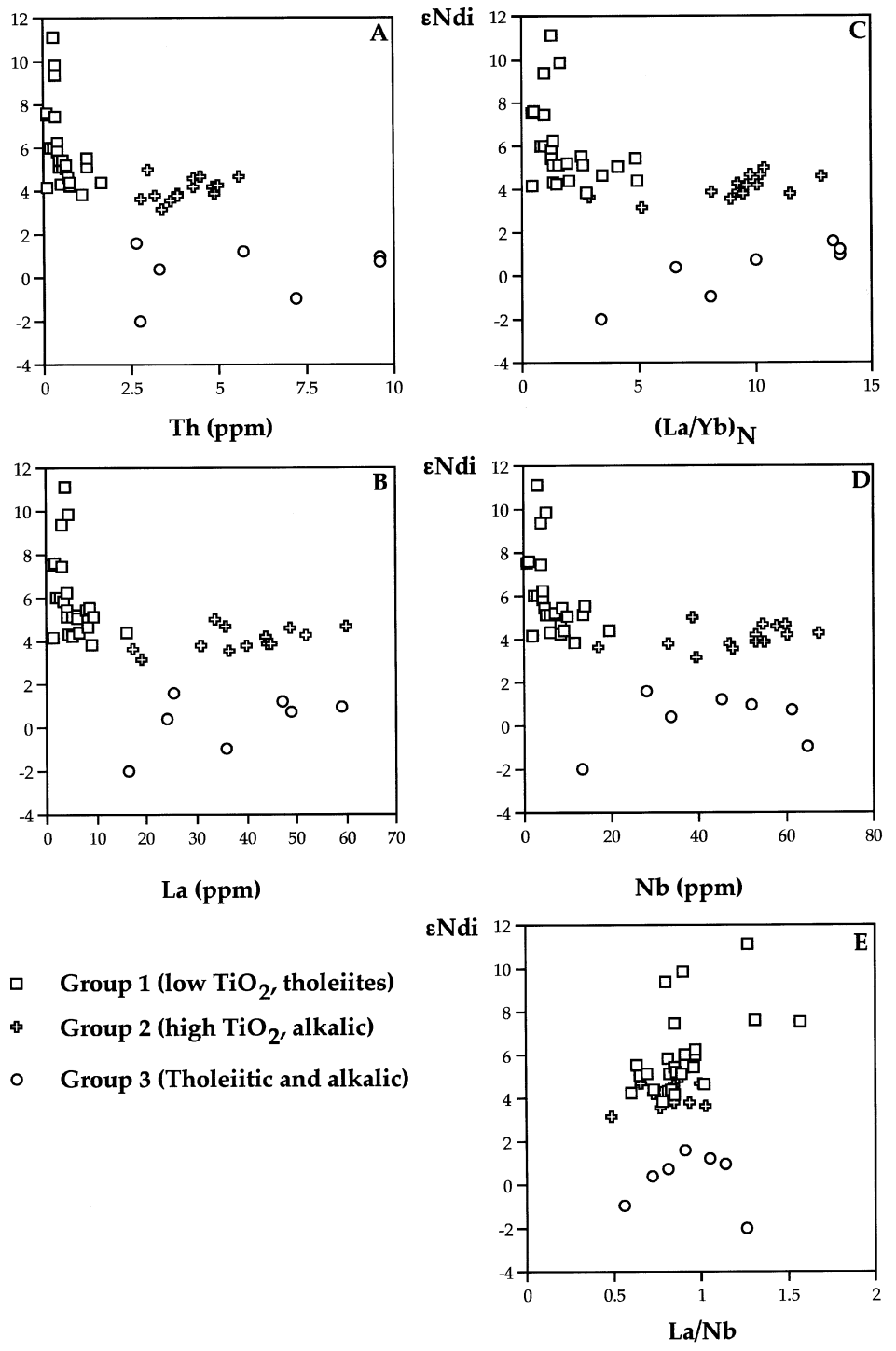

Fig. 7. εNd_i vs. Th (A), La (B), $(La/Yb)_N$ (C), Nb (D), and La/Nb (E) for the Middle Permian volcanics from Oman.

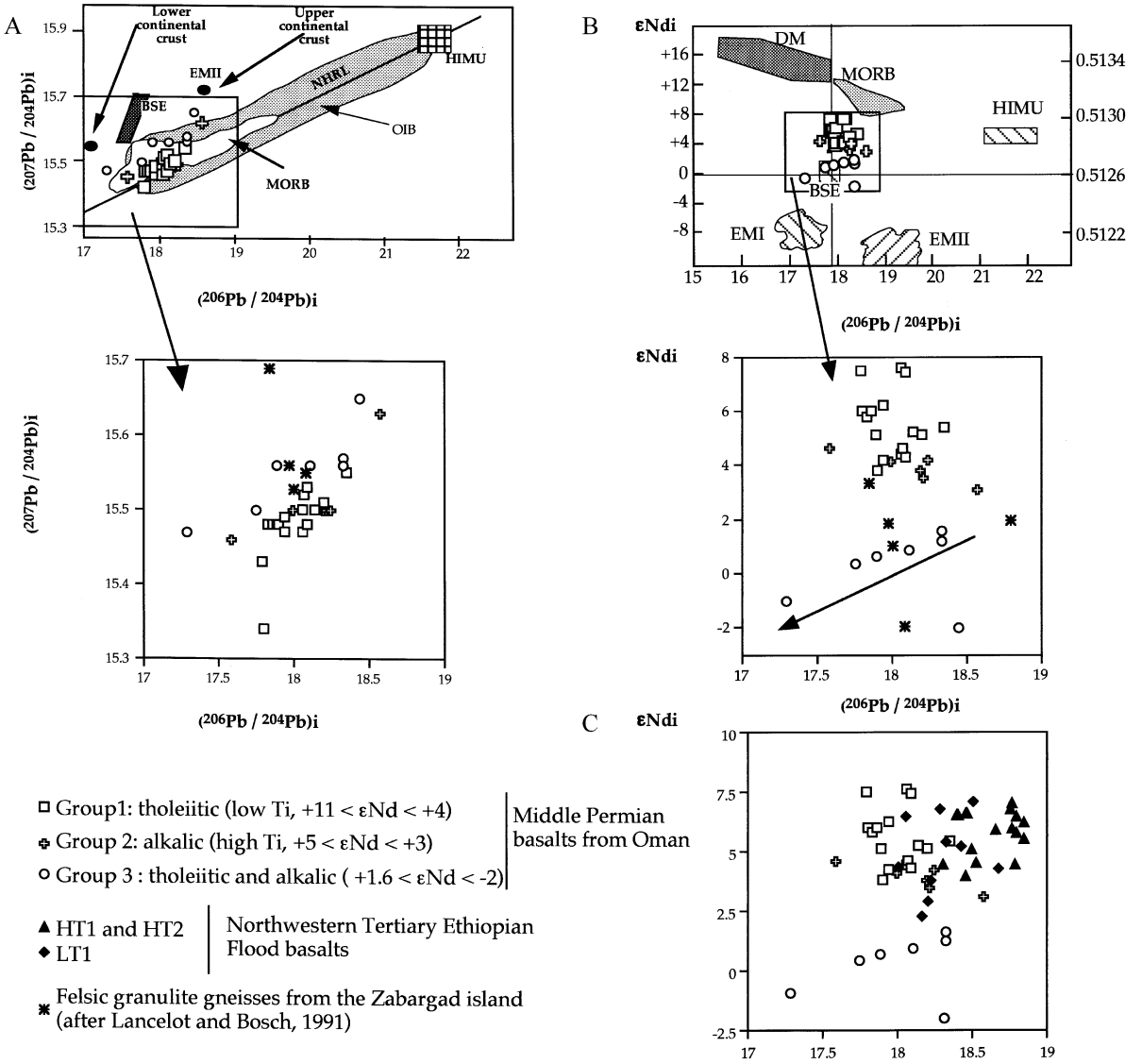

Fig. 8. Lead isotopic features. 8A and 8B: $(^{207}Pb/^{204}Pb)_i$–$(^{206}Pb/^{204}Pb)_i$, and εNd_i vs. $(^{206}Pb/^{204}Pb)_i$ correlation diagrams for the Middle Permian volcanics from Oman, 8C: Comparison of the Middle Permian volcanics from Oman with the Tertiary flood basalts from northwestern Ethiopia (data are after Pik et al., 1999). Note that the $(^{206}Pb/^{204}Pb)_i$ of the Tertiary flood basalts from Ethiopia are higher than those of the Middle Permian volcanics from Oman.

and depletions in HREE and Y (Fig. 6). No correlations are observed for this group in the εNd_i vs. Th, $(La/Yb)_N$, La and Nb plots (Fig. 7). Most of the Group 2 volcanics share with Group 1 similar initial Pb ratios with the exception of two samples (OM131 and OM210, Table 2) which differ by significantly lower and higher initial Pb ratios, respectively. OM131 is the less radiogenic in Pb while OM210, characterized by the highest initial isotopic Pb ratios, falls near the BSE and EM2 fields in the $(^{207}Pb/^{204}Pb)_i$–$(^{206}Pb/^{204}Pb)_i$ correlation diagram (Fig. 8A).

Group 3 is composed of two tholeiitic (low-Ti) dolerites from Wadi Al Hulw (OM88, OM96, Table

1) and alkali (TiO_2-rich) basalts, trachy-basalts and dolerites characterized by low to negative εNd_i (+1.6 to −2; Table 2). Most of the latter have been sampled in the Wadi Aday sequence with the exception of two samples from Al Ajal (OM126, OM216) which are associated with distal sediments near the structural top of the thrust pile (HD4 unit, Maury et al., 2003). The trace element chemistry of Group 3 is similar to that of Group 2. However, some samples (OM240, OM241) differ from the others by their higher Th contents (Th = 9.6 ppm, Table 1) or by lower LREE enrichments (OM88, Table 1, Fig. 6F). No correlations are observed for this group between εNd_i and incompatible elements (Fig. 7). Group 3 shares with Group 2 similar $(^{207}Pb/^{204}Pb)_i$ and $(^{208}Pb/^{204}Pb)_i$ ratios (Table 2) but differs by lower $(^{206}Pb/^{204}Pb)_i$ ratios (Table 2, Fig. 8A). Group 3 displays a positive correlation between εNd_i and $(^{206}Pb/^{204}Pb)_i$ (Fig. 8B) with the exception of sample OM88 (Table 2). Samples OM216 and OM96 are characterized by the lowest and highest εNd_i and $(^{206}Pb/^{204}Pb)_i$ ratios, respectively (Table 2, Fig. 8B).

5. Discussion

5.1. Geochemical relationships between the three groups of Middle Permian basalts and dolerites from Oman

Group 1 tholeiitic basalts exhibit positive correlation trends in the La vs. Th, Nb vs. Th, and $(La/Yb)_N$ vs. La plots (Fig. 9). Group 2 alkali basalts display similar trends in the La and Nb vs. Th plots only. This evolution from LREE-depleted to slightly LREE-enriched tholeiites (Group 1) and alkali basalts (Group 2) can be attributed either to a decrease of the partial melting degree assuming a homogeneous mantle source or to the mixing of a depleted (DMM) and an enriched mantle (OIB-type) sources. The large range of the εNd_i values of Group 1 indicates that the mantle source of this group is heterogeneous. The positive correlations between incompatible elements typical of Group 1 can be attributed to the mixing of a depleted and an enriched sources, respectively. This is well expressed in the Nb/Nd vs. La/Nd plot (Fig. 9) where Group 1 exhibits a linear trend between N-MORB and E-MORB fields. Some samples do not plot on the trend, a feature likely due to variations of partial melting degree. Most of the Group 2 samples plot between E-MORB and OIB fields but with a large scatter. Thus, we can assume that: (i) Group 1 likely derived from the mixing of two mantle sources, a depleted MORB-type (DMM) and an enriched OIB-type; (ii) variations of the trace element and isotopic compositions of Group 1 can be attributed to the mixing of these two mantle sources, (iii) the rather restricted range of the εNd_i values of Group 2 (Table 2) suggests that the variations of the trace element composition of this group can be attributed to variable degrees of partial melting of an enriched source. Finally, the trace element and isotopic compositions of Groups 1 and 2 do not suggest involvement of a continental crust in the genesis of these tholeiitic and alkaline volcanic rocks, respectively.

Group 3 does not show any correlation between incompatible elements (Fig. 9). This feature suggests that the variations of the trace element compositions of this group can be attributed to variable degrees of partial melting and/or the involvement of different enriched components (mantle and continental crust). The low to negative values of the εNd_i of Group 3 basalts suggest that crustal contamination or recycled sediments are involved in the genesis of this group. However, Group 3 does not show the Nb and Ta negative anomalies (Fig. 6F) which are systematically documented in flood basalts contaminated by the upper continental crust (Gibson et al., 1995; Pik et al., 1998, 1999; Fitton et al., 1998). The most likely hypothesis to explain such low to negative εNd_i values is the involvement of the lower Arabian–Nubian continental crust in the genesis of Group 3 (Bosch, 1990; Lancelot and Bosch, 1991). Indeed, Group 3 samples exhibit a positive correlation bewteen εNd_i and $(^{206}Pb/^{204}Pb)_i$ and differ from Groups 1 and 2 ones by their lower $(^{206}Pb/^{204}Pb)_i$. Such low Pb ratios are characteristic of the granulitic lower crust of the late Precambrian Arabian–Nubian shield (McGuire and Stern, 1983; Brueckner et al., 1988; Seyler and Bonatti, 1988; Teklay et al., 1998; Bosch, 1990). Thus, it seems reasonable to assume that the lower crust of the late Precambrian Arabian–Nubian shield contaminated Group 3 magmas during their ascent towards the surface.

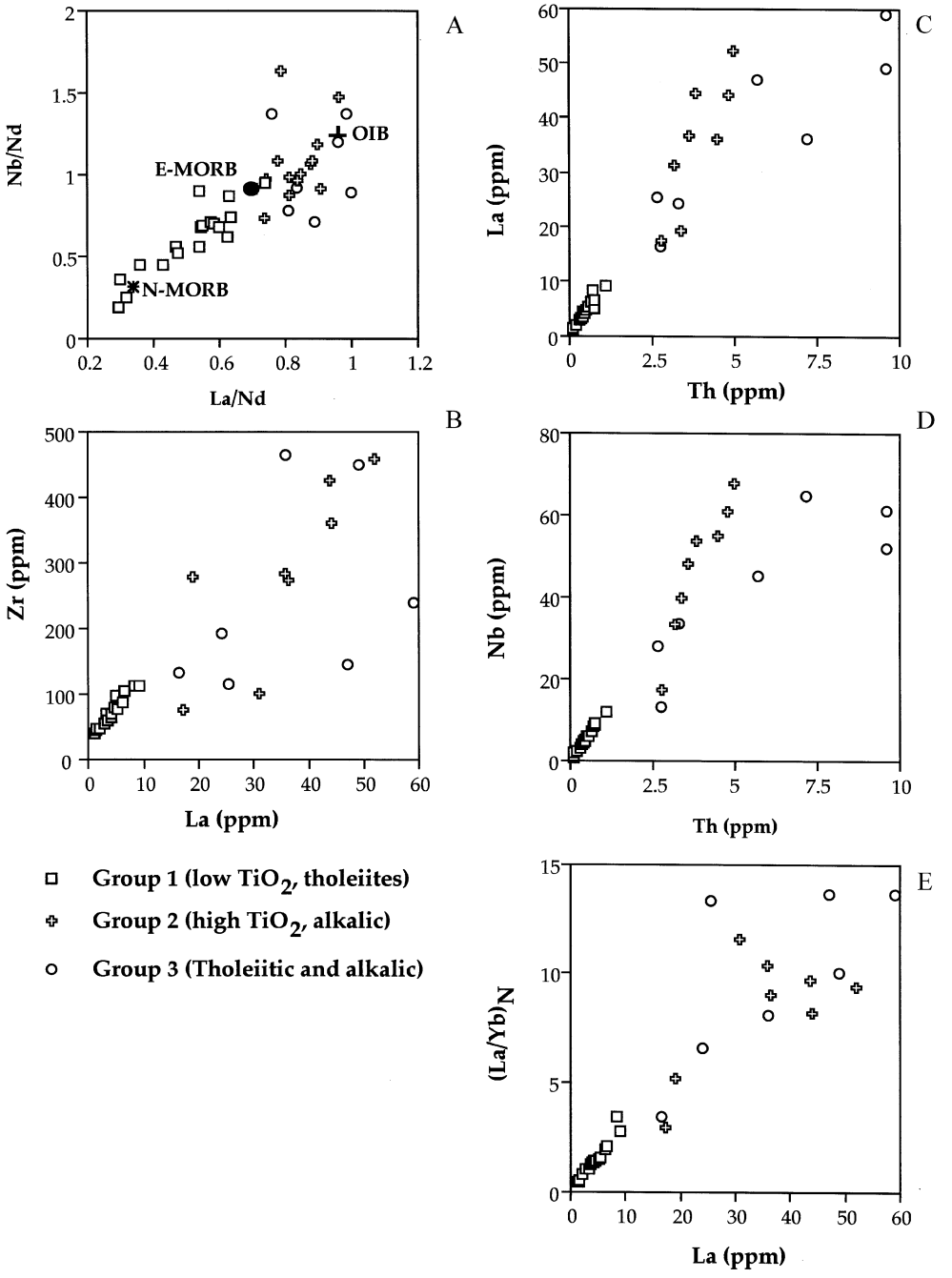

Fig. 9. Selected trace element plots. (A) Nb/Nd vs. La/Nd, (B) Zr vs. La, (C) La vs. Th, (D) Nb vs. Th, (E) $(La/Yb)_N$ vs. La plots for the Middle Permian volcanics from Oman.

5.2. Geochemical comparison of the Middle Permian volcanic rocks from Oman with those of similar ages emplaced along the southern margin of the Neo-Tethyan ocean

The Middle to Late Permian volcanism related to the Neo-Tethys opening is known in Kashmire (Panjal traps), and along the northern margin of the Indian shield involved in the Himalayas collisional Ranges (Lahul–Spiti and SE Zanskar, northwest India, Gupta et al., 1983; Vannay and Spring, 1993; Drakkar Po units and Shergol Melange along the Ladakh Indus suture zone in western Ladakh, Bassoulet et al., 1980; Honegger et al., 1982; Searle, 1983; Colchen and Reuber, 1986; Cannat and Mascle, 1990; Gaetani and Garzanti, 1991; Garzanti et al., 1994, 1996a, 1996b; Reuber et al., 1992; Searle et al., 1997; Robertson, 1998; Corfield et al., 1999; Hodges, 2000) (Fig. 1). These Middle to Upper Permian volcanics were emplaced either on the northern rifted margin of the Indian–Arabian shields or in the neighbouring basins. They are likely to represent the remnants of the southern volcanic margin of the Neo-Tethys ocean. The trace element geochemical comparison of the Panjal Traps, and alkaline volcanics of the Indus–Tsangpo suture zone with those of the Hawasina Nappes shown in Fig. 10 is based on preliminary data on the former occurrences.

The Panjal traps are coeval with the Middle Permian volcanics of the Saik Formation (Figs. 3 and 4B, Saih Hatat window). Both volcanics were emplaced onto continental crust. The Panjal traps erupted mainly as subaphyric flows in subaerial or shallow marine environments where minor amounts of pillow basalts have been recognized. Subordinate amounts of nepheline-bearing basalts, leucite basalts, ankaramites, trachytes and rhyolites occur (Honegger et al., 1982). Panjal basalts are metamorphosed into the low grade amphibolite facies (Vannay and Spring, 1993). They show typical features of continental crust-contaminated tholeiites with moderate LREE enrichments and marked Nb and Ta negative anomalies (Fig. 10A). The Saik Formation mafic lavas are predominantly alkalic and differ from the Panjal basalts by their greater LREE enrichments and lack of negative Nb and Ta anomalies (Fig. 6F).

The Upper Permian volcanic rocks of the Ladakh–Indus suture occur as blocks caught in a olistrostrome (Drakkar Po). Among the exotic blocks of the Drakkar Po olistostrome (Colchen et al., 1987; Colchen, 1999; Corfield et al., 1999), some consist of Upper Permian limestones associated with alkaline volcanic rocks (Fig. 10B). The latter can be correlated with those emplaced in the Hawasina basin. They differ from the Middle Permian alkaline lavas of Oman by their significantly higher contents in incompatible elements such as LREE, Nb, Th, Zr and Hf (Fig. 10B).

Thus, during the Late Middle to Late Permian, continental breakup took place along the Gondwana eastern and north-eastern margin along with the emplacement of continental flood tholeiites (Panjal traps) and alkalic or tholeiitic (Saih Hatat) volcanics. Concomitantly, alkali and tholeiitic basalts were emplaced in a marine basin which formed along the rifted and submerged Gondwana eastern margin. The development of this basin will lead to the formation of the Neo-Tethys oceanic realm.

5.3. Geochemical comparison of the middle permian volcanic rocks from oman with younger analogs

Rifting processes associated with continental breakup and opening of oceans are illustrated by the Afar/Red Sea and North Atlantic ocean developments. In both cases, continental rifting and extension began with emplacement of continental flood basalts.

The Afar plume, centered in northeastern Ethiopia, resulted in the separation of Arabia from East Africa and the opening of the Red Sea. The temporal relationships between rifting processes associated with the breakup of the Afro-Arabian plate and the opening of the Red Sea have been studied on the uplifted volcanic margin in western Yemen. Menzies et al., Group 1 (1997) show that volcanism started at 29–31 Ma and was very important until 29 Ma. Then it decreased with time. The exposed volcanic sequence is dominated by a thick pile of Group 1 subaerial basalts overlain by rhyolites and ignimbrites. The isotopic compositions of the volcanic rocks from Yemen LIP define a range in Sr and Nd ratios from values similar to those of oceanic rocks to compositions typical of upper and lower crustal rocks (Baker et al., 1996). Elemental and isotopic data also show that magmas evolved with time from deep-mantle mafic melts that are variably contaminated by lower crust to silicic melts contaminated with

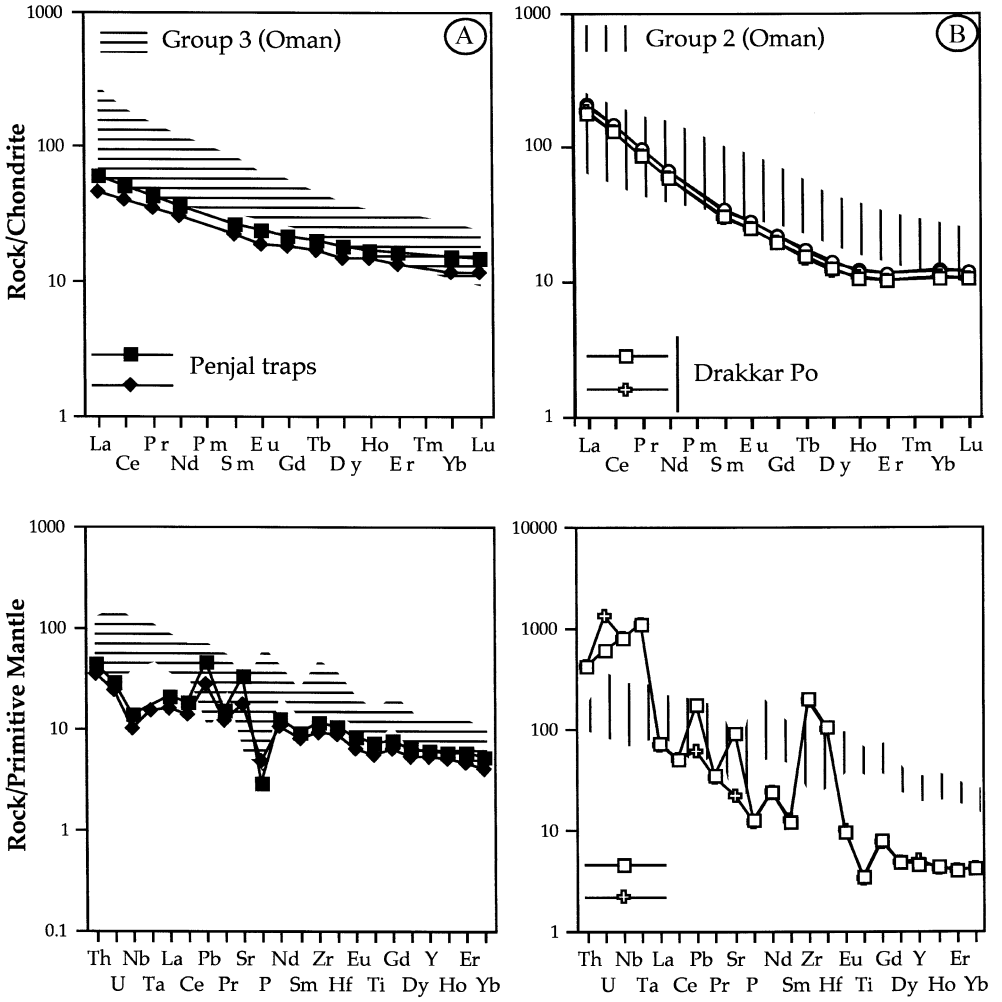

Fig. 10. A geochemical comparison of the Late Permian volcanics from Oman with those of similar ages exposed in the Indian Himalayas (Panjal Traps, Shergol tectonic Melange and Spotang thrust sheet of the Indus–Tsangpo suture zone). Data from the Panjal traps are after Vannay and Spring (1993). Data of the Drakkar Po volcanics thrust are after Prudhon-Chatelain's (1999) unpublished report, Université Claude Bernard, Lyon, France), respectively.

upper crust (Chazot and Bertrand, 1993). In contrast, basalts erupted in the Red Sea and Gulf of Aden spreading axes exhibit isotopic compositions typical of local asthenosphere. LIP volcanism from Yemen is not associated with extension which clearly postdates the emplacement of the basalts and rhyolites ($\sim < 26$ Ma). Then, the volcanic margin was rapidly and deeply exhumed at the earliest, in the Oligo-Miocene.

In the North Atlantic Igneous Province, two phases of magmatism occurred. During the first phase (62 Ma) continent-based magmatism emplaced in Baffin Island, W and SE Greenland, the British Isles and probably in central East Greenland. The second phase (56 Ma) is represented by the seaward-dipping reflector sequences (SDRS) along the continental margins, the Main Series basalts in central East Greenland, the Greenland–Faeroes Ridge and Iceland (Saunders et al., 1997). SRDS basalts from the North Atlantic Province are TiO_2-poor and more depleted in incompatible elements, compared to their continent-based equivalents. Group 1 tholeiites of the Hawasina Nappes can be compared to the seaward-dipping

reflectors (SRDS) basalts from the North Atlantic (Fig. 11).

In the Hawasina Nappes, there is a clear correlation between the geochemical types and their sedimentary environment (Maury et al., 2003). Thus, we can assume that: (1) Group 1 low-TiO_2 tholeiites interbedded with distal sediments (Rustaq, Buday'ah and the top of the Al Ajal thrust pile) erupted in the Hawasina basin far away from the continent, (2) Group 2 high TiO_2 alkali basalts associated with proximal basin sediments (Wadi Wasit, base of the Al Ajal thrust pile) erupted in the Hawasina basin, close to the continent, (3) Group 3 lavas were mostly emplaced on the thinned Arabian continental margin (Wadi Aday, Al Hulw), although a sample (OM126) associated to distal sediments near the top of the Al Ajal thrust pile also displays the chemical features typical of Group 3.

The geochemical and isotopic results developed above show that the Middle Permian volcanics located at the base of the Hawasina Nappes are clearly distinct from N-MORB and display features considered as characteristic of plume-related magmas. Indeed, we have shown that the Middle Permian lavas display geochemical features of LTi tholeiites and HTi alkali basalts. Group 1 likely derives from the mixing of two mantle sources, a depleted MORB type, and an enriched OIB type. Pb and Nd isotopic compositions of Group 2 clearly show features typical of an OIB type signature. Finally, Group 3 is geochemically similar to Group 2 but differs from Group 2 by its low to negative εNd values and low $^{206}Pb/^{204}Pb$ ratios suggesting a contamination of plume-derived magmas by the Arabian–Nubian lower crust. The apparent lack of N-MORB in the Hawasina basin or within the Ladakh Indus suture

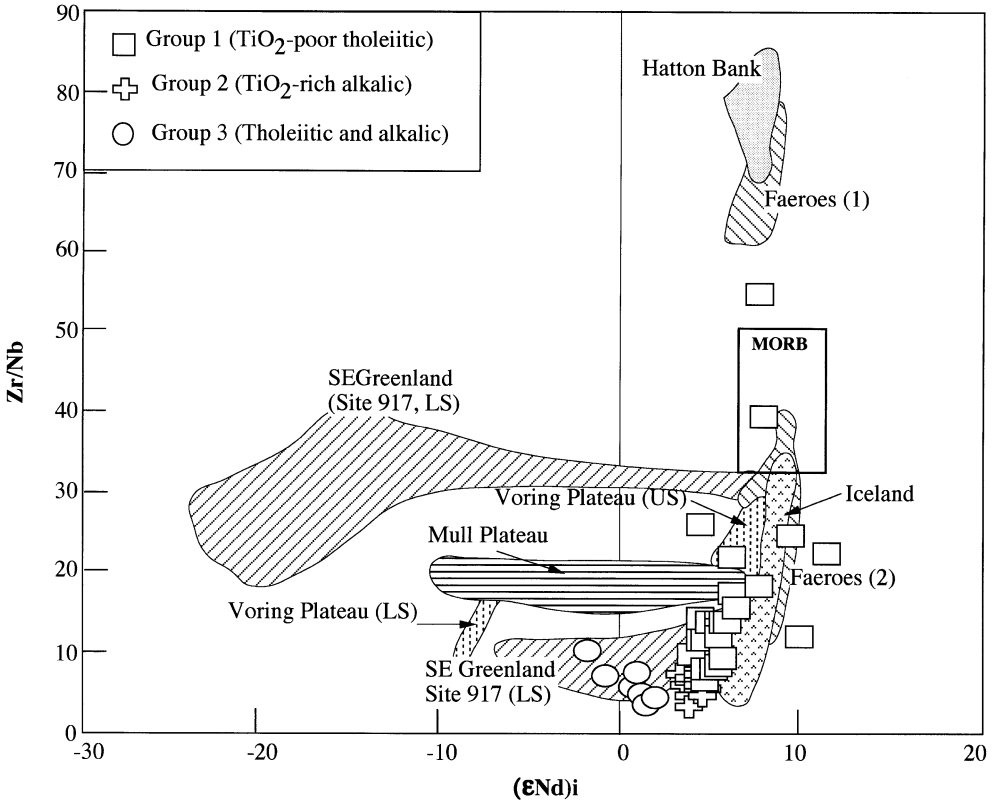

Fig. 11. Geochemical comparison between the Middle Permian volcanism from Oman and the Tertiary North Atlantic igneous province. Data are after Saunders et al. (1997).

(according to the literature) suggests that the remnants of the truly oceanic part of the Middle Permian Tethys have yet to be found. In addition, geochemical indications of contamination of mafic magmas by the lower continental crust (Group 3 basalts) are found not only on the para-autochtonous Arabian margin (Saih Hatat) but also, although less commonly, in the distal part of the Hawasina basin.

Thus, the Middle Permian plume-related alkaline and tholeiitic suites of the Saiq Formation, exposed on the submerged margins of the Arabian Platform and the Al Jil Formation, located in the adjacent Hamrat Duru Basin, represent the remnants of the Neo-Tethyan southern rifted volcanic passive margin.

6. Conclusions

The Middle Permian submarine mafic volcanics of the southern Neo-Tethyan margin in Oman exhibit trace element and isotopic characteristics of plume-related magmas. Group 1 tholeiites are geochemically similar to seaward-dipping reflectors basalts. The Nd and Pb isotopic composition of the tholeiitic (low-Ti, Group 1) and alkaline suites (high-Ti, Group 2) from the Hamrat Duru Basin show that these suites derived from the melting of enriched OIB sources and are mostly devoid of crustal contamination.

The geochemical data discussed in this paper represent the first attempt of isotopic characterization of the Tethyan plume, the heterogeneity of which is supported by the large range of Nd and Pb isotopic compositions of the Middle Permian tholeiitic and alkalic basalts from Oman. Similar heterogeneities are also common features of Tertiary plumes, i.e. Afar/Red Sea and North Atlantic/Iceland.

Acknowledgements

This work was supported by the Institut National des Sciences de l'Univers, programme "Intérieur de la Terre". We thank M. Caroff and F. Cordey for their contribution to geochemical and palaeontological studies, respectively, and C. Basile, G. H. Mascle and M. Tardy for the discussions on the Tethyan geodynamics. Many thanks to T.J. Peters and anonymous reviewer for their constructive reviews.

References

Acharyya, S.K., 1992. Pan-Indian Gondwana plate break-up, rewelding and evolution of the Himalaya, Indo-Burmese range and Andaman island arc. In: Sinha, A.K. (Ed.), Himalayan Orogen and Global Tectonics. Wiley, Hoboken, pp. 77–89.

Al-Riyami, K., Robertson, A.H.F., Xenophontos, C., Danelian, T., Dixon, E.J., 2000. Tectonic evolution of the Mesozoic Arabian passive continental margin and related ophiolite: Baër-Bassit (NW Syria). In: Panayides, I., et al., (Ed.), Proceedings Third International Conference on the Geology of the Eastern Mediterranean, Geol. Survey Cyprus, Nicosia, pp. 61–81.

Baker, J.A., Thirlwall, M.F., Menzies, M.A., 1996. Sr–Nd–Pb and trace element evidence for crustal contamiantion of a mantle plume: oligocene flood volcanism in western Yemen. Geochim. Cosmochim. Acta 60, 2559–2581.

Barrat, J.-A., Keller, F., Amossé, J., Taylor, R.N., Nesbitt, R.W., Hirata, T., 1996. Determination of rare earth elements in sixteen silicate reference chromatography procedures. Geostand. Newsl. 20, 133–139.

Bassoulet, J.-P., Colchen, M., Juteau, T., Marcoux, J., Mascle, G.H., 1980. L'édifice des nappes du Zanskar (Ladakh, Himalaya). C. r. Acad. Sci., Sci. Paris 290 (Série D), 389–392.

Béchennec, F., 1988. Géologie des Nappes Hawasina dans les parties orientale et centrale des Montagnes d'Oman. Thèse Doct. D'Etat, Universté P. et M. Curie, Paris VI, Bur. Rech. Géol. Min. Document 127, Orléans, France. 474 pp.

Béchennec, F., Le Métour, J., Rabu, D., Villey, M., Beurrier, M., 1988. The Hawasina basin: a fragment of a starved passive continental margin, thrust over the Arabian platform during obduction of the Semail Nappe. Tectonophysics 151, 323–343.

Béchennec, F., Tegyey, M., Le Métour, J., Lemière, B., Lescuyer, J.L., Rabu, D., Milési, J.P., 1991. Igneous rocks in the Hawasina nappes and the Hajar supergroup, Oman mountains: their significance in the birth and evolution of the composite extensional margin of Eastern Tethys. Min. of Petroleum and Minerals of Sultanate of Oman (Ed.), Ophiolite Genesis and Evolution of the Oceanic Lithosphere, pp. 569–611.

Béchennec, F., Roger, J., Le Métour, J., Wyns, R., 1992a. Geological map of Seeb, Sheet NF 40-03, scale 1/250 000, with Explanatory notes. Sultanate of Oman, Ministry of Petroleum and Minerals, Directorate of Minerals, BRGM, Orleans, France, ed., 104 pp.

Béchennec, F., Roger, J., Le Métour, J., Wyns, R., Chevrel, S., 1992b. Geological map of Ibri, Sheet NF 40-02, scale 1/250 000, with Explanatory notes. Sultanate of Oman, Ministry of Petroleum and Minerals, Directorate of Minerals, BRGM, Orleans, France, ed., 94 pp.

Berberian, M., King, G.C.P., 1981. Towards a paleogeography and tectonic evolution of Iran. Can. J. Earth Sci. 18, 210–265.

Blendinger, W., van Liet, A., Hugues Clarke, M.W., 1990. Updoming, rifting and continental margin development during the Late Paleozoic in Northern Oman. In: Robertson, A.H.F., Searle, M.P., Ries, P. (Eds.), The Geology and Tectonics of the Oman Region. Spec. Publ.-Geol. Soc., vol. 49, pp. 27–37.

Blendinger, W., Furnish, W.M., Glenister, B.F., 1992. Permian

cephalopod limestones, Oman mountains: evidence of a Permian seaway along the northern margin of Gondwana. Palaeogeogr. Palaeoclimatol. Palaeoecol. 93, 13–20.

Bosch, D., 1990. Evolution géochimique initiale et précoce d'un rfit: systématique isotopique, Pb, Sr et Nd du diapir mantellique de Zabargad, de son encaissant gneissique et de son hydrothermalisme. Comparaison avec les sédiments métallifères et les MORB de la Mer Rouge, Thèse Docto. Uniiversité Montpellier II. 230 pp.

Brueckner, H.K., Zindler, A., Seyler, M., Bonatti, E., 1988. Zabargad and the isotopic evolution of the sub-Red Sea mantle and crust. Tectonophysics 150, 163–176.

Cannat, M., Mascle, G.H., 1990. Réunion extraordinaire de la Société géologique de France en Himalaya du Ladakh. Bull. Soc. Géol. Fr. 8 (VI), 553–582.

Chazot, G., Bertrand, H., 1993. Mantle sources and magma–continental crust interactions during early Red Sea–Aden rifting in southern Yemen: elemental and Sr, Nd, Pb isotopic evidence. J. Geophys. Res. 98, 1819–1835.

Chemenda, A.I., Mattauer, M., Bokun, A.N., 1996. Continental subduction and a mechanism for exhumation of HP metamorphic rocks: new modelling and field data from Oman. Earth Planet. Sci. Lett. 143, 173–182.

Coffin, M.F., Eldholm, O., 1992. Volcanism and continental breakup: a global compilation of large igneous provinces. In: Storey, B.C., Alabaster, T., Pankhurst, R.J. (Eds.), Magmatism and the Causes of Continental Break-Up. Spec. Publ.-Geol. Soc. Lond., vol. 68, pp. 17–30.

Coffin, M.F., Eldholm, O., 1994. Large igneous province: crustal structure, dimensions, and external consequences. Rev. Geophys. 32, 1–36.

Colchen, M., 1999. Ophiolitic melanges in the Ladakh Indus suture zone: a key to understanding the geodynamic evolution of the Indian and Tibetan Tethyan margin. 14th Himalayan–Karakorum–Tibet Workshop, Tubingen, Germany. Terra Nostra, vol. 99, p. 128.

Colchen, M., Reuber, I., 1986. Les mélanges ophiolitiques du Zanskar, Himalaya du Ladakh. C. r. Acad. Sci., Sci. Paris 303, 719–724.

Colchen, M., Reuber, I., Bassoulet, J.P., Belier, J.P., Blondeau, A., Lys, M., De Wever, P., 1987. Données biostratigraphiques sur les mélanges ophiolitiques du Zanskar Himalaya du Ladakh. C. r. Acad. Sci., Sci. Paris 305, 403–406.

Cordey, F., Baud, A., Béchennec, F., Gorican, S., Krystyn, L., 2001a. Permian–Triassic deep water sediments of the Wadi Wasit revisited. International Conference Geology of Oman. Sultanate of Oman Ministry of Commerce and Industry, Muscat, p. 29. Abstract volume.

Cordey, F., Béchennec, F., Maury, R., 2001b. Buday'ah: a Late Permian Hawasina basinal unit, MORB pillow basalt and radiolarian units. The Oman Ministry of Commerce and Industry. Permo-Triassic Deposits: From Shallow Water to Base of Slope, Excursion B01, International Conference on the Geology of Oman, pp. 23–25.

Corfield, R.I., Searle, M.P., Green, O.R., 1999. Photang thrust sheet: an accretionary complex structurally below the Spontang ophiolite constraining timing and tectonic environment of ophiolite subduction, Ladakh Himalaya, NW India. J. Geol. Soc. (Lond.) 156, 1031–1044.

Cotten, J., Le Dez, A., Bau, M., Caroff, M., Maury, R.C., Dulski, P., Fourcade, S., Bohn, M., Brousse, R., 1995. Origin of anomalous rare-earth element and yttrium enrichments in subaerially exposed basalts: evidence from French Polynesia. Chem. Geol. 119, 115–138.

Courtillot, V., Jaupart, C., Manighetti, I., Tapponnier, P., Besse, J., 1999. On causal links between flood basalts and continental breakup. Earth Planet. Sci. Lett. 166, 177–195.

De Wever, P., Bourdillon-de-Grissac, C., Béchennec, F., 1988. Permian age from radiolarites of the Hawasina nappes, Oman mountains. Geology 16, 912–914.

Fitton, J.G., Hardarson, B.S., Ellam, R.M., Rogers, G., 1998. Sr-, Nd- and Pb-isotopic compositions of volcanic rocks from the Southeast Greenland margin at 63°N: temporal variation in crustal contamination during continental breakup. In: Saunders, A.D., Larsen, H.C., Wise Jr., S.W. (Eds.), Proceedings of the Ocean Drilling Program. Scientific Results, vol. 152, pp. 351–357.

Gaetani, M., Garzanti, E., 1991. Multicyclic history of the Northern India continental margin (Northwestern Himalaya). AAPG Bull. 75, 1427–1446.

Garzanti, E., Sciunnach, D., 1997. Early Carboniferous onset of Gondwanian glaciation and Neo-Tethyan rifting in Southern Tibet. Earth Planet. Sci. Lett. 148, 359–365.

Garzanti, E., Nicora, A., Tintori, D., Sciunnach, D., Angiolini, L., 1994. Late Palaeozoic stratigraphy and petrography of the Thini Chu Group (Manang, Central Nepal): record of Gondwana glaciation and rifting of Neo-Tethys. Riv. Ital. Paleontol. Stratigr. 100, 155–194.

Garzanti, E.L., Angiolini, A., Sciunnach, D., 1996a. The Permian Kuling Group (Spiti, Lahaul and Zanskar; NW Himalaya): sedimentary evolution during rift/dritf transition and initial opening of Neo-Tethys. Riv. Ital. Paleontol. Stratigr. 102, 175–200.

Garzanti, E., Nicora, A., Tintori, A., Sciunnach, D., 1996b. The Mid-Carboniferous to lowermost Permian succession of Spiti (Po Group and Ganmachidam Formation: Tethys Himalaya, northern India): Gondwana glaciation and rifting of Neo-Tethys. Geodin. Acta 9, 78–100.

Garzanti, E., Le Fort, P., Sciunnach, D., 1999. First report of Lower Permian basalts in South Tibet: tholeiitic magmatism during breakup and incipient spreading in Neo-Tethys. J. Asian Earth Sci. 17, 533–546.

Gibson, S.A., Kirkpatrick, R.J., Emmermann, R., Schmincke, P.-H., Pritchard, G., Okay, P.J., Thorpe, R.S., Marriner, G.F., 1982. The trace element composition of lavas and dykes from a 3 km vertical section through a lava pile in Eastern Iceland. J. Geophys. Res. 87, 6532–6546.

Gibson, S.A., Thompson, R.N., Dickin, A.P., Leonardos, O.H., 1995. High-Ti and low-Ti mafic potassic magmas: key to plume–lithosphere interactions and continental flood-basalt genesis. Earth Planet. Sci. Lett. 136, 149–165.

Glennie, K.W., Bœuf, M.G.A., Hugues Clarke, M.W., Moody-Stuart, M., Pilaart, W.F.H., Reinhart, B.M., 1974. Geology of the Oman mountains. Geol. Mijnb. I (423 pp).

Gupta, K.R., Gergan, J.T., Kumar, S., 1983. Geochemistry of the volcanic rocks of northwestern Himalaya and its bearing on

tectonics—a review. In: Sinha, A.K. (Ed.), Contemporary Geoscientific Researches in Himalaya, vol. 2, pp. 9–18. Dehra Dun.

Hodges, K.V., 2000. Tectonics of the Himalaya and southern Tibet from two perspectives. Geol. Soc. Amer. Bull. 112 (3), 324–350.

Honegger, K., Dietrich, V., Frank, W., Gansser, W., Thöni, M., Trommsdorff, V., 1982. Magmatism and metamorphism in the Ladakh Himalayas (the Indus–Tsangpo suture zone). Earth Planet. Sci. Lett. 60, 253–292.

Kent, R.W., Storey, A.D., Saunders, A.D., 1992. Large igneous provinces: sites of plume impact or plume incubation. Geology 20, 891–894.

Kozur, H.W., Wardlaw, B.R., Baud, A., Béchennec, F., Marcoux, J., Richoz, S., 2001. Middle Permian conodonts from Oman. Permophiles 38, 10–15.

Lancelot, J.R., Bosch, D., 1991. A Pan African age for the HP–HT granulite gneisses of Zabargad island: implications for the early stages of the Red Sea rifting. Earth Planet. Sci. Lett. 107, 539–549.

Lapierre, H., Rocci, G., 1976. Le volcanisme alcalin du Sud-Ouest de Chypre et le problème de l'ouverture des régions téthysiennes au Trias. Tectonophysics 30, 299–313.

Lapierre, H., Dupuis, V., Mercier de Lépinay, B., Ruíz, J., Tardy, M., Maury, R.C., Hernandez, J., Loubet, M., 1997. Is the lower Duarte igneous complex (Hispaniola) a remnant of the Caribbean plume-generated oceanic plateau? J. Geol. 105, 111–120.

Lapierre, H., Narros, A., Bosch, D., Mascle, G.H., Tardy, M., Demant, A., The Mamonia Comples (SW Cyprus) revisited: remnant of Late Triassic intra-oceanic volcanism along the Tethyan southwestern passive margin. Chem. Geol. (submitted for publication).

Le Métour, J. 1988. Géologie de l'Autochtone des Montagnes d'Oman: la fenêtre du Saih Hatat, Thèse Doct. d'Etat, Université P. et M. Curie, Paris VI, Bur. Rech. Géol. Min., Document 129, Orléans, France, 430 pp.

Le Métour, J., Rabu, D., Tegyey, M., Béchennec, F., Beurrier, M., Villey, M., 1990. Subduction and obduction: two stages in the Eo-Alpine tectonometamorphic evolution of the Oman mountains. In: Robertson, A.H.F., Searle, M.P., Ries, A.C. (Eds.), The Geology and Tectonics of the Oman Region. Spec. Publ.-Geol. Soc., vol. 49, pp. 327–339.

Le Métour, J., Béchennec, F., Roger, J., Wyns, R., 1992. Geological map of Muscat, Sheet NF 40-04, scale 1/250 000, with Explanatory notes, edited by Sultanate of Oman, Ministry of Petroleum and Minerals, Directorate of Minerals, BRGM, Orléans, France.

Lippard, S.J., Shelton, A.W., Gass, I.G., 1986. The ophiolite of Northern Oman. Mem. Geol. Soc. Lond. 11 (178 pp).

Malpas, J., Calon, T., Squires, G., 1993. The development of a late Cretaceous microplate suture zone in SW Cyprus. In: Prichard, H., Alabaster, T., Harris, N.B.W., Neary, C.R. (Eds.), Magmatic Processes and Plate Tectonics. Special Publication-Geol. Soc. London, vol. 76, pp. 177–195.

Marcoux, J., 1987. Histoire et topologie de la Néo-Téthys. Thèse de Doctorat-es-Sciences, Paris .350 pp.

Matte, P., 2002. The Variscan collage and orogeny (480–290 Ma) and the tectonic definition of the Armorica microplate: a review. Terra Nova 13 (2), 122–128.

Maury, R.C., Cotten, J., Béchennec, F., Caroff, M., Marcoux, J., 2001. Magmatic Evolution of the Tethyan Permo-Triassic Oman margin. Geology of Oman, Pangea Symposium: Muscat, Oman.

Maury, R.C., Béchennec, F., Cotten, J., Caroff, M., Cordey, F., Marcoux, J., 2003. Middle Permian plume-related magmatism of the Hawasina Nappes and the Arabian Platform: implications on the evolution of the Neotethyan margin in Oman. Tectonics 22 (6), 1073 (doi:10.129/2002TC001483).

McCulloch, M.T., Wasserburg, G.J., 1978. Sm–Nd and Rb–Sr chronology of continental crust formation. Science 200 (4345), 1003–1011.

McGuire, A.V., Stern, R.J., 1983. Granulite xenoliths from western Saudi Arabia: the lower crust of the Late Precambrian Arabian–Nubian shield. Contrib. Mineral. Petrol. 144, 395–408.

Menzies, M., Baker, J., Chazot, G., Al'Kadasi, M., 1997. Evolution of the Red Sea, Volcanic Margin, Western Yemen. In: Mahoney, J.J., Coffin, M.F. (Eds.), The Large Igneous Provinces, Continental, Oceanic and Planetary Flood Vocanism. Geophysical Monograph, vol. 100, pp. 29–43.

Michard, A., Goffé, B., Saddiqi, O., Oberhansli, R., Wendt, A.S., 1994. Late Cretaceous exhumation of the Oman blueschists and eclogites: a two stage extensional mechanism. Terra Nova 6, 404–413.

Miller, J.M.C.L., Gray, D.R., Gregory, R.T., 1998. Exhumation of high-pressure rocks in NE Oman. Geology 26, 235–238.

Nikishin, A.M., Ziegler, P.A., Abbott, D., Brunet, M.-F., Cleotingh, S., 2002. Permo-Triassic intraplate magmatism and rifting in Eurasia: implications for mantle plumes and mantle dynamics. Tectonophysics 351, 3–39.

Parrot, J.-F., 1974. L'emblage ophiolitique du Baër-Bassit (N–W de la Syrie): étude pétrographique et géochimique du complexe filonien, des laves qui lui sont associées et d'une partie des formations éffusives comprises dans le volcano-sédimentaire. Cah.-ORSTOM, Géol. VI (2), 97–126.

Pik, R., Deniel, C., Coulon, C., Yirgu, G., Hofmann, C., Ayalew, D., 1998. The northwestern Ethiopian Plateau flood basalts: classification and spatial distribution of magma types. J. Volcanol. Geotherm. Res. 81, 91–111.

Pik, R., Deniel, C., Coulon, C., Yirgu, G., Marty, B., 1999. Isotopic and trace element signatures of Ethiopian flood basalts: evidence for plume–lithosphere interactions. Geochim. Cosmochim. Acta 63, 2263–2279.

Pillevuit, A., 1993. Les blocs exotiques du Sultanat d'Oman: évolution paléogéographique d'une marge passive flexurale. Mém. Géol. Univ. Lausanne, Suisse 17 (249 pp).

Pillevuit, A., Stampfli, G., Baud, A., Marcoux, J., 1992. Late Permian opening of the Neotethys in Oman. Géochronique 42, 85 (abstract).

Pillevuit, A., Marcoux, J.G., Stampfli, G., Baud, A., 1997. The Oman exotics: a key to the understanding of the Neotethyan geodynamic evolution. Geodin. Acta 10, 209–238.

Rabu, D., Le Métour, J., Béchennec, F., Beurrier, M., Villey, M., Bourdillon-Jeudy de Grissac, C., 1990. Sedimentary aspects of the Eo-Alpine cycle on the northeast edge of the Arabian platform (Oman mountains). In: Robertson, A.H.F., Searle, M.P., Ries, A.C. (Eds.), The Geology and Tectonics of the Oman Region. Spec. Publ.-Geol. Soc., vol. 49, pp. 49–68.

Reuber, I., Colchen, M., Mevel, C., 1992. The Spotang Ophiolite and ophiolitic mélanges of the Zanskar, N. W. Himalya, tracing the evolution of the closing Tethys in the upper Cretaceous to the early Tertiary. In: Sinha, A.K. (Ed.), Himalayan Orogen and Global Tectonics. Mohan Primlani, New Delhi, pp. 235–266.

Robertson, A.H.F., 1998. Rift-related sedimentation and volcanism of the north-Indian margin inferred from a Permian–Triassic exotic block at Layamuru, Indus suture zone (Ladakh Himalaya) and regional comparisons. J. Asian Earth Sci. 16, 159–172.

Roberston, A.H.F., 2000. Formation of mélanges in the Indus Suture Zone, Ladakh Himalaya by successive subduction-related, collisional and post-collisional processes during the Late Mesozoic–Late Tertiary time. In: Khan, M.A., Treloar, P.J., Searle, M.P., Jan, M.Q. (Eds.), Tectonics of the Nanga Parbat Synataxis and the Western Himalaya. Special publication-Geological Society of London, vol. 170. The Geological Society, London, UK, pp. 333–374.

Robertson, A.H.F., Searle, M.P., 1990. The northern Oman Tethyan continental margin: stratigraphy, structure, concepts and controversies. In: Robertson, A.H.F., Searle, M.P., Ries, A.C. (Eds.), The Geology and Tectonics of the Oman Region. Spec. Publ.-Geol. Soc., vol. 49, pp. 3–25.

Robertson, A.H.F., Waldron, J.W.F., 1990. Geochemistry and tectonic setting of Late Triassic and Late Jurassic–Early Cretaceous basaltic extrusives from the Antalya Complex, -west Turkey. In: Savascin, M.Y., Eronat, A.H. (Eds.), International Earth Sciences Congress on Aegean Regions, Proceedings, vol. 2. Geol. Soc. London Spec. Pub., pp. 279–299.

Robertson, A.H.F., Blome, C.D., Cooper, D.W.J., Kemp, A.E.S., Searle, M.P., 1990. Sedimentary and structural evolution of a continental margin transform lineament: the Hatta zone, Northern Oman mountains. In: Robertson, A.H.F., Searle, M.P., Ries, A.C. (Eds.), The Geology and Tectonics of the Oman Region. Spec. Publ.-Geol. Soc., vol. 49, pp. 3–25.

Rollinson, H., 1993. Using Geochemical Data: Evaluation, Presentation, Interpretation. Logman Scientific and Technical Wiley, New York, USA. 352 pp.

Samper, A., 2002. Le Volcanisme Permien des Nappes De Hawasina, Sultanat D'Oman: Témoin D'une Marge Passive Volcanique, Mémoire De DEA Dynamique de la Lithosphère Université Aix-Marseille III. 30 pp.

Saunders, A.D., Fitton, J.G., Kerr, A.C., Norry, J.C., Kent, R.W., 1997. The North Atlantic igneous province. In: Mahoney, J.J., Coffin, M.F. (Eds.), The Large Igneous Provinces, Continental, Oceanic and Planetary Flood Vocanism. Geophysical Monograph, vol. 100, pp. 45–93.

Scotese, C.R., Golonka, J, 1993. PALEOMAP Paleogeographic Atlas, PALEOMAP Progress Report # 20. Department of Geology, University of Texas at Arlington, 28 maps.

Searle, M.P., 1983. Stratigraphy, stucture and evolution of the Tibetan–Tethys zone in Zanskar and the Indus suture zone in the Ladakh Himalaya. Trans. R. Soc. Edinb. Earth Sci. 73, 205–219.

Searle, M.P., Corfield, R.I., Stephenson, B., McCarron, J., 1997. Structure of the north Indian continental margin in the Ladakh–Zanskar Himalayas: implications for the timing of obduction of the Spontang ophiolite, India–Asia collision and deformational events in the Himalaya. Geol. Mag. 134, 297–316.

Sëngor, A.M.C, 1990. A new model for the late Paleozoic–Mesozoic evolution of Iran and implications for Oman. In: Robertson, A.H.F., Searle, M.P., Ries, A.C. (Eds.), The Geology and Tectonics of Oman Region. Spec. Publ.-Geol. Soc. Lond., vol. 49, pp. 797–831.

Sengör, A.M.C., Cin, A., Rowley, D.B., Nie, S.Y., 1993. Space–time patterns of magmatism along the Tethysides: a preliminary study. J. Geol. 101, 51–84.

Seyler, M., Bonatti, E., 1988. Petrology on gneiss-amphibolite lower crust unit from Zabargad island, Red Sea. Tectonophysics 150, 177–207.

Stampfli, G.M., Pillevuit, A., 1993. An alternative Permo-Triassic reconstruction of the kinematics of the Tethyan realm. In: Dercourt, J., Ricou, L.E., Vrielinck, B. (Eds.), Atlas Tethys Palaeoenvironmental Maps. Gauthier-Villars, Paris, pp. 55–62.

Stampfli, G., Marcoux, J., Baud, A., 1991. Tethyan margins in space and time. Paleogeogr. Paleoclimatol. Paleoecol. 87, 373–409.

Stampfli, G.M., Mosar, J., Favre, P., Pillevuit, A., Vannay, J.-C., 2001. Late Palaeozoic to Mesozoic evolution of the Western Tethyan realm: the Neotethys—East Mediterranean basin connection. In: Ziegler, P.A., Cavazza, W., Roberston, A.H.F., Crasquin-Soleau, S. (Eds.), Peri-Tethys Mem. 6: PeriTethyan Rift/Wrench Basins and Passive Margins. Mém. Mus. Natl. Hist. Nat. Paris, vol. 186, pp. 51–108.

Sun, S.S., McDonough, W.F., 1989. Chemical and isotopic systematics of ocean basalts: implications for the mantle composition and processes. In: Saunders, A.D., Norry, M.J. (Eds.), Magmatism in the Ocean basins. Spec. Publ. – Geol. Soc. Lond., vol. 42, pp. 313–345.

Teklay, M., Kröner, A., Mezger, K., Oberhänsli, R., 1998. Geochemistry, Pb–Pb single zircon ages and Nd–Sr isotope composition of Precambrian rocks from southern and eastern Ethiopia: implications for crustal evolution in East Africa. J. Afr. Earth Sci. 26 (2), 207–227.

Todt, W., Cliff, R.A., Hanser, A., Hofmann, A.W., 1996. Evaluation of a $^{202}Pb-^{205}Pb$ double spike for high-precision lead isotope analysis. In: Basu, A., Hart, S. (Eds.), Earth Processes: Reading the Isotopic Code. AGU, Washington, D.C, pp. 429–437.

Vannay, J.C., Spring, L., 1993. Geochemistry of the continental basalts within the Tethyan Himalaya of Lahul–Spiti and SE Zanskar, northwest India. In: Treloar, P.J., Searle, M.P. (Eds.), Himalayan Tectonics, Geological Society London Special Publication, N°74, London, UK, pp. 237–249.

White, M.W., Albarède, F., Telouk, F., 2000. High-precision analysis of Pb isotopic ratios by multi-collector ICP-MS. Chem. Geol. 167, 257–270.

Wilson, M., Guiraud, R., 1998. Late Permian to recent magmatic activity on the African–Arabian margin of Tethys. In: Macgregor, D.S., Moody, R.T.J, Clark-Lowes, D.D. (Eds.), Petroleum Geology of North Africa. Spec. Publ.-Geol. Soc., vol. 132, pp. 231–263.

Zingler, A., Hart, S.R., 1986. Chemical systematics. Annu. Rev. Earth Planet. Sci. 14, 493–571.

Résumé
L'utilisation de la technique K-Ar Cassignol-Gillot nous a permis de définir les limites temporelles du volcanisme effusif sub-aérien de l'île de Basse-Terre (Guadeloupe) et de préciser les périodes d'activité des quatre principaux massifs constituant l'île, jusque-là mal contraintes. Le Complexe Basal [2,79 ± 0,04 - 2,68 ± 0,04 Ma], la Chaîne Septentrionale [1,81 ± 0,03 - 1,15 ± 0,02 Ma], la Chaîne Axiale [1023 ± 25 - 435 ± 8 ka] et le complexe récent de la Grande-Découverte [205 ± 28 - actuel] illustrent la migration du volcanisme à Basse-Terre depuis 3 Ma suivant une direction principale Nord-Sud et une vitesse moyenne de l'ordre de 20 km/Ma. Nous proposons que les principales directions d'extraction des magmas soient contrôlées par les systèmes de graben E-W et failles normales en échelon NW-SE affectant l'archipel de la Guadeloupe. Les taux d'extrusion, calculés sur la base d'observations et modélisations morphologiques sont compris entre 1,4 10^{-5} (Complexe Basal) et 4,5 10^{-4} km^3/yr (Chaîne Axiale). Les principales périodes d'activité du complexe le plus récent de l'île ont été déterminées. Le complexe de Trois-Rivières - Madeleine, situé au sud du volcan de la Grande-Découverte, est contraint entre 87 ± 5 ka et l'actuel. C'est la première fois que des âges K-Ar sont réalisés dans cette zone. Ils démontrent que les diverses phases d'activité effusive de ce complexe sont contemporaines de celles du volcan de la Grande-Découverte. Les coulées de Trois-Rivières (87 ± 5 ka) puis la mise en place de l'alignement E-W du dôme de la Madeleine et des coulées du Palmiste entre 70 et 45 ka permettent de dater une phase de propagation du rift de Marie-Galante. La reconnaissance et la datation de coulées jeunes < 10 ka dans l'environnement du dôme de la Madeleine permettent d'étendre la zone d'activité volcanique actuelle à l'extrémité sud de l'île. De fait, ceci nous conduit à considérer l'aléa volcanique dans une zone qui n'est plus restreinte uniquement au dôme de la Soufrière et à son voisinage immédiat, mais à l'étendre jusqu'au sud de l'île dans la zone du massif de La Madeleine - Trois-Rivières. Enfin, des phénomènes d'effondrements de flancs majeurs, ont pu être datés sur les îles de Basse-Terre (640 et 550 ka), La Dominique (100 ka), Martinique (330 ka) et Sainte-Lucie (100 ka), et nous proposons une relation causale entre la récurrence de ces phénomènes catastrophiques et les changements climatiques globaux.

Abstract
The use of the K-Ar Cassignol-Gillot technique enabled us to define the temporal bounds of the sub-aerial effusive volcanism in Basse-Terre (Guadeloupe), and to constrain the active periods of the four main massifs that make the island, which were poorly defined so far. The Basal Complex [2.79 ± 0.04 – 2.68 ± 0.04 Ma], the Septentrional Chain [1.81 ± 0.03 – 1.15 ± 0.02 Ma], the Axial Chain [1023 ± 25 - 435 ± 8 ka] and the most recent volcanic complex of Grande-Découverte [205 ± 28 - actuel] illustrate the southwards migration of volcanism through time in Basse-Terre since 3 Ma, along a main N-S direction, at a rate of roughly 20 km/Ma. We propose magma extraction to be linked to the E-W striking graben and en-échelon normal fault systems that affect the Guadeloupe archipelago. Extrusion rates, on the basis of morphological observations and modeling spread from 1.4 10^{-5} (Basal Complex) to 4.5 10^{-4} km^3/yr (Axial Chain). The main building stages of the most recent complex in Basse-Terre have been determined. The Trois Rivières – Madeleine Complex, located South of the Grande-Découverte Volcano has been constrained between 87 ± 5 ka and present time. For the first time K-Ar ages are provided for this area. These show that the various stages of effusive activity are contemporaneous with the Grande-Découverte volcano ones. The Trois-Rivières lava flows (87 ± 5 ka) and the subsequent emplacement of the E-W alignment of La Madeleine dome and Le Palmiste lava flow, between 70 and 45 ka, constrain the age of a Marie-Galante rift propagation phase. Recognition and dating of lava flows younger than 10 ka in the surroundings of the La Madeleine dome lead to extend the present time volcanic activity up to the extreme south of the island, hence to consider volcanic hazards in a larger zone spreading from La Soufrière area up to the La Madeleine -Trois Rivières volcanic complex. Finally, dating of major flank-collapse events in Basse-Terre (640 and 550 ka), Dominica (100 ka), Martinique (330 ka) and St. Lucia (100 ka) have been realized and we propose in this work a causal link between the recurrence of such catastrophic events and global climate changes.